UNIVERSITE MONTPELLIER 2
SCIENCES ET TECHNIQUE DU LANGUEDOC

Demande d'Habilitation à Diriger des Recherches

Ecole Doctorale
Systèmes Intégrés en Biologie, Agronomie, Géosciences, Hydrosciences et Environnement (SIBAGHE)

Spéciation, mécanismes d'acquisition de la composition chimique des solutions du sol et modélisation des cycles biogéochimiques

par

Frédéric Gérard

le 05 novembre 2008

Devant le jury composé de :

M. Marc Benedetti	Professeur Université Paris VII, rapporteur
M. Jérôme Balesdent	Directeur de Recherches INRA, rapporteur
M. Jean-Luc Chotte	Directeur de Recherches IRD.
M. Etienne Dambrine	Directeur de Recherches INRA
M. Benoît Jaillard	Directeur de Recherches INRA
Mme Catherine Keller	Professeur Université Aix-Marseille III, rapporteur

Pour Thérèse

Sommaire

Sélection d'articles……75

« Spéciation de l'aluminium dissous et Al_{13} »

Gérard F., Boudot J.-P., et Ranger J. (2001) Consideration on the occurence of the Al_{13} polycation in natural soil solutions and surface waters. *Applied Geochemistry* **16**, 513-529.

« Silice dans les solutions gravitaires et capillaires faiblement liées »

Gérard F., François M., et Ranger J. (2002) Processes controlling silica concentration in leaching and capillary soil solutions of an acidic brown forest soil (Rhône, France). *Geoderma* **107**, 197-226.

« Silice et solutions extraites par centrifugation »

Gérard F., Ranger J., Ménétrier C., et Bonnaud P. (2003) Silicate weathering mechanisms determined using soil solutions held at high matric potential. *Chemical Geology* **202**, 443-460.

« Transferts hydriques : pédotransfert et écoulements préférentiels »

Gérard F., Tinsley M., et Mayer K. U. (2004) Preferential flow revealed by hydrologic modeling based on predicted hydraulic properties. *Soil Science Society of America Journal* **68**, 1526-1538 (+ Errata **70**, 305).

« Synthèse : prise en compte de la matière organique naturelle dans les modèles de spéciation et applications »

Dudal Y. et Gérard F. (2004) Accounting for natural organic matter in aqueous chemical equilibrium models: a review of the theories and applications. *Earth-Science Reviews* **66**, 199-216.

« Spéciation du carbone organique dissous »

Jaffrain J., Gérard F., Meyer M., et Ranger J. (2007) Assessing the quality of dissolved organic matter in forest soils using ultraviolet absorption spectrophotometry. *Soil Science Society of America Journal* **71**, 1851-1858.

« Modélisation du cycle biogéochimique du silicium »

Gérard F., Mayer K. U., Hodson M. J., et Ranger J. (2008) Modelling the biogeochemical cycle of silicon in soils: application to a temperate forest ecosystem. *Geochimica Cosmochimica Acta* **72**, 741-758.

REMERCIEMENTS

Mes premiers contacts avec la recherche sont arrivés précocement dans mon parcours professionnel, à supposer bien sûr qu'être étudiant est une profession. Ce fût à l'occasion de mon stage de DUT « Mesures Physiques », il y a déjà près de vingt ans, effectué au Laboratoire « *Microstructures et microélectronique* » (CNRS) d'Athis-Mons (91). L'objectif était de caractériser des hétérojonctions GaAs/GaAlAs. Il a vraiment fallut de l'initiative et de l'imagination pour mener à bien ce stage !

Dès lors, une question se posait : comment faire pour que la recherche soit mon métier ? Concilier amour et passion a été la solution, qui prie forme à Strasbourg, haut lieu des Géosciences et lieu de résidence d'une jeune fille qui allait devenir mon épouse des années plus tard. L'Alsace et ses alsaciens au curieux accent et dialecte fut un choc culturel pour le banlieusard que j'étais. Heureusement qu'il y avait la Géologie pour fédérer et les copains (Alain et Cathy en particulier) pour m'intégrer en « Alssssace ». Je me rappellerai toujours le baptême du feu que j'ai dû passer : l'ascension de nuit de la cathédrale de Strasbourg par ses échafaudages …

Ces années alsaciennes passèrent très vite, jalonnées par les diplômes, l'armée (à Mutzig, et c'est pas en Allemagne…) et puis me voilà en thèse. Sans doute la meilleure époque dans une carrière scientifique. Merci à mon directeur de thèse, Bertrand Fritz, de m'avoir laissé « carte blanche » dans la manière de mener cette thèse, et à Alain Clément de m'avoir soulagé du travail considérable, trop souvent méconnu, qu'est la programmation informatique (en Fortran qui plus est). Ce fût aussi l'occasion de mon premier congrès international, en 1993, à l'EUG de Strasbourg. Ce genre de manifestation aide pas mal aussi dans une carrière. Je voudrais donc remercier le collègue espagnol rencontré à cette occasion : Joseph Soler, pour son appuis « très appuyé » des années plus tard alors que j'étais, terminant la rédaction de mon mémoire, à la recherche d'un postdoc. J'ai donc eu la chance de réaliser ma formation postdoctorale au Lawrence Berkeley National Laboratory (LBNL). Ce fut l'occasion de ma rencontre avec Tianfu Xu, avec lequel j'ai partagé une trop courte année de recherche dans le « lab ». Tianfu m'a marqué par son sens aigu de l'amitié, et ses connaissances approfondies des méthodes de résolution numériques des systèmes d'équations non linéaires. On se reverra toujours avec plaisir. J'ai également pu y rencontrer des experts de la modélisation couplée (bio)géochimie-transferts, comme Carl Steefel, Peter Lichtner, Klaus Ulrich Mayer (dit Uli), et Karsten Pruess. Merci pour leurs encouragements à poursuivre dans cette difficile et austère thématique qu'est la modélisation « mécaniste » des processus géochimiques et de leur couplage avec les transferts de masse en milieu poreux.

Depuis cette période, Uli, actuellement « Associate Professeur » à l'Université de Colombie-Britannique (Vancouver, Canada), n'a cessé de m'accompagner en sa qualité de concepteur du modèle couplé biogéochimie-transferts MIN3P. J'ai sélectionné cet outil il y a déjà 7 ans, afin qu'il serve de modèle « plateforme » devant accueillir les développements nécessaires à la réalisation de mes recherches à l'INRA. A ce titre, je souhaite remercier tout particulièrement Jacques Ranger de m'avoir ouvert les portes de son unité nancéienne. Là aussi il m'a été laissé « carte blanche » sur les orientations de mes recherches, et surtout j'ai pu avoir accès aux nombreuses données des sites forestiers expérimentaux (une condition nécessaire mais pas suffisante pour publier). Le personnel technique du laboratoire doit être remercié pour les mesures réalisées, qui furent fastidieuses autant par leur nombre que par les longs et récurrents déplacements sur le terrain. J'aimerais également souligner l'aide de Jean-Pierre Boudot (LIMOS, CNRS, Nancy), en tant que modélisateur et analyste de la spéciation de l'aluminium, et pour m'avoir fait souvent crédit... Une mention spéciale également pour Martin Hodson, de l'Oxford-Brookes University (Angleterre), qui m'a aussi beaucoup aidé sur le cycle biologique du silicium dans les écosystèmes forestiers. Le

silicium ?! Vous savez, cet élément non indispensable pour les plantes mais dont certaines regorgent et dont les effets bénéfiques sont bien réels…

L'histoire ne s'arrête pas là. Elle a continué à partir de ma récente affectation à l'INRA de Montpellier. Merci donc aux départements EA et EFPA, et bien sûr au responsable de l'Unité d'accueil, Benoît Jaillard, de l'avoir acceptée. L'une des conditions, imposée par mon nouvel hôte, était la rédaction de ce manuscrit

Enfin, la rédaction de ce mémoire et les années de travail pour y arriver n'auraient certainement pas été possibles si j'eusse été célibataire. Une pensée forte à Mylène et à mes enfants, Lucas, Eliott et Julie.

Curriculum vitae

Frédéric GERARD

Né le 31 janvier 1966 à L'häy-les-Roses (94), France

Nationalité Française, marié (1996), 3 enfants

Anglais courant

Adresse professionnelle : UMR1222 INRA/SupAgro.M
« Biogéochimie du Sol et de la Rhizosphère »
34060 Montpellier
Tél. : 04 99 61 30 24 ; Fax : 04 99 61 30 88
Couriel : gerard@supagro.inra.fr

Membre « *Soil Science Society of America* » depuis 1998, de la « *Geochemical Society of America* » depuis 2005, de l' « *International Humic Substance Society* » depuis 2007.

ENCADREMENT

→ Deux postdocs étrangers (anglais et coréen)
→ Une thèse de l'Université Nancy I, soutenue oct. 06 « *Fonctionnement Organo-minéral des Sols Forestiers* ».
→ Sept M2 ou DEA (6 à l'UHP de Nancy, spécialité « *Sciences Agronomiques* » et « *Physique et Chimie de la Terre* », et 1 à Montpellier Master « *FENEC* »).

L'ensemble a donné lieu directement à 5 publications de rang A.

→ Deux M1 ou équivalent (1 IUP Nantes « *Mesures Physiques* » et 1 Maîtrise « *Physique et Chimie de la Terre* » Nancy).
→ Deux stagiaires de DUT (informatique, Montpellier).

Participation aux comités de 3 thèses, au jury d'une thèse, et au comité de pilotage d'un jeune chercheur de l'INRA. Rapporteur stage M2 Master FENEC (Montpellier).

ENSEIGNEMENT

- Deux semaines de formation en 1997 à l'utilisation d'un modèle géochimique (EQ3/6) auprès d'ingénieurs chimistes de la compagnie de Géothermie Salvadorienne. Intervention en tant que consultant international.
- De 1998 à 2006, en moyenne 3 heures de cours ou de TD sur la modélisation biogéochimique dans le cadre du module « *Ecosystèmes à bas intrants* » (J. Ranger) du DEA national de Science du Sol et du M2 l'ayant remplacé.
- Module « *Modélisation* » (L. Martinez) de la Maîtrise « *Sciences de la Terre et de l'Univers* », commune aux Universités de Nancy et de Strasbourg : 7 heures de cours et 30 heures de TP.

- Intervention de 3 heures en 2003 sur l'acidification des eaux auprès de techniciens ONF (formation continue CNFF « *La forêt et les modifications environnementales d'origine humaine : CO_2, pollution, climat* »).
- TP en hydrologie des sols (M. Jauzein) du M2 « *Géosciences et Génie Civil*» de Nancy (une dizaine d'heures), en 2005.
- Cours de 4 heures dans le cadre du module « *Cycles biogéochimiques* » (R. Poss) du Master « FENEC » de Montpellier.
- Intervention d'une semaine enn 2005 au sein d'une école chercheurs « *Understanding and Modelling of the Rhizosphere* » organisée par B. Novak (ETH Zurich) dans le cadre de l'action COST 631.
- Prise en charge en 2006 de deux formations permanentes INRA « *Modélisation des interactions sol-plante avec le modèle MIN3P* » (4 jours chacune).

EXPERTISES SCIENTIFIQUES

Expert pour 10 journaux scientifiques internationaux ; Analytica Chimica Acta, Chemical Geology, European Journal of Soil Science, Environmental Science and Technology, Forest Ecology and Management, Geochimica et Cosmochimica Acta, Geoderma,, Journal of Environmental Quality, Soil Science Society of America Journal, Vadose Zone Journal.

Expert pour projet ANR « Blanche » et la « Czech Science Foundation ».

RESPONSABILITE PROJETS

- Projet « *Jeunes équipes* », région Lorraine, en 1999-2000 (100 kF)
- Projet « *Fonds France Canada pour la Recherche* » 2002-2003 (6.5 k€)
- Programme d'Action Intégrée France-Autriche (PAI Amadeus) 2004-2005 (2.5 k€)
- Projet « *Emergent* », région Lorrain, en 2004-2006 (10 k€)
- Projet « *Innovant* », INRA département EFPA, 2007 (8 k€)

PARTICIPATION PROJETS

- ➔ Projet ECOFOR « *Biodiversité et Gestion forestière* » coord. J. Ranger (2000-2003).
- ➔ Deux programmes GESSOL, coord. J. Ranger (1999-2002) et G. Echevarria (2001-2003).
- ➔ Une programme GESSOL II, coord. G. Richard (2004-2007).
- ➔ Deux ACI « *Ecologie Quantitative* », coord. M.-P. Turpault (2001-2004) et J. Ranger (2003-2005).
- ➔ Une ACI PNSE, coord. P. Renault (2001-2003).
- ➔ Deux ACI ECCO « *Ecosphère Continentale : Processus et Modélisation* », coord. J. Gaillardet (2004-2005) et J.-D. Meunier (2005-2007).
- ➔ Un projet ANR « *Agriculture et Développement Durable* », coord. G. Richard (2005-2008).
- ➔ Un projet « *Innovant* » SupAgro Montpellier, coord. E. Le Cadre (2007-2008).

ORGANISATION DE SEMINAIRES

- En 1999, à Nancy, dans le cadre de la venue d'un chercheur Américain (Thomas DeLuca, Univ. Montana), sur le thème des effets de l'éradication des feux de forêt sur la dynamique de N dans les sols.

- En 2001, à Nancy, deux séminaires autours de la venue de M. Hodson (Oxford-Brookes Univ., Angleterre) et de F. Dassonville (INRA Avignon, CSE). Ces chercheurs sont respectivement des spécialistes des interactions entre Al et Si dans les plantes et des interactions activités microbiennes anaérobiques et géochimie.
- En 2005, co-organisation de deux séminaires à l'INRA de Nancy, avec des participants de différents laboratoires Français. L'un portait sur l'étude et la modélisation des transferts hydriques dans les sols. Le second portait sur la modélisation couplée biogéochimie-transferts dans les sols.

Titres et travaux

2006 1er novembre, mobilité vers l'UMR1222 INRA/SupAgroM. « *Biogéochimie du Sol et de la Rhizosphère* ».

2002 Nommé Chargé de Recherche 1ière classe.

1998 1er août, nommé Chargé de Recherche 2ième classe, UPR1138 « *Biogéochimie des Ecosystèmes Forestiers* », INRA, Nancy.

1997 Postdoc aux Etats-Unis. Lawrence Berkeley National Laboratory, Earth Science Division, Berkeley, Californie. L'objectif était de coupler le modèle hydrodynamique TOUGH2 au modèle géochimique EQ3/6 et de réaliser de premiers tests dans le cadre de l'étude d'un dépôt supergène de cuivre (Atacama, Chili).

1996 Thèse en Géochimie, Université Louis Pasteur, Strasbourg (co-direction B. Fritz et J.-L. Crovisier). Titre « *Modélisation géochimique thermodynamique et cinétique avec prise en compte des phénomènes de transport de masse en milieu poreux saturé* », 250pp.

1993 DEA Géosciences, mention bien. Université Louis Pasteur de Strasbourg.

1991 Maîtrise Sciences de la Terre, mention Géologie Fondamentale et Appliquée, mention bien. Université Louis Pasteur de Strasbourg.

1990 Licence Sciences de la Terre, mention Géologie Fondamentale et Appliquée, mention assez bien. Université Louis Pasteur de Strasbourg.

1989 DUT Mesures Physiques, option mesures et contrôles physico-chimiques. Université d'Orsay (Paris XI).

1987 Baccalauréat technologique, spécialité électrotechnique (série F3), Athis-Mons (91).

1982 CAP et BEP en électrotechnique et électricité d'équipements, Ecole Privée Technique et Professionnelle Citroën, Paris XV.

LISTE DES PUBLICATIONS

- Articles de Rang A -

Publiés

Wonisch H., **Gérard F.,** Dietzel M., Jaffrain J., Nestroy O., Boudot, J.-P. 2008. Occurrence of polymerized silicic acid and aluminum species in two forest soil solutions with different acidity. *Geoderma*. **Sous presse**

Gérard F., Mayer K. U., Hodson M. J., et Ranger J. 2008. Modelling the biogeochemical cycle of silicon in soils: application to a temperate forest ecosystem. *Geochim. Cosmochim. Acta*. **doi:10.1016/j.gca.2007.11.010**.

Jaffrain J., **Gérard F.**, Meyer M., and Ranger J. 2007. Assessing the quality of dissolved organic matter in forest soils using ultraviolet absorption spectrophotometry. *Soil Sci. Soc. Am. J.* 71:1851-1858.

Sangster A. G., Ling L., **Gérard F.**, and Hodson M. J. 2007. X-ray microanalysis of needles from Douglas fir growing in environments of contrasting acidity. *Water, Air and Soil Pollution: Focus* 7:143-149.

Nowack B., Mayer K. U., Oswald S. E., Van-Beinum W., Appelo C. A. J., Jacques D., Seuntjens P., **Gérard F.**, Jaillard B., Schnepf A., and Roose T. 2006. Verification and intercomparison of reactive transport codes to describe root-uptake. *Plant & Soil* 285:305-321.

Dudal, Y., et **F. Gérard**. 2004. Accounting for natural organic matter in aqueous chemical equilibrium models: a review of the theories and applications. *Earth-Sci. Rev.* 66:199-216.

Gérard, F., M. Tinsley, et K.U. Mayer. 2004. Preferential flow revealed by hydrologic modeling based on predicted hydraulic properties. *Soil Sci. Soc. Am. J.* 68:1526-1538 (errata en 2006, 70, 305).

Gérard, F., J. Ranger, C. Ménétrier, et P. Bonnaud. 2003. Silicate weathering mechanisms determined using soil solutions held at high matric potential. *Chem. Geol.* 202:443-460.

Ranger, J., **F. Gérard**, M. Lindemann, D. Gelhaye, et L. Gelhaye. 2003. Dynamics of litterfall in a chronosequence of Douglas-fir (*Pseudotsuga menziesii* Franco) stands in the Beaujolais mounts (France). *Ann. For. Sci.* 60:475-488.

Ryder, M., **F. Gérard**, D.E. Evans, et M.J. Hodson. 2003. The use of root growth and modelling data to investigate amelioration of aluminium toxicity by silicon in Picea abies seedlings. *J. Inorg. Biochem.* 97:52-58.

Gérard, F., M. François, et J. Ranger. 2002. Processes controlling silica concentration in leaching and capillary soil solutions of an acidic brown forest soil (Rhône, France). *Geoderma* 107:197-226.

Gérard, F., et J. Ranger. 2002. Silicate weathering mechanisms in a forest soil, p. 383-415, In I. Océanographique, ed. The Biogeochemical silicium cycle: elemental to global scale, Vol. 28. Institut Océanographique de Paris, Paris.

Brulé, C., P. Frey-Klett, J.-C. Pierrat, S. Courrier, **F. Gérard**, M.-C. Lemoine, J.-L. Rousselet, G. Sommer, et J. Garbaye. 2001. The survival in the soil of the ectomycorhizal fungus Laccaria bicolor S238N and the effects of a mycorrhiza helper Pseudomonas fluorescens. *Soil Biol. Biochem*. 33:1683-1694.

Gérard, F., J.-P. Boudot, et J. Ranger. 2001. Consideration on the occurence of the Al13 polycation in natural soil solutions and surface waters. *Appl. Geochem*. 16:513-529.

Gérard, F., A. Clément, et B. Fritz. 1998. Numerical validation of an Eulerian hydrochemical code using a 1-D multisolute mass transport system involving heterogeneous kinetically-controlled reactions. *J. Contam. Hydrol.* 30:201-216.

Gérard, F., B. Fritz, A. Clément, et J.-L. Crovisier. 1998. General implications of aluminium speciation-dependent kinetic dissolution rate law in water-rock modelling. *Chem. Geol.* 151:247-258.

Gérard, F., A. Clément, B. Fritz, et J.-L. Crovisier. 1996. Introduction of transport phenomena into the thermo-kinetic code KINDIS: The code KIRMAT. *C.R. Acad. Sci. Paris* 322IIa:377-384.

Soumis

Le Cadre E., **Gérard F.**, Génermont S., Morvan T., Recous S. 2008. Which formalism to model the pH and temperature dependence of the microbiological processes in soils? Emphasis on nitrification. *Environm. Model. Assess.*

Devau N., **Gérard F.**, Le Cadre E., Roger L., Ashad M., Hinsinger P., Jaillard B., 2008. Using a mechanistic adsorption model to understand the influence of soil pH on phosphorus availability: application to a Chromic Cambisol. *Ecological Modelling*.

- Congrès -

Le Cadre E., **Gérard F.**, Devau N, Clairotte M., Li. H., Aznar JL., Arshad M., Jaillard B., Hinsinger P. (2007) Soil pH modifications in the rhizosphere : a real impact on P availability in soil ? Rhizosphere II, Montpellier, 26-31 août (**poster**).

Devau N., Le Cadre E., **Gérard F.**, Roger L., Arshad M., Aznar JL., Jaillard B., Hinsinger P. (2007) Modelling of an environmental indicator of phosphorus availability according to pH variations: application to a cambisol. Rhizosphere II, Montpellier, 26-31 août (**poster**).

Nowack, B., Mayer, K. U., Oswald S. E., Van-Beinum W., Appelo C. A. J., Jacques D., Seuntjens P., **Gérard F.**, Jaillard B., Schnepf A., Roose T. (2006) Verification and intercomparison of reactive transport codes to describe root-uptake. EGU General Assembly 2006, Vienna, Austria, 2.-7. April 2006 (**poster**).

Gérard F., Mayer K. U., Hodson M. J., and Meunier J.-D. (2006) Modelling the biogeochemical cycle of silicon in soils using the reactive transport code MIN3P. *Eos Trans. AGU* **87**(52), H11F-1299 (**poster**).

Gérard F., Jaffrain J., Boudot J.-P. et Ranger J., 2005. Influence of SOM on aluminium mobility in a forested brown acidic soil : a view from soil solutions held at different matrix potential. 15th Goldschmidt Conf., 20-25th May 2005, Moscow, Idaho (USA) **(communication)**.

Subramaniyam P., **Gérard F**., Evans D.E., et M.J. Hodson. 2005. Mineral analysis of needles from Douglas fir and Norway spruce growing in Breuil Forest, Morvan, France. Acid Rain Conf., June 2005, Prague **(poster)**.

Sangster A.G., Ling L., **Gérard F.**, et Hodson M.J., 2005. X-ray microanalysis of needles from Douglas fir growing in environments of contrasting acidity. Acid Rain 2005, 7th Conf. On Acid desposition, 12-17 June 2005, Prague **(communication)**.

Nowack B., Jacques D., Oswald S., Roose T. Schnepf A., Seuntjens P., Van-Beinum W., **Gérard F.**, Mayer K.U., Kirk G., Nietfeld H., et Jaillard B., 2005. Validation of coupled speciation-transport models to describe root-uptake. Acid Rain 2005, 7th Conf. On Acid desposition, 12-17 June 2005, Prague **(poster)**.

Gérard F., Jaffrain J., Boudot J.-P., Clément C. et Ranger J., 2005. Mechanisms controlling the mobility of aluminium in a brown acidic soil : influence of the planted tree species and matric potential. Sixth Keele Meeting on Aluminium:"Aluminium : Lithosphere to Biosphere (and back)", 26th Feb.- 2nd March 2005, Buçaco (Portugal) **(poster + presentation)**.

Wonisch H., Dietzel M., Gérard F., Jaffrain J., Köhler S. J., Nestroy O. et Boudot, J.-P., 2005. Aluminium and Silica Speciation in Acidic Soil Solutions (France and Austria). Sixth Keele Meeting on Aluminium:"Aluminium : Lithosphere to Biosphere (and back)", 26th Feb.- 2nd March 2005, Buçaco (Portugal) **(poster)**.

Nowack B., Jacques D., Mayer K.U., Oswald S., Roose T., Schnepf A., Seuntjens P., Van-Beinum W., **Gérard F.**, Kirk G., Nietfeld H., et Jaillard B., 2004. Validation of coupled speciation-

transport models to describe root-uptake. Rhizosphere, 12-17 Sept. 2004, Munich (Germany) **(poster)**.

Jaffrain J., **Gérard F.**, Ranger J., et Meyer M., 2004. Using UV spectrometry to assess the effect of the tree species on the DOC properties. Eurosoil, 4-12 Sept. 2004, Freiburg (Germany) **(poster)**.

Wonisch H., **Gérard F.**, Dietzel M., Jaffrain J., Köhler S. J., Nestroy O., Boudot J.-P., et Möller A. 2004. Occurrence and stability of polymeric silica in acidic soil solutions. Eurosoil, 4-12 Sept. 2004, Freiburg (Germany) **(poster).**

Gérard F., Tinsley M. and Mayer K.U., 2003. Simulating water transfers at a forest field site by using pedo-transfer functions. AGU fall meeting, 8-12 Dec. 2003, San Francisco (USA) **(poster)**.

Dietzel M., Gérard F., Jaffrain J., Nestroy O., Weber H., Möller A. , et Hillebrecht J., 2003. New aspects on the mechanisms of silicate weathering - impact of polysilicic acids and hydroxyaluminosilicate colloids. MINPET 2003, 15-21 Sept. 2003, Neukirchen am Großvenediger (Austria) **(communication)**.

Tinsley M., Mayer K.U., et **Gérard F.**, 2003. Comparison of pedo-transfer functions in a field situation. EGS-AGU-EUG Joint Assembly, 6-11 Apr. 2003, Nice (France) **(poster)**.

Gérard F., Jaffrain J., Boudot J.-P., et Ranger J., 2003. Complexation de l'aluminium par la matière organique dissoute dans les solutions gravitaires de sols forestiers : utilisation de la modélisation pour l'étude des propriétés des substances humiques. 5ème Colloque sur la matière organique naturelle, Groupe Français de l'IHSS, Université Blaise Pascal, 26-28 Mar. 2003, Clermont-Ferrand (France) **(poster)**.

Jaffrain J., **Gérard F.,** et Ranger J, 2003. Effets des essences forestières sur le fonctionnement organo-minéral d'un sol forestier : observation et modélisation. Etat de l'art, protocole, objectifs et perspectives. 5èmes Journées d'Ecologie Fonctionnelle, Centre National de Formation Forestière (CNFF-ONF), 12-14 Mar. 2003, Nancy (France) **(poster)**.

Möller A., Dietzel M., **Gérard F.**, Weber H., Bäumler H.P., Heinrichs H., et Hillebrecht J., 2003. Interaction of dissolved aluminium with polysilicic acid and the formation of hydroxyaluminosilicate complexes and colloids in acidic solutions. Fifth Keele Meeting on Aluminium :"Aluminium in life: from acid rain to Alzheimer's disease", 22-25 Feb. 2003. Keele (England) **(communication)**.

Ryder M., **Gérard F.**, Evans D.E., et Hodson M.J., 2003. The use of root growth and modelling data to investigate amelioration of aluminium toxicity by silicon in picea abies seedlings. Fifth Keele Meeting on Aluminium:"Aluminium in life: from acid rain to Alzheimer's disease", 22-25 Feb. 2003, Keele (England) **(poster; 1er prix)**.

Gérard F., 2002. Solutions capillaires et étude des mécanismes actuels et in situ contrôlant la dissolution des silicates dans un sol brun acide. Journées Nationales d'Etude du Sol, 22-24 Oct. 2002, Orléans (France) **(poster)**.

Gérard F., 2002. Silicate weathering in forest soils: capillary solutions and the study the mechanisms controlling the dissolution rate of silicates. Séminaire de l'Institut Océanographique de Paris "The biogeochemical Si cycle Elemental to global scales", 22 Oct. 2002, Paris (France) **(communication)**.

Ryder M., **Gérard F.**, Evans D.E., et Hodson M.J., 2002. Aluminium toxicity and silicon amelioration for hydroponically grown Picea Abies seedlings: a comparison of root growth and modelling data. 13th congress of the federation of European societies of plant physiology, 1-6 Sept. 2002, Heraklion (Greece) **(poster)**.

Gérard F. et Ranger J., 2001. Use of extracted soil solutions to study the reaction mechanism Controlling in-situ and present-day silicate weathering rate. 11th Goldschmidt Conf., 20-25 May 2001, Hot Springs, Virginia (USA) **(communication)**.

Gérard F. and Ranger J., 2000. Asserting the toxicity risk caused by the Al_{13} polycation at mildly acidic to near-neutral pH in soil solutions and surface waters. *Internat. Symp. "Managing Forest Soils for Sustainable Productivity", 18-22 Sept. 2000, Vila Real (Portugal)* **(speech).**

Ménétrier C., **Gérard F.**, Ranger J., and François M., 2000. Influences comparées de la coupe rase d'un peuplement de Douglas sur le flux d'altération. *6èmes Journées Nationales de l'Etude des Sols: "Les enjeux actuels de l'anthropisation des sols", 25-28 Apr. 2000, Nancy (France).*

François M., Ranger J., **Gérard F.**, and Ménétrier C., 2000. Effets comparés de la coupe rase d'un peuplement de Douglas sur la chimie des solutions du sol. *6èmes Journées Nationales de l'Etude des Sols: "Les enjeux actuels de l'anthropisation des sols", 25-28 Apr. 2000, Nancy (France).*

Gérard F., Genon J.G. and Ranger J., 1999. Long-term thermodynamic and kinetic study of mineral-soil solutions interactions in an acid brown soil. *2nd Karlsruher Geochemical Workshop "Mineral/Water Interactions Close to Equilibrium", 25-26 Mar. 1999, Karlsruhe (Germany).*

Gérard F., Genon J.G. and Ranger J., 1999. Long-term thermodynamic and kinetic study of mineral-soil solutions interactions in an acid brown soil. *10th European Union of Geosciences (EUG-X), 28 Mar. -1 Apr. 1999, Strasbourg (France).*

Gérard F., Brimhall G., Pruess K., and Xu T., 1998. Influences of thermodynamic and kinetic constraints in supergene copper enrichment modelling. *European Research Conference "Geochemistry of Crustal Fluids", Aghia Pelaghia (Greece).*

Xu T., Pruess K., **Gérard F.**, and Brimhall G., 1997. Modeling non-isothermal multiphase multi-species reactive chemical transport in porous and fractured porous media. *AGU fall meeting, San Francisco (USA)*.

Gérard F., Clément A. and Fritz B., 1997. The model KIRMAT: formulation, numerical methods and applications. *A Workshop on Subsurface Reactive Transport Modeling*, *Pacific Northwest National Laboratory, 29 Oct.-1 Nov., Richland, Washington (USA).*

Gérard F., 1996. Some general implications of aluminum speciation-dependent kinetic dissolution rate law in water-rock interaction modeling. *European Research Conference «Geochemistry of Crustal Fluids», Seefeld (Austria).*

Gérard F., Fritz B., Oelkers E. H., and Clément A., 1996. Modélisation de l'altération hydrothermale d'un grès: effets de la dispersion hydrodynamique et des lois cinétiques faisant intervenir l'effet inhibiteur de l'aluminium. *16ème Réunion des Sciences de la Terre « Dynamique et Economie de la Terre », Orléans (France).*

Gérard F., Clément A., Crovisier J.-L., and Fritz B., 1995. The 1D reactive computer code KIRMAT. Numerical algorithm validation and possibilities of application to nuclear waste storage. *8th European Union of Geosciences (EUG-VIII), Strasbourg (France).*

Gérard F., Clément A., Fritz B., and Crovisier J.-L., 1995. Modeling mineral solution mass transfer with transport phenomena. *Congrès Minéralogie-95, Strasbourg (France).*

Abdelouas A., Crovisier J.-L., Lutze W., and **Gérard F.**, 1995. Rhyolitic glass as natural analogue for R7T7 borosilicate glass altered in salt. *Congrès Minéralogie-95, Strasbourg (France).*

Advocat T., Crovisier J.-L., Clément A., **Gérard F.**, and Vernaz E., 1995. Modeling of solution renewal with the KINDIS code: Example of R7T7 glass dissolution at 90°C. In: Scientific basis for nuclear management. *Mat. Res. Soc. Symp., Japan*.

Gérard F., Martinez L. and Fennouh A., 1994. Sandstones texture characterization with quantitative image analysis. *I Congreso Internacional de Materiales, 16th Encuentro de Investigacion Metalurgica Mem., Saltillo (Mexique)*

Fennouh A. , Martinez L., Fritz B., Belin-Geindre S., and **Gérard F.**, 1994. Characterization of reservoir pore-complex geometry using image analysis procedure, Cambrian of Hassi Messaoud oild field, Algeria. *I Congreso Internacional de Materiales, 16th Encuentro de Investigacion Metalurgica Mem., Saltillo (Mexique).*

SYNTHESE DES TRAVAUX

1. Introduction

Depuis ma prise de fonction à l'INRA Nancy (équipe Cycles biogéochimiques, devenue UPR « Biogéochimie des Sols Forestiers »), je me suis attaché à développer le programme de recherche intitulé « Mécanismes d'acquisition de la composition chimique des solutions du sol et modélisation des cycles biogéochimiques ». Ce travail a pris place dans le cadre de sites expérimentaux en forêt plantée mis en place et suivis par l'Unité, et tous situés sur des sols acides (Alocrisols).Depuis ma mobilité montpelliéraine en novembre 2006, j'ai commencé des recherches sur l'identification et la modélisation des mécanismes contrôlant la disponibilité du phosphore pour les plantes. Ce domaine, celui du cycle biogéochimique du P, constituera l'essentiel de mes perspectives de recherche et d'encadrement. A Nancy, les principaux objectifs de mes travaux étaient:

(i) d'identifier les processus et les mécanismes qui contrôlent la dynamique des solutés dans les sols ;

(ii) de développer puis d'appliquer un modèle numérique (i.e. un modèle informatique et mathématiques) capable de simuler sur des bases mécanistes la composition chimique des solutions de sol.

Face à une thématique si ouverte, se situant qui plus est à l'interface de plusieurs disciplines du vivant et du minéral, j'ai d'abord décidé de cibler les solutés à étudier selon leur importance pour le fonctionnement et la fertilité des sols étudiés. Mon choix s'est porté sur l'aluminium, la silice et le carbone organique dissous (COD). Les méthodes mises en œuvres ont été :

(a) l'utilisation de données physiques et chimiques provenant de sites expérimentaux. Plus concrètement, il s'agissait de mesures *in situ* (e.g. humidité par sonde TDR) et/ou des mesures réalisées au laboratoire sur des échantillons du sol. Les mesures classiquement réalisées par l'Unité se sont parfois avérées insuffisantes pour l'étude des mécanismes, et cela m'a amené à développer et utiliser de nouvelles méthodes. Mes activités ne se sont donc pas confinées à la modélisation, mais ont également touché la paramétrisation et le suivi du fonctionnement du sol ;

(b) le développement et les applications d'un modèle de transfert-réactif jugé performant, d'un point de vue numérique et au niveau du nombre et de la manière dont les processus de transfert, les processus biologiques et processus géochimiques y étaient intégrés. Le modèle MIN3P (Mayer, 1999 ; Mayer et al., 2002) a été sélectionné au cours de la première phase du projet (1998-2000), afin de servir de modèle « plateforme » accueillant les développements nécessaires aux objectifs de modélisation couplée.

Durant les premières années, je me suis attaché à l'étude du site expérimental de Vauxrenard (Rhône, sol brun acide, chronoséquence de plantations de Douglas (*Pseudotsuga menziesii* Franco)). Ce site était fortement équipé et a été suivi de fin 1992 et fin décembre 1999. En conséquence, une imposante base de données avait été constituée et permettait la réalisation de premières études. Mes activités de recherche se sont ensuite petit à petit déplacées vers le nouveau site expérimental de Breuil (Morvan), mis en place afin d'étudier les effets de l'essence sylvicole (7 essences) sur le fonctionnement de l'écosystème et du sol en particulier. Les effets de deux essences plantées, le hêtre (*Fagus sylvatica L.*) et le Douglas (*Pseudotsuga menziesii* Franco), ont été plus spécifiquement étudiés dans le cadre de la thèse de J. Jaffrain (2007).

J'ai employé différents outils, statistiques, informatiques (modèles) et analytiques, au cours de ces recherches. La figure (1) illustre succinctement la méthode qui a été suivie.

Brièvement, des modélisations non couplées des processus géochimiques (thermodynamiques et cinétiques) et des transferts hydriques ont permis une étude fine et rapide des processus. L'étude des données à l'aide des statistiques a également permis de mettre en évidence la nature des processus dans les sols étudiés, et ce souvent indépendamment de la modélisation. Ces travaux en amont ont abouti à l'établissement d'un modèle conceptuel de fonctionnement du site, servant de guide aux développements et aux applications du modèle couplé MIN3P. Outre le calcul des flux, l'utilisation de MIN3P a également servi à vérifier la pertinence du modèle conceptuel à justifier des retours aux développements numériques (i.e. allers retours applications-développements).

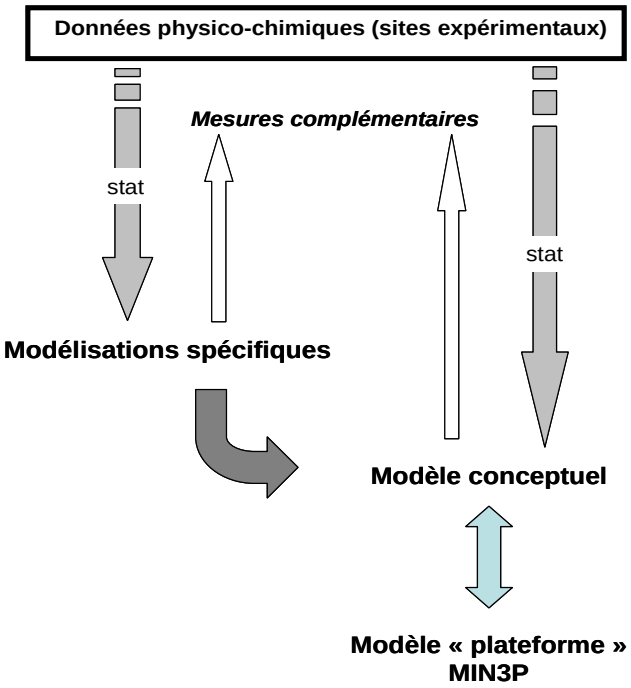

Figure 1. Méthode suivie pour étudier les processus et mécanismes contrôlant la composition chimique des solutions du sol, développer et appliquer le modèle couplé biogéochimie-transfert MIN3P.

Ma formation fait que j'ai abordé ce programme sous l'angle de la géochimie. Les mécanismes géochimiques sont relativement bien connus à l'échelle du laboratoire. Il fallait donc en premier lieu tenter d'établir leur validité sur le terrain, de les hiérarchiser, puis de paramétrer les équations correspondantes. De façon très schématique, la méthode a consisté à retrouver certaines tendances « mécanistes » du laboratoire (issues de la littérature) parmi des données issues des sites expérimentaux. Une bonne correspondance signifierait que les mécanismes étudiés au laboratoire (et les paramètres intrinsèques) peuvent être utilisés dans une modélisation mécaniste à l'échelle du terrain. Des variables mesurées (concentrations totales, pH ...) et des variables issues de la modélisation (par exemple, l'indice de saturation d'un minéral, l'activité chimique des ions, la réactivité du COD) ont été considérées.

Mon projet de recherche nancéien était également basé sur un modèle conceptuel général de fonctionnement des sols élaboré au sein de l'Unité (e.g. Marques et al., 1996). Il décrit l'existence de différents types de solution de sol selon le potentiel hydrique (ψ) du sol (Figure 2A). Il existe une relation entre le potentiel et la taille maximale des pores (assimilés

à des capillaires cylindriques : loi de Jurin), et donc aussi avec le temps de résidence de l'eau dans le sol. Différents processus, ou bien encore des processus identiques mais plus ou moins exacerbés, peuvent contrôler la composition chimique de l'eau selon son temps de résidence dans le sol. La séparation des différents types d'eau du sol est opérationnelle. Elle correspond aux différents dispositifs utilisés pour collecter les solutions de sol : plaques lysimétriques, lysimètres microporeux sous tension, centrifugation. Ce modèle conceptuel a été conforté plusieurs fois par les résultats de mes recherches. La figure 2B montre un agrandissement de l'interface entre l'eau et le solide, avec une description physico-chimique de ce que revêt la notion de « complexe d'échange » usitée en science du sol. Diverses extractions permettent d'accéder peu ou proue aux éléments adsorbés aux solides du sol, mais aussi à certains minéraux néoformés (souvent mal cristallisés) et à la matière organique du sol (MOS). La minéralogie est nécessaire à l'identification des phases cristallisées, comme les minéraux primaires et les argiles, à condition qu'elles soient suffisamment abondantes pour être détectées par diffraction des rayons X.

Une synthèse des recherches que j'ai réalisé est présentée dans ce qui suit. Mes travaux ont été consacrées à l'étude et à la modélisation:

- ⇨ de la spéciation de Al, Si et du COD;
- ⇨ des processus et mécanismes contrôlant la mobilité de Al, Si et du COD ;
- ⇨ des transferts de l'eau dans un sol forestier ;
- ⇨ du cycle biogéochimique de Si.

A noter que les deux premiers items sont interdépendants, puisque la connaissance de la spéciation aqueuse de Al, Si et du COD est essentielle à l'étude des processus et des mécanismes contrôlant ces solutés.

Enfin, les principales publications sont données en annexe, et indiquées en caractère gras dans le texte qui suit. Ces documents suivent également l'exposé de mon projet de recherche et de formation.

2. Spéciation de Al, Si et du COD

Les formes chimiques de l'aluminium sont nombreuses. Dans des conditions acides, l'espèce aqueuse la plus connue, mais pas nécessairement la plus abondante, est l'ion Al^{3+}. La silice possède une spéciation plus simple, dominée par l'acide orthosilicique ($H_4SiO_4°$).

Il existe des incertitudes au sujet de l'abondance des espèces combinant Si et Al dans des conditions acides à moyennement acides, et sur l'occurrence (et l'abondance) de polymères (silice polymérique) pouvant être libérés en solution lors de la dissolution des silicates (e.g. Dietzel, 2000).

Quand au COD, la diversité des molécules le composant est reconnue, ainsi que leur interactions avec les métaux, essentiellement des cations du fait de l'abondance des groupes fonctionnels acides dans le COD.

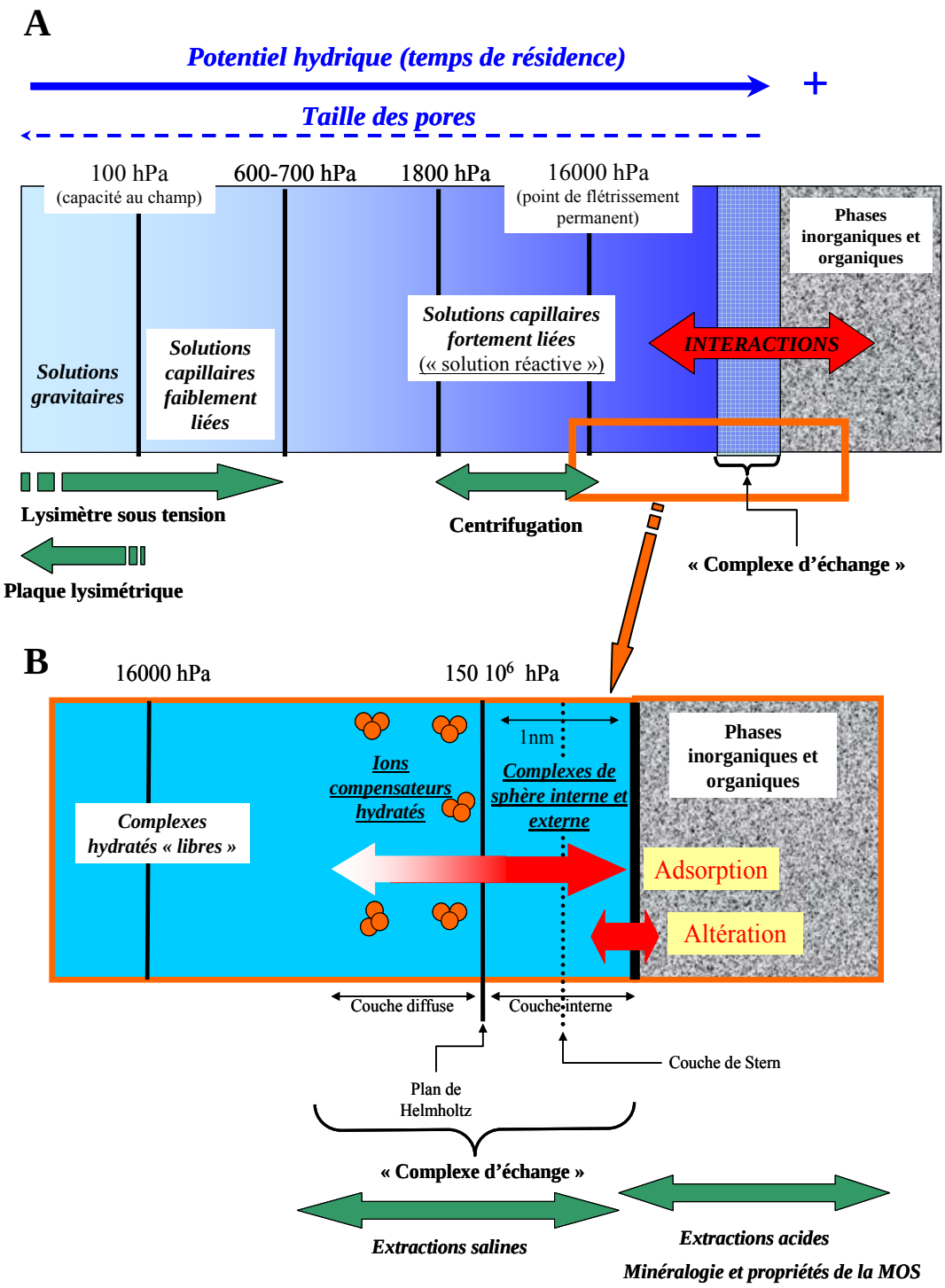

Figure 2. A) Schéma conceptuel représentant les différents types d'eau du sol selon le potentiel hydrique (ψ), et leur relation vis-à-vis des interactions se produisant avec les solides (minéraux et matière organique du sol). Les méthodes disponibles afin d'accéder à ces différents compartiments sont également indiquées. **B)** Agrandissement de l'interface solution-solide. Le complexe d'échange est représenté par des ions adsorbés plus ou moins fortement aux solides (adsorption spécifique et non spécifique). Les méthodes utilisées afin d'accéder à ces compartiments sont également indiquées.

2.1. Al et Si polymérique

Mes premiers travaux sur la spéciation aqueuse de Al et Si ont porté sur l'occurrence d'une espèce polymérique de Al, l'Al_{13} ($Al_{13}(O_4)(OH)_{24}^{7+}$), dans les solutions naturelles (sol et eaux de surface). L'influence de cette espèce sur la toxicité aluminique est majeure (e.g. Boudot et al., 1994), mais sa présence dans le milieu naturel pouvait être questionnée. En effet, les premiers calculs effectués dans la littérature ignoraient la présence de nombreux ligands susceptibles de complexer Al, et de ce fait capables de déstabiliser Al_{13} provoquant ainsi sa disparition des solutions. Dans le cadre de cette étude, j'ai pu montrer que la concentration de l'Al_{13} est négligeable dans les eaux naturelles **(Gérard et al., 2001)**.

Depuis lors, tous les calculs de spéciation que j'ai réalisé dans des solutions de différents sites ont confirmé voire même exacerbé la tendance (Figure 3). Cette figure illustre également le fait que l'espèce Al^{3+} n'est pas nécessairement l'espèce la plus abondante en sol acide. Dans le site autrichien, le plus acide, les espèces Al-sulfate et Al-fluor sont au moins d'importance équivalente.

Les premiers calculs de spéciation de Al ont également été l'occasion de mettre en place une base de données thermodynamiques intégrant les avancées les plus récentes dans le domaine de la géochimie. En particulier, le formalisme de Helgeson-Kirkham-Flowers (HKF) de Shock et Helgeson (1988) a été utilisé, sur la base des paramètres publiés pour les espèces hydroxylées de Al, pour Al^{3+}, et pour un complexe Al-Si monomérique (Shock et al., 1997; Salvi et al., 1998). Ce formalisme permet de calculer des valeurs cohérentes des constantes thermodynamiques d'équilibre à partir du logiciel Supcrt92 (Johnson et al., 1992). Depuis, j'ai amélioré la base de données grâce à l'avancée des travaux dans le domaine, en particulier l'article de synthèse de Tagirov et Schott (2001) et des travaux sur les complexes entre Al^{3+} et les sulfates (Xiao et al., 2002). La version la plus récente de la base de données thermodynamiques a été utilisée dans la thèse de J. Jaffrain, et dans le cadre du PAI entre la France et l'Autriche (Amadeus) que j'ai coordonné (Wonisch et al., 2007).

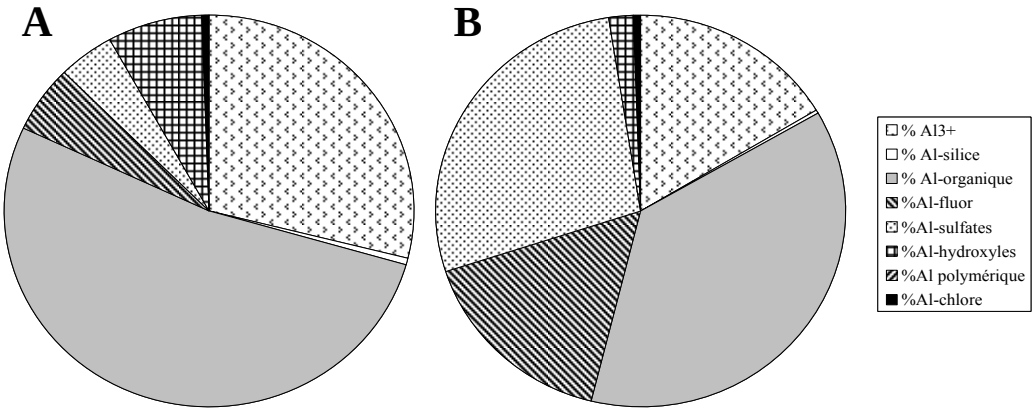

Figure 3. Spéciation de l'aluminium dans des solutions capillaires fortement liées (Wonish et al., 2007). Calculs réalisé à l'aide du modèle WHAM-VI (Tipping, 1998). A) Solutions du site de Breuil. B) Solutions du site de Bruck an den Mur.

Le travail réalisé par Wonish et al. (2008) portait sur l'occurrence Si polymérique dans les solutions de deux sols (Dystric Cambisols) d'acidité contrastée. L'un des sols est moyennement acide (site de Breuil, Nièvre, France) et l'autre est très acide (site de Bruck an dem Mur, Styrie, Autriche). La présence de Si polymérique dans les solutions de sols acides semblait possible du fait de premiers travaux dans le domaine (Xu and Harsh, 1993), et la

dissolution des silicates pourrait en être la source (Dietzel, 2000). Cependant, la question de l'abondance de Si polymérique dans ce milieu restait posée. Dans cette étude la silice polymérique a été dosée à partir de mesures par spectrophotométrie d'absorbance UV, qui constituait la méthode maîtrisée au sein du laboratoire autrichien co-participant au projet. Les résultats montrent une occurrence sporadique de Si polymérique dans les solutions de sol collectées dans les deux sites. Sa concentration peut atteindre jusqu'à 23% (pondéral) de l'élément total dissous. Les solutions collectées dans l'horizon de surface contiennent plus de Si polymérique. Cette dernière observation est conforme vis-à-vis de plus la forte acidité et des concentrations plus élevées d'Al mesurées dans les solutions de surface. En effet, ces conditions devraient impliquer une dissolution plus intense des silicates (source) et une plus grande stabilité de Si polymérique (effets stabilisateurs de Al).

2.2. Associations organométallique et substances humiques

Les premiers calculs de spéciation de Al ont été réalisés en collaboration avec J.-P. Boudot (LIMOS, CNRS Nancy). Ce chercheur utilisait un formalisme empirique pour la complexation de Al par le COD. Ce formalisme, développé par Schecher et Driscoll (1993) et Driscoll et al. (1994), repose sur la considération d'un acide organique équivalent, possédant trois protons et les constantes d'acidité associées. Les constantes de complexation entre les ligands équivalents et Al^{3+} sont également disponibles. Les valeurs prises par ces variables ont été optimisées au regard de mesures (titration acido-basique et spéciation de Al) réalisées dans des échantillons d'eaux de surface.

Les intérêts de ce formalisme empiriques sont nombreux. Il s'agit d'une approche simple des interactions entre Al et le COD, qui peut être aisément introduite dans les bases de données thermodynamiques des modèles géochimiques. Enfin, la concentration en COD est la seule variable pouvant être mesurée pour utiliser ce formalisme. Quand aux limites, elles n'auront certainement échappé à personne, en particulier le fait que l'on suppose que le COD possède les mêmes propriétés acide/base et la même réactivité vis-à-vis de Al si l'on utilise les valeurs publiées par Schecher et Driscoll (1993) et Driscoll et al. (1994). La détermination de valeurs propres aux situations étudiées est chose difficile du fait du nombre important de paramètres à ajuster, qui se monte à cinq. Il faut ajouter que l'étude de la spéciation du COD et des processus/mécanismes susceptibles de la contrôler ne peut pas être conduite en adoptant une approche par ligand équivalent. Ce formalisme a néanmoins obtenu un certain succès au cours de mes premiers travaux et de ceux de J.-P. Boudot. En particulier, les calculs de la spéciation de Al réalisée selon cette méthode ont donné des résultats cohérents en terme d'équilibre des solutions vis-à-vis des minéraux du sol. Cet aspect de mes travaux, touchant les processus et les mécanismes contrôlant notamment la mobilité de Al, sera présenté plus en détail dans la partie suivante.

Indépendamment de ces succès relatifs, il m'a semblé important d'utiliser progressivement de modèles plus mécanistes disponibles dans la littérature. Etant donné le contexte de mes travaux (sols forestiers, échelle de la parcelle), je me suis orienté sur la prise en compte en modélisation géochimique des effets des substances humiques (SH) sur la spéciation des métaux. Il est reconnu dans la littérature que les SH sont des composés ubiquistes dans les solutions de sol et les eaux de surface. Cette fraction du COD, appelée également fraction hydrophobe, présente une forte affinité pour la complexation des cations, en particulier d'ions Al^{3+}. Ces travaux ont commencé en 2002 par l'encadrement d'un stagiaire en M1 (F. Huybretchs, Maitrîse « Physique et Chimie de la Terre »). L'objectif du stage était d'utiliser un modèle reconnu dans le domaine; le modèle WHAM-VI (Tipping, 1998) afin de calculer la spéciation de Al dans les solutions de sol du site de Vauxrenard, et d'en préciser les contraintes et limites. Ensuite, un article de synthèse réalisé avec un jeune chercheur (à l'époque) de l'Unité CSE de l'INRA d'Avignon, Y. Dudal **(Dudal and**

Gérard, 2004), a permis de faire une synthèse des applications du modèle WHAM-VI au milieu naturel, d'en discuter les limites, et de pointer l'existence d'un modèle équivalent : NICA-Donnan (Kinniburgh et al., 1999).

En bref, il ressort notamment de ce travail de synthèse bibliographique que les modèles WHAM-VI et NICA-Donnan utilisent des bases de données contenant des valeurs génériques des propriétés des SH, dont la spéciation est scindée entre acides fulviques (AF) et en acides humiques (AH). En appliquant ces modèles au milieu naturel, il est généralement considéré que les SH sont entièrement composées d'AF quand l'étude concerne le COD et d'AH quand l'étude porte sur la MOS. De plus, la concentration en SH est rarement connue par mesures, dans les solutions de sol en particulier à cause du faible volume disponible comparé à la lourdeur des mesures. Dans ces conditions, les utilisateurs de ces modèles mécanistes de simulation des interactions entre la MON et les métaux supposent, arbitrairement que 50% du COD est composé de SH et que le reste est « inerte », ou du moins sans effet significatif sur la complexation des métaux.

Pour une application un minimum rigoureuse, il faut disposer de mesures de spéciation d'au moins un métal. Ainsi, il est possible d'en estimer la concentration des SH par calibration. Cela a pu être démontré dans le site de Vauxrenard, à l'aide de mesures de la spéciation de Al et en calibrant la concentration des SH jusqu'à obtenir une bonne correspondance avec le modèle (Figure 4). Un intérêt accru pour cette méthode peut être trouvé en disposant de mesures de la spéciation de plusieurs métaux. La précision de constantes de complexation métaux-SH (constantes dites intrinsèques) peut alors être testée et les valeurs ajustées si nécessaire. Bien que la nature de ces constantes soit intrinsèque, un ajustement est généralement justifié par le petit nombre d'expérience ayant servi à l'estimer le valeurs en base de données (e.g. Christensen and Christensen, 1999).

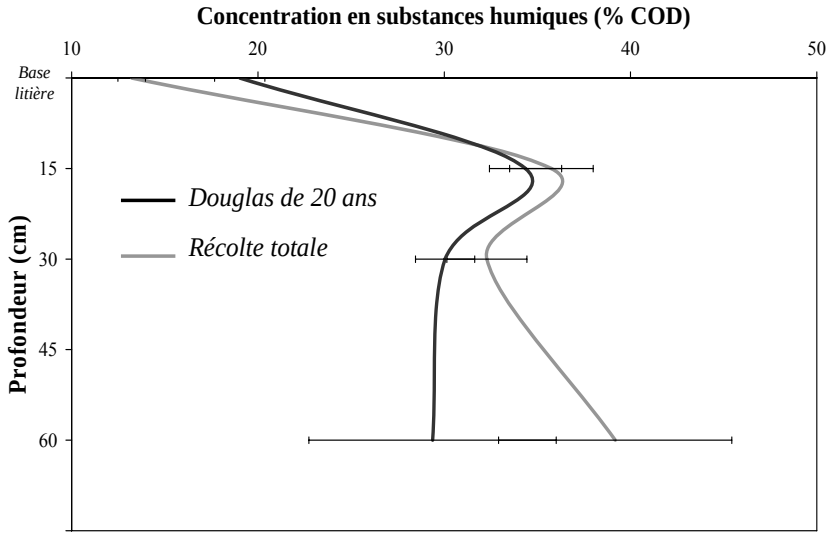

Figure 4. Variations avec la profondeur du sol du % de COD complexant Al (correspondant au % de substances humiques, assimilées à des acides fulviques). Valeurs calculées par le modèle WHAM-VI calibré par des mesures de spéciation de Al. Résultats pour des solutions du site de Vauxrenard (Rhône), collectées à l'aide de plaques lysimétriques. Deux parcelles ont été étudiées ; l'une accueillant un peuplement de Douglas d'un vingtaine d'année, et l'autre un peuplement de 60 ans venant d'être récolté.

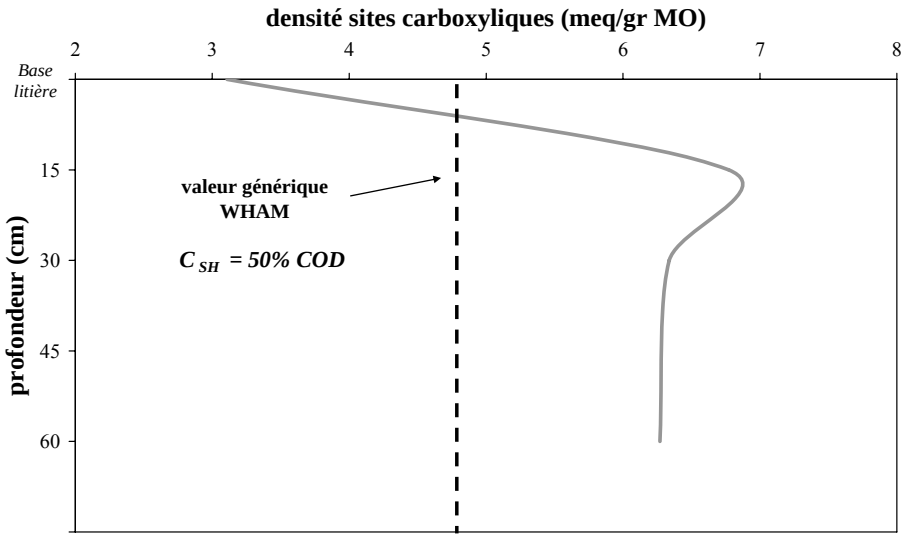

Figure 5. Variations avec la profondeur du sol de la densité des sites carboxyliques des SH estimées par calibration du modèle WHAM-VI. Dans cet exemple, la concentration des substances humiques (assimilés à des acides fulviques) a été fixée à 50% du COD et les calculs réalisés dans des solutions du site de Vauxrenard (Rhône) collectées par des plaques lysimétriques.

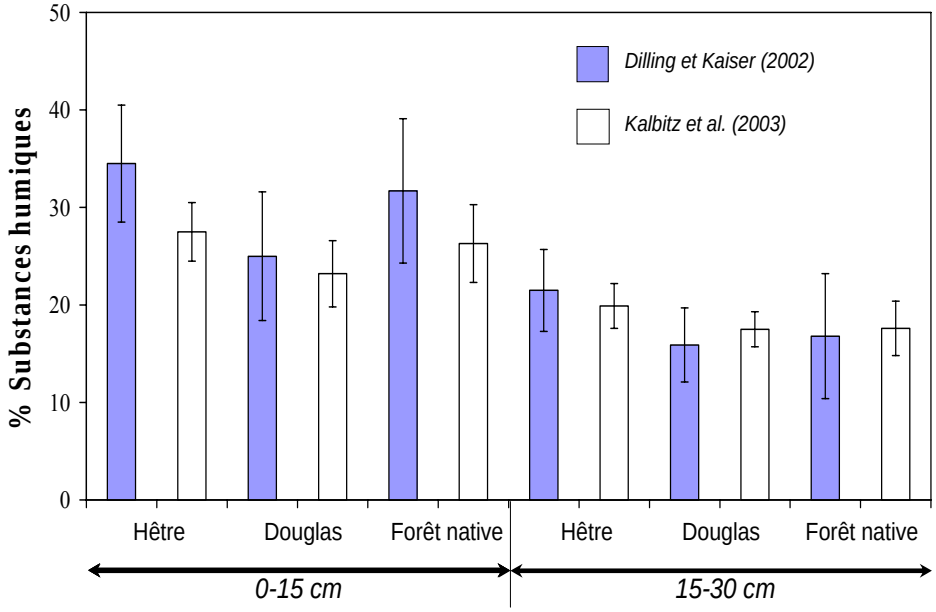

Figure 6. Estimations de la concentration en substances humiques réalisées à partir des mesures d'absorbance UV/visible et des fonctions proposées par Dilling et Kaiser (2002) et par Kalbitz et al. (2003). Résultats des solutions capillaires fortement liées du site expérimental de Breuil (Jaffrain, 2007). Echantillons collectés à deux intervalles de profondeur (0-15 cm et 15-30 cm) et dans trois parcelles (plantations de hêtre et de Douglas, et parcelle de forêt native).

Si l'on connaît la concentration des SH en plus des mesures de spéciation des métaux, il est possible de *calibrer la densité des sites complexant* (carboxyliques et phénoliques). De

tels calculs ont été effectués dans Benedetti (1996) et par moi-même, en étudiant les solutions du site de Vauxrenard (Figure 5). La calibration de ces variables n'a pas que des raisons pratiques, provoquées par l'absence de données propres aux conditions étudiées. En effet, la densité des sites complexant peut varier lors de l'extraction et la purification des SH. Ces variations s'expliquent par la nature « supra-moléculaire » des SH (Piccolo, 2001), impliquant que ces composés correspondraient à un ensemble instable de molécules organiques s'agrégeant entre elles sous l'effet de forces de type Van der Waals. A noter que la *composition des SH* en acides humiques (AH) et acides fulviques (AF) doit aussi influencer les valeurs de densité calibrées. Dans la base de données du modèle WHAM-VI, la densité des sites carboxyliques des AH est environ 30% plus faible que celle des AF.

Enfin, il est important de connaître la *spéciation de la fraction non humique* du COD, en particulier concernant les acides organiques de faible poids moléculaire (AOFPM). Peu d'études prennent en compte les effets des SH et des composés non humiques sur la spéciation des métaux. Une contribution significative de AOFPM a été pourtant calculée dans la poignée d'études réalisées à ce jour (**Dudal and Gérard, 2004**).

2.3. Qualité de la matière organique

La concentration en SH et en substances non humiques, les proportions en AF et AH ainsi que plusieurs autres indicateurs de la qualité du COD (poids moléculaire moyen, biodégradabilité etc.) peuvent être estimés par spectrophotométrie d'absorption entre 200 nm et 500 nm (Jaffrain, 2007; Jaffrain et al., 2007). Les liaisons aromatiques des constituants du COD, essentiellement les SH, absorbent la lumière dans cette gamme de longueur d'onde. L'absorption par les nitrates et le fer peut être corrigée. La spectrophotométrie d'absorption est une méthode non invasive, se contentant d'un très petit volume d'échantillon. Ces particularités font que la méthode est bien adaptée à l'étude de la qualité du COD dans les solutions du sol.

La quantification de ces propriétés, par exemple la concentration en SH, repose sur l'utilisation de fonctions prédictives utilisant une ou plusieurs valeurs d'absorbances spécifiques (absorbance/COD) mesurées à des longueurs d'onde clés. L'utilisation de ces fonctions suppose bien entendu qu'elles soient valides dans les conditions de l'étude. Une telle généricité est matière à débat. Toutefois, je considère que la généricité des ces fonctions est raisonnable car elles reposent souvent sur l'utilisation d'échantillons d'origine très diverse, allant des eaux de surface aux extractions aqueuses de litière et de sol. De plus, les concentrations en SH calculées en utilisant plusieurs fonctions publiées peuvent être très similaires (Figure 6). Les concentrations en SH estimées via ces fonctions prédictives ont été comparées à celles provenant de la calibration du modèle WHAM-VI (Figure 7). Cette comparaison montre que les estimations des deux méthodes sont proches. Par calibration, il existe une tendance de à surestimer ces concentrations dans la gamme des faibles valeurs, et à sous estimer quand les concentrations sont élevées. Ces résultats confortent l'assez bonne généricité des propriétés contenues dans la base de données du modèle.

L'abondance relative des AF et des AH dans le COD a également été estimée à partir de la spectrophotométrie UV dans les solutions du sol du site de Breuil (Figure 8). Des résultats cohérents ont été obtenus. On note en effet la tendance « AH » du COD des solutions collectées sous la litière, et la tendance « AF » des solutions capillaires faiblement liées collectées dans le sol. Le COD des solutions capillaires fortement liées, notre meilleure approximation de la solution « réactive » du sol, montre plutôt logiquement une tendance « AH ».

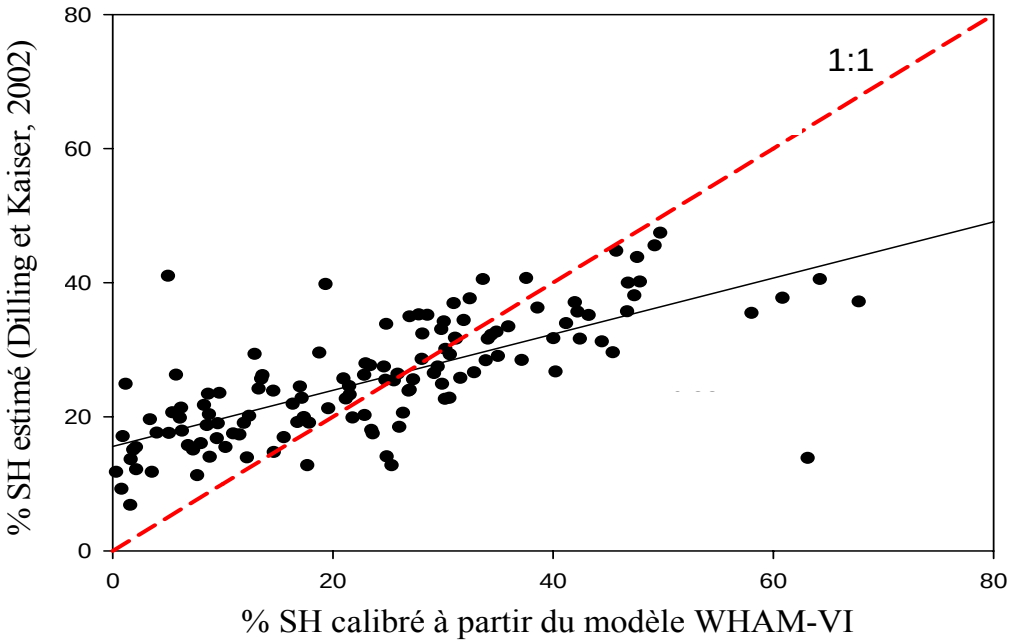

Figure 7. Comparaison entre les concentrations en substances humiques calculées par la fonction prédictive de Dilling et Kaiser (2002) et celles issues de la calibration du modèle WHAM-VI. Solutions capillaires fortement liées, site de Breuil parcelles de hêtre, de Douglas et forêt native groupées (Jaffrain, 2007).

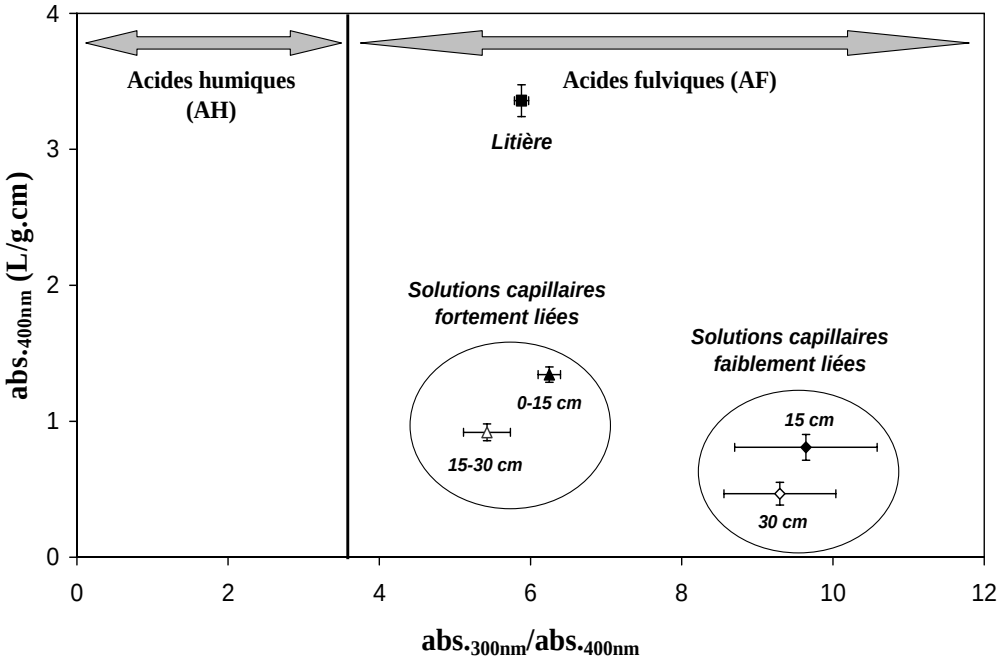

Figure 8. Valeurs moyennes de l'index acides fulviques/acides humiques (Artinger et al., 2000; Claret et al., 2003) selon le type de solutions capillaires et la profondeur du sol. Site de Breuil, parcelles de hêtre, de Douglas et forêt native groupées (comm. Pers. J. Jaffrain).

Il est bien admis que l'absorbance spécifique à 254 nm est un bon indicateur relatif de l'aromaticité du COD et des propriétés associées (poids moléculaire, biodégradabilité, etc.). Des mesures réalisées dans différents types de solution collectées à plusieurs profondeurs nous ont apporté des informations sur le fonctionnement organo-minéral du sol **(Jaffrain et al., 2007)**. Les effets (30 après) de la plantation de hêtre ou de Douglas ont pu être étudiés par comparaison à une parcelle de référence non plantée (taillis sous futaie, essentiellement composé de hêtre et de quelques chênes). Les principaux résultats de cette étude indiquent que la plantation de hêtre perturbe encore de nos jours l'aromaticité du COD des solutions capillaires du sol, quelles soient fortement ou faiblement liées à la matrice. Les résultats obtenus sous Douglas ne sont pas significativement différents de ceux acquis dans le sol de la forêt de référence. Cependant, il n'est pas sûr que l'état de quasi équilibre observé dans le sol planté de Douglas ne soit pas de nature apparente, et qu'en fait le système ne tende pas lentement vers un équilibre différent. Cette tendance observée dans les solutions du sol s'inverse dans les solutions collectées à la base de la litière (dynamique court terme). Dans type de solution, le COD collecté sous Douglas est différent de celui de la forêt native et de la parcelle de hêtre. Ce résultat est cohérent avec l'épaisseur singulièrement faible de l'horizon organique sous plantation de Douglas. On observe également un manque d'influence de la saison sur l'aromaticité du COD, ce qui semble indiquer que les effets des plantations sur l'aromaticité du COD a persisté durant toute la période de l'étude (1-2 ans).

3. Processus et mécanismes contrôlant le COD, Si et Al

3.1. Mobilité du COD

L'étude de **Jaffrain et al. (2007)** montre en outre une diminution de l'aromaticité du COD avec la profondeur du sol, sans doute du fait de l'adsorption préférentielle de la fraction aromatique (i.e. les SH). Ce travail a par ailleurs montré que le processus d'adsorption est d'une manière ou d'une autre affecté par le type de plantation. En effet, le passage dans le sol minéral du COD contenu par les solutions sortant de la litière provoque des effets différents sur l'aromaticité selon qu'il s'agisse de la plantation de hêtre (apparition de différences dans le sol) ou à la plantation de Douglas (disparition des différences).

Enfin, il a été évoqué plus haut que le COD des solutions capillaires fortement liées montrait une tendance AH (cf. Figure 8). Ce résultat est certainement à mettre sur le compte de la relative proximité de la MOS et des effets d'une plus forte interaction (à l'équilibre ou non) de cette MOS avec ce type de solution capillaire.

3.2. Spéciation et mécanismes

Les calculs de la spéciation de Al ont également montré que l'Al_{13} ne devant pas intervenir de manière significative dans la formation des hydroxydes d'Al en milieu naturel **(Gérard et al., 2001)**, contrairement à ce qui avait été invoqué dans la littérature (e.g. Bourrié et al., 1989).

La silice polymérique possède la capacité de s'associer à l'Al^{3+} et de fait pourrait jouer le rôle de précurseur dans la formation des aluminosilicates. Une relation inverse entre occurrence de Si polymérique et proximité de l'équilibre vis-à-vis du groupe des imogolites a été calculée dans le site de Breuil (Figure 9), ce qui semble confirmer le rôle précurseur de la silice polymérique dans la formation des aluminosilicates (Wonish et al., 2008).

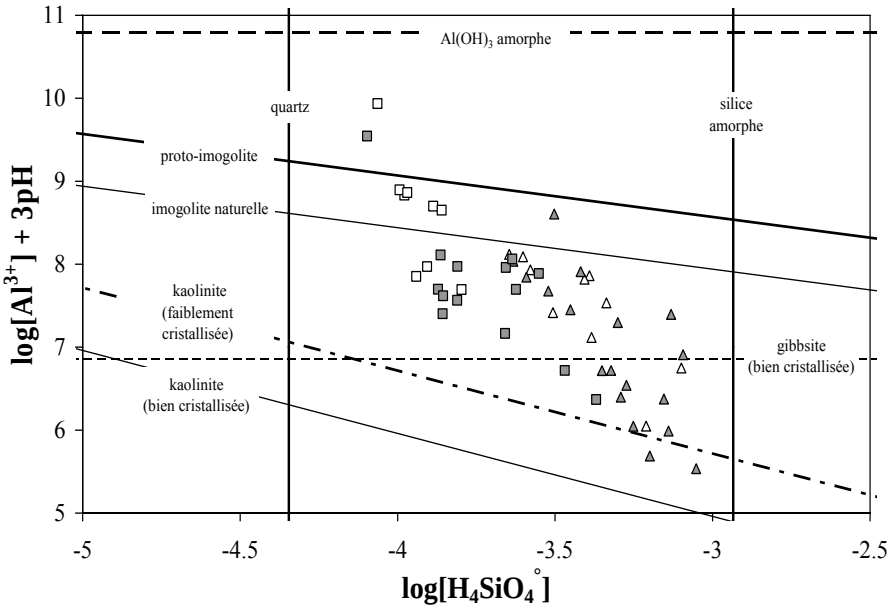

Figure 9. Diagramme d'activité dans le système Al-Si (Wonish et al., 2008). Calculs de spéciation réalisés par le modèle WHAM-VI. Solutions capillaires fortement liées. Symboles carrés : échantillons du site de Breuil (Nièvre, France); symboles triangulaires : échantillons du site de Bruck an den Mur (Styrie, Autriche). Symboles pleins : échantillons présentant des quantités détectables de Si polymérique (> 5%). Symboles vides : échantillons dépourvus de Si polymérique.

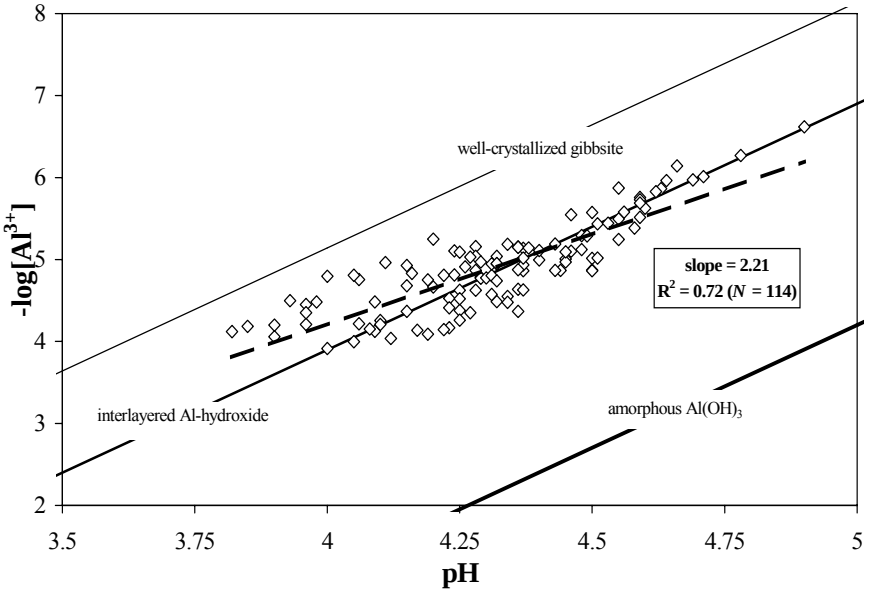

Figure 10. Diagramme d'activité dans le système Al-H **(Gérard et al., 2003)**. Calculs réalisées à l'aide du modèle Phreeqc 2 (Parkhurst and Appelo, 1999), en utilisant le formalisme de ligands organiques équivalents pour simuler la complexation organo-métallique. Solutions capillaires fortement liées du site de Vauxrenard (Rhône).

Les résultats de ces premiers calculs de spéciation de Al, réalisés en utilisant le formalisme de ligands organiques équivalents, ont confirmé ce qui pouvait être déduit des observations minéralogiques **(Gérard et al., 2002; 2003)**. Comme l'indique les diagrammes d'activité, l'activité de l'ion Al^{3+} semble essentiellement contrôlée par la néoformation d'hydroxydes d'Al (Figure 10). Malgré ces résultats cohérents, la précision de ces calculs et des observations qui en ont été faites pouvaient être questionnées, du fait de :

- l'absence de mesures de spéciation de Al, qui auraient rendues possible l'évaluation du modèle de ligands équivalents, et l'ajustement très probable des constantes pour un calcul plus précis de l'activité de Al^{3+} ;

- la pente relativement faible de la régression linéaire réalisée au travers les données du diagramme d'activité (cf. Figure 10). En effet, une pente égale ou proche de 3 unités devrait être calculée dans le cas d'un contrôle franc par néoformation d'hydroxydes d'Al (Al(OH)3 libres ou en interfoliaire des argiles 2 :1). Une valeur plus faible peut révéler l'existence d'un contrôle mixte de Al^{3+} par adsorption avec la MOS et néoformation d'hydroxydes (e.g. Berggren and Mulder, 1995).

Ces limites justifient d'autant plus le choix d'un modèle plus mécaniste pour la simulation des interactions organo-minérales (WHAM-VI), et le fait de combiner la modélisation à des mesures de la spéciation.

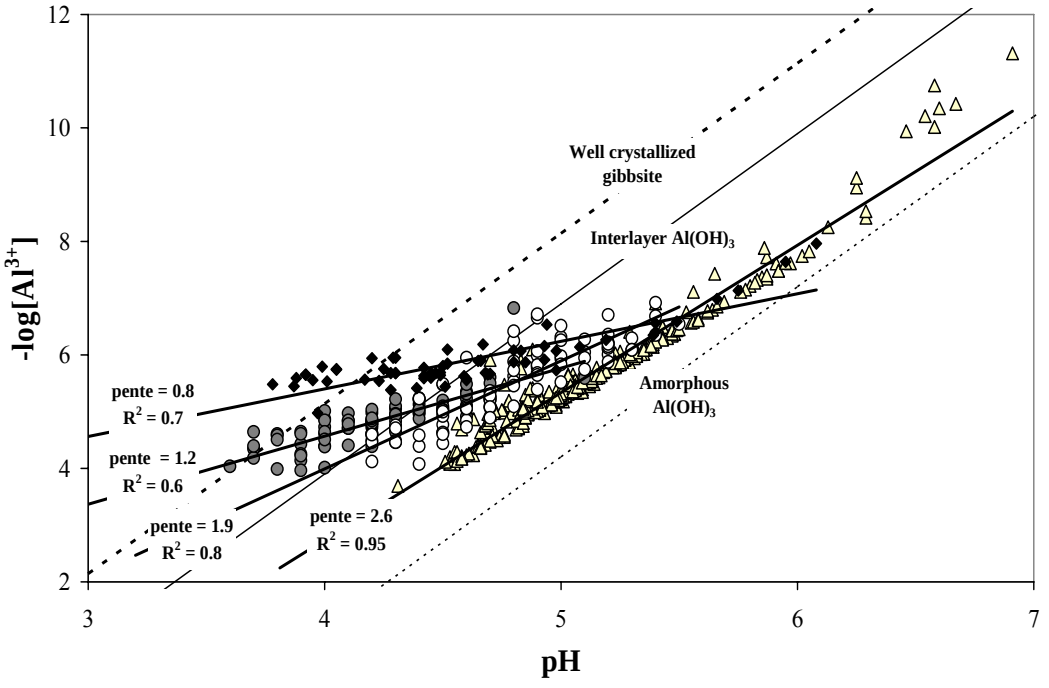

Figure 11. Diagramme d'activité dans le système Al-H réalisé à l'aide des calculs du modèle WHAM-VI (Gérard et al., 2005). Les losanges noirs correspondent aux solutions collectées sous la litière. Les ronds gris et blancs correspondent aux solutions capillaires fortement liées (micropores) collectées entre 0-15 et 15-30 cm, respectivement. Les triangles blancs correspondent aux solutions capillaires faiblement liées collectées à 15 et 30 cm de profondeur. Données issues du site expérimental de Breuil (Nièvre). Echantillons collectés sous les plantations de hêtre et de douglas, et sous la parcelle de forêt native.

Ces conditions ont été recueillies dans le site de Breuil, avec les échantillons de solution ayant déjà été l'objet de l'étude de la spéciation du COD par spectophotométrie d'absorbance. Des résultats très intéressant ont été obtenus. La pente des régressions et la position des points dans le diagramme vis-à-vis des droites de stabilité des phases minérales pures indiquent que Al^{3+} est contrôlé par des mécanismes différents selon le type de solution de sol, selon qu'il s'agisse de solutions collectées sous la litière, ou bien de solutions capillaires circulant dans les macropores et les micropores du sol (Figure 11). Dans les pores les plus larges (solutions capillaires faiblement liées), le mécanisme serait la néoformation d'hydroxydes d'Al tandis que dans les micropores (solutions capillaires fortement liées), en particulier dans l'horizon de surface (0-15 cm), cette néoformation serait associée à l'adsorption de Al^{3+} par la MOS. Un contrôle très marqué de Al^{3+} par l'adsorption avec la matière organique est observé à la sortie de la litière (solutions collectées sous la litière). La pente est de l'ordre de l'unité. Elle indique la stoechiométrie de l'échange Al^{3+}/H^{+} au niveau de la SOM (e.g. Cronan et al., 1986).

Les calculs de la spéciation de Al sont également intéressants pour les processus contrôlant la silice dissoute (Si). Les diagrammes d'activités réalisés dans le système Al-Si ont tous montré l'absence d'un contrôle de Si (et par là même de Al) par une précipitation rapide d'allophanes ou d'imogolite (Figure 12). Les solutions du sol sont globalement sous saturées vis-à-vis de ces phases, en particulier à pH acide (points possédant les plus fortes activités). De plus, bien que des régressions linéaires significatives aient été obtenues, leur pente (indiquant la stoechiométrie Si/Al du précipité potentiel) est bien trop élevée pour correspondre à une phase qui ait déjà été identifiée dans un sol **(Gérard et al., 2002, 2003)**.

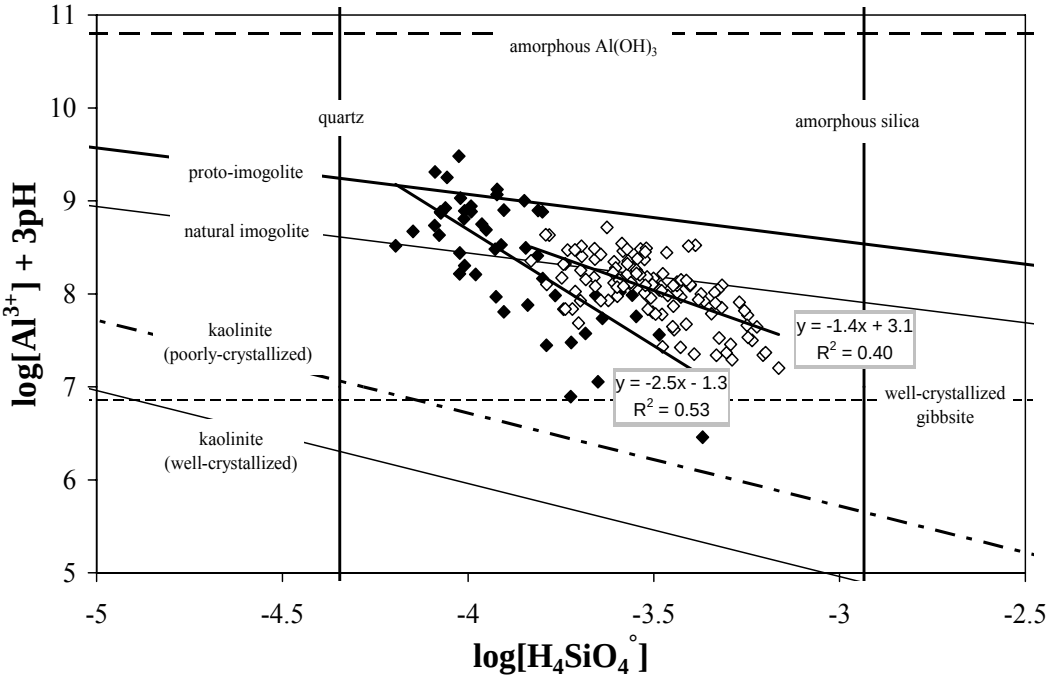

Figure 12. Diagramme d'activité dans le système Al-Si. Solutions capillaires fortement liées du site de Vauxrenard (symboles blancs) et du site de Breuil (symboles noirs). Les régressions linéaires correspondantes sont également indiquées.

Ces résultats de modélisation géochimique sont conformes aux observations minéralogiques, et notamment aux extractions de la fraction faiblement cristalline (extractions Tamm) à laquelle on soustrait l'Al adsorbé à la MOS (Ezzaïm et al., 1999; Jaffrain, 2007). Le rapport Al/Si ainsi obtenu renseigne sur la présence d'allophanes (e.g. Simonsson and Berggren, 1998). Un rapport supérieur à 2 montrerait que les hydroxydes d'Al amorphes à faiblement cristallisés sont les principaux minéraux secondaires contenant de l'aluminium. Cela n'exclue cependant pas la présence de quantités traces d'imogolites et autres allophanes dans les sols étudiés. Cette considération a d'ailleurs été faite par Wonish et al. (2008), afin d'étayer le rôle précurseur de la silice polymérique (stabilisée par Al) dans la formation des silicates secondaires.

3.3. Extractions chimiques

Etant donné l'importance des résultats des méthodes d'extraction, j'ai essayé d'améliorer le protocole utilisé pour extraire les cations adsorbés à la MOS. Ces travaux ont été réalisés dans le site de Breuil, où il a été possible de montrer les biais de la méthode utilisée classiquement par le laboratoire afin d'accéder à Al adsorbé par la MOS. Il s'agissait d'une extraction au Na-pyrophosphate. En toute rigueur, le fait de soustraire la concentration de Al extraite par cette méthode à celle extraite par la méthode de Tamm (1922) devrait aboutir à une valeur positive (ou nulle) correspondant aux quantités d'Al contenues dans les phases faiblement cristallisées. Or, cela n'est vérifié que dans les horizons profonds du site de Breuil, (Forêt, 2003). Une différence négative est calculée dans le sol de surface (Figure 13).

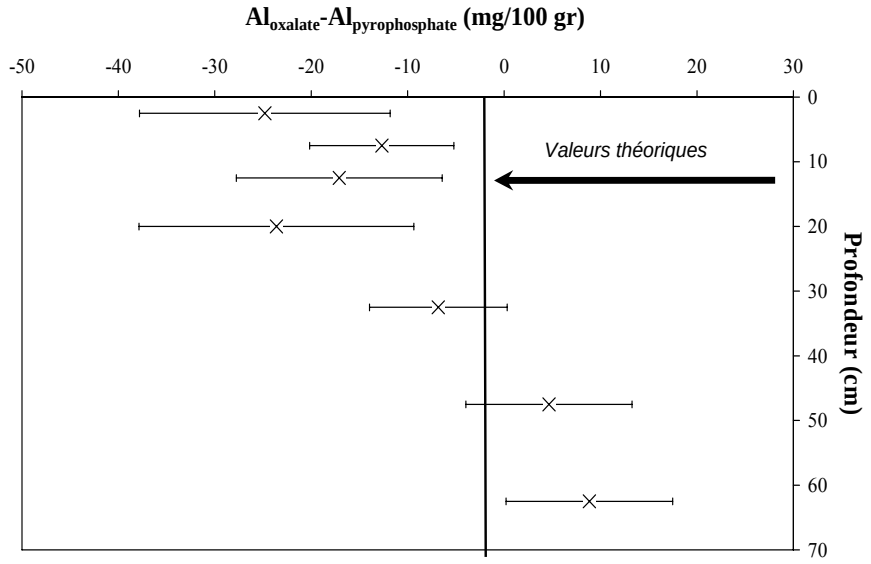

Figure 13. Evolution de la différence entre aluminium extrait par oxalate et aluminium extrait par pyrophosphate (Forêt, 2003). Données acquises dans le sol du peuplement de Douglas du site de Breuil.

Ce biais dans la méthode par pyrophosphate avait déjà été remarqué par Kaiser (1996). Il aurait pour cause les effets de la dissolution des minéraux ciblés par l'oxalate, qui serait favorisée par le pH très alcalin de l'extractant pyrophosphate. L'utilisation d'un autre extractant a été mise en place dans la thèse de J. Jaffrain (Jaffrain, 2007). Il s'agit du chlorure de cuivre ($CuCl_2$). L'utilisation du $CuCl_2$ afin d'extraire l'Al adsorbé à la MOS est

connue depuis longtemps (Juo and Kamprath, 1979). Les mesures réalisées sur le site de Breuil donnent toutes des résultats cohérents vis-à-vis de l'Al extrait par oxalate (Figure 14). Ces résultats montrent également la présence d'une quantité d'hydroxydes d'Al (amorphes et faiblement cristallisés) largement supérieure (5 à 10 fois) à celle de l'Al adsorbé à la MOS. Il apparaît donc que la dynamique de Al dans le sol serait plus fortement contrôlée par les néoformations d'hydroxydes d'Al (dissolution et/ou précipitation) que par des réactions d'adsorption avec la MOS. Cette tendance est exacerbée si l'on ajoute à ce compartiment inorganique les concentrations d'Al-hydroxydes dans l'espace interfoliaire des argiles 2:1, extraites à l'aide de tricitrate de sodium.

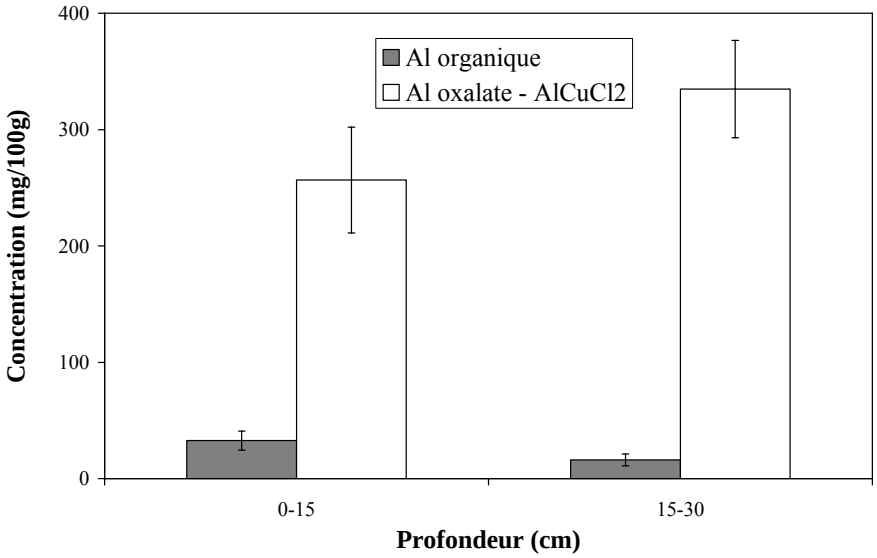

Figure 14. Concentration en aluminium adsorbé à la MOS et différence entre Al extrait par oxalate et Al extrait par chlorure de cuivre, correspondant à la concentration d'Al sous forme d'hydroxyde amorphe et faiblement cristallisé. Sol du peuplement de Douglas, site de Breuil (Baton, 2004)

Une telle hégémonie d'un mécanisme inorganique sur le contrôle de Al dans le sol a été déduite d'observations réalisées sur la phase solide. Elle est en contradiction avec les résultats obtenus en calculant la spéciation de Al dans les différents types de solutions capillaires (cf. Figure 11). En effet, la présence d'une adsorption de Al^{3+} n'avait été observée que dans les solutions capillaires fortement liées, en particulier celles issues de l'horizon de surface. Deux explications peuvent être invoquées afin d'expliquer cette différence:

i) nous ne connaissons pas le volume relatif des micropores, contenant les solutions capillaires fortement liées, et des pores plus larges, contenant les solutions capillaires faiblement liées (exhibant un contrôle « minéral » très marqué). Dans ces conditions, les effets d'un contrôle de Al par la MOS peuvent très bien être dilués à l'échelle du sol si ce mécanisme est limité à un faible volume poral;

ii) les faibles concentrations d'Al adsorbé pourraient révéler une certaine saturation de sites d'adsorption. Dans la gamme de pH des solutions du site de Breuil, la quantité d'Al adsorbé dépend en grande partie de la densité des fonctions carboxyliques de la MOS. Ces sites ne seraient alors pas suffisamment nombreux pour contrôler les flux d'Al.

La validité du deuxième point a été confortée par des résultats obtenus en mettant en relation le pH du sol (pH eau) et les concentrations d'Al adsorbé à la MOS (Jaffrain, 2007). En effet, un contrôle par la MOS devrait être privilégié à pH acide, au détriment d'un contrôle par les néoformations minérales (e.g. Cronan et al., 1986 ; Berggren and Mulder, 1995). En conséquence, les concentrations d'Al associé à la MOS devraient augmenter avec l'acidité. Cependant, le résultat inverse a été trouvé dans le sol de Breuil. La corrélation est faible, certes, mais significative et plus marquée dans l'horizon de surface du sol (Figure 15). Il apparaît donc que la quantité d'Al adsorbé diminue avec l'acidité, comme si Al^{3+} était excédentaire dans les micropores et que sa concentration adsorbée dépendait uniquement de la déprotonation des sites (qui augmente avec le pH).

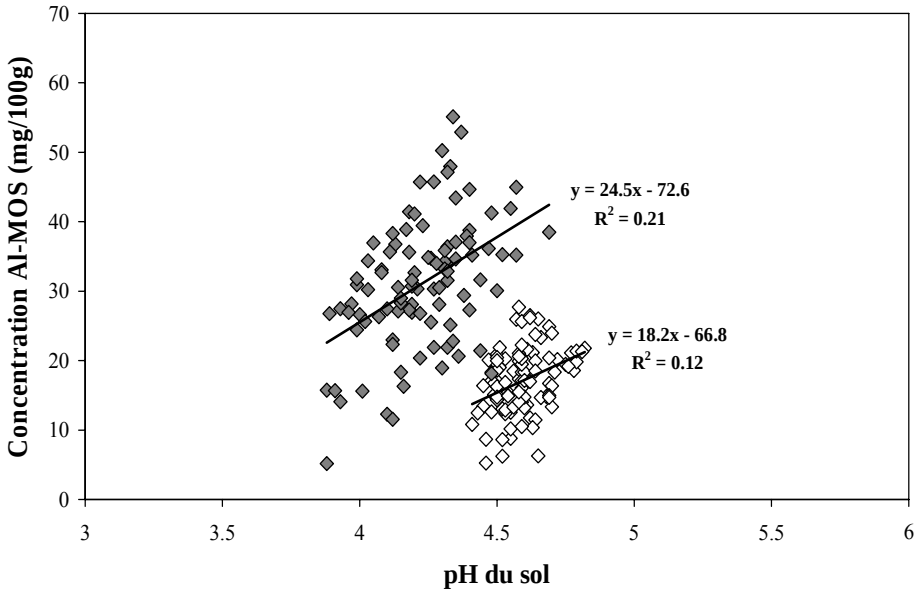

Figure 15. Concentration en aluminium adsorbé à la MOS (mg/100g) en fonction du pH du sol (pH eau). Symboles grisés : horizon de surface (0-15 cm) ; symboles blancs : horizon profond (15-30 cm).

3.4. Dynamique du silicium

La modélisation de la spéciation aqueuse de Al et de Si, ainsi que l'examen des diagrammes d'activités et les observations minéralogiques ont montré l'absence d'un effet significatif des néoformations d'aluminosilicates sur la concentration de Si dans les solutions du sol des sites de Vauxrenard et de Breuil. La question du ou des mécanismes contrôlant la dynamique de Si restait donc posée. Afin de tenter d'y répondre, des travaux ont été réalisés principalement dans le site de Vauxrenard. Nous verrons plus loin que les résultats sont confortés par les premières observations effectuées dans le site de Breuil.

La première étape a été consacrée aux mécanismes contrôlant la concentration de Si dans les solutions gravitaires (plaques lysimétriques) et dans les solutions capillaires faiblement liées (**Gérard et al., 2002**). Des variations saisonnières antagonistes de la concentration en Si ont été observées selon le type de solution du sol. Dans le cas des solutions capillaires, un maximum est atteint en été et un minimum en hiver. Ces variations temporelles de la concentration sont fortement corrélées à celles de la température du sol (Figure 16).

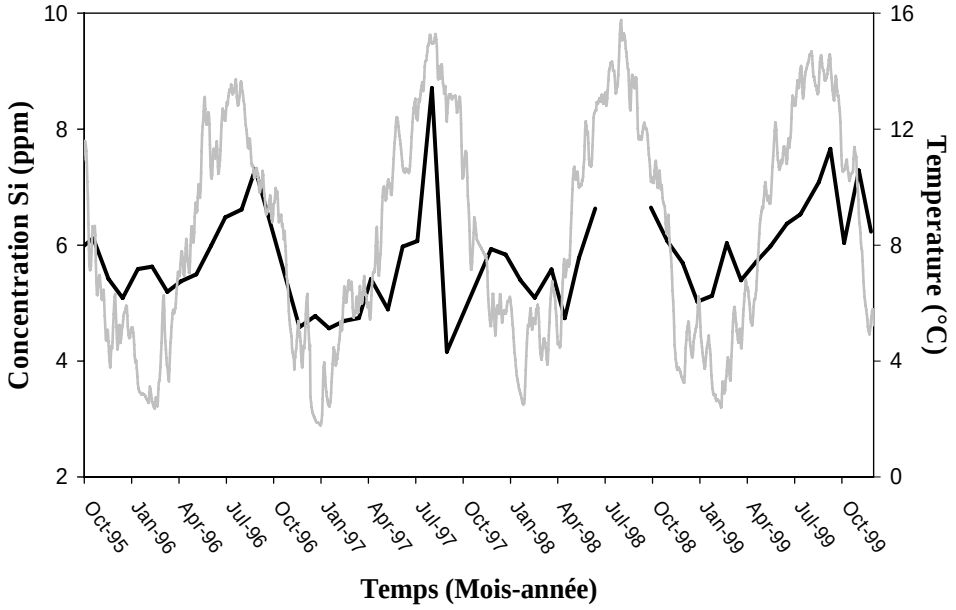

Figure 16. Concentration moyenne en silice mesurée dans les solutions capillaires (trait noir) et température du sol (trait gris). Site de Vauxrenard, exemple à 30 cm de profondeur.

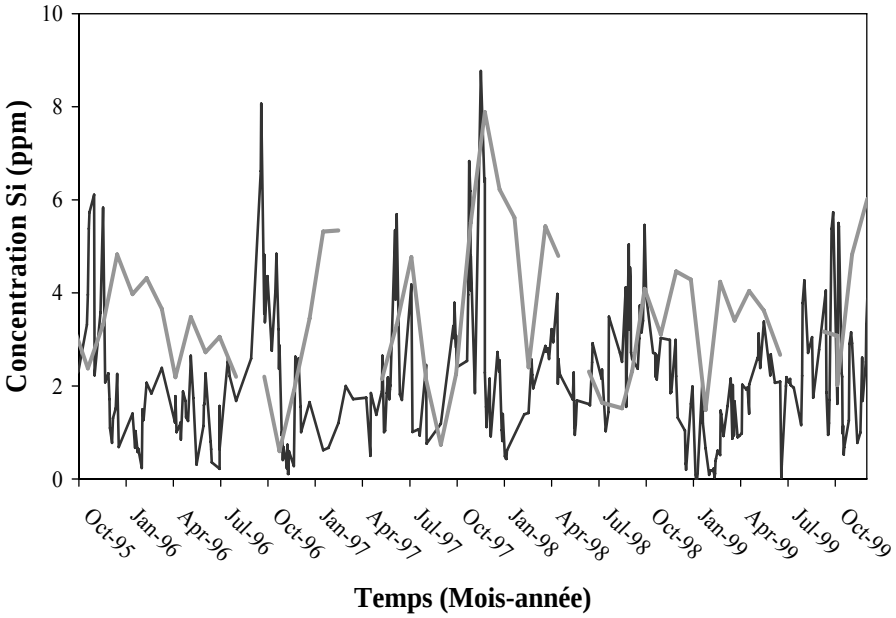

Figure 17. Concentration moyenne en silice mesurée dans les solutions gravitaires collectées à 15 cm de profondeur (trait gris) et dans les solutions collectées sous la litière (trait noir). Site de Vauxrenard.

La corrélation positive entre Si et T donne un autre argument pour écarter un effet significatif d'une précipitation rapide de minéraux silicates. De plus, cet argument est indépendant de la modélisation de la spéciation. En effet, la solubilité des minéraux secondaires potentiels (allophanes, imogolites) y compris les argiles (kaolinite et vermiculites notamment) présente une dépendance inverse vis-à-vis de la température

(**Gérard et al., 2002**). Cela peut être apprécié à partir des bases de données thermodynamiques utilisées par des modèles géochimiques très répandus, tels que PHREEQC.

En l'absence d'un contrôle de Si par la néoformation de silicates, la corrélation positive de Si et de T ne pouvait s'expliquer que par l'effet de la dissolution des silicates primaires. Le processus d'altération des silicates primaires contrôlerait donc la concentration en Si des solutions capillaires. En ce qui concerne le processus/mécanisme responsable des variations saisonnières dans les solutions gravitaires, où la concentration en Si est maximum en hiver et minimum en été, il n'a été aussi clairement établi. Plusieurs hypothèses existent, par exemple le transfert préférentiel de colloïdes silicatés dans les eaux gravitaires, ou bien encore la libération de silice par la litière associée à un enrichissement par diffusion à partir des eaux capillaires. Les effets de processus du sol sont nécessaires car les concentrations mesurées dans les solutions de litière sont plus faibles que celles mesurées dans les solutions gravitaires (Figure 17). L'origine colloïdale de Si dans les eaux gravitaires n'a pas été infirmée par l'étude récente de l'occurrence de Si polymérique (Wonish et al., 2008).

Le contrôle de la concentration de Si dans les solutions capillaires par la dissolution des silicates primaires a ensuite été confirmé et précisé par l'étude des solutions fortement liées (**Gérard et al., 2003**). Une méthode originale a été employée à cette occasion, puisqu'elle consiste à rechercher parmi les données mesurées dans la « solution réactive » du sol l'existence d'une *relation mécaniste*, bien établie dans les conditions plus maîtrisées du laboratoire. Son obtention révèlerait la présence du mécanisme en question dans le sol. Sur la base des travaux précédents, suggérant donc une relation de proportionnalité entre Si et vitesse de dissolution des silicates primaires (**Gérard et al., 2002**), une relation linéaire significative a été obtenue entre le log de la concentration de Si (i.e. proportionnel au log de la vitesse de dissolution) et le pH (Figure 18).

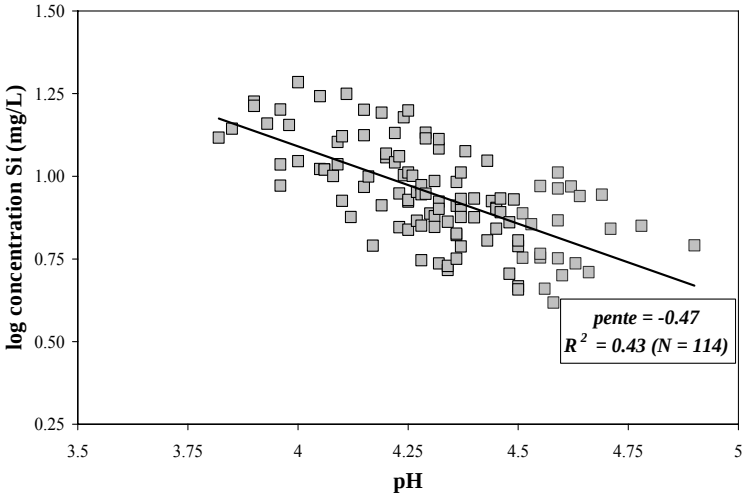

Figure 18. Relation linéaire entre le log de la concentration en Si et le pH des solutions capillaires fortement liées. Site de Vauxrenard (**Gérard et al., 2003**).

L'établissement d'une telle relation implique que la dissolution des silicates primaire est essentiellement contrôlée par des réactions de surface, et que les protons constituent la principale espèce réactive (**Gérard et al., 2003**). De plus, la valeur de la pente est caractéristique de la dissolution des feldspaths alcalins. Les deux feldspaths alcalins

présents dans le sol (feldspath-K, albite) se dissolvent suffisamment loin de l'équilibre thermodynamique pour qu'une relation linéaire entre logSi et le pH soit observable.

L'établissement d'une relation linéaire entre logSi et le pH suggère aussi que la surface réactive des silicates primaires varie peu d'un échantillon de sol à l'autre. Les valeurs relatives (moyennes) de la surface réactive des différents silicates primaires du sol ont pu être calculées à partir des données de minéralogie quantitative. Elles ont été utilisées pour calculer des vitesses de dissolution. Les calculs ont montré que le feldspath-K devait être de loin le minéral se dissolvant le plus rapidement. Ces résultats impliquent donc que la concentration de Si dans les solutions capillaires du sol serait principalement contrôlée par la dissolution du feldspath-K (**Gérard et al., 2003**).

Ce type de relation linéaire a également été obtenu à partir des solutions capillaires fortement liées de plusieurs parcelles du site de Breuil (Jaffrain, 2007), ainsi que dans des solutions d'un sol plus acide situé dans les alpes autrichiennes (Figure 19). Il semblerait donc que la dissolution des silicates primaires, visiblement celle des feldspaths alcalins, y contrôlerait aussi la concentration en Si. Sur le site de Breuil, un contrôle par l'altération a été confirmé par l'étude des variations saisonnières de Si dans les solutions capillaires faiblement liées, bien que le petit nombre de données disponibles en été, voire selon l'essence sylvicole leur absence totale, gêne considérablement l'observation des pics de concentration (Figure 20).

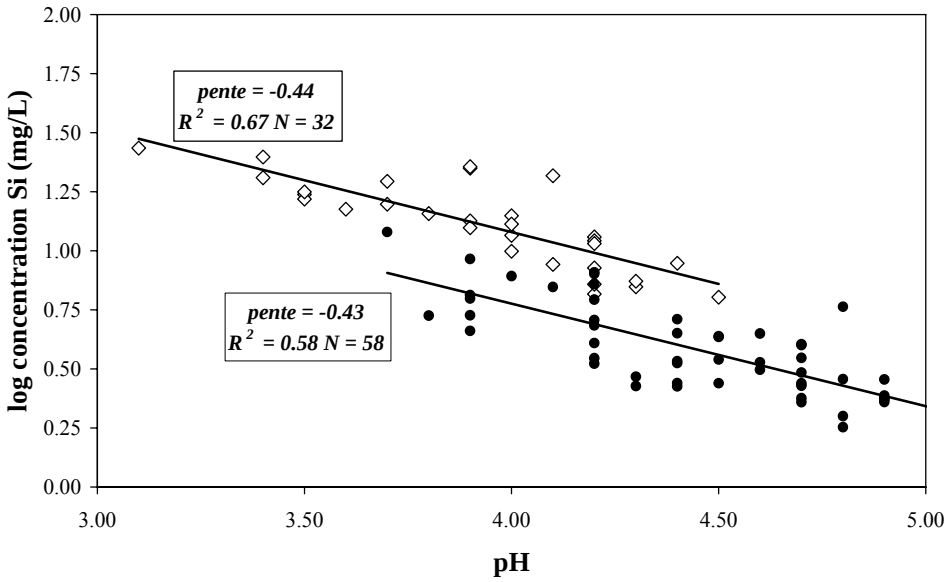

Figure 19. Relation linéaire entre le log de la concentration en Si dans les solutions capillaires fortement liées et leur pH. Symboles noirs : site de Breuil, parcelle de Douglas ; symboles blancs : site de Bruck an den Mur.

3.5. Bilan

L'étude et la modélisation de la spéciation de Si et de Al associées à des données sur la phase solide du sol ont abouti à l'identification des mécanismes géochimiques, voire biogéochimiques (du fait de la place de la MO dans le système), susceptibles de contrôler la dynamique de ces éléments dans des sols forestiers acides.

La démarche adoptée ces dernières années a également abouti à des résultats génériques sur :

- l'occurrence et le rôle de Al_{13} et de la silice polymérique dans la formation des minéraux secondaires (**Gérard et al., 2001** ; Wonisch et al., 2007) ;
- les mécanismes contrôlant Al selon la taille des pores (Gérard et al., 2005) ;
- la dynamique de la MO et la qualité du COD (**Jaffrain et al., 2007**) ;
- et le processus contrôlant Si dans les solutions capillaires (**Gérard et al., 2002, 2003**).

Les limites de la modélisation géochimique ont également été mises en évidence, lors de l'étude des mécanismes contrôlant Al selon la taille des pores et en comparant les résultats « vus » à partir de la phase aqueuse et ceux « vu » à partir de la phase solide. En effet, seule, la modélisation géochimique ne permet de quantifier les flux. Cet outil peut apporter des informations qualitatives voir semi-quantitatives (vitesses relatives) sur le fonctionnement organique et minéral des sols. Ces connaissances sont un préalable à une étude couplée, permettant de donner accès aux flux contrôlant les cycles biogéochimiques. Cependant, cet objectif nécessite d'abord la quantification des transferts hydriques dans le sol.

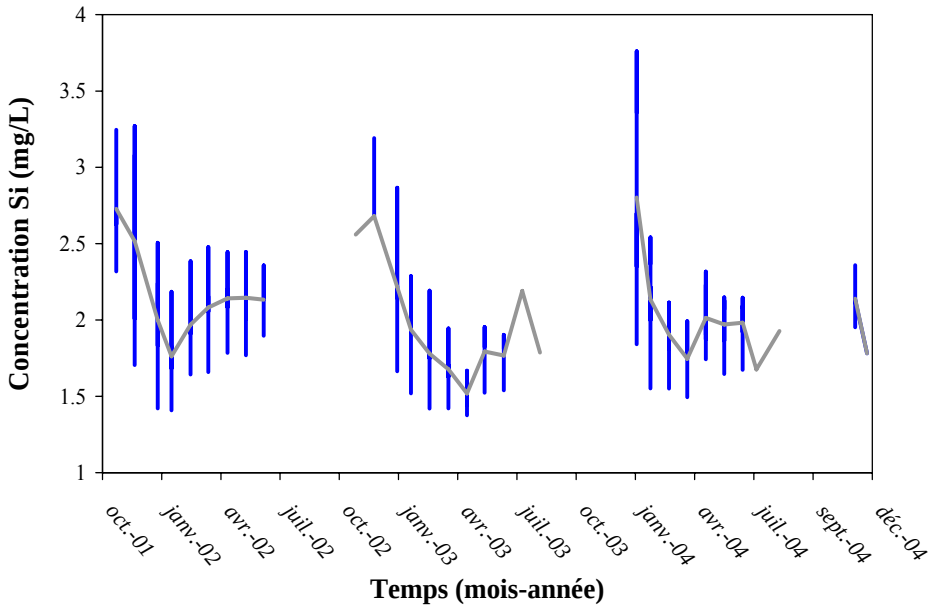

Figure 20. Concentration en silice dans les solutions capillaires faiblement liées du site de Breuil. Echantillons collectés à 60 cm de profondeur, peuplement de Douglas. Trait noir : différence entre valeurs max et min ; trait gris : concentration moyenne.

4. Transferts hydriques

4.1. Méthode

Afin de préparer le terrain pour la modélisation couplée biogéochimie-transfert, le modèle MIN3P a été développé dans le domaine des transferts de l'eau. Les processus d'évapotranspiration on été intégrés dans le modèle. Le modèle MIN3P utilise la loi de

Richards pour quantifier les flux d'eau. Les relations de van Genuchten (1980) entre humidité-potentiel hydrique (θ-ψ) et humidité-conductivité hydraulique (θ-K) sont utilisées. Les processus d'évaporation ont été introduits par M. Tinsley dans le cadre de sa formation postdoctorale effectuée dans notre laboratoire. La méthode a consisté à ajouter un terme puits à l'équation de Richards (**Gérard et al., 2004, 2006**). La transpiration potentielle est calculée selon l'équation de bilan suivante :

$$ETP = T + E_u + f\,I \tag{1}$$

avec *ETP* correspondant à l'évapotranspiration potentielle (m/s), *T* étant la transpiration potentielle (m/s), E_u l'évaporation physique potentielle (m/s), *I* l'interception de la végétation (m/s), et *f* (s.d.) un facteur spécifique à la végétation, permettant de tenir compte de la diminution de la transpiration les jours de pluie.

Ces variables sont traitées par le modèle MIN3P comme des variables externes, c'est à dire que les valeurs en fonction du temps sont lues dans un fichier. L'évaporation physique potentielle correspond à une fraction de l'ETP, fixée par le rapport entre énergie solaire au sol et énergie solaire incidente (Vilette, 1994). La transpiration réelle de la végétation est limitée par le stress hydrique et dépend du leaf area index (LAI). Ces effets sont pris en compte par la fonction de Battaglia and Sands (1997). La transpiration réelle est répartie dans les horizons du sol en fonction de la densité de longueur racinaire (m/m^3) et de l'humidité (e.g. Tiktak and Bouten, 1994).

4.2. Site de Vauxrenard

Les transferts de l'eau dans le sol du site de Vauxrenard avaient fait l'objet d'une première étude en 1994, qui avait pour objet la paramétrisation des processus écophysiologiques nécessaires à l'application du modèle BILJOU (Vilette, 1994). Ces fonctions et leurs paramètres ont été utilisés dans le modèle MIN3P. Le modèle BILJOU ne prend pas en compte la vitesse de transfert de l'eau dans le sol, puisque la notion de conductivité hydraulique, c'est-à-dire de capacité du sol à laisser passer l'eau, est absente. Dans ce modèle, l'eau passe instantanément d'un horizon de sol à l'horizon sous jacent quand la réserve utile en eau est atteinte (Granier et al., 1999). La prise en compte des remontées capillaires n'est pas possible avec ce formalisme, qui est très empirique.

Il est nécessaire de connaître les propriétés hydrodynamiques du sol pour simuler les transferts de l'eau avec MIN3P. Elles ont été estimées à l'aide de la fonction de pédo-transfert (FPT) ROSETTA (Schaap et al., 2001). Les FPT sont utilisées pour prédire les propriétés hydrodynamiques du sol à l'aide de propriétés facilement mesurables (densité apparente, granulométrie, etc.). La validité des prédictions de ROSETTA avait été testée dans la littérature par comparaison avec des mesures en laboratoire. De plus, cette FPT utilise une méthode de réseau neuronal pour les calculs des propriétés hydrodynamiques du sol. Cette méthode implique qu'aucune hypothèse *a priori* ne doit être faite sur la paramétrisation des relations entre les variables prédictives et les variables prédites, contrairement aux FPT classiques qui reposent sur des fonctions polynomiales prédéfinies. La FPT ROSETTA n'avait jamais été évaluée d'un point de vue fonctionnel, c'est-à-dire pour sa capacité à prédire l'humidité du sol sur le terrain. Cette étape essentielle est dans la pratique limitée par la difficulté (coup) des mesures de terrain. Le site de Vauxrenard disposait d'une vaste base de données de mesures *in situ* de l'humidité du sol (TDR), couvrant plusieurs années et plusieurs profondeurs. A cet égard, de bonnes conditions étaient réunies dans ce site expérimental pour une évaluation fonctionnelle de la FPT ROSETTA.

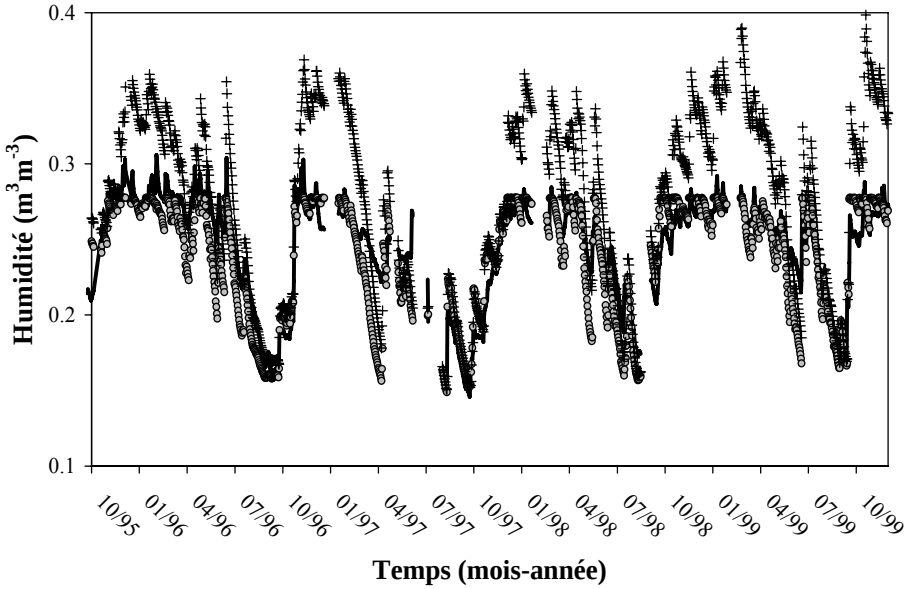

Figure 21. Humidité moyenne journalière du sol de Vauxrenard en fonction du temps. Exemple à 30 cm de profondeur. Trait noir : mesure TDR ; croix : modélisation réalisée en tenant compte des prédictions de la FTP ROSETTA ; cercles gris : modélisation avec prise en compte des écoulements préférentiels.

Les simulations réalisées dans le site de Vauxrenard ont été basée sur un profil 1-D de sol, de 1.2 m de profondeur et découpé en cinq horizons de taille et de propriétés hydrodynamiques différentes. Le domaine spatial a été discrétisé par 120 volumes élémentaires de taille (Δz) identique. Les valeurs journalières de pluviométrie (pluviolessivats), d'interception et d'ETP sont issues du modèle BILJOU. La densité racinaire ainsi que la réserve extractible en eau ont été calibrées sur la première partie de la série temporelle de mesures TDR (environ 2 ans). Les valeurs calibrées ont été conservées durant le reste de la période de temps afin de valider la simulation.

Les résultats des simulations sont bons en période de faible humidité, mais largement surestimés en période de forte humidité (Figure 21).Une telle surestimation systématique des fortes humidités illustre la présence d'écoulements préférentiels de l'eau dans des macropores. Ce processus viendrait en quelque sorte court-circuiter les écoulements plus lents se produisant dans la matrice, pour laquelle d'ailleurs les paramètres semblent avoir été correctement prédits par la FTP ROSETTA (**Gérard et al., 2004, 2006**). Pour tenir compte de ce nouveau processus en modélisation il a été nécessaire de retourner à une phase de développement du modèle MIN3P. Deux méthodes ont été employées. La première, assez réaliste, repose sur la description de deux sous milieux (deux colonnes de sol : l'une pour la matrice et l'autre pour les macropores) et d'un terme de transfert entre eau libre et eau liée (Gerke and van Genuchten, 1993b, a). Il s'agit d'une méthode dite « hors équilibre » (e.g. Simunek et al., 2003), car les potentiels hydriques des deux sous-milieux peuvent être différents. Sa limite réside dans le nombre de paramètres nécessaire à son utilisation : 11. La seconde méthode introduite dans le modèle MIN3P a été proposée par Mohanty et al. (1997). C'est une méthode dite « à l'équilibre ». Elle consiste à ajouter à l'équation standard de la conductivité hydraulique un terme décrivant l'effet des macropores, de forme exponentielle et n'opérant qu'à partir d'un seuil de potentiel hydrique. Ainsi, seulement deux paramètres sont à optimiser avec la seconde méthode: la conductivité hydraulique à

saturation des macropores (κ) et la valeur seuil de potentiel hydrique (ψ_{pf}). Ce dernier formalisme a été utilisé pour l'application du module hydrique de MIN3P au site de Vauxrenard. Après calibration de κ et de ψ_{pf} dans tous les horizons de sol, il permet au modèle MIN3P de simuler précisément l'humidité du sol en période de forte humidité (Figure 21).

4.3. Extension au site de Breuil

Le site de Breuil, et en particulier le sol de parcelle de Douglas, a été le second terrain d'application du modèle MIN3P pour les transferts de l'eau. Cette seconde application a été réalisée au travers de deux projets coordonnées par G. Richard (INRA Orléans) et s'inscrivant dans des programmes nationaux (Gessol et ANR « ADD »). Les objectifs étaient d'étudier, de prévoir et de prévenir les risques de tassement des sols et les effets sur les transferts de l'eau. Comparée à la précédente application au site de Vauxrenard, l'intérêt de cette seconde application du modèle au site de Breuil était aussi de disposer de mesures plus complètes des propriétés du sol, en particulier les courbes θ-ψ mesurées sur des échantillons collectés à différentes profondeurs. En effet, ces mesures physiques ont permis l'utilisation de la FPT ROSETTA dans des conditions mieux contraintes puisque de manière optionnelle cette FPT peut utiliser des *mesures d'humidité à de potentiel hydriques clés* (330 hPa et 15000 hPa, en valeur absolue) pour effectuer ses prédictions. Les propriétés prédites devraient être plus précises.

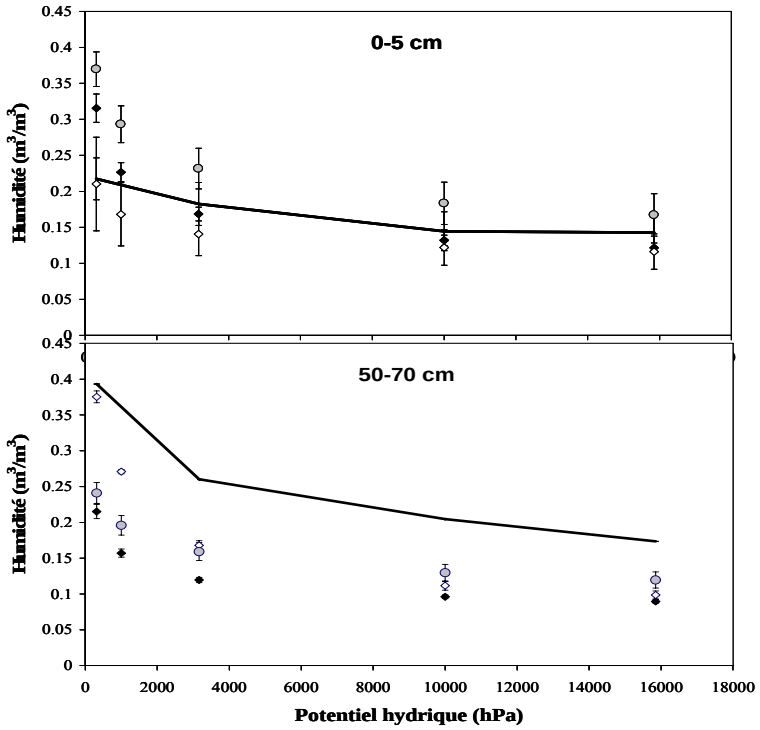

Figure 22. Comparaison entre les mesures et les prédictions de la courbe humidité-potentiel hydrique. Site de Breuil, parcelle de Douglas, exemple à 0-5 cm et 50-70 cm. Trait noir : mesures ; cercles gris : prédictions par la FPT de Wösten et al. (1999) ; losanges noirs : prédictions par la FPT ROSETTA sans les deux mesures d'humidité ; losanges blancs : prédictions par ROSETTA en utilisant les deux mesures d'humidité.

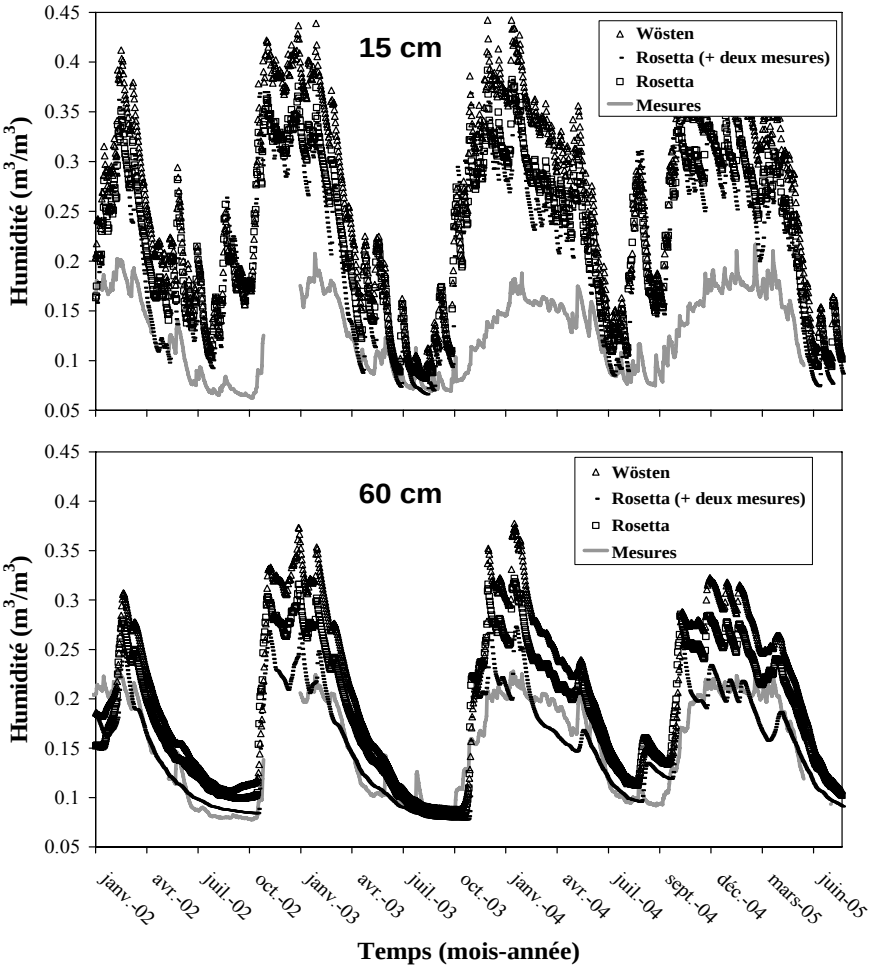

Figure 23. Comparaison entre les mesures et les simulations de l'humidité moyenne du sol de la parcelle de Douglas du site expérimental de Breuil. Simulations réalisées en considérant les propriétés hydrodynamiques du sol prédites à l'aide de la FPT ROSETTA, avec et sans prise en compte des deux mesures d'humidité, et de la FPT de Wösten et al. (1999).

De plus, une seconde FPT a pu être évaluée. Il s'agit des équations polynomiales proposées par Wösten et al. (1999). Cette FTP, standard, nécessite en entrée une donnée supplémentaire : le pourcentage de MOS (en plus de la densité apparente et de la granulométrie dans Rosetta). Les prédictions des deux FPT ont d'abord été comparées aux mesures θ-ψ réalisées sur des échantillons collectés entre 0 et 70 cm de profondeur (Figure 22). Cette confrontation montre que les prédictions de ROSETTA sont généralement plus précises que celles prédites par les équations de Wösten et al. (1999). Cette dernière FPT conduit à surestimer l'humidité des échantillons collectés dans les horizons de surface.

Dans les horizons profonds, les prédictions de toutes les FPT fournissent des valeurs d'humidité très sous-estimées (environ 25% d'erreur). En tenant compte des deux mesures d'humidité, les prédictions de ROSETTA sont plus précises pour les faibles potentiels (i.e. proche de la saturation) et ce quelque soit la profondeur du sol.

Les différences observées entre mesures et prédictions à l'échelle de l'échantillon de sol ont des répercutions équivalentes sur les humidité simulées à l'échelle de la parcelle. En effet, sur le terrain les meilleurs résultats ont été obtenus en utilisant les valeurs prédites par la FPT ROSETTA en tenant compte des deux mesures d'humidité (Figure 23). Les

humidités simulées en dessous de 15 cm de profondeur sont fortement améliorées en période de forte humidité. A 15 cm de profondeur, la surestimation de l'humidité du sol n'est que partiellement corrigée, ce qui pose de nouveau le problème des écoulements préférentiels, comme à Vauxrenard. Il a été possible de corriger ce biais en introduisant ce processus et en calibrant les deux paramètres contrôlant son intensité (κ et ψ_{pf}). A noter que les résultats calculés à 30 et 60 cm de profondeur n'ont pas été détériorés de manière significative en prenant en compte les écoulements préférentiels en surface (Figure 24).

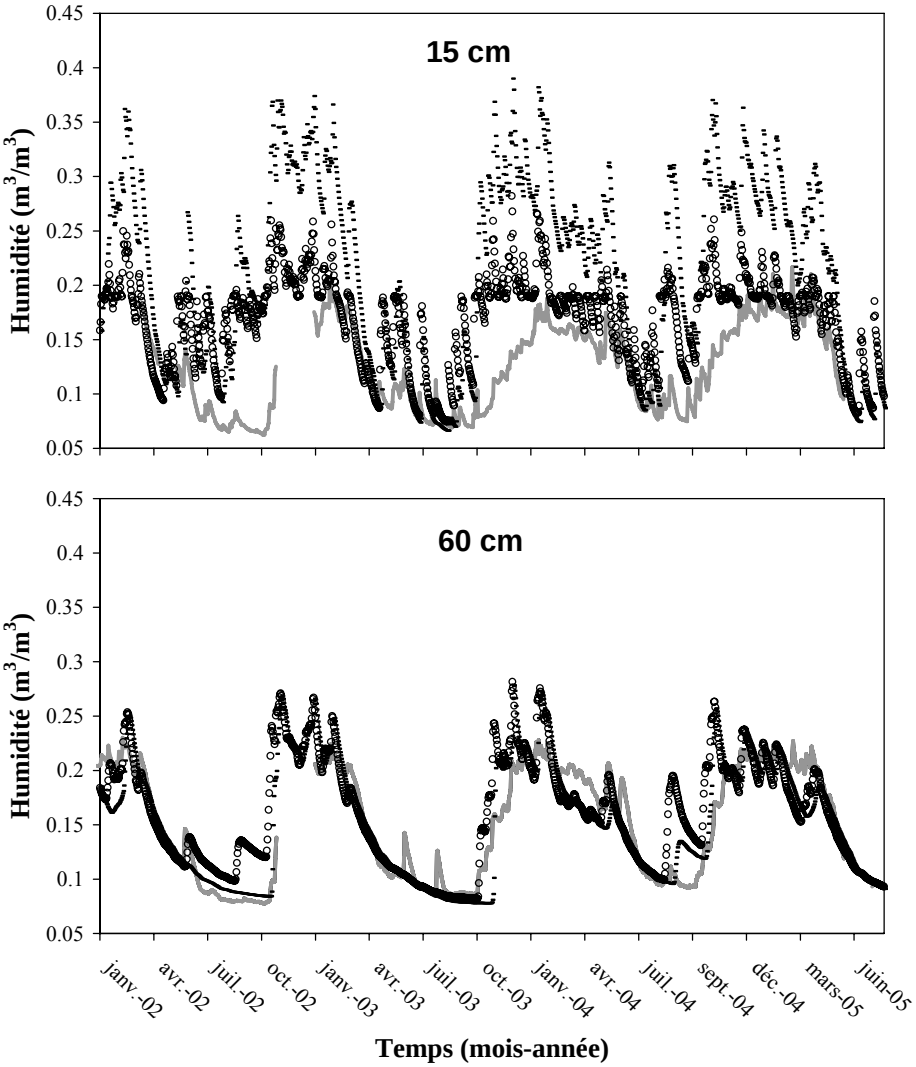

Figure 24. Comparaison entre les mesures et les simulations de l'humidité moyenne du sol de la parcelle de Douglas du site expérimental de Breuil. Simulations réalisées en utilisant les propriétés hydrodynamiques du sol prédites par la FPT ROSETTA avec prise en compte des deux mesures d'humidité. Trait gris : mesures TDR ; petits rectangles noirs : sans écoulements préférentiels ; cercles : avec prise en compte des écoulements préférentiels.

5. Cycle biogéochimique du silicium

L'ensemble des recherches réalisées sur le site expérimental de Vauxrenard constituait une base pour la modélisation mécaniste du cycle biogéochimique de Al et de Si par le modèle MIN3P. En effet, les mécanismes contrôlant la mobilité de Al^{3+} et de Si ont été précisés au cours de l'étude de leur spéciation et des interactions avec la phase solide (**Gérard et al., 2001, 2002, 2003**). Les transferts de l'eau dans le sol du site ont également été modélisés avec succès (**Gérard et al., 2004, 2006**).

J'ai décidé de m'intéresser au cycle de Si plutôt qu'à celui de Al pour les raisons suivantes :

- une *spéciation aqueuse simple,* essentiellement réduite à l'espèce $H_4SiO_4°$. La spéciation de Al est quand à elle beaucoup plus complexe, car non réduite à la seule espèce Al^{3+} du fait de la présence de nombreux ligands organiques et inorganiques. Dans ces conditions, une modélisation ciblant Al imposerait de considérer les mécanismes contrôlant la concentration des différents ligands, et en particulier celle du COD (et de sa spéciation). De plus, la spéciation de Al étant fortement dépendante du pH, il serait également nécessaire de modéliser le cycle des protons afin de simuler le cycle de Al.
- La *relative simplicité du mécanisme contrôlant Si* dans les solutions capillaires : la dissolution (loin de l'équilibre) du feldspath potassique, comparé à Al^{3+} dont la mobilité devrait être contrôlée par deux mécanismes : l'adsorption avec la MOS et la néoformation d'hydroxydes d'Al.
- La *neutralité de Si en solution*, évitant ainsi l'éventualité de la question sur la nature de la réaction d'absorption équilibrant les charges.
- L'*importance du cycle de Si pour l'altération des silicates primaires*, qui est un processus important en sol acide soumis à de faibles intrants car il constitue l'une des seules sources d'éléments nutritifs.
- La *méconnaissance du cycle biogéochimique de Si dans les écosystèmes terrestres*, particulièrement en climat tempéré et dans les écosystèmes forestiers, malgré son importance à l'échelle globale (e.g. Meunier, 2003).

La modélisation du cycle de Si a débuté par d'élaboration d'un premier modèle conceptuel (Figure 25). Il est basé sur l'identification des mécanismes géochimiques contrôlant cet élément, sur la modélisation des transferts de l'eau et sur l'hypothèse communément répandue du non prélèvement significatif de Si par le Douglas.

Le consensus existant sur l'absence d'un prélèvement de Si par le Douglas avait justifié le non dosage de cet élément dans la biomasse. En l'absence d'un retour au sol de Si par les chutes de litière, Si mesurée dans les solutions collectées sous la litière (cf. Figure 17) devrait être issue de la dissolution des silicates du sol apportés dans l'horizon organique par bioturbation (Figure 25).

La validité de ce premier modèle conceptuel, limitant donc le cycle biogéochimique de Si à sa composante géochimique, a été testée en confrontant les résultats de simulations couplées géochimie-transfert aux concentrations mesurées. Les mesures réalisées dans les solutions capillaires faiblement liées ont été utilisées, puisqu'elles constituaient une base de données très importante (pluriannuelle) et donc idéale pour confronter le modèle à la réalité. Dans ce type de solution du sol, les précédents travaux avaient montré que la concentration en Si était contrôlée par la dissolution du feldspath-K, procédant loin de l'équilibre et dont la cinétique était principalement affectée par la température du sol (**Gérard et al., 2002, 2003**).

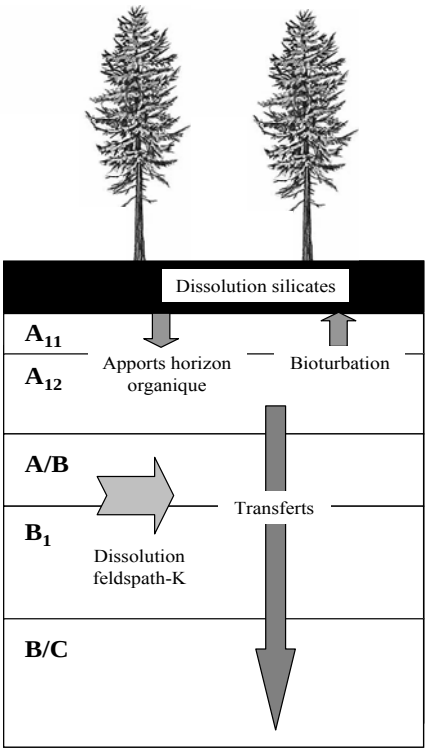

Figure 25. Premier modèle conceptuel du cycle de Si dans le site de Vauxrenard. Le non prélèvement de Si par le Douglas y est considéré.

Concernant les transferts de l'eau, les simulations couplées ont été effectuées en considérant les mêmes conditions et paramètres que dans l'étude préliminaire. Les concentrations mesurées quasi quotidiennement (partiteur) dans la solution collectée sous la litière (cf. Figure 17) ont été considérées en entrée du profil de sol, ainsi que les valeurs journalière de la température du sol mesurées sous la litière (0 cm) et à 15, 30, 60 et 120 cm de profondeur (Figure 26).

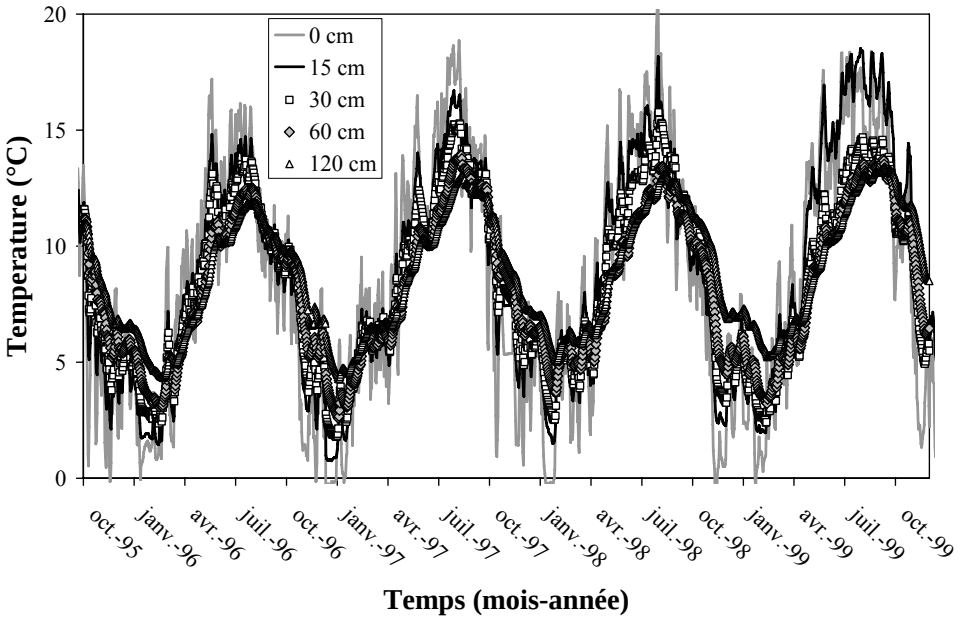

Figure 26. Températures mesurées à différentes profondeurs du sol du site de Vauxrenard, considérées dans le modèle MIN3P afin de simuler la concentration de Si mesurées dans les solutions capillaires faiblement liées.

Ces valeurs ponctuelles de température sont extrapolées linéairement dans l'espace afin de tenir compte en modélisation des effets d'un gradient de température. Les effets de la température sur la cinétique de dissolution sont pris en compte par la loi d'Arrhénius faisant intervenir une énergie d'activation apparente de réaction.

Les simulations couplées géochimie-transfert ont rapidement montré l'invalidité du premier modèle conceptuel, du fait de la présence de pics de concentration beaucoup trop importants. Ces pics sont causés par le processus de transpiration excluant le prélèvement de Si, et donc concentrant cet élément dans le milieu. Le résultat à 15 cm de profondeur est donné Figure (27) à titre d'exemple.

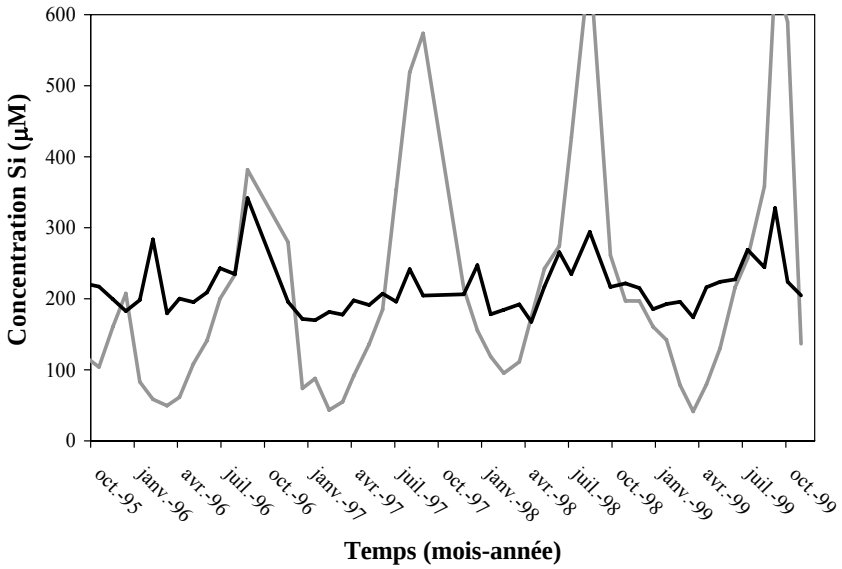

Figure 27. Comparaison entre les concentrations moyennes mesurées et simulées selon le premier modèle conceptuel, c'est-à-dire en excluant le prélèvement de Si par la végétation (cf. Figure 25).

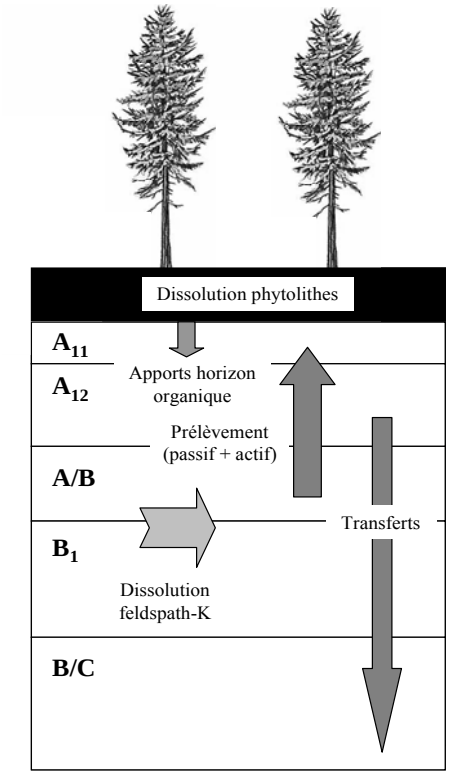

Figure 28. Second modèle conceptuel du du cycle de Si dans le site de Vauxrenard, considérant la présence d'un prélèvement (passif et actif) de Si par le Douglas

Les résultats illustrent aussi le fait que l'effet concentration du non prélèvement de Si par la végétation ne permet pas expliquer les variations constatées sur le terrain. L'ajout d'une dissolution du feldspath-K à cette simulation provoque une augmentation encore plus importante des pics de concentration, même si les points bas (obtenus en hiver, quand la transpiration est minimale) peuvent arriver à des niveaux conformes aux mesures.

Etant donné cet échec, il a été nécessaire d'introduire le prélèvement de Si par la forêt de Douglas dans le modèle conceptuel (Figure 28). Les fondements et les résultats de la modélisation correspondante sont détaillés dans une publication soumise à *Geochimica Cosmochimica Acta* **(Gérard et al., 2008)**. Les résultats obtenus sont bons (Figure 29), et valident donc ce modèle conceptuel, puisqu'il a été possible de reproduire avec précision (environ de 10% de Normalized Root Mean Square Error) les mesures de concentration en Si dans les solutions capillaires faiblement liées.

A l'image de l'application consacrée aux transferts hydriques, qui a rendu nécessaire l'introduction des écoulements préférentiels, la révision du modèle conceptuel pour le cycle de Si a imposé un nouveau retour aux développements numériques de MIN3P. En effet, il a fallut modifier les équations contrôlant le transfert des solutés afin de prendre en compte le prélèvement passif des solutés. Ce travail de développement numérique a été réalisé en collaboration avec H.W. Kim, un étudiant coréen en formation postdoctorale. La méthode a consisté à introduire un terme puits dans l'équation de transfert des solutés :

$$\frac{\partial}{\partial t}\left(S_a \phi T_j^a\right) = \nabla.\left(S_a \phi D_a \nabla T_j^a\right) - \nabla.\left(\nu T_j^a\right) - R_j - q T_j^a \qquad (2)$$

avec S_a la saturation en eau, ϕ la porosité, T_j^a la concentration totale de l'élément chimique j (mol L^{-1}), v la vitesse de Darcy (m s^{-1}), D_a le coefficient de dispersion hydrodynamique (m^2 s^{-1}), R_j est le terme source/puits des réactions cinétiques (mol L^{-1} s^{-1}) et q est le flux d'eau prélevé par la végétation (s^{-1}).

La possibilité d'un prélèvement actif de Si par la végétation a également été incluse dans le modèle conceptuel. La présence de ce mécanisme de prélèvement est indiquée par la diminution des concentrations en Si en fonction de la profondeur du sol (Figure 30), qui ne peut être expliquée par des néoformations. Ce mécanisme de prélèvement a été modélisé de manière classique, à l'aide d'une loi cinétique de type Monod. L'utilisation de ce type de loi était possible via la loi cinétique générale utilisée dans MIN3P (Mayer et al., 2002).

Des analyses de Si dans les différents compartiments de la biomasse sur pied et restituée sous forme de litière au sol ont du être réalisées. Les mesures de Si dans la biomasse, se présentant sous forme d'opale communément appelée *phytolithe*, ont été réalisées dans un laboratoire étranger, celui de M. Hodson (Oxford-Brookes University), spécialiste de Si dans les végétaux. Connaissant les flux et stocks des différents compartiments de la biomasse, le flux de Si prélevé annuellement a été calculé : 157 mmol m^{-2} an^{-1} (~ 44 kg ha^{-1} an^{-1}). Cette valeur est élevée comparée aux valeurs disponibles pour des écosystèmes forestiers équivalents (Bartoli and Souchier, 1978; Bartoli, 1983). Ce flux est de l'ordre de ceux calculé plus récemment pour des écosystèmes forestiers situé sous les tropiques (e.g. Lucas, 2001). Il apparaît également qu'environ 90% du flux prélevé par le Douglas est recyclé au sol par le biais des chutes de litière. L'importance de ce chiffre suggère que la concentration de Si dans les solutions collectées sous l'horizon organique devrait principalement provenir de la dissolution des phytolithes. D'autres arguments confirment cette considération (**Gérard et al., 2008**).

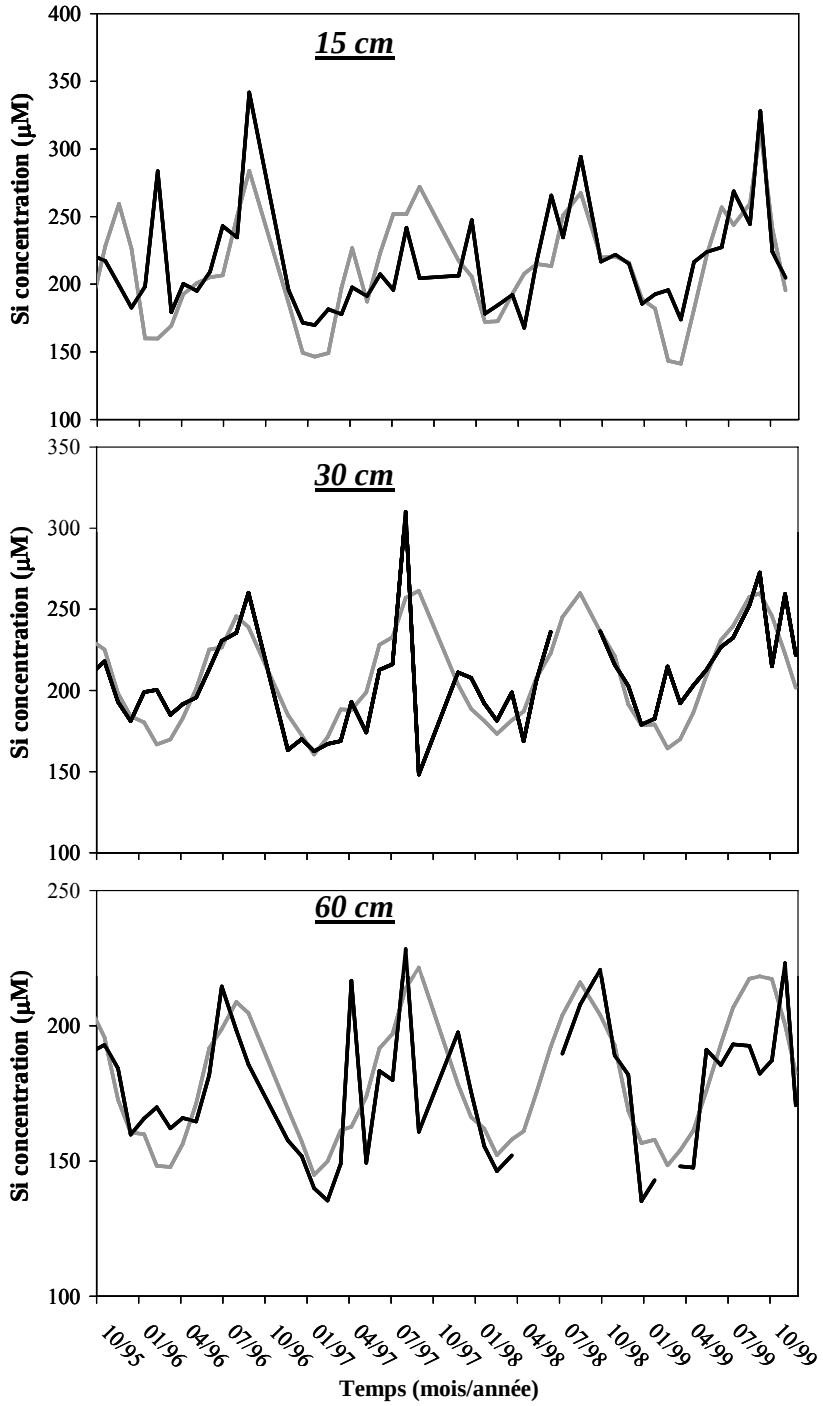

Figure 29. Comparaison entre la concentration moyenne mesurée et simulée par le modèle MIN3P. Résultats obtenus en considérant le modèle conceptuel incluant un prélèvement de Si par le Douglas (cf. Figure 28).

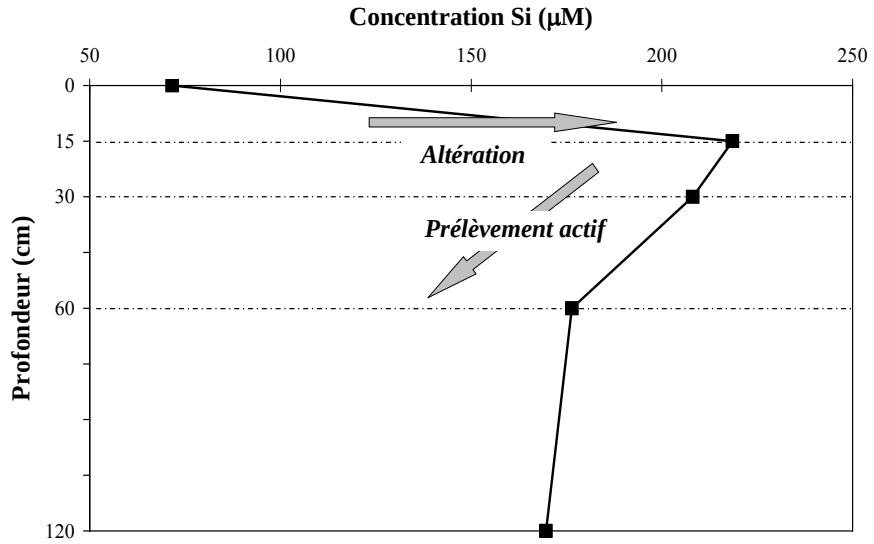

Figure 30. Variations de la concentration moyenne en Si en fonction de la profondeur du sol, et interprétation des mécanismes contrôlant ces variations.

Les analyses de Si dans la biomasse fournissent deux arguments allant dans le sens d'un prélèvement actif de Si par le Douglas. Ces arguments sont basés des travaux en agronomie (Ma and Takahashi, 2002), étant donné le déficit de connaissances concernant les plantes ligneuses. Le premier argument est la concentration élevée de Si mesurée dans les feuilles des Douglas, impliquant le classement de cette espèce en tant que plante hyper-accumulatrice, comme le riz et le blé, reconnues depuis longtemps pour leur capacité à prélever activement Si. Le second argument est une teneur en Si plus élevée que celle du calcium, toujours dans les feuilles. Enfin, un troisième argument a été fourni par les résultats de la modélisation couplée. En effet, il apparaît que le flux de Si prélevé de manière passive par la forêt de Douglas, qui est contraint par le flux de transpiratoire et la concentration de Si dans les solutions (cf. Eqn. 2), n'est pas suffisant pour couvrir le flux calculé à partir des analyses et des flux de biomasse. L'ajout d'un terme actif était donc nécessaire pour répondre à ce critère et donc réaliser une modélisation cohérente.

Cette première modélisation mécaniste du cycle biogéochimique de Si a permis de quantifier les flux associés aux différents processus contrôlant Si (Figure 31). Si l'on tient compte des incertitudes régnant sur ces flux, les résultats indiquent que la contribution du cycle biologique au cycle biogéochimique de Si est au moins équivalent à celle du cycle géochimique (**Gérard et al., 2008**).

L'importance de la composante biologique ne signifie pas nécessairement que Si dans les eaux de surface doit être affectée par ces processus plutôt que par l'altération des silicates, puisque les résultats concernent l'échelle du profile de sol. A une échelle supérieure, à celle du bassin versant, le processus contrôlant Si dépendra notamment du temps des résidence des solutions et de leur trajets dans le sous-sol.

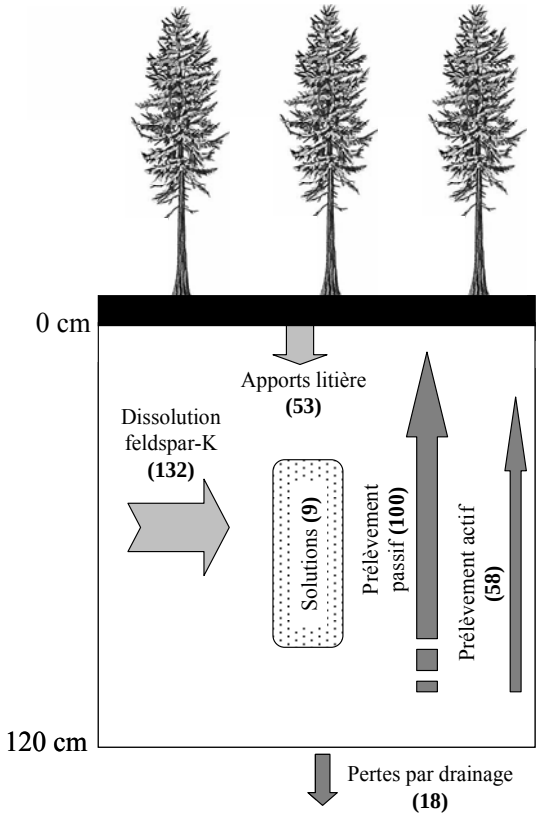

Figure 31. Flux contrôlant le cycle biogéochimique de Si dans l'écosystème de Vauxrenard (Douglas, climat tempéré, sol acide). Les valeurs entre parenthèses sont exprimées en mmol m^{-2} an^{-1}.

6. Conclusions et perspectives

Concernant toujours le cycle de Si, les travaux précurseurs de F. Bartoli et collaborateurs (Bartoli and Souchier, 1978; Bartoli, 1981, 1983) avaient abouti à des résultats similaires pour un écosystème forestier tempéré sur sol acide composé d'un mélange de feuillus (hêtre) et de conifères (sapins). Sous feuillus uniquement (hêtre), ces auteurs ont calculés que le cycle biologique était très supérieur au cycle géochimique, à l'image des résultats trouvés dans les forêts tropicales (Alexandre et al., 1997; Meunier et al., 1999). Sous pins par contre, Bartoli (1983) a trouvé que l'altération prédominait. Ces premiers travaux des années 80, trop longtemps oubliés, ainsi que le présent travail (qui a eu au moins le mérite de les réactiver), devraient être approfondis avec les outils d'aujourd'hui, tant analytiques que numériques. Des situations et des échelles variées peuvent être étudiées à l'aide du modèle MIN3P, en tenant compte ou non des minéraux secondaires, sous différents couverts végétaux, etc. De telles études devraient contribuer à une meilleure connaissance de la dynamique de Si et de l'altération des silicates en milieu continental.

Les résultats de la modélisation du cycle biogéochimique de Si viennent quelque peu mettre à mal ceux obtenus au travers de l'étude des solutions du sol (statistiques, modélisation de la spéciation, diagrammes d'activité), à partir desquels il avait été conclu au contrôle de Si dans les solutions capillaires par l'altération des silicates primaires. Or, la modélisation couplée a permis de montrer une influence au moins équivalente de la biologie. Cependant, l'apparent contrôle de l'altération sur la concentration de Si provient du fait que le principal mécanisme de prélèvement de Si est passif (cf. Figure 31). En effet, ce mécanisme n'altère pas les concentrations. Les variations saisonnières observées dans les solutions capillaires faiblement liées étaient effectivement provoquées par la dissolution des silicates primaires, mais ont été conservées malgré l'importance de la biologie sur cette dynamique. L'application du modèle MIN3P au cycle biogéochimique de Si illustre bien l'intérêt d'une modélisation couplée des processus, permettant de valider des modèles conceptuels de fonctionnement biogéochimique du sol, de quantifier les flux et d'en obtenir des informations sur les processus dominants. Cependant, de nombreuses étapes sont nécessaire afin d'atteindre rigoureusement ce stade d'application de MIN3P. Il s'agit d'abord de préciser les mécanismes géochimiques affectant la dynamique des solutés, puis de simuler les transferts de l'eau, d'en élaborer un modèle conceptuel qui seulement ensuite sera testé, éventuellement ajusté (y compris le modèle numérique) et enfin seulement une quantification est possible.

Le lecteur attentif aura remarqué l'absence de modélisation couplée ciblant la composition chimique des autres types de solutions de sol, c'est-à-dire des solutions capillaires fortement liées (solutions « réactives ») et des solutions gravitaires. Cela reste à faire, en effet. Comme l'indique également les résultats obtenus dans le site de Breuil pour le contrôle de Al^{3+} selon le type de solution de sol, il sera nécessaire de développer les possibilités de MIN3P de prendre en compte l'existence de plusieurs sous milieux dans la porosité totale du sol, où prennent place des processus de nature ou d'intensité différentes.

Pour finir, quelques mots sur mes travaux dédiés à la qualité du COD et la modélisation de la spéciation des cations à l'aide des modèles WHAM-VI ou NICA-Donnan. Les problèmes de paramétrisation peuvent paraître impressionnants, ainsi que les différentes manière de calibrer le modèle selon les données disponibles. Cependant, il faut avoir conscience du fait que l'objectif des diverses calibrations effectuées n'était pas limité aux calculs de la spéciation des métaux. En effet, leur but était aussi d'en déterminer des

variables difficilement mesurables, voir non mesurables dans une solution du sol, comme la concentration en substances humiques ou la densité des sites complexant. Des valeurs moyennes peuvent ainsi en être calculées ainsi qu'une idée de la variabilité. Ces valeurs pourraient être ultérieurement utilisées dans le modèle en ne disposant pas mesures de spéciation mais tout en assurant une relative précision des résultats. Il serait donc important de répéter la démarche dans des écosystèmes identiques, à des fins d'évaluation de la pertinence des résultats présents, et sur des écosystèmes différents dans le but de généraliser l'information et d'utiliser plus facilement les modèles.

PROJET

Préambule

Mes activités de recherche et d'encadrement devraient continuer à concerner l'étude, par la modélisation, des processus biogéochimiques couplés ou non aux processus de transfert. L'utilisation en amont de modèles spécifiques à certains processus, aux processus géochimiques en particulier, devrait être poursuivie, dans l'objectif d'aider à l'étude d'un processus spécifique et à hiérarchiser les mécanismes. Ces connaissances sont nécessaires pour optimiser les modifications du modèle couplé et pouvoir raisonnablement l'appliquer à un système naturel.

Je n'envisage pas d'opérer un tournant radical dans la nature de mes activités. Cependant, le contexte Montpelliérain justifie l'ouverture du contenu à de nouveaux objets d'étude, aussi bien en terme de type de sol que d'échelle ou bien encore d'espèce végétale.

Les thèmes de recherche que je souhaite conduire s'inscrivent dans l'objectif général d'une meilleure prise en compte des processus biologiques en modélisation géochimique. L'élément « modèle » devrait être phosphore (P). Les plantes « modèles » pourront être aussi bien forestières que de grande culture. Les sols seront d'abord méditerranéens et tropicaux, étant donné le contexte. L'étude plus ponctuelle de sols tempérés est possible à des fins de connaissances des processus.

Mes activités de recherche et d'encadrement auront pour objectifs d'identifier et de modéliser les processus et les mécanismes contrôlant (i) *la biodisponibilité* et (ii) *la disponibilité environnementale* de P. Ces deux critères de qualité des sols et de risques associés au lessivage de P seront désormais désignés sous le terme de *disponibilité de P*.

La disponibilité de P est proportionnelle à la concentration des formes inorganiques de cet élément, notées Pi. La différence P – Pi correspond aux formes organiques du P, regroupées sous le terme de Po. Les concentrations des différentes formes du P, dans la rhizosphère et dans le sol en général, sont contrôlées par de nombreux processus (Figure 32).

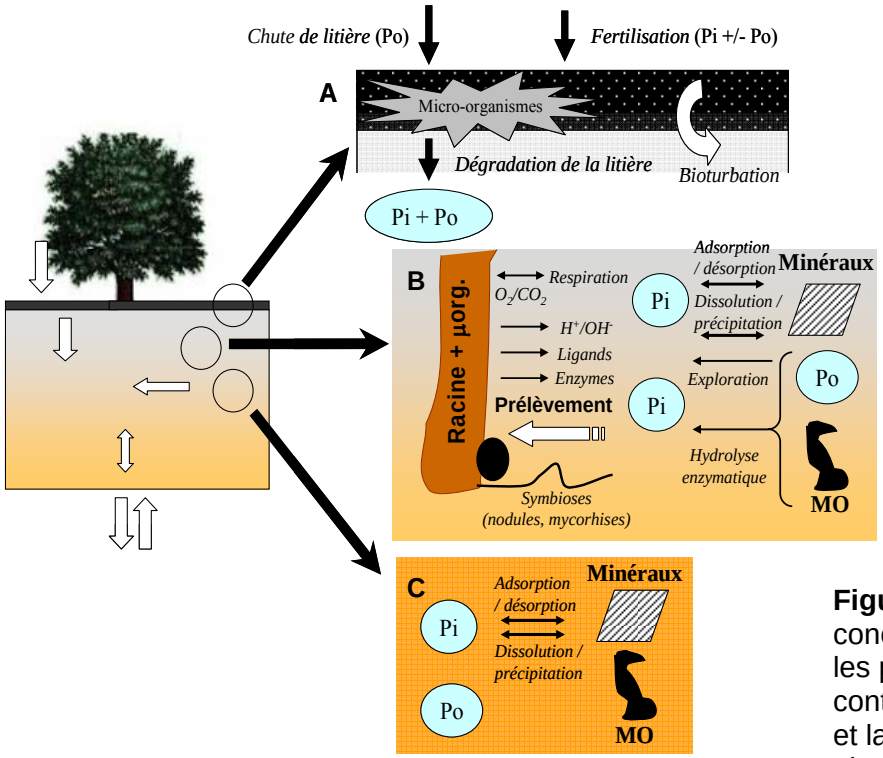

Figure 32. Schéma conceptuel représentant les principaux processus contrôlant la concentration et la spéciation du phosphore dans un écosystème terrestre.

Le *développement de techniques analytiques* soutiendra mes activités. Ces techniques seront sélectionnées selon leur aide pour une meilleure connaissance des processus et des mécanismes. Le but est d'améliorer la fiabilité de la modélisation. Les travaux de modélisation que je souhaite diriger seront en priorité appliqués au *milieu sol*, dans toute sa complexité, notamment en ce qui concerne l'hétérogénéité de ses constituants et la diversité des processus.

Des données acquises à différentes échelles de temps et d'espace soutiendront également mes travaux, qui se dérouleront de l'échelle *de l'échantillon à celle du profil de sol*. L'échelle de l'échantillon, au laboratoire, sera l'objet de mes premiers travaux sur le P, car la compétence expérimentale est disponible localement. Les travaux sur le terrain pourront trouver comme cadre le site du « chantier Méditerranée », devant être mis en place par la nouvelle UMR. Des travaux dans les sites forestiers du CIRAD et de l'INRA sont également possibles au travers des projets ou le co-encadrement d'étudiants et de chercheurs en formation.

Plusieurs *axes de recherches et de développement* seront donc poursuivis dans l'objectif principal de **modéliser la disponibilité du P à différentes échelles de temps et d'espace**. Brièvement, les axes envisagés portent sur :

A. Les processus géochimiques. L'objectif sera d'abord de déterminer les processus géochimiques contrôlant la disponibilité du Pi, c'est-à-dire sa concentration en solution. Les processus d'adsorption jouent souvent un rôle central. Ils seront particulièrement étudiés. La modélisation géochimique sera utilisée afin d'étudier ce processus dans le sol. Ces travaux s'appuieront sur des *expériences visant à mimer l'effet de la présence d'une plante* sur la concentration en Pi, qui sera issue de différentes extractions utilisées comme indicateur de disponibilité de P. Je prévois également de *manipuler d'autres facteurs* comme le type de sol, la température, la salinité, ou bien encore les intrants, afin de vérifier et améliorer la généricité de nos connaissances et de l'approche. Selon la correspondance « mesures-modélisation » obtenue, les mécanismes géochimiques pourront être déterminés. En appliquant l'approche à des expériences réalisées en présence de plantes, il devrait aussi être possible d'évaluer les effets de processus biologiques sur la dynamique du P. L'étude des mécanismes géochimiques contrôlant la disponibilité de P doit être accompagnée en second plan par celle d'éléments majeurs tels que Al, Si, Fe, Ca (selon le pH), pour les cations, et SO_4^{2-}, CO_3^{2-}/CO_2 et O_2 pour les anions et les gaz. Des travaux seront également engagés sur ces éléments, en particulier Al et Si.

B. Les processus biologiques. L'échelle des études qui seront conduites dans cet axe se veut résolument celle du laboratoire, à l'image de l'axe précédent consacré à la géochimie. De nombreux processus biologiques peuvent *affecter directement* la disponibilité de P (Figure 32). Cet axe concerne plus particulièrement les processus d'hydrolyse enzymatique, d'immobilisation ou de solubilisation de Pi liée à l'activité des microorganismes symbiotiques ou non (bactéries, mycorhize, nodule fixateur de N_2), et enfin les changements de disponibilité induits par l'activité de la macrofaune. Je compte particulièrement m'appuyer sur les travaux des collègues de l'UMR pour la modélisation de ces processus. Pour leur couplage, une *approche modulaire* sera privilégiée, en particulier pour la prise en compte de l'architecture racinaire (exploration) et des effets de la macrofaune (vers de terre) sur les processus affectant la disponibilité de P. L'intégration d'un processus biologique au modèle MIN3P ouvre la voie à son étude couplée aux processus géochimiques et aux processus transferts. Les développements de la modélisation dans ce domaine

devraient s'*accompagner d'expériences permettant d'évaluer, de caler, et de valider les modèles*.

C. ***Le Cycle de C, N et de P.*** De nombreux modèles permettent de simuler le cycle de ces éléments dans les systèmes sol-plante. Très peu d'entre eux cependant permettent le couplage de ces trois cycles. Des clés pour le couplage en modélisation des cycles de C, N et de P sont proposées. Des développements significatifs du modèle MIN3P seront nécessaires, mais ils permettront d'améliorer très fortement la manière dont les processus géochimiques, les processus de transferts, et certains processus biologiques, sont considérés en modélisant le cycle de C, N et de P. Cet axe concerne également les processus *affectant indirectement la disponibilité de P*. Le processus de « priming effect » sera particulièrement visé, du fait de son importance et des compétences locales. Ce travail inclura une première phase d'étude des mécanismes responsables du couplage entre le « priming effect » et la géochimie du sol.

D. ***Le transfert des gaz.*** Dans ce domaine, mes travaux porteront sur l'amélioration de la prise en compte du transfert des gaz dans le sol en modélisation couplée. La dynamique des gaz est importante pour de nombreux processus biologiques et géochimiques affectant directement ou indirectement la disponibilité de P. Des applications de terrain sont prévues, notamment sur la thématique des *gaz à effet de serre*, où il sera possible d'étudier le couplage des transferts gazeux aux processus biologiques, microbiologiques et aux transferts hydriques.

E. ***Les mesures et expérimentations.*** Un ensemble de mesures physico-chimiques sera mis en place afin de répondre à l'objectif principal de mon projet de recherche et d'encadrement. Beaucoup des mesures prévues peuvent être réalisées en routine (extractions, chimie de l'eau). D'autres sont plus pointues ou plus lourdes, par exemple l'isotopie du P, la micro-fluorescence X ou bien encore la diffractométrie X. Leur utilisation devra faire appel à des collaborations à l'extérieur du laboratoire. Concernant les expérimentations, les techniques d'étude des interactions sol-plante et de physiologie de la plante sont bien maîtrisées dans l'Unité. Le terrain sera fourni par la mise en place d'un site autour de cette structure, et il pourra l'être au travers des collaborations avec le CIRAD et l'INRA.

F. ***La diffusion vers l'extérieur.*** L'objectif est de diffuser le modèle auprès d'un nombre plus important d'utilisateurs. A cette fin, il est prévu de l'équiper rapidement d'une interface d'entrée «user-friendly ». La diffusion de son utilisation devrait pouvoir se réaliser au travers de l'enseignement universitaire et de formations permanentes.

A. Processus géochimiques

Dans une première étape une approche physico-chimique sera développée afin de tenter de simuler la disponibilité environnementale du P dans un sol. La disponibilité de cet élément sera appréhendée au travers des *indicateurs utilisés couramment en écologie et en agronomie* : extractions à l'eau, au $CaCl_2$, méthode Olsen.

Cet axe de recherche apportera l'essentiel des travaux expérimentaux que je compte diriger. Leur contenu, associé à la présentation d'autres travaux, constitue un axe détaillé par la suite.

Brièvement, les sols étudiés devront être caractérisés au niveau de leur minéralogie, texture, quantité et qualité de la matière organique. Des extractions du P du sol seront d'abord réalisées sur des sols au sein desquels *les effets biologiques sont réduits au minimum* (i.e. sans contact avec des plantes, éventuellement stérilisés), afin de limiter les processus affectant la disponibilité de P aux seuls processus géochimiques. Les modélisations géochimiques seront utilisées pour simuler les concentrations de P extraites ou directement mesurées dans l'eau du sol. Les avancées théoriques dans le domaine de la géochimie des environnements de surface permettent à certains modèles géochimiques de simuler rigoureusement, c'est-à-dire de manière mécaniste, les processus d'adsorption et de dissolution-précipitation. Ces outils géochimiques seront utilisés et les paramètres génériques issus de la littérature et des bases de données des modèles pourront également être utilisées pour la paramétrisation des simulations.

Selon les succès et les échecs de la modélisation, confinée donc pour l'instant à des systèmes essentiellement géochimiques, il devrait être possible de :

- ⇨ comprendre le *déterminisme des indicateurs* de disponibilité du P, c'est-à-dire de préciser la nature des processus et des mécanismes géochimiques contrôlant la concentration en Pi extraite selon ces méthodes très populaires;

- ⇨ de *hiérarchiser* les processus et mécanismes, en vue de simplifier la modélisation ;

- ⇨ de *prévoir* Pi dans des conditions physico-chimiques changeantes (variations de pH, de température, de salinité).

En filigrane aux expérimentations et aux modélisations qui seront conduites afin de réaliser les objectifs précédents, des confrontations mesures-modèle seront effectuées dans des expérimentations beaucoup plus complexes, car réalisées *en présence de plantes*. Les résultats permettront de mettre en évidence l'influence d'autres processus, en particulier des processus biologiques. Il devrait donc être possible par ce type de travaux de « peser » le poids relatif de la géochimie et de la biologie dans le déterminisme de la disponibilité de P. Les travaux réalisés dans le cadre du stage de M2 de N. Devau illustrent bien la philosophie de l'approche envisagée (Devau, 2007; Devau et al., 2008). De premiers résultats très prometteurs ont été obtenus dans le cadre de son stage de M2 (Figure 33).

Les résultats de cette première phase de modélisation devront être intégrés dans le modèle couplé MIN3P. Une étape intermédiaire de *comparaison entre les résultats des modèles géochimiques et ceux de MIN3P* devra être réalisée. En effet, le modèle MIN3P est fondamentalement moins complet en ce qui concerne les processus d'adsorption que ne l'est un modèle géochimique spécialisé. Le modèle MIN3P ne tient pas compte de l'existence d'une couche diffuse à la surface de solides en contact avec de l'eau. Dans ces conditions, les réactions ne se produisent que sur un seul plan : la surface du solide, et cela à des

conséquence sur les quantités adsorbées. L'intérêt est la diminution du nombre de variables à résoudre, atténuant ainsi la lourdeur des calculs du modèle. Cependant, le modèle MIN3P n'apparaît pas nécessairement moins précis dans une situation donnée. Ses bases sont fondamentalement identiques à celles des modèles géochimiques. Les constantes d'équilibre des réactions pourraient être calibrées afin de compenser les effets de la couche diffuse. Selon les résultats de la comparaison entre MIN3P et le modèle géochimique, il pourrait être rapidement nécessaire de le modifier de manière significative, ce que réclame l'introduction d'un formalisme plus complexe pour l'adsorption dans MIN3P.

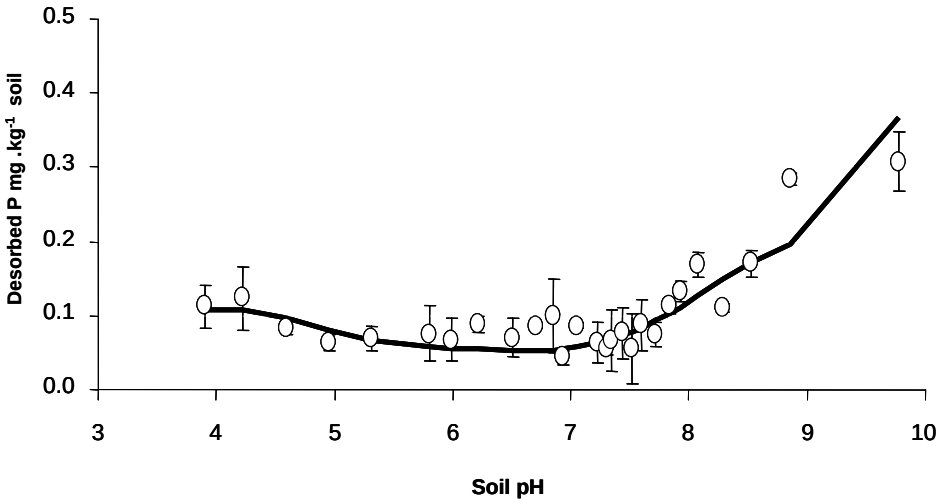

Figure 33. Comparaison mesure-modélisation des concentrations en P inorganique extraites par $CaCl_2$ dans l'horizon de surface d'un Cambisol (0-20 cm) (fersialitique, pH neutre) (Devau, 2007). Les symboles blancs correspondent aux mesures, le trait continu à la modélisation.

L'étude des processus géochimiques affectant la disponibilité de P doit être associée en second plan à celle d'éléments majeurs tels que Al, Si, Fe, Ca (selon le pH), pour les cations, et SO_4^{2-}, CO_3^{2-}/CO_2 et O_2 pour les anions et les gaz. La dynamique de ces solutés et de ces gaz peut avoir un effet important sur celle du P dans le sol. Parmi ces éléments minéraux, une attention particulière sera placée sur les cycles de Si et de Al, importants à différents titres, et s'inscrivant dans la continuité de mes travaux nancéiens.

Outre la perspective d'une meilleure valorisation de mon travail sur la dynamique de Al, je prévois *à moyen terme* de poursuivre mes travaux dans le domaine du cycle biogéochimique de Si. Ce cycle est connecté au cycle du C du fait de l'influence des allophanes (andosols) et des phytolithes dans la séquestration du carbone. Un autre intérêt de Si provient de l'influence des allophanes sur l'adsorption du P, et du rôle de compétiteur de Si pour l'adsorption de P par les oxydes métalliques (Gustafsson, 2001). Sur le terrain, mes travaux sur le cycle de Si pourront se dérouler *via* la poursuite de ma collaboration avec le CEREGE (J.-D. Meunier) sur les herbacées cultivées, et/ou avec l'INRA de Nancy (J. Ranger) sur les plantations forestières sous climat tempéré, et/ou sur des sites IRD (où la thématique du couplage Si-C s'avérerait pertinente). Etant donné l'importance du cycle de Si, des opportunités devraient se présenter à l'échelle européenne, par exemple avec le groupe dédié à cet élément, récemment mis en place en Allemagne (Sommer et al., Bayreuth).

En outre, des applications sur les éléments minéraux pourraient se présenter selon les problématiques des sites du chantier Méditerranée de la future UMR avec Seqbio. Par exemple, des recherches visant le cycle et la toxicité de Al sont envisageables (sols acides, tropicaux en particulier), ou bien encore la problématique du cuivre dans les anciens terrains viticoles de la région Languedoc-Roussillon.

B. Processus biologiques

La réalisation du premier axe de recherche aura donc permis la modélisation de la disponibilité environnementale de P. Son rôle sera aussi de préciser l'importance des processus biologiques comparés aux processus géochimiques.

Le premier objectif de cet axe sur les processus biologiques sera d'appliquer le modèle MIN3P à des expériences d'interaction sol-plante du type *culture en pot*. Le couplage d'un module dit « plante entière » sera nécessaire selon l'échelle de temps considérée (croissance de la plante effective ou non). Cela nécessitera de gérer les interactions entre le niveau de Pi en solution (et Pi contrôlé par les réactions, selon leur cinétique) sur la croissance de la biomasse. Les compétences en écophysiologie végétale pour le module de croissance pourront être mobilisées localement (LEPSE, CIRAD) et à l'échelle nationale (UMR EPHYSE et TCEM, INRA Bordeaux).

Les premières modélisations couplées, selon leurs résultats, guideront les modifications du modèle MIN3P. Selon les conditions, il pourrait être nécessaire de prendre en compte les micro-organismes pour leurs effets sur l'*immobilisation/solubilisation* de Pi dans la rhizosphère et la transformation du Po en Pi par *hydrolyse enzymatique*. Ma participation récente à l'école chercheurs « Modélisation et Ecologie Microbienne » de la Grande Motte (34) m'a donné la possibilité de faire le point sur les avancées dans le domaine, et de préciser un certain nombre de pistes pour de futures collaborations. Ces travaux pourront s'appuyer sur les compétences analytiques de L. Bernard, qui vient d'être recrutée par l'IRD « Seqbio », et par celles de A. Brauman (chercheur senior de la même unité) et de R. Lensi (CEFE). Coté INRA, ces travaux pourront s'appuyer sur les compétences analytiques et expérimentales de C. Plassard et de l'équipe « Protéines dans l'Environnement » (H. Quiquanpoix et al.). Coté modélisation, le campus de SupAgro Montpellier accueille une unité (Analyse de Systèmes et Biométrie) composée d'informaticiens et de mathématiciens (MIA INRA et INRIA) travaillant sur le thème. La cinétique des réactions enzymatiques pourra aussi être considérée, avec en particulier les effets du pH et de la force ionique, le tout étant étudié dans un projet innovant EA (2008) porté par E. Le Cadre et Y. Dudal.

L'activité rhizobienne des légumineuses et la disponibilité du P semblent couplées ; c'est à dire que la fixation symbiotique de N_2 est influencée par la disponibilité de P et surtout cette dernière est influencée par la fixation. Cet effet peut être provoqué par un déséquilibre du flux de protons (e.g. Schulze and Drevon, 2005; Kouas et al., 2007). Des travaux ont été engagés afin de prendre en compte la symbiose rhizobienne en tant que fonction racinaire dans le modèle MIN3P. Ils ont fait l'objet d'une proposition de stage de M1 co-encadré avec Jean-Jacques Drevon, le spécialiste du sujet de l'UMR. Ce sous thème devrait bénéficier du séjour de 6 mois d'un thésard tunisien dans le cadre d'un projet financé par le MAE (programme Utique). Les premiers objectifs seront de développer un modèle conceptuel, qui se voudra générique et mécaniste, de fonctionnement de l'interface nodule-sol en relation avec la disponibilité de P. Il conviendra également de proposer des formalismes mathématiques permettant de simuler ce fonctionnement. Après ce bilan, des expériences ciblées pourront être engagées, ainsi que des développements numériques du modèle MIN3P.

Le processus de bioturbation, induits pas exemple par les vers de terre, provoque le remaniement physique et chimique du sol. Ce sont des processus importants et plusieurs chercheurs de l'Unité Seqbio sont impliqués dans des projets de *modélisation « centrée objet »* appliquée aux vers de terre et aux microorganismes (E. Blanchard, A. Brauman, J.-L. Chotte). Les sorties de ces modèles développés à l'IRD pourraient « alimenter » le modèle MIN3P, par exemple en remettant à jour la texture du sol etc., et à l'inverse les sorties de MIN3P pourraient alimenter les modèles biologiques. En effet, de nombreux processus biologiques sont influencés par la physico-chimie du système.

Enfin, l'exploration racinaire devrait aussi faire l'objet de travaux de développement numériques de MIN3P. La prospection racinaire est un mécanisme important permettant aux plantes d'augmenter la disponibilité de P. Bien que les premières expériences seront réalisées au laboratoire en minimisant l'influence de la prospection racinaire (physiquement), l'influence de ce processus ne peut pas être ignorée dans un modèle se voulant générique et applicable au terrain.

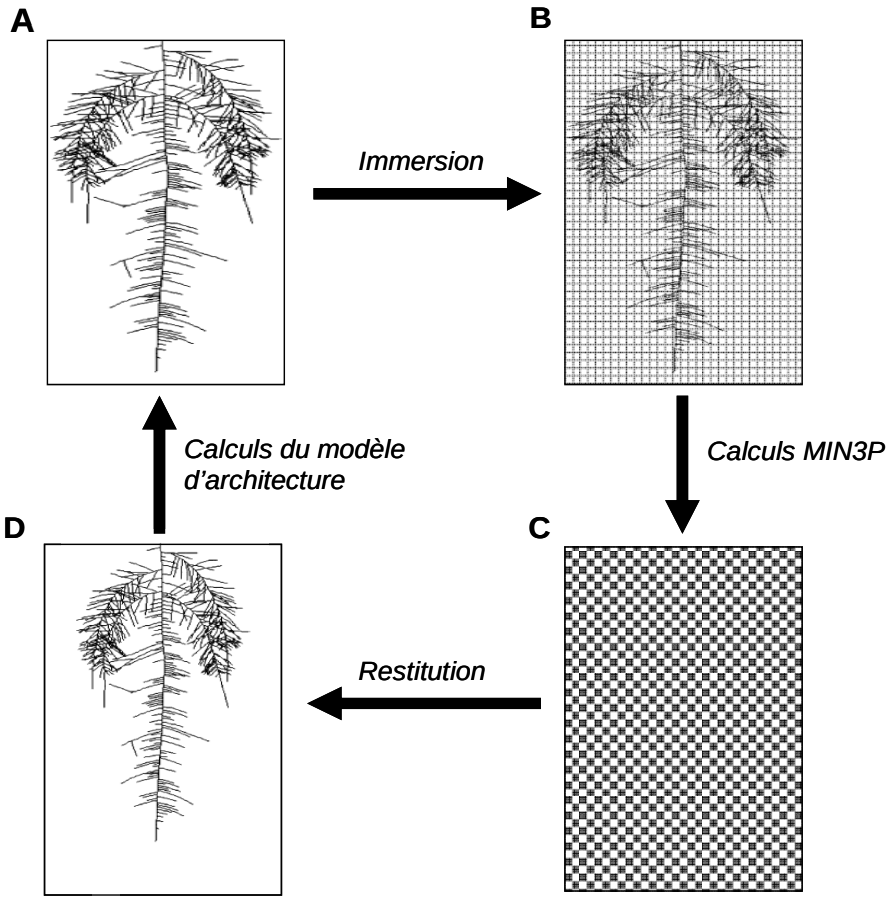

Figure 34. Représentation des principales étapes du couplage envisagé entre un modèle d'architecture et le modèle MIN3P. **A** : la géométrie du système racinaire est calculée par le modèle d'architecture au temps t. **B** : le résultat est immergé dans le maillage de MIN3P, via l'utilisation de valeurs de densités de fonctions racinaires (apex, symbioses, etc…). **C** : les transferts réactifs sont simulés par MIN3P entre t et t + Δt. **D** : les paramètres chimiques et physiques à t + Δt sont transférés au modèle d'architecture pour calculer une nouvelle géométrie du système racinaire.

Plusieurs modèles d'architecture racinaire existent (cf. synthèse de Doussan et al., 2003). Les modèles les plus performants permettent de simuler la dynamique 3D de systèmes racinaire avec une très bonne résolution. Plusieurs fonctions racinaires ont été prises en compte dans ces modèles, telles que le prélèvement de l'eau, de P et l'exsudation de composés organiques (e.g. Somma et al., 1998; Ma et al., 2001; Doussan et al., 2006; Dunbabin et al., 2006). Par contre, les interactions avec le sol sont faiblement représentées dans les modèles d'architecture racinaire. Ce manque provient certainement du nombre trop important des variables à résoudre. En effet, les modélisations de l'architecture des racines sont caractérisées par un très grand nombre de mailles ou de volumes élémentaires (voxel), nécessaire pour discrétiser suffisamment finement le domaine spatial pour aboutir à une représentation géométriquement réaliste des racines.

Je souhaite adopter l'approche inverse dans ce projet, en favorisant la modélisation des processus physico-chimique et en simplifiant la géométrie et la croissance des racines. Pour ce faire, je propose que la géométrie du système racinaire calculée par un modèle d'architecture soit « immergée » dans le maillage plus grossier de MIN3P (Figure 34). Des valeurs de densité de fonction racinaire, c'est-à-dire d'apex, de poils, de rhizobium, etc. seront calculées pour faire le lien entre les deux modèles. Les propriétés du sol calculées par MIN3P seront ensuite retournées dans le maillage plus fin du modèle d'architecture pour mettre à jours la géométrie du système racinaire. Le modèle d'architecture racinaire sera couplé au modèle MIN3P en utilisant une approche séquentielle, permettant de résoudre séparément les équations simulant l'architecture et celles pour les transferts réactifs.

De erreurs numériques seront induits par les échanges entre modèles de résolutions spatiale et temporelle différentes. Je considère que les erreurs introduites sont faibles comparées à l'erreur phénoménologique qu'induiraient la non prise en compte de l'architecture, et donc de l'exploration du système racinaire dans le modèle couplé MIN3P. De plus, il est rassurant de savoir que les échelles de temps et d'espace entre la rhizosphère et les racines sont suffisamment différentes pour que ces objets puissent être traités séparément (Darrah et al., 2006).

Le choix du modèle d'architecture racinaire à coupler à MIN3P devra se faire au regard de ses possibilités de tenir compte des variables du sol et de leurs effets sur la croissance et l'architecture du système racinaire. Certains modèles utilisent des fonctions de densité de traits morphologiques des racines afin de simuler la géométrie du système racinaire (e.g. Dupuy et al., 2005). Cependant, l'influence des propriétés physiques et chimiques locales du sol n'y est pas considérée. Le modèle de Doussan et al. (2006) est spécialisé dans les transferts hydriques, la géométrie du système racinaire est statique et non influencée par l'humidité locale du milieu. Le modèle SimRoot (e.g. Ma et al., 2001) ne semble également pas permettre le couplage géométrie-variables du sol, bien qu'il soit possible de tenir compte des effets de compétition induits par le système racinaire d'autres plantes (Rubio et al., 2001). Somma et al. (1998) proposèrent le premier modèle d'architecture possédant la possibilité de tenir compte d'un couplage avec plusieurs variables du sol, telles que l'humidité et la concentration en nutriments. Développé plus récemment, le modèle RootMap permet de tenir compte d'effets de la disponibilité locale des nutriments sur l'architecture du système racinaire (Dunbabin et al., 2002; Dunbabin et al., 2004). Il sera important de faire le point avec C. Doussan (CSE, INRA Avignon) sur les derniers développements et les projets de développement de son outil. Le terrain devrait être le programme EA « Sol virtuel », dont l'un des axes, que nous coordonnons à trois avec A. Mollier (TCEM, INRA Bordeaux), est dédié à ce couplage. A. Mollier devrait apporter son expertise sur la modélisation de la partie aérienne et de la demande optimale en P.

C. Cycles de C, N et de P

Une rapide *synthèse des modèles de cycle de C, N, et P* est nécessaire dans l'objectif de préciser quelques pistes de modèles conceptuels et de formalismes décrivant les flux de C, N et P, qui pourront être introduits dans le modèle biogéochimie-transfert MIN3P.

Le travail de Wang et al. (2007) illustre assez bien le type de couplage visé dans cette modélisation du cycle de C, N, et P. Dans leur modèle, les cycles de N et de C sont couplés par le biais de la minéralisation de la litière et de la MO du sol (modèle à deux compartiments) et de la croissance des plantes (Figure 35). La fixation symbiotique de N est considérée. Les cycles de N et de P sont couplés via la production de phosphatases, riches en N, donc grandes consommatrices, et la transformation du Po en Pi. La cinétique des processus contrôlant le cycle de C, N et P est linéaire. Ce type de loi cinétique est disponible dans le modèle MIN3P. Par contre, certains flux échangés entre les différents compartiments sont calculés à l'aide de fonctions non linéaires, faisant partiellement intervenir une cinétique Michaelis-Menten. Ce type de cinétique peut être pris en compte dans MIN3P.

Les modèles développés par M. Pansu de l'IRD, en particulier la version la plus élaborée (MOMOS-6), ne permettent pas de simuler le cycle de P. La fixation de l'azote atmosphérique n'est pas non plus considérée et le modèle ne possède pas de module pour simuler les prélèvements de N et C par les plantes (Figure 36). Par contre, le modèle MOMOS-6 permet de décrire avec une bonne précision la dynamique de C et de N dans de sols agricoles en tenant compte de la respiration de la biomasse microbienne (Pansu et al., 2004; Pansu et al., 2007). Des lois cinétiques linéaires sont également utilisées dans ce modèle. La matière organique du sol (nécromasse incluse) est représentée par cinq compartiments, contre deux dans le modèle de Wang et al. (2007). En outre, ce modèle a été appliqué pour l'étude de l'effet des racines sur la dynamique de la MO du sol, et a permis d'en estimer les rhizodépositions (Bottner et al., 1999).

De nombreux autres modèles de cycle de C, N, P dans les écosystèmes terrestres existent dans la littérature. Certains sont plus spécialisés dans le cycle de P. Par exemple, Daroub et al. (2003) proposent un modèle pour le cycle de P dans les sols déficients en P (sols calcaires et tropicaux). Un nombre assez complet de compartiments est considéré (Figure 37). Des lois cinétiques du premier ordre sont utilisées et la géochimie y est simplifiée à l'extrême (adsorption linéaire de P etc.).

Cet axe de recherche concerne également les processus biologiques n'affectant pas directement la disponibilité du P, tels que la nitrification (effets sur nutrition N) et la dégradation de la MO (apports DOC pouvant rentrer en compétition avec Pi pour l'adsorption, apports CO_2 modifiant le pH etc.). Ces deux processus sont du domaine d'expertise de E. Le Cadre (Le Cadre et al., 2008) et de plusieurs collègues de l'IRD (M. Pansu, T. Chevalier, M. Bernoux et al. etc.). Enfin, un aspect novateur et important de mon travail dans le domaine du cycle de C, N et P sera de prendre en compte l'effet des apports de matières organiques fraîches (MOF) sur la vitesse minéralisation ou la dégradation de la MO du sol (e.g. Kuzyakov et al., 2000). Cet effet, décrit communément sous le terme de « priming effect », n'est pas intégré dans les modèles de cycle (e.g. Fontaine et Barot, 2005).

En relation avec L. Bernard, chercheuse microbiologiste récemment recrutée à l'IRD (UR Seqbio), et ses collaborateurs, j'envisage de travailler à l'introduction du modèle microbiologique de S. Fontaine (Fontaine and Barot, 2005) dans le modèle MIN3P. Outre le développement d'un modèle « classique » de cycle de C, N et de P qui tiendrait également

compte de l'effet « priming » sur la dégradation de la MO du sol, ces travaux permettraient le développement d'un outil rendant possible le couplage du « priming effect » aux variables géochimiques. Un tel couplage a déjà été observé (e.g. Rasmussen et al., 2007). D'ailleurs, mes travaux dans ce domaine devront porter au préalable sur l'étude des mécanismes géochimiques responsable de ce couplage. L'approche reposera sur mesures physico-chimiques et l'analyse statistique des données, à l'image de celle mise en place à Nancy pour l'étude de Si, Al et du COD (cf. synthèse des travaux).

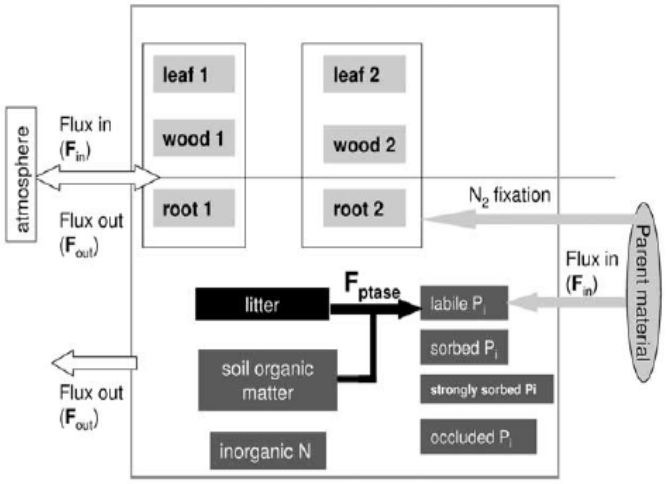

Figure 35. Modèle conceptuel représentant le couplage des cycles de C, N et P dans le modèle de Wang et al. (2007).

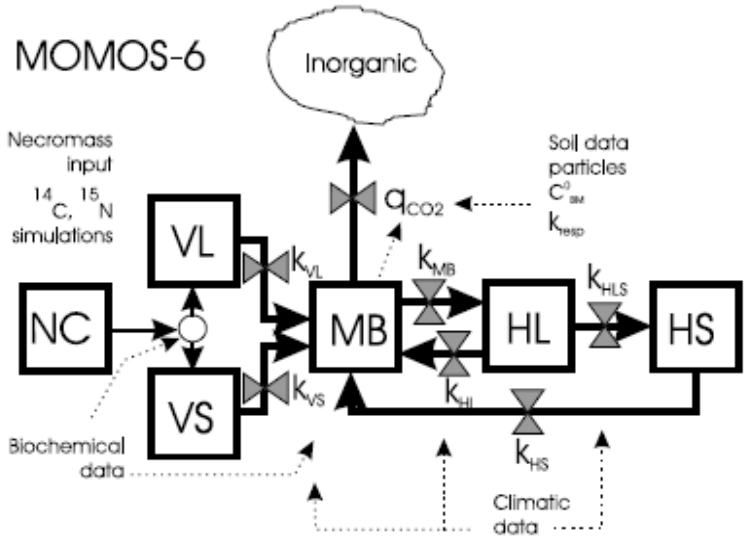

Figure 36. Modèle conceptuel utilisé dans le modèle MOMOS-6 pour simuler le cycle de C et de N dans les écosystèmes terrestres (Pansu et al., 2004). NC : nécromasse ; VL : nécromasse labile ; VS = nécromasse stable ; MB : biomasse microbienne ; HL = MO humifiée labile ; HS : MO humifiée stable. Les variables k sont en fait les constantes des lois cinétiques d'ordre 1 contrôlant les flux entre les différents compartiments. qCO_2 est le flux de CO_2 respiré par les microorganismes.

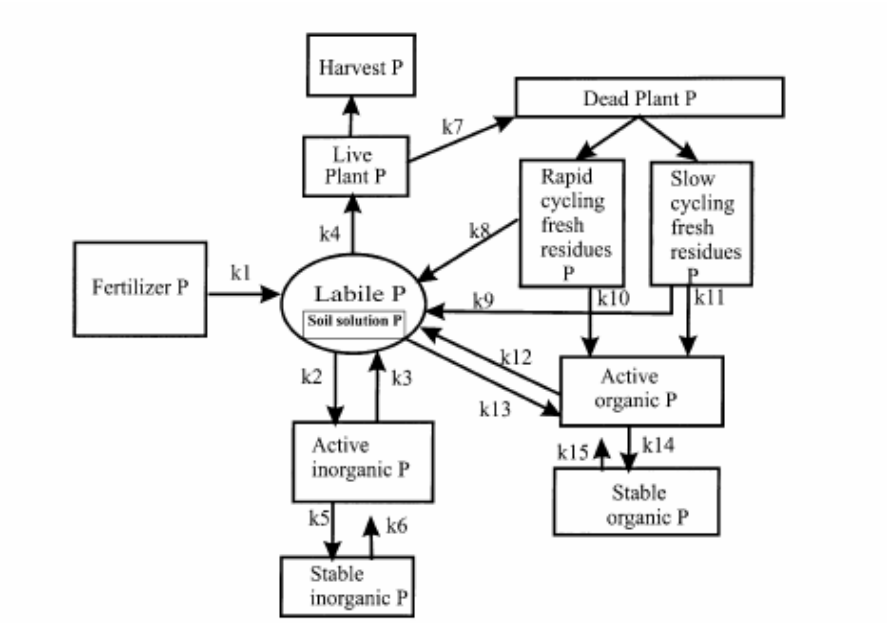

Figure 37. Modèle conceptuel du modèle de Daroud et al. (2003) de simulation du cycle du P dans les sols calcaires et tropicaux (limitants en P).

Les possibilités des modèles de cycle et plusieurs de leurs limites ont été discutées dans des articles de synthèse (Wu and McGechan, 1998; Lewis and McGechan, 2002). D'un point de vue général, le niveau de prise en compte des processus physiques et chimiques y est faible. Par exemple, le COD est souvent ignoré dans les modèles de cycle, comme dans les précédents. Le calcul des pertes de l'azote par drainage profond est également très simplifié et la fraction organique de N n'est pas prise en compte. Enfin, les processus d'interaction entre le sol et le phosphore sont simulés à l'aide d'équations empiriques (isothermes d'adsorption etc.), quand ils ne sont pas totalement ignorés s'agissant du Po, etc.

Les limites fondamentales et conceptuelles des modèles de cycles de C, N et P fondent l'intérêt de la démarche de modélisation que je compte poursuivre avec MIN3P, et de ma collaboration privilégiée avec le concepteur, K.U. Mayer. En effet, le couplage des formalismes contenus dans les modèles de cycle aux équations de transport réactif résolues par MIN3P doit permettre de développer un nouvel outil qui devra permettre entre autres choses:

- ➔ d'*améliorer le caractère prédictif et générique* des modélisations des cycles de C, N, et P, étant donné que les processus géochimiques et les processus de transfert pourront être considérés de manière mécaniste et couplée ;
- ➔ de *contribuer à répondre à des questions de recherche*. Par exemple, quels sont les effets du COD (adsorption compétitive, dissolution/précipitation) ou du « priming » sur la biodisponibilité du P ?
- ➔ d'étudier par la *modélisation de l'évolution des écosystèmes sur le long terme*, sous des contraintes naturelles et anthropiques, à l'image des applications réalisées par Wang et al. (2007) ou bien Herbert et al. (2003).

D. Transfert des gaz du sol

Les transferts des gaz dans le sol sont limités aux transferts par diffusion moléculaire dans le modèle MIN3P. Ce processus de transfert y est simulé de manière standard, à partir de la résolution de la loi de Fick. Cette possibilité est insuffisamment générique et pas assez mécaniste. Les transferts gazeux méritent une attention particulière car ils peuvent affecter de nombreux processus biologiques, géochimiques et physiques (évaporation). Des modifications doivent être réalisées en priorité afin d'améliorer la manière dont les transferts gazeux peuvent être considérés dans MIN3P. Il s'agit principalement :

- *d'introduire le processus de transfert des gaz par convection (advection)* ;

Le transfert convectif d'un gaz peut être provoqué par un gradient de pression, dont les causes peuvent être nombreuses : fluctuation de la nappe phréatique, déplacement d'un front d'infiltration, variation de la pression atmosphérique, et bien sûr la présence de réactions biologiques et géochimiques (dégradation de composés organiques, respiration, dissolution/précipitation des carbonates etc.). Bien que l'importance de ce processus soit potentiellement importante, la convection des gaz est très peu introduite dans les modèles couplés.

- *d'améliorer la méthode de simulation de la diffusion des gaz.*

La méthode classiquement utilisée en modélisation de ce processus, dite 'Fickienne', c'est-à-dire à partir de la résolution de la loi de Fick, se révèle inadaptée en cas de concentration élevée des gaz (e.g. Webb, 1998). Une approche plus mécaniste, dite de 'gaz poussière' (Dusty gaz model) a été introduite dans certains modèles de transfert (e.g. Webb, 2001). Cette approche sera introduite dans MIN3P.

Ce travail de modélisation vient d'être initié en partenariat avec l'UBC (K.U. Mayer), le BRGM (service « eau ») et le FZH de Liepzig (projet SAFIRA, sur l'utilisation des zones humides pour le traitement des eaux; U. Maier et al.).

Concernant les applications du modèle couplé, plusieurs possibilités existent mais des sites précis n'ont pas été définis à ce jour, puisque à ce stade les développements numériques du modèle sont toujours en cours de réalisation Une application que je souhaite soutenir concerne le site de Madagascar suivi par l'Unité IRD « Seqbio » (L. Chapuy-Lardy). Les gaz du sol (flux de NO_2 et CO_2 à la surface et concentrations en profondeur) y sont suivis et des travaux sont conduits afin de comprendre leur déterminisme, de modéliser les flux, et de préciser les sources. D'autres applications, sans doute plus tournées vers la contamination du sol, devront voir le jour en relation avec mon partenaire du BRGM (M. Azaroual, service « eau », Orléans).

E. Mesures et expérimentations

La réalisation des recherches envisagées dans l'axe consacré à l'étude et à la modélisation des processus géochimiques contrôlant la disponibilité de P demandera des mesures physico-chimiques en vue d'une meilleure connaissance du système. Ces mesures seront réalisées localement et en s'appuyant sur les équipements et compétences d'autres laboratoires.

Les expérimentations envisagées concernent principalement les axes sur les processus géochimiques et biologiques contrôlant la disponibilité de P. Elles s'échelonneront dans le temps, selon un degré de complexité croissante, servant de support aux développements de la modélisation. La réussite des confrontations mesures-modèle conditionnera le passage à un niveau supérieur de complexité. Les expérimentations envisagées correspondent à :

- de « simples » incubations d'un sol sans plante. Différents sols seront utilisés et les conditions physico-chimiques (pH, salinité…) seront manipulées. Il est également prévu de mettre en contact le sol avec une résine mimant l'effet puits de P provoqué par le prélèvement préférentiel de cet élément par le végétal ;

- un sol en contact avec une plante (rhizobox) ;

- un sol contenu dans un pot soutenant la croissance de plantes. La manipulation des conditions environnementales est également prévue à ce niveau de complexité.

1. Mesures physico-chimiques

Il s'agira en premier lieu de déterminer la spéciation du P dans le sol au travers de:

- l'analyse des solutions extraites ou collectées (chimie totale, Pi et Po) ;

- la réalisation d'extractions chimiques (eau, $CaCl_2$, Olsen, oxalate, séquentielles), dont l'utilité est multiple puisque selon la nature de l'extraction chimique réalisée la concentration en P extrait sert d'indicateur de disponibilité, indique la quantité totale de Pi adsorbée par le sol, la présence de P minéral, la compartimentation du P organique etc. ;

- des mesures physiques et isotopiques.

Les extractions chimiques pourront être réalisées localement, avec l'appui si nécessaire des services d'analyse de l'INRA et/ou du CIRAD. Concernant les mesures physiques, je pense développer des liens avec le CEREGE (J. Rose, P. Garnier) et l'Ecole des Mines d'Alès (J.C. Bénezet). La minéralogie des sols peut en partie être déterminée par des mesures de diffraction de rayons X. Ces techniques sont largement maîtrisées par ses laboratoires. Les pré-traitements (fraction argileuse) pourraient être réalisés sur place à Montpellier. Des mesures de potentiel Zéta serviront à l'identification des processus géochimiques (adsorption *vs.* dissolution/précipitation) contrôlant la concentration de Pi (Li and Stanforth, 2000). En complément, la technique de microanalyse par fluorescence X pourrait permettre de préciser la localisation du P par rapport aux constituants minéraux et organiques du sol (e.g. Fitzgerald et al., 2006).

L'isotopie du P revêt plusieurs aspects. En effet, les mesures de cinétique d'échange isotopique (^{32}P) renseignent la dynamique de mise en solution du P ; i.e. sur les aspects cinétiques de la disponibilité. Ces mesures peuvent donc aider à déterminer les mécanismes contrôlant la disponibilité à différentes échelles de temps. La cinétique de dilution isotopique du P peut être mesurée à l'INRA de Bordeaux (e.g. Morel and Hinsinger, 1999; Stroia et al., 2007). Les mesures sur ^{31}P par spectromètre de Résonance Magnétique Nucléaire (RMN) s'avèrent très intéressantes pour l'étude de la spéciation du P, inorganique (Pi) et organique (Po). Ces mesures peuvent être réalisées sur la phase solide (e.g.

MacDowell et al., 2002) et en milieu aqueux (e.g. Koopmans et al., 2003). Un spectromètre RMN adapté pour des échantillons liquides est disponible sur le campus SupAgro de Montpellier. Il a déjà été utilisé dans l'Unité. Concernant l'appareil permettant l'analyse des solides (Solid-state RMN), il en existe dans plusieurs laboratoires français et étrangers. Une collaboration est à développer le cas échéant, car cette technique d'analyse est limitée par la présence de fer, rendant donc *a priori* délicate l'étude de nombreux sols, en particulier de sols tropicaux. Cela n'exclut cependant pas l'analyse d'échantillons aqueux, selon la concentration en Fe soluble.

2. Expérimentations : laboratoire et terrain

Comme indiqué en début de partie, les premières expériences seront réalisées dans un sol sans plante, afin de simplifier un peu le système et cibler les processus géochimiques. Des travaux sur sol nu dont le pH avait été manipulé ont été conduits durant le stage de M2 de N. Devau (Devau, 2007 ; Devau et al., 2008). Ils seront approfondis en thèse, toujours en étudiant le sol « modèle » de l'UMR : un Cambisol (fersialitique, pH neutre). Il est aussi prévu de tester cette modélisation sur plusieurs types d'extraction et sur plusieurs sols possédant des propriétés physiques et chimiques contrastées, de part leur origine ou leur passé agricole ou sylvicole (fertilisation etc.) différents. Par exemple, les processus de dissolution/précipitation des minéraux secondaires riches en P peuvent être amplifiés en manipulant un sol très fertilisés, car ce processus contrôle la solubilité du P (McDowell et al., 2003). De même, il est prévu à plus long terme de manipuler la température et la salinité du milieu afin de vérifier et d'améliorer la généricité de nos connaissances et de l'approche. Par exemple, la modélisation des effets d'une variation de la température sur la solubilité du P peut aider à vérifier la nature du processus/mécanisme déterminant, ou bien encore nous permettre de déterminer les paramètres contrôlant les effets de la température en modélisation (enthalpie, énergie d'activation), etc.

Au laboratoire, des dispositifs de type rhizobox devraient permettre de collecter du sol et des solutions « rhizophériques », voir le long d'un gradient de distance par rapport aux racines. Le cas échéant, selon notamment le type de sortie souhaité (i.e. fonctionnement de la rhizosphère ou perte de P de la zone d'enracinement), des mesures plus intégratrices sont envisageables au travers de la récolte des solutions drainées à la base d'un réacteur. Ces expériences peuvent être conduites sur place, où ces techniques ont été développées depuis plusieurs années. Une approche équivalente pourra être menée sur le terrain. A cette échelle, les solutions du sol pourront être collectées par des techniques de lysimétrie. Il serait également intéressant d'utiliser des solutions extraites par centrifugation, reprenant ainsi la démarche débutée à Nancy pour Si, Al et le COD (solution « réactive » du sol etc.), d'autant que l'une des forces de cette technique est son utilisation possible dans de nombreux sites, sans avoir recours à de lourds dispositifs. Une approche « nomade » est donc envisageable, offrant la possibilité d'une généralisation spatiale « raisonnée » de cette modélisation. Quand à la nature des écosystèmes étudiés, ceux sous climat tropical et subtropical seront privilégiés, puisque les sols présentent souvent un déficit en P disponible (Hinsinger, 2001; Vance et al., 2003). Sous climat plus tempéré, le site de Landes (pin maritime) constitue un cas d'étude intéressant car situé sur sol pauvre. Le rôle du Po y est central, pour sa capacité à fournir du Pi par hydrolyse enzymatique. L'étude de sols riches sous climat tempéré serait intéressante à plus long terme, afin d'étendre le champ pédoclimatique des applications.

Un élément clé pour la sélection des sites de terrain est la possibilité de réaliser des analyses de P dissous à proximité et rapidement de lieu de collecte, à cause des risques d'évolution de sa spéciation (Worsfold et al., 2005). De tels artefacts peuvent également se produire à plus long terme, durant le transport vers le laboratoire ou du fait du conditionnement des échantillons (congélation). A noter que les analyses de la phase solide

et adsorbée pose également des problèmes de préparation et de stockage des échantillons de sol, puisqu'il apparaît que le séchage et le tamisage des sols peut induire la précipitation de phosphates de calcium en particulier dans les sols carbonatés (Penn and Bryant, 2006).

Le pin maritime pourra constituer l'espèce forestière « modèle » de ce projet au titre déjà des travaux importants réalisés par C. Plassard sur cette l'espèce (sites des Landes). Cependant, cela sera conditionné par la mise en place d'un site de terrain pour le suivi des variables du sol, tel que ceux mis en place sous les tropiques par le CIRAD (UPR 80). Coté plantes de grande culture, la première plante modèle devrait être le blé. Cette céréale est étudiée dans le cadre de la thèse de N. Devau sur la biodisponibilité de P en fonction du pH. Le haricot ou une autre légumineuse de grande culture constituera une seconde espèce modèle, car elle possède la particularité d'accueillir une symbiose rhizobienne fixatrice de N_2.

F. Diffusion du modèle

Des efforts de diffusion du modèle couplé MIN3P doivent être réalisés afin de bénéficier en retour de l'expérience d'un nombre plus important d'utilisateur.

Le premier vecteur de diffusion sera la réalisation de formations permanentes, à l'INRA et en dehors de cet institut. Un second vecteur devrait être la mise en place d'un enseignement spécifique, dans le cadre d'un Master ou de l'enseignement par correspondance (UVED).

La diffusion du modèle vers une communauté élargie est suspendue à la réalisation d'une interface d'entrée « user-friendly ». Une première version est désormais opérationnelle (Figure 38), mais limitée aux fonctions de transfert hydrique. Elle est en cours d'extension aux autres possibilités du modèle couplé MIN3P.

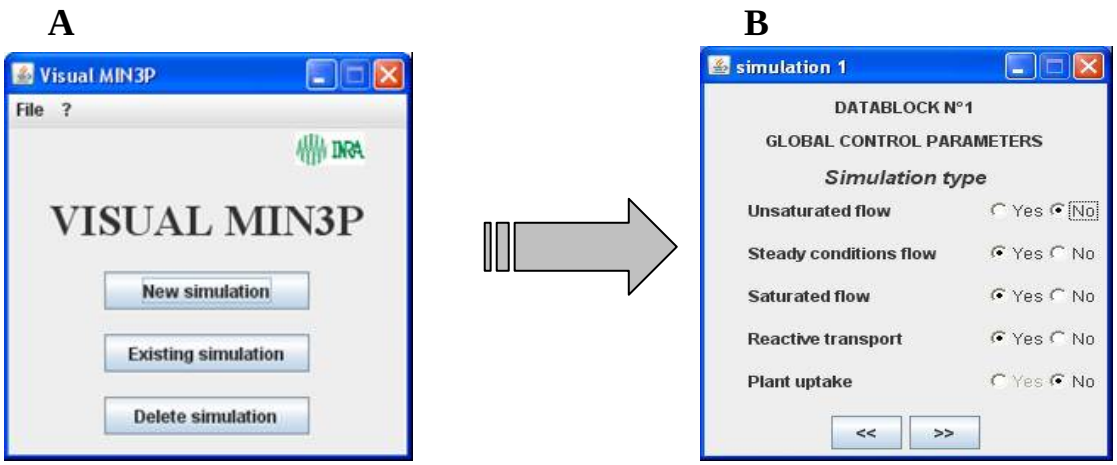

Figure 38. Interface d'entrée du modèle MIN3P. Exemple correspondant à la fenêtre d'accueil (**A**) et à celle de saisie du type de simulation à réaliser (**B**) (transferts uniquement, milieu non saturé ou saturé, état stationnaire, couplage avec la géochimie, avec les prélèvements hydro-minéraux de la plante etc.).

Bibliographie

Alexandre A., Meunier J.-D., Colin F., and Koud J.-M. (1997) Plant impact on the biogeochemical cycle of silicon and related weathering processes. *Geochim. Cosmochim. Acta* **61**, 677-682.

Artinger R., Buckau G., Geyer S., Fritz P., Wolf P., and Kim J. I. (2000) Characterization of groundwater humic substances: influence of sedimentary organic carbon. *Appl. Geochem.* **15**, 97-116.

Bartoli F. (1981) Le cycle biogeochimique du silicium sur roche acide : application à deux écosystèmes forestiers tempérés (Vosges). *Thesis, Univ. Henri Poincaré, Nancy, France*, pp. 188.

Bartoli F. (1983) The biogeochemical cycle of silicon in two temperate forest ecosystems. *Environm. Biogeochem. Ecol. Bull.* **35**, 469-476.

Bartoli F. and Souchier B. (1978) Cycle et rôle du silicium d'origine végétale dans les écosystèmes tempérés. *Ann. Sci. Forest.* **35**, 187-202.

Baton M. (2004) Influence des essences forestières sur les propriétés complexantes de la matière organique du sol, pp. 25. INRA.

Battaglia M. and Sands P. (1997) Modelling site productivity of Eucalyptus Globulus in response to climatic and site factors. *Aus. J. Plant Physiol.* **24**, 831-850.

Benedetti M. F., van Riemsdijk, W.H., Koopal, L.K., Kinniburgh, D.G., Goody, D.C. & Milne, C.J. (1996) Metal ion binding by natural organic matter : From the model to the field. *Geochim. Cosmochim. Acta* **60**(14), 2503-2513.

Berggren D. and Mulder J. (1995) The role of organic matter in controlling aluminium solubility in acidic mineral soil horizons. *Geochim. Cosmochim. Acta* **59**, 4167-4180.

Bottner P., Pansu M., and Sallih Z. (1999) Modelling the effect of active root on soil organic matter turnover. *Plant & Soil* **216**, 15-25.

Boudot J.-P., Becquer T., Merlet D., and Rouiller J. (1994) Aluminium toxicity in declining forests: a general overview with seasonal assessment in a silver fir forest in the Vosges mountains (France). *Ann. For. Sci.* **51**, 27-51.

Bourrié G., Grimaldi C., and Régeard A. (1989) Monomeric versus mixed monomeric-polymeric models for aqueous aluminium species: Constraints from low-temperature natural waters in equilibrium with gibbsite under temperate and tropical climate. *Chem. Geol.* **76**, 403-417.

Christensen J. B. and Christensen T. H. (1999) Complexation of Cd, Ni, and Zn by DOC in polluted groundwater: a comparison of approaches using resin exchange, aquifer material sorption and computer speciation models (WHAM and MINTEQA2). *Environmental Science and Technology* **33**, 3857-3863.

Claret F., Schäfer T., Bauer A., and Buckau G. (2003) Generation of humic and fulvic acid from Callovo-Oxfordian clay under high alkaline conditions. *The Science of the Total Environment* **317**, 189-200.

Cronan C. S., Walker W. J., and Bloom P. R. (1986) Predicting aqueous aluminium concentrations in natural waters. *Nature* **324**, 140-143.

Daroub S. H., Gerakis A., Ritchie J. T., Friesen D. K., and Ryan J. (2003) Development of a soil-plant phosphorus simulation model for calcareous and weathered tropical soils. *Agricultural Systems* **76**, 1157-1181.

Darrah P. R., Jones D. L., Kirk G. J. D., and Roose T. (2006) Modelling the rhizosphere: a review of methods for 'upscaling' to the' whole-plant scale. *Eur. J. Soil Sci.* **57**, 13-25.

Devau N. (2007) Modélisation de deux indicateurs de la disponibilité environnementale du phosphore en fonction des variations de pH d'un cambisol, pp. 15. INRA/SupAgro Montpellier (France).

Devau N., Gérard F., Le Cadre E., Roger L., Ashad M., Hinsinger P., and Jaillard B. (2008) Using a mechanistic adsorption model to understand the influence of soil pH on phosphorus availability: application to a Chromic Cambisol. *Ecological Modelling* **soumis**.

Dietzel M. (2000) Dissolution of silicates and the stability of polysilicic acid. *Geochim. Cosmochim. Acta* **19**, 3275-3281.

Dilling J. and Kaiser K. (2002) Estimation of the hydrophobic fraction of dissolved organic matter in water samples using UV photometry. *Water Res.* **36**, 5037-5044.

Doussan C., Pages L., and Pierret A. (2003) Soil exploration and resource acquisition by plant roots: an architectural and modelling point of view. *Agronomie* **23**(5-6), 419-431.

Doussan C., Pierret A., Garrigues E., and Pages L. (2006) Water uptake by plant roots: II - Modelling of water transfer in the soil root-system with explicit account of flow within the root system - Comparison with experiments. *Plant and Soil* **283**(1-2), 99-117.

Driscoll C. T., Lehtinen M. D., and Sullivan T. J. (1994) Modeling the acid-base chemistry of organic solutes in Adirondack, New York, lakes. *Water Resour. Res.* **30**(2), 297-306.

Dudal Y. and Gérard F. (2004) Accounting for natural organic matter in aqueous chemical equilibrium models: a review of the theories and applications. *Earth-Sci. Rev.* **66**(3-4), 199-216.

Dunbabin V., McDermott S., and Bengough A. G. (2006) Upscaling from rhizosphere to whole root system: Modelling the effects of phospholipid surfactants on water and nutrient uptake. *Plant and Soil* **283**(1-2), 57-72.

Dunbabin V., Rengel Z., and Diggle A. J. (2004) Simulating form and function of root systems: efficiency of nitrate uptake is dependent on root system architecture and the spatial and temporal variability of nitrate supply. *Functional Ecology* **18**(2), 204-211.

Dunbabin V. M., Diggle A. J., Rengel Z., and van Hugten R. (2002) Modelling the interactions between water and nutrient uptake and root growth. *Plant and Soil* **239**(1), 19-38.

Dupuy L., Fourcaud T., Stokes A., and Danjon F. (2005) A density-based approach for the modelling of root architecture: application to Maritime pine (Pinus pinaster Ait.) root systems. *J. Theor. Biol.* **236**(3), 323-334.

Ezzaïm A., Turpault M.-P., and Ranger J. (1999) Quantification of weathering processes in an acid brown soil developed from tuff (Beaujolais, France). Part II. Soil formation. *Geoderma* **87**, 155-177.

Fitzgerald S., Chaurand P., and Rose J. (2006) X-ray fluorescence micro-analysis for environmental science. *X-ray application* **18**, 8-10.

Fontaine S. and Barot S. (2005) Size and functional diversity of microbe populations control plant persistence and long-term soil carbon accumulation. *Ecology Letters* **8**, 1075-1087.

Forêt M. (2003) Effets des essences sur l'évolution des sols dans le site atelier de la forêt de Breuil-Chenue (Morvan). Rapport 2ème année ENSA Rennes, INRA Nancy. pp. 50.

Gérard F., Boudot J.-P., and Ranger J. (2001) Consideration on the occurence of the Al_{13} polycation in natural soil solutions and surface waters. *Appl. Geochem.* **16**, 513-529.

Gérard F., François M., and Ranger J. (2002) Processes controlling silica concentration in leaching and capillary soil solutions of an acidic brown forest soil (Rhône, France). *Geoderma* **107**, 197-226.

Gérard F., Mayer K. U., Hodson M. J., and Ranger J. (2008) Modelling the biogeochemical cycle of silicon in soils: application to a temperate forest ecosystem. *Geochim. Cosmochim. Acta* **doi:10.1016/j.gca.2007.11.010**.

Gérard F., Ranger J., Ménétrier C., and Bonnaud P. (2003) Silicate weathering mechanisms determined using soil solutions held at high matric potential. *Chem. Geol.* **202**, 443-460.

Gérard F., Tinsley M., and Mayer K. U. (2004) Preferential flow revealed by hydrologic modeling based on predicted hydraulic properties. *Soil Sci. Soc. Am. J.* **68**, 1526-1538.

Gérard F., Tinsley M., and Mayer K. U. (2006) Errata "Preferential flow revealed by hydrologic modeling based on predicted hydraulic properties" 68, 1526-1538. *Soil Sci. Soc. Am. J.* **70**, 305.

Gerke H. H. and van Genuchten M. T. (1993a) A dual porosity model for simulating the preferential movement of water and solutes in structure porous media. *Water Resour. Res.* **29**, 305 - 319.

Gerke H. H. and van Genuchten M. T. (1993b) Evaluation of a first order water transfer term for variably saturated dual-porosity models. *Water Resour. Res.* **29**, 1225-1238.

Granier A., Bréda N., Biron P., and Vilette S. (1999) A lumped water balance model to evaluate duration and intensity of drought constraints in forest stands. *Ecol. Model.* **116**, 269-283.

Gustafsson J. P. (2001) Modelling competitive anion adsorption on oxide minerals and an allophane-containing soil. *Eur. J. Soil Sci.* **52**, 639-653.

Herbert D. A., Williams M., and Rastetter E. B. (2003) A model analysis of N and P limitation on carbon accumulation in Amazonian secondary forest after alternate land-use abandonment. *Biogeochemistry* **65**(1), 121-150.

Hinsinger P. (2001) Bioavailability of soil organic P in the rhizosphere as affected by root-induced chemical changes: a review. *Plant & Soil* **237**, 173-195.

Jaffrain J. (2007) Effet des essences forestières sur le fonctionnement organo-minéral d'un sol brun acide : observations et modélisations. INRA/UHP Nancy, pp. 360.

Jaffrain J., Gérard F., Meyer M., and Ranger J. (2007) Assessing the quality of dissolved organic matter in forest soils using ultraviolet absorption spectrophotometry. *Soil Sci. Soc. Am. J.* **71**, 1851-1858.

Johnson J. W., Oelkers E. H., and Helgeson H. C. (1992) SUPCRT92: A software package for calculating the standard molal thermodynamic of minerals, gases, aqueous species, and reactions from 1 to 5000 bars and 0° to 1000°C. *Computer & Geosciences* **18**, 899-947.

Juo A. S. R. and Kamprath E. J. (1979) Copper chloride as an extractant for estimating the potentially aluminium pool in acids soils. *Soil Sci. Soc. Am. J.* **43**, 35-38.

Kaiser K., Zech, W. (1996) Defects in estimation of aluminium in humus complexes of podzolic soils by pyrophosphate extraction. *Soil Sci.* **161**, 452-458.

Kalbitz K., Schmerwitz J., Schwesig D., and Matzner E. (2003) Biodegradation of soil-derived dissolved organic matter as related to its properties. *Geoderma* **113**, 273-291.

Kinniburgh D. G., Van Riemsdijk W. H., Koopal L. K., Borkovec M., Benedetti M. F., and Avena M. J. (1999) Ion binding to natural organic matter : competition, heterogeneity, stoichiometry and thermodynamic consistency. *Colloids and surfaces. A, Physicochemical and engineering aspects* **151**(1-2), 147-166.

Koopmans G. F., Chardon W. J., Dolfing J., Oenema O., van der Meer P., and Van Riemsdijk W. H. (2003) Wet chemical and phosphorus-31 nuclear magnetic resonance analysis of phosphorus speciation in a sandy soil receiving long-term fertilizer or animal manure applications. *Journal of Environmental Quality* **32**, 287-295.

Kouas S., Alkama N., Abdelly C., and Drevon J.-J. J. (2007) Proton efflux by nodulated-roots varies among common bean (*Phaseolus vulgaris*) under phosphorus deficiency. *Plant Nutritition and Soil Science* **in press**.

Kuzyakov Y., Friedel J. K., and Stahr K. (2000) Review of mechanisms and quantification of priming effects. *Soil Biol. Biochem.* **32**, 1485-1498.

Le Cadre E., Gérard F., Génermont S., Morvan T., and Recous S. (2008) Which formalism to model the pH and temperature dependence of the microbiological processes in soils? Emphasis on nitrification. *Environm. Model. Assess.* **soumis**.

Lewis D. R. and McGechan M. B. (2002) A review of field scale phosphorus dynamics models. *Biosystems Engineering* **82**, 359-380.

Li L. and Stanforth R. (2000) Distinguishing adsorption and surface precipitation of phosphate on goethite. *Journal of Colloid and Interface Science* **230**, 12-21.

Lucas Y. (2001) The role of plants in controlling rates and products of weathering: Importance of biological pumping. *Annu. Rev. Earth Planet. Sci.* **29**, 135-163.

Ma J. F. and Takahashi E. (2002) *Soil, fertilizer, and plant silicon research in Japan*. Elsevier Science.

Ma Z., Walk T. C., Marcus A., and Lynch J. P. (2001) Morphological synergism in root hair length, density, initiation and geometry for phosphorus acquisition in Arabidopsis thaliana: A modeling approach. *Plant and Soil* **236**(2), 221-235.

MacDowell R. W., Condron L. M., Mahieu N., Brookes P. C., Poulton P. R., and Sharpley A. N. (2002) Analysis of potentially mobile phosphorus in arable soils using solid state nuclear magnetic resonance. *Journal of Environmental Quality* **31**, 450-456.

Marques R., Ranger J., Gelhaye D., Pollier B., Ponette Q., and Gobert O. (1996) Comparison of chemical composition of soil solutions collected by zero-tension plate lysimeters with those from ceramic cup lysimeters in a forest soil. *Eur. J. Soil. Sci.* **47**, 407-417.

Mayer K. U., Frind E. O., and Blowes D. W. (2002) Multicomponent reactive transport modeling in variably saturated porous media using a generalized formulation for kinetically controlled reactions. *Water Resour. Res.* **38**, 1174-1195.

McDowell W. H., Mahieu N., Brookes P. C., and Poulton P. R. (2003) Mechanisms of phosphorus solubilization in a limed soil as a function of pH. *Chemosphere* **51**, 685-692.

Meunier J.-D. (2003) Le rôle des plantes dans le transfert du silicium à la surface des continents. *C. R. Geoscience* **335**, 1199-1206.

Meunier J.-D., Colin F., and Alarcon C. (1999) Biogenic silica storage in soils. *Geology* **27**, 835-838.

Mohanty B. P., Bowman R. S., Hendrick J. M. H., and van Genuchten M. T. (1997) New piecewise-continuous hydraulic functions for modelling preferential flow in an intermittent flood-irrigated field. *Water Resour. Res.* **33**, 2049-2063.

Morel C. and Hinsinger P. (1999) Root-induced modifications of the exchange of phosphate ion between soil solution and soil solid phase. *Plant and Soil* **211**(1), 103-110.

Pansu M., Bottner P., Sarmiento L., and Metselaar K. (2004) Comparison of five soil organic matter decomposition models using data from a 14C and 15N labeling field experiment. *Global Biogeochemical Cycles* **18**, 1020-1034.

Pansu M., Sarmiento L., Metselaar K., Hervé D., and Bottner P. (2007) Modelling the transformations and sequestration of soil organic matter in two contrasting ecosystems of the Andes. *Eur. J. Soil Sci.* **58**, 775-785.

Parkhurst D. L. and Appelo C. A. J. (1999) User's guide to PHREEQC (Version 2). U. S. Geol. Surv.

Penn C. J. and Bryant R. B. (2006) Incubation of dried and sieved soils can induce calcium phosphate precipitation/adsorption. *Commun. Soil Sci. Plant Anal.* **37**, 1437-1449.

Piccolo A. (2001) The supramolecular structure of humic substances. *Soil Sci.* **166**(11), 810-832.

Rasmussen C., Southard R. J., and Horwath W. R. (2007) Soil mineralogy affects conifer forest soil carbon source utilization a microbial priming. *Soil Sci. Soc. Am. J.* **71**, 1141-1150.

Rubio G., Walk T., Ge Z., Yan X., Liao H., and Lynch J. P. (2001) Root gravitropism and below-ground competition among neighbouring plants: A modelling approach. *Annals of Botany* **88**, 929-940.

Salvi S., Pokrovski G. S., and Schott J. (1998) Experimental investigation of aluminium-silica aqueous complexing at 300°C. *Chem. Geol.* **151**, 51-67.

Schaap M. G., Leij F. J., and van Genuchten M. T. (2001) ROSETTA: a computer program for estimating soil hydraulic parameters with hierarchical pedotransfer functions. *J. Hydrol.* **251**, 163-176.

Schecher W. D. and Driscoll C. T. (1993) ALCHEMI: A chemical equilibrium model to assess the acid-base chemistry and speciation of aluminum in dilute solutions. In *Chemical Equilibrium and Reaction Models*, Vol. special publication 42 (ed. R. Loeppert, Schwab, A.P., Goldberg, S.), pp. 325-356. Soil Science Society of America Div. S-1 V.

Schulze J. and Drevon J. J. (2005) P-deficiency increases the O-2 uptake per N-2 reduced in alfalfa. *J. Exp. Bot.* **56**(417), 1779-1784.

Shock E. L. and Helgeson H. C. (1988) Calculation of the thermodynamic and transport properties of aqueous species at high pressures and temperatures: Correlation algorithms for ionic species and equation of state predictions to 5kb and 1000°C. *Geochim. Cosmochim. Acta* **53**, 2009-2036.

Shock E. L., Sassani D. C., Willis M., and Sverjensky D. A. (1997) Inorganic species in geologic fluids: Correlations among standard molal thermodynamic properties of aqueous ions and hydroxide complexes. *Geochim. Cosmochim. Acta* **61**, 907-950.

Simonsson M. and Berggren D. (1998) Aluminium solubility related to secondary solid phases in upper B horizons with spodic characteristics. *Eur. J. Soil Sci.* **49**, 317-326.

Simunek J., Jarvis N. J., van Genuchten M. T., and Gärdenäs A. (2003) Review and comparison of models for describing non-equilibrium and preferential flow and transport in the vadose zone. *J. Hydrol.* **272**, 14-35.

Somma F., Hopmans J. W., and Clausnitzer V. (1998) Transient three-dimensional modeling of soil water and solute transport with simultaneous root growth, root water and nutrient uptake. *Plant & Soil* **202**, 281-293.

Stroia C., Morel C., and Jouany C. (2007) Dynamics of diffusive soil phosphorus in two grassland experiments determined both in field and laboratory conditions. *Agriculture Ecosystems & Environment* **119**(1-2), 60-74.

Tagirov B. and Schott J. (2001) Aluminium in crustal fluids revisited. *Geochim. Cosmochim. Acta* **65**, 3965-3992.

Tiktak A. and Bouten W. (1994) Soil water dynamics and long-term water balances of a Douglas fir stand in the Netherlands. *J. Hydrol.* **156**, 265-283.

Tipping E. (1998) Humic ion-binding model VI: an improved description of the interactions of protons and metal ions with humic substances. *Aqu. Geochem.* **4**, 3-48.

van Genuchten M. T. (1980) A closed-form equation for predicting the hydraulic conductivity of unsaturated soils. *Soil Sci. Soc. Am. J.* **44**, 892 - 898.

Vance C. P., Uhde-Stone C., and Allan D. L. (2003) Phosphorus acquisition and use: critical adaptations by plants for securing a nonrenewable resource. *New Phytol.* **157**, 423-447.

Vilette S. (1994) Etablissement du bilan hydrique sur une chronosequence de peuplement de Douglas (*Pseudotsuga menziesii* (Mirb.) Franco), pp. 52. ENESA-ENITA/INRA.

Wang Y.-P., Houlton B. Z., and Field C. B. (2007) A model of biogeochemical cycles of carbon, nitrogen, and phosphorus including symbiotic nitrogen fixation and phosphatase production. *Global Biogeochemical Cycles* **21**, GB1018.

Webb S. W. (1998) Gas-phase diffusion in porous media - evaluation of an advective-dispersive formulation and the dusty-gas model for binary mixtures. *Transport in Porous Media* **1**, 187-199.

Webb S. W. (2001) Modification of TOUGH2 to include the dusty gas model for gas diffusion. *Sandia Report* **Sandia National Laboratory, Albuquerque, USA.**

Wonisch H., Gérard F., Dietzel M., Jaffrain J., Nestroy O., and Boudot J.-P. (2007) Occurrence of polymerized silicic acid and aluminum species in two forest soil solutions with different acidity. *Geoderma* **soumis**.

Wonisch H., Gérard F., Dietzel M., Jaffrain J., Nestroy O., and Boudot J.-P. (2008) Occurrence of polymerized silicic acid and aluminum species in two forest soil solutions with different acidity. *Geoderma* **In press**.

Worsfold P. J., Gimbert L. J., Mankasingh U., Omaka O. N., Hanrahan G., Gardolinski P., Haygarth P. M., Turner B. L., Keith-Roach M. J., and McKelvie I. D. (2005) Sampling, sample treatment and quality assurance issues for the determination of phosphorus species in natural waters and soils. *Talanta* **66**(2), 273-293.

Wösten J. H. M., Lilly A., Nemes A., and Le Bas C. (1999) Development and use of a database of hydraulic properties of European soils. *Geoderma* **90**, 169-185.

Wu L. and McGechan M. B. (1998) A review of carbon and nitrogen processes in four soil nitrogen dynamics models. *J. agric. Engng Res* **69**, 279-305.

Xiao C., Wesolowski D. J., and Palmer D. A. (2002) Formation quotients of aluminium sulfate complexes in $NaCF_3SO_3$ media at 10, 25, and 50°C from potentiometric titrations using a mercury/mercurous sulfate electrode concentration cell. *Environmental Science & Technology* **36**, 166-173.

Xu S. and Harsh J. B. (1993) Labile and nonlabile aqueous silica in acid solutions: relation to the colloidal fraction. *Soil Sci. Soc. Am. J.* **57**, 1271-1277.

SELECTION D'ARTICLES

Spéciation de l'aluminium dissous et Al_{13}

Gérard F., Boudot J.-P., et Ranger J. (2001) Consideration on the occurrence of the Al_{13} polycation in natural soil solutions and surface waters. *Applied Geochemistry* **16**, 513-529.

PERGAMON

Applied Geochemistry 16 (2001) 513–529

Applied Geochemistry

www.elsevier.com/locate/apgeochem

Consideration on the occurrence of the Al_{13} polycation in natural soil solutions and surface waters

Frédéric Gérard [a,*], Jean-Pierre Boudot [b], Jacques Ranger [a]

[a] *Centre de Recherches Forestières (INRA), Cycles Biogéochimiques, Forêt d'Amance, Champenoux, F-54280 Nancy, France*
[b] *Centre de Pédologie Biologique (CNRS), UPR 6831, Université de Nancy I, 17 rue Notre-Dame des Pauvres, BP5, F-54501, Vandoeuvre-lès-Nancy cedex, France*

Received 31 August 1999; accepted 11 April 2000
Editorial handling by R.L. Bassett

Abstract

Equilibrium speciation calculations were performed (1) for soil solutions and streamwaters collected in central and eastern France and (2) for simulated waters at 0 and 25°C, to assess the highest concentration of Al_{13} that could be reached in waters in the absence of complexing ligands other than OH^-. A comprehensive and updated set of aqueous Al species, including polymeric hydroxyaluminosilicates (HAS), and their corresponding thermodynamic formation constants, were used. Results suggest that the concentration of the Al_{13} polycation in natural waters has been largely overestimated in some past studies using equilibrium models to calculate Al speciation, owing to oversimplification (many Al ligands not considered) and the unrecognised temperature dependence of some formation constants. The Al_{13} concentration in mildly acidic natural waters may not exceed a few μmol l^{-1} at Al_T on the order of 10^{-4} mol l^{-1} and should be less than 1 μmol l^{-1} at $Al_T = 10^{-5}$ mol l^{-1}. Monomeric Al–Si species may not significantly interfere with the formation of Al_{13}, but the formation of both HAS polymers (proto-imogolite precursors) and organo-Al complexes have a marked detrimental effect on the Al_{13} concentration. The maximum concentration of Al_{13} decreased upon increasing temperature from 0 to 25°C. In contrast, the pH range wherein Al_{13} may occur increases slightly with temperature and the most acidic pH value above which Al_{13} may be formed has been underestimated. At $T = 25$°C, the Al_{13} polycation may be a significant Al species (4 to 5% of Al_T) at pH < 4.5 if $Al_T > 10^{-4}$ mol l^{-1}. The results of this study and the use of HAS polymers to calculate Al speciation in moderately natural acidic soil solutions were in better accordance with soil mineralogy. This research suggests strongly that Al_{13} should be negligible in natural soil and surface waters and may not control either Al^{3+} activity or Al-trihydroxide formation through polymerisation/depolymerisation steps. Also, from a biological point of view, the toxicity of Al_{13} to plants and aquatic organisms in natural conditions may be considered to be very low.

1. Introduction

The question of the occurrence of the tridecameric Al polycation $Al_{13}(O_4)(OH)_{24}^{7+}$, known as Al_{13}, in natural soil solutions and streamwaters is of considerable interest. The Al_{13} polycation is highly toxic to several plant species (Parker et al., 1989; Shann and Bertsch, 1993; LaZerte et al., 1997) and can decrease heavy metal mobility (Badora et al., 1998). Moreover, Al_{13} may form a metastable pool that regulates the formation of various Al mineral phases and buffers Al^{3+} activity (Bottero et al., 1987; Bourrié, 1990). Equilibrium calculations carried out for tropical and temperate soil solutions led to an Al speciation scheme more compatible with soil mineralogy when including the Al_{13} polymer than when excluding it (Bourrié et al., 1989; Bourrié, 1990). These authors calculated that Al_{13} may dominate monomeric hydroxo complexes at pH 5 with Al_T in the range 10^{-5}–10^{-6} mol l^{-1}, since the addition of the Al_{13} polycation decreases the solution saturation with respect

* Corresponding author. Fax: +33-3-8339-4069.
E-mail address: gerard@nancy.inra.fr (F. Gérard).

0883-2927/01/$ - see front matter
PII: S0883-2927(00)00048-2

to Al hydroxides by almost two orders of magnitude. In simulated natural waters, Furrer et al. (1992, 1993) calculated that at a total Al concentration (Al_T) of 10^{-4} mol l^{-1} and $T=25°C$, over 2/3 of the metal may be present in the Al_{13} form at pH 4.7–6 and the Al_{13} polymer remained as significant at Al_T of 10^{-5} mol l^{-1} and pH 5–6. These results may be alarming for ecosystems since Parker et al. (1989) and Shann and Bertsch (1993) reported that Al_{13} concentrations as low as 3–5 μmol l^{-1} inhibit root growth in several plant species.

The real occurrence of Al_{13} in natural waters may be questioned, however, as its formation involves the previous appearance of the aluminate ion, $Al(OH)_4^-$ (in alkaline conditions), the latter interacting subsequently with 12 octahedral Al (in acidic conditions) (Bertsch, 1989), a succession of conditions which are not obviously relevant to pedogenesis in acidic and mildly acidic soils. Additionally, many potentially interfering anions occur in most soil solutions (Boudot et al., 1994). Accordingly, other Al-containing polymers are also able to form and to decrease Al^{3+} activity, and to improve discrepancies between speciation calculations and soil mineralogy. For instance, the addition of phosphate to Al solutions may induce the formation of Al–PO_4 polymers in acidic conditions (Alva et al., 1986), which remain in solution at low or moderate ionic strength (depending on Al concentration). The Al–PO_4–H_2O system is poorly understood and poorly reliable. This is in some instances of little importance, as soluble phosphate is rather scarce in natural acidic soil solutions and unpolluted streamwaters. Silica also favours the polymerisation of Al as hydroxyaluminosilicate polymers (HAS) and proto-imogolite colloids (PI). Thermodynamic parameters have recently been published for the Al–Si–H_2O system (Browne and Driscoll, 1992; Farmer and Lumsdon, 1994; Pokrovski et al., 1996, 1998; Salvi et al., 1998). Although some discrepancies remain with respect to HAS, this is great progress, as nearly all soil solutions and surface waters contain appreciable amounts of silica.

It should be pointed out that, despite recent improvements (Faust et al., 1995), there is a lack of analytical tools available to reveal the occurrence of Al_{13} in natural waters, due to the low concentrations of total Al and the presence of many interfering anions. This paper aims at studying the stability of the elusive Al_{13} polycation in soil solutions and surface waters. Aqueous Al thermodynamics have been better constrained during the last decade and the study of the possible occurrence of Al_{13} in surface waters and soil solutions may be handled with more confidence. Here, the formation of monomeric Al–Si species and soluble polymeric HAS in natural soil solutions and surface waters will be considered to examine the consequences of their occurrence on Al_{13} concentration. The authors will also include ion pairs other than those formed with Al and OH, as the amounts of SO_4, F, and organic anions are far from negligible in even weakly polluted natural media in Europe, due to natural biological cycles and atmospheric deposition. This is particularly relevant with respect to the formation of the Al_{13} polymer, as all these anions are able to complex more or less Al, that will decrease Al^{3+} activity and may thus impede the formation of Al_{13}.

In what follows, solutions from forest soils as well as streamwaters will first be studied in order to calculate their likely Al_{13} content. Particular attention will be paid to mineral/water equilibria in studying Al speciation in soil solutions, since the nature of the weathering products occurring in the soils studied have been well documented (Ezzaïm et al., 1999). All the waters used in this study are supersaturated with respect to well-crystallised gibbsite, which is a prerequisite for polynuclear Al stability (Hem and Roberson, 1990). Theoretical calculations will also be carried out in order to assess the maximum Al_{13} concentration that could be reached in natural surface waters and soil solutions in temperate and tropical climates.

2. Materials and methodology

2.1. Natural surface waters

More than 100 soil solutions and streamwater samples were examined. Furrer et al. (1992) showed that the Al_{13} polycation loses almost its entire positive charge between pH 6 and 7 and could interact with dissolved metal cations, leading to completely new equilibrium conditions. Therefore, only a selected set of samples having pH values below neutrality has been considered.

The speciation calculations were first performed for soil solutions collected at 15 and 120 cm below the litter layer. A detailed list of water sample selections used for calculations can be found in the Appendix. The studied soil is an acid brown soil, classified as a 'Typic Dystrochrept' (USDA, 1994) or an Alocrisol (AFES, 1992), and covered by a plantation of Douglas fir. The studied area is situated in the 'Montagne des Aiguilettes' in the Beaujolais (Rhône, France). Stand characteristics, ecological situation and nutrient dynamics have been discussed in several studies (e.g. Ranger et al., 1995; Marques et al., 1996, Marques and Ranger, 1997). Soil solutions were collected monthly from 1992 to 1997. After sampling, solutions were taken to the laboratory, filtered (0.45 μm), maintained at 4°C and analysed as quickly as possible. The pH was measured with a single-rod pH electrode (Ingold-xerolit®) plugged to a Mettler DL21 pH-meter. ICP emission spectroscopy (JY 38 plus spectrometer) was used to measure total Si and Al concentrations. Dissolved organic carbon (DOC) was measured on a Shimadzu TOC 5050. Sulphate and F^- were analysed by ionic chromatography. Long-term survey of

this site has provided leaching soil solutions with large pH and concentration variations. Solution pH had values ranging from acid to slightly above neutral. Collected capillary solutions were not considered in this study because most of them exhibited a pH < 4.7, below the limit for presence of Al_{13} in surface waters at a total Al concentration (Al_T) on the order of 10^{-4} mol l^{-1} or less (Furrer et al., 1993). Al_T ranged from 10^{-5} mol l^{-1} to almost 10^{-3} mol l^{-1} in leaching solutions. In solutions collected in the upper soil horizon, Al_T was on the order of 10^{-4} mol l^{-1}. Leaching soil solutions collected at 120 cm depth contained significantly more dissolved Al (up to 5.10^{-4} mol l^{-1}). Conversely, DOC was on the order of 40 mg l^{-1} in upper solutions and 6 mg l^{-1} at 120 cm depth. The variations of the silica concentration indicated that the soil solutions were either undersaturated or slightly supersaturated with respect to quartz (10^{-5}–2.10^{-4} mol l^{-1}). Sulphate concentrations varied from 10^{-5} to 10^{-3} mol l^{-1} and F^- concentrations may reach a maximum of 10^{-5} mol l^{-1}.

The occurrence of the Al_{13} polycation was also investigated by means of equilibrium speciation calculations in streamwaters collected across the Vosges massif (France). The effects of forest ecosystem acidity on soil fertility, streamwater chemistry and biotoxicity have been extensively studied for 10 a in this area (Probst et al., 1990; Boudot et al., 1994, 1996; Party et al., 1995; Dambrine et al., 1998). Recently, Thomas et al. (1999) and Probst et al. (1999) have related streamwater pH to geology and relief. Most solutions ranged from neutral to mildly acidic pH and Al_T was on the order of 10^{-5} mol l^{-1}. Aqueous silica concentration stood on average close to quartz saturation (5×10^{-5} mol l^{-1}). Sulphate, F^- and DOC concentrations were on the order of 10^{-4} mol l^{-1}, 10^{-5} mol l^{-1} and 3 mg l^{-1}, respectively.

2.2. The aluminium speciation model

Aqueous Al distribution was calculated with the EQ3NR computer program (Wolery, 1992) at the in situ season temperature for soil solutions (3–14°C) and at the mean annual temperature for stream waters (7°C), as can be seen in the Appendix A. Both the aqueous species and thermodynamic equilibrium constants (K) compiled from the literature and used in this study are listed in Table 1 at 25 and 0°C. The estimation method used to account for the temperature dependence of K will be discussed in the following. When available, errors associated to the values of K constants were also listed in Table 1 at both temperatures. All the uncertainties correspond to ± standard deviation.

2.3. Monomeric aluminium species

The thermodynamic database used by default in EQ3NR is derived from the SUPCRT92 program (Johnson et al., 1992). This software makes it possible to calculate a set of internally consistent equilibrium constants from 0° to 300°C. Knowledge of the revised Helgeson–Kirkham–Flowers (HKF) model parameters is required for aqueous reactions (Shock and Helgeson, 1988). These parameters can be found in Shock et al. (1997) and Salvi et al. (1998) for hydroxo-Al complexes and the monomeric alumino-silica species $AlH_3SiO_4^{2+}$ (hereafter referred to as AlHSi) respectively. The uncertainties associated to HKF parameters were known for the AlHSi species only and were introduced in the SUPCRT92 program to calculate the error on K constants at 0 and 25°C. Equilibrium constants calculated by SUPCRT92 for the hydroxo-Al complexes may be considered as accurate given that Shock et al. (1997) successfully reproduced with the HKF formulation a number of K constants retrieved from studies which have been carried out for years at different temperatures, ranging from low to hydrothermal values.

The HKF model parameters remain undetermined for Al–F and Al–SO_4 complexes as well as for the second monomeric Al–Si species $Al(OH)_3H_3SiO_4^-$ (termed as AlOHSi). For the Al–F and AlOHSi species, the Van't Hoff Eq. (1) had been used to make calculations at temperatures other than the reference temperature (298.15 K):

$$\log K_T = \log K_{Tr} - \frac{\Delta H_r^0}{2.303R}\left(\frac{1}{T} - \frac{1}{T_r}\right) \quad (1)$$

in which ΔH_r^0 is the standard enthalpy change for the reaction (or heat of reaction) expressed in J mol^{-1}, R is the universal gas constant (8.31451 J mol^{-1} K^{-1}), T is the Kelvin temperature at which K is to be calculated, T_r is the reference Kelvin temperature, K_{T_r} is the equilibrium constant at the reference temperature, and K_T is the equilibrium constant at the required temperature.

Equilibrium constants at 25°C and the values of ΔH_r^0 used in Eq. (1) were from Nordstrom and May, (1989) and Pokrovski et al. (1998). Concerning Al–SO_4 species, large discrepancies for the K values at low temperature have been outlined in the literature (Nordstrom and May, 1989; Ridley et al., 1999). As suggested by Ridley et al. (1999), more reliable values at 0 and 25°C have been determined in this study by extrapolating the function they have proposed which is based on direct measurements done at higher temperatures ($T \geqslant 50$°C). Unfortunately, the error on K constants at lower temperatures was unavailable with this method. However, the complexing of SO_4 with Al is recognised to be strong and it thus appeared important to consider some uncertainties. Therefore, values provided at 50°C by Ridley et al. (1999) were considered in this study.

The formation of metal-organic complexes plays a predominant role in aqueous chemistry and mineral weathering rates (Drever and Stillings, 1997). Dissolved

Table 1
Dissociation constants at 25 and 0°C (1 atm) and standard heats of reaction (kJ mol^{-1}) used for Al speciation calculations[a]

Species	$\log K_{25°C}$	$\log K_{0°C}$	ΔH_r^0 (kJ mol^{-1})
$AlOH^{2+}$ [b]	5.00	5.76	−47.39
$Al(OH)_2^+$ [b]	10.34	11.97	−101.63
$Al(OH)_3^0$ [b]	15.60	18.05	−162.76
$Al(OH)_4^-$ [b]	22.20	24.98	−173.34
$Al_2(OH)_2^{4+}$ [c]	7.69±0.30	8.88±0.34	−74.20
$Al_3(OH)_4^{5+}$ [c]	13.88±0.10	16.00±0.19	−132.19
$Al_{13}(OH)_{32}^{7+}$ [c]	98.65±0.05	117.06±0.70	−1147.91
$AlH_3SiO_4^{2+}$ [d]	1.70±0.15	2.64±0.17	−58.61
$Al(OH)_3SiO_4^-$ [e]	18.43±0.13	20.96±0.13[j]	−157.75
$AlSO_4^+$ [f]	−4.17±0.13[k]	−5.40± 0.13[k]	76.69
$Al(SO_4)_2^-$ [f]	−5.90±0.23[k]	−7.34±0.23[k]	89.79
$Al_2(SO_4)_{3(aq)}$ [g]	1.88	1.88	Unknown
AlF^{2+} [h]	−7.0±0.1	−6.93±0.1[j]	−4.44
AlF_2^+ [h]	−12.7±0.2	−12.57±0.2[j]	−8.28
$AlF_{3(aq)}$ [h]	−16.8±0.3	−16.66±0.3[j]	−9.04
AlF_4^-	−19.4±0.4	−19.25±0.4[j]	−9.20
AlF_5^{2-} [h]	−20.6±0.5	−20.48±0.5[j]	−7.70
AlF_6^{3-} [h]	−20.6±1.0	−20.39±1.0[j]	−13.00
Alorg [i]	−8.38±0.13	−8.38±0.13[j]	Unknown
Al(H)org$^+$ [i]	−13.10±0.11	−13.10±0.11[j]	Unknown

[a] The corresponding equilibrium reactions are written in terms of the species Al^{3+}, $H_4SiO_4°$, F^-, SO_4^{2-}, H^+, and water molecules.
[b] Shock et al. (1997).
[c] Plyasunov and Grenthe (1994).
[d] Salvi et al. (1998); error calculated at 0 and 25°C with the SUPCRT92 program from the uncertainties on the standard partial molar thermodynamic properties at 25°C and 1 bar.
[e] Pokrovski et al. (1998).
[f] Ridley et al. (1999).
[g] Reported in Su et al. (1995).
[h] Nordstrom and May, (1989).
[i] Schecher and Driscoll, (1993).
[j] Uncertainty determined at 25°C.
[k] Uncertainty determined at 50°C.

Al is known to form strong complexes with a variety of organic constituents that differ in size, composition and function. It is difficult to characterise the heterogeneous mixture of naturally occurring organic solutes found in soil and surface waters, mostly humic and fulvic acids, which contain diverse functional groups (carboxylic, phenols, alcohols...). A number of modelling approaches have been used to estimate the formation of Al complexes with naturally occurring organic constituents (Schecher and Driscoll, 1993; Driscoll et al., 1994; Tipping, 1994; Grzyb, 1995). The choice of the model depends on the degree of knowledge of the dissolved organic constituents. In the water samples described herein, only DOC concentrations are known. The WHAM program of Tipping (1994) requires the amount of fulvic and humic acids. Alternatively, one may use the model developed by Grzyb (1995), where only DOC concentration is required as an input parameter to cope with organic Al speciation. However, this model is not suitable for DOC concentrations below 3 mg/l (Grzyb, 1995) and a number of surface water compositions used here did not meet this condition.

The empirically based model proposed by Schecher and Driscoll (1993) and later revised by Driscoll et al. (1994) was much more adaptable: Al complexation by naturally occurring organic solutes was modelled with a triprotic analogue, wherein organic acid/base reactions were described by the following reaction series and related dissociation constants (Table 1):

$$H_3org = H^+ + H_2org^- \quad (2)$$

$$H_2org^- = H^+ + Horg^{2-} \quad (3)$$

$$Horg^{2-} = H^+ + org^{3-} \quad (4)$$

$$Al^{3+} + org^{3-} = Alorg \quad (5)$$

$$Al^{3+} + H^+ + org^{3-} = Al(H)org^+ \quad (6)$$

where the species org stood for the triprotic organic analogue.

The triprotic model can be easily introduced in any speciation program, as shown for instance by Boudot et al. (1996) in the MINEQL+ speciation program (Schecher and McAvoy, 1992). The temperature dependencies of the equilibrium constants of the above reactions unfortunately remain unknown, so that they have to be kept constant to calculate aqueous Al speciation. The error introduced by this uncertainty may be at least partly balanced by the reliability of the K values used for reactions (2)–(6). Owing to these uncertainties, organo-Al complexes will be added into the model for test purposes only, in order to assert their effect on the occurrence of Al_{13} in natural waters.

2.4. Polynuclear aluminium species

The temperature dependence of the stability constants of various polynuclear Al species may be predicted on the basis of a simple electrostatic model of electrolytic dissociation proposed by Bryzgalin and Rafal'skiy (1982). Plyasunov and Grenthe (1994) used this model to calculate $K(T)$ from 0 to 250°C for the formation reactions of the Al_2, Al_3 and Al_{13} polycations, expressed in terms of OH^- and Al^{3+}. They checked its validity in several ways, against the mononuclear Al^{3+}–OH^- system, the available stability constants for polynuclear hydroxy-Al species, and by comparing the calculations to additional experimental data for the formation of polynuclear hydrolytic complexes of few divalent cations.

Whether or not the occurrence of monomeric Al–Si species has been comprehensively determined in acidic and basic solutions (Farmer and Lumsdon, 1994; Pokrovski et al., 1996, 1998; Salvi et al., 1998), the nature and stability of polymeric HAS occurring in mildly acidic solutions has been hotly debated for at least a decade (Birchall et al., 1989; Browne and Driscoll, 1992; Farmer and Lumsdon, 1995; Exley and Birchall, 1995, 1996; Lumsdon and Farmer, 1996). The dimeric species $Al_2(OH)_2OSi(OH)_3^{3+}$ and $Al_2(OH)_2(OSi(OH)_3)_2^{4+}$ proposed by Browne and Driscoll (1992) at pH $\approx$ 5 have been convincingly ascribed by Farmer and Lumsdon (1994) to an experimental artefact involving the persistence of polysilicic acids in the aqueous Si solution used. However, the occurrence of relatively stable HAS polymers under mildly acidic conditions in the absence of polysilicic acids seems to be a reality. This is outlined by Lumsdon and Farmer (1995), who failed to account for the decrease of the Al biotoxicity induced by the addition of silicic acid to aqueous Al (Birchall et al., 1989) when including only the AlHSi species in their speciation modelling. Lumsdon and Farmer (1995) failed as well when invoking the formation of PI sols as a possible explanation of the observations made by Birchall et al. (1989), since experimental solutions were undersaturated with respect to this phase. Lastly, Exley and Birchall (1996) persisted and stressed that the occurrence of polymeric HAS in moderately acidic media can actually be regarded as being responsible for the decrease of aqueous Al toxicity. These authors gave convincing experimental arguments and cited a number of papers supporting the formation of HAS at laboratory time scales (a few months).

So far, however, an accurate description of the nature and stability of HAS is badly lacking, and remains a widely open matter of debate. Reliable thermodynamic data addressing the formation of PI (Lumsdom and Farmer, 1995) are obviously not suitable to model the formation of soluble HAS. PI should be regarded as a heterogeneous mixture ranging from soluble HAS polymers, as attested by its ability to adsorb within the expandable interlayer space of clays such as montmorillonite (Huang, 1991), to a highly dispersed colloidal phase forming a sol, as attested by its ability to be precipitated by fulvic acids (Farmer, 1979; Wada and Wada, 1980; Lou and Huang, 1988; Huang, 1991). Consequently, in order to estimate the effect of the formation of soluble HAS on the occurrence of Al_{13} in natural waters, the authors used the thermodynamic database (Table 1) to determine a value for the formation constant of HAS polymers from the experiments done by Birchall et al. (1989). Such an approach was a proxy but it was also the most efficient and finally the most acceptable way to study the effect of the formation of soluble HAS polymers on Al_{13} contents. Because in mildly acidic environments soluble HAS may be precursors of solid phases such as imogolite and PI (Birchall et al., 1989; Exley and Birchall, 1995, 1996), the authors considered an equivalent aqueous species of the same stoichiometry ($[Al_2SiO_3(OH)_{4(aq)}]_n$). The best fit for $\log K = 18.01$ (± 0.65) was found for the formation reaction with $n = 1$.

Speciation calculations were first performed without simulating the formation of the soluble HAS polymers. For testing only, the possible influence of the formation of HAS on Al_{13} content was then addressed. The temperature dependence of the HAS formation constant remains so far unknown, so that the $\log K$ value was kept constant during calculations.

2.5. Uncertainty analysis

The influence of the reported errors on the $\log K$ of Al species (Table 1) was considered in the following calculations, in order to study their effect on the calculated Al_{13} concentration in soil solutions and surface waters. The maximum contribution of Al_{13} to Al speciation was calculated by simply increasing the thermodynamic stability of the other Al species and by decreasing Al_{13} stability. The inverse method was used to obtain the minimum contribution of Al_{13}. The influence of errors

associated to the formation constants for polymeric HAS species and organo-Al complexes was not simulated, because those species will be tested in the following on a binary basis, i.e. by either considering their occurrence or not.

2.6. The activity model

The studied soil solutions and streamwaters were weakly concentrated and their ionic strength was always below 0.01 molal. Accordingly, either the Davies or the B-dot formulation of the Debye–Hückel extended law may be used with the same level of accuracy (Wolery, 1992). Because of its validity for a larger temperature range, the B-dot equation was used in this study. The hard core diameter, a^0, contained in the B-dot equation is unknown for a few aqueous species such as those involved in the triprotic organic analogue model and the dimeric and trimeric hydroxy-Al species. A comprehensive discussion of the value of a^0 to be used for Al_{13} may be found in Bourrié et al. (1989), who pointed out the uncertainty prevailing on the applicability of the Debye–Hückel extended law to ions having a charge as high as +7. Moreover, as can be seen by testing the effect of different values of a^0 with EQ3NR, the choice of a^0 has a minor influence owing to the very low ionic strength of the solutions. Therefore, the activity coefficients of organic and polynuclear Al species including Al_{13} were all set to unity in the calculations.

2.7. Mineral stability

The mineralogy and chemical properties of the soil at the Vauxrenard site, from which the soil solutions were collected, have been extensively studied (Ezzaïm et al., 1999). Kaolinite, hydroxy-Al interlayered vermiculites and interstratified vermiculite–biotite have been identified as the main weathering products. Since the kaolinite precipitation rate is typically slow at low temperature, amorphous $Al(OH)_3$ or hydroxy-Al interlayers in vermiculites may control aqueous Al (e.g. Bourrié et al., 1989; Su et al., 1995). This must be particularly true at moderately acidic pH, as Al bound to solid organic matter has a weak influence at pH > 4.5 in organo-mineral and mineral soil layers (Cronan et al., 1989).

The equilibrium constants compiled in Table 2 were used to study the effect of the formation of Al_{13} on the stability of minerals in contact with the soil solutions. The uncertainties corresponding to ±1 standard deviation were also listed when available. The uncertainties at $T = 0°C$ are scarcely known for minerals or may not be calculated from the data provided by the authors. In such cases, as for aqueous species, the same error was assumed at 0 and 25°C. Furthermore, it is widely recognised that the thermodynamic equilibrium constant of minerals are influenced by atomic ordering and crystal size. Amorphous forms and a large variety of crystal size are typically found in nature. Several equilibrium constants were thus selected from the literature for each of the identified weathering products, primarily interlayer $Al(OH)_3$ and kaolinite, in order to cope with the natural heterogeneity of their K constants. The temperature dependence of amorphous and interlayer $Al(OH)_3$ was assumed identical to that of the well-crystallised gibbsite, calculated with SUPCRT92 by Johnson et al. (1992) from the data of Pokrovski and Helgeson (1995). The same approximation was made for poorly crystallised kaolinite (Kittrick, 1966) and the well-crystallised form (Devidal et al., 1996) as well, based on the data proposed by Helgeson et al. (1978) for this mineral and calculated with the SUPCRT92 program.

Thermodynamic consistency was preserved for interlayer $Al(OH)_3$ by re-interpreting the solubility experiments performed by Su et al. (1995) with the present database complemented by the Al–chloride complexes (Gruaer, 1993) because of the very large Cl concentrations in their solutions. Otherwise, a good agreement was found between the thermodynamic data used here and those considered in the solubility studies carried out in order to assert the K constants of the two kaolinites considered here and PI. Quartz was also included in the calculations and served as a reference for the activity of orthosilicic acid, which seemed relevant to the relatively low silica concentrations measured in the natural solutions. Equilibrium constants calculated with SUPCRT92 were used for quartz. Results were in good agreement with those recently revised by Rimstidt (1997).

3. Results

3.1. Expected Al_{13} contents in natural soil solutions and surface waters

When the formation of HAS and organo-Al complexes was not considered, the calculated amount of the so-called Al_{13} polycation in soil solutions reached approximately 7.2±0.1% of Al_T (Fig. 1). The dimeric and trimeric hydroxy-Al species were always present in negligible amounts. The Al_{13} content was slightly higher in waters collected at 120 cm than at 15 cm depth (7.2±0.1% against 6.7±0.2%, respectively). As expected and whatever the depth, the contribution of the Al_{13} polymer to Al speciation was pH dependent and increased from approximately pH 5 to reach a maximum or plateau near pH 6. This was more or less maintained up to the upper pH limit (pH = 7) determined by Furrer et al. (1992) for the occurrence of Al_{13}. The corresponding Al_{13} concentrations culminated at 3.9±0.1 μmol l^{-1} in soil solutions from 15 cm depth and at approximately 25±2 μmol l^{-1} in those from 120 cm depth. As illustrated for instance in Fig. 2 for soil solutions from

Table 2
Equilibrium constants in the system SiO_2–Al_2O_3–H_2O at 1 atm, 0 and 25°C and standard heats of reaction (kJ mol^{-1})[a]

Minerals	$\log K_{25°C}$	$\log K_{0°C}$	ΔH_r^0 (kJ mol^{-1})
gibbsite[b]	7.07±0.21	8.59±0.23	−94.78
Amorphous $Al(OH)_3$[c]	10.80	12.32	−94.78
Interlayer $Al(OH)_3$[d]	8.89±0.12	10.41±0.12[i]	−94.78
Kaolinite-A[e]	3.92±0.15	5.87±0.15[i]	−121.59
Kaolinite-B[f]	6.20	8.15	−121.59
Proto-imogolite (PI)[g]	14.04±0.10	15.59±0.10[i]	−96.65
quartz[h]	−3.99	−4.63	39.91

[a] The corresponding equilibrium reactions are written in terms of the species Al^{3+}, $H_4SiO_4^\circ$, H^+, and water molecules.
[b] Pokrovski and Helgeson (1995); error calculated at both temperatures with the SUPCRT92 program from the uncertainties on the standard partial molar thermodynamic properties at 25°C and 1 bar.
[c] Stumm and Morgan (1981).
[d] From Su et al. (1995), revised at $T = 25°C$ for the purpose of this study in order to be consistent with the authors' thermodynamic database for aqueous species (Table 1). The uncertainty was recalculated as well.
[e] Well-crystallised kaolinite from Devidal et al. (1996). Uncertainty corresponding to that given for the standard Gibbs free energy of formation (25°C and 1 bar).
[f] Poorly crystallised kaolinite from Kittrick (1966), revised by Devidal et al. (1996).
[g] From Lumsdon and Farmer (1995). Uncertainty calculated at $T = 22 \pm 2°C$ directly from K values
[h] Helgeson et al. (1978).
[i] Uncertainty determined at 25°C.

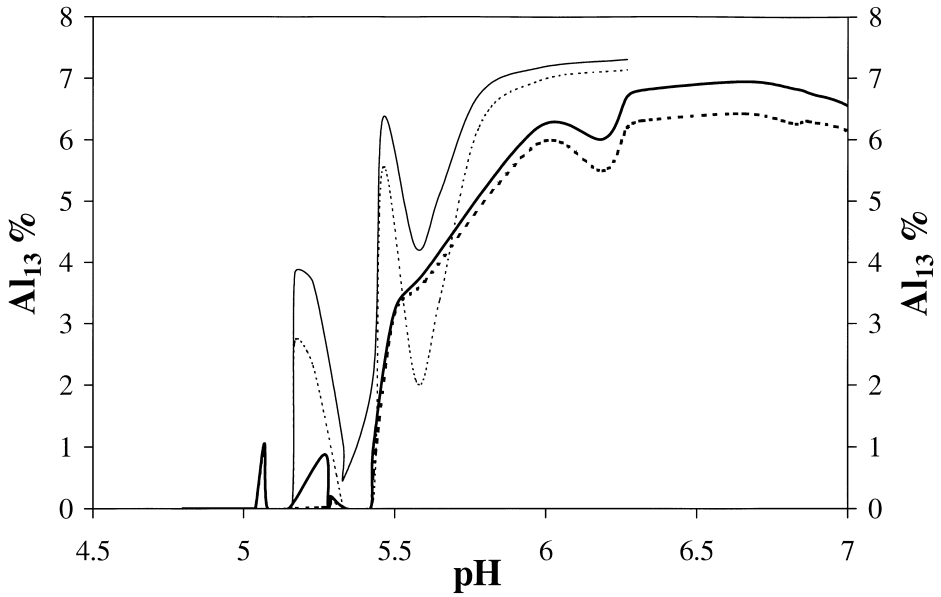

Fig. 1. Maximum and minimum calculated distribution of Al_{13} in soil solutions (15 cm depth = thick lines; 120 cm depth = narrow lines) as a function of pH, expressed in % of total dissolved Al. Calculations excluded the formation of HAS and organic complexes.

the upper soil horizon, the occurrence of inorganic ligands such as SO_4^{2-} and F^- in the acidic and moderately acidic pH ranges induced the formation of Al–F and Al–SO_4 complexes, which lower Al^{3+} activity and therefore hindered the formation of Al_{13}. A relatively small amount of monomeric Al-Si species was also formed, due to the occurrence of dissolved silica. The monomeric species denoted AlOHSi appeared at near neutral to neutral pH and affected the Al_{13} concentration. In contrast, the Al–Si species termed AlHSi, which is the dominant Al–Si species at acidic to mildly acidic pH, was always found in very minor amounts (< 1% of Al_T).

The Al_{13} polycation largely dominated the dimeric and trimeric Al species in streamwaters as well. As expected due to the lower Al_T concentration, on the

order of 10^{-5} mol l^{-1}, at a similar pH range, the calculated concentration and percentage of Al_{13} in streamwaters is much less than in soil solutions. This polymer did not form more than 3.6±0.5% of Al_T (Fig. 3) and its maximal concentration did not exceed 0.31±0.4 μmol l^{-1}.

By comparing Fig. 4 to Fig. 1, it can be seen that the concentration of Al_{13} as calculated at equilibrium in both soil solutions and streamwater significantly decreases when accounting for organic ligands or HAS polymers. Organic ligands form organo-Al complexes and HAS

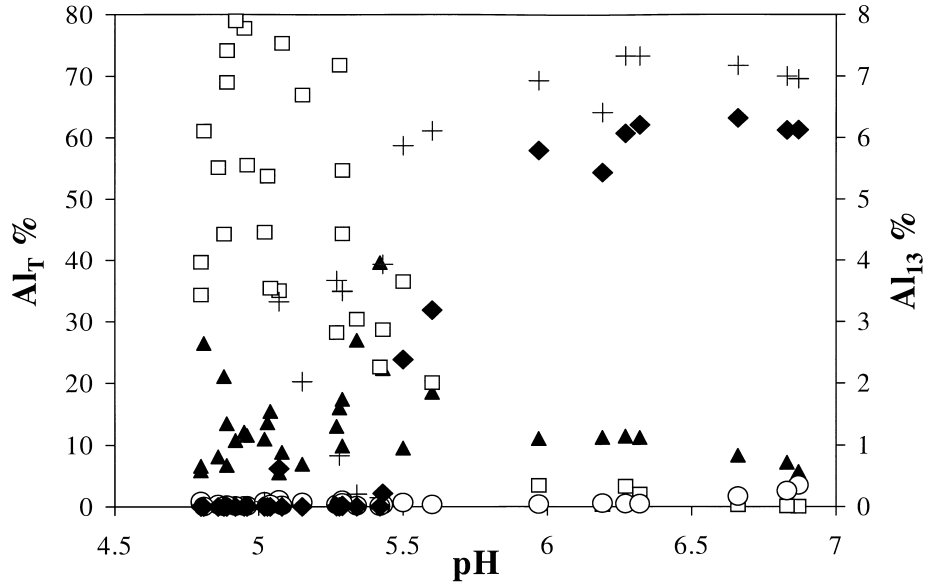

Fig. 2. Calculated distribution of aqueous Al species in soil solutions collected in the upper soil horizon (15 cm depth) illustrating the competition effect between Al–F, Al–SO_4, monomeric Al–Si species and the aqueous polymer Al_{13}. Open squares:Al–SO_4 species; dark triangles: Al–F species; open circles: Al–Si species; dark diamonds: Al_{13} polymer in the simulation with ligands; crosses: Al_{13} polymer in the simulation done without any ligands other than OH^-.

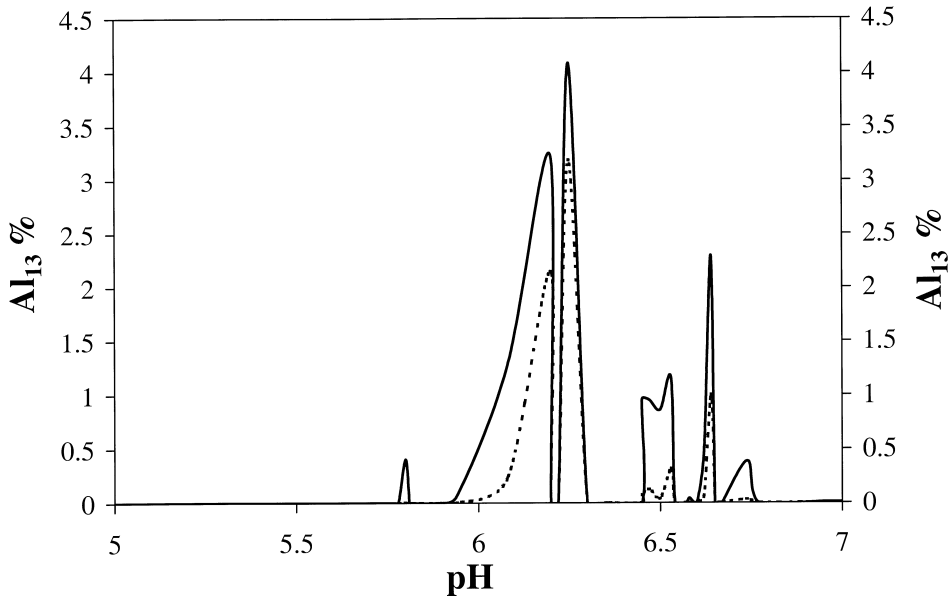

Fig. 3. Maximum and minimum calculated distribution of Al_{13} in streamwaters as a function of pH, expressed in % of total dissolved. Calculations excluded the formation of HAS and organic complexes.

polymers take up aqueous Al at mildly acidic to near neutral pH and therefore compete with Al_{13}. As shown in Fig. 4, the Al_{13} concentration in soil solutions collected at 15 cm depth was lowered to a maximum of 4.0±0.5% of Al_T only (2.4±0.3 μmol l^{-1}), against 6.7±0.2% (3.9±0.1 μmol l^{-1}), due to the inhibiting effect of organic Al. Moreover, Al_{13} became significant within a more restricted pH range (6.5–7). On the other hand, the Al_{13} concentration in soil waters collected at 120 cm depth was essentially unmodified by the presence of organic Al, owing to lower DOC concentrations (6 mg/l) and larger Al_T contents (5×10^{-4} mol l^{-1}) compared to soil solutions collected at the upper soil horizon. The Al_{13} concentration culminated to approximately 6.3±0.1% of Al_T and its maximal value is about 23±2 μmol l^{-1}, against 7.2±0.1% and 25±2 μmol l^{-1}.

If only the formation of HAS is tested in the calculations, the Al_{13} content mostly disappeared in soil solutions collected at 15 cm depth. In deep soil solutions (120 cm depth), the Al_{13} content was brought down to a lesser extent, since Al_T is larger than in the upper soil solutions and dissolved silica concentrations measured at both depths were on the same order. However, Al_{13} did not take more than 2.2±0.1% of Al_T (≈3.3±0.2 μmol l^{-1}) and was significant within a more restricted pH range (6–6.5). When accounting for the formation of both organic Al and HAS polymers, the Al_{13} concentration in deep soil solutions reached a maximal value of 2.1±0.1 μmol l^{-1} only (1.4±0.1% of Al_T).

Dissolved Al concentrations were much less in streamwaters (10^{-5} mol l^{-1}) than in deep soil waters, whereas DOC concentrations were similar. Consistently, the concentration of the Al_{13} polycation decreased markedly when the complexation of Al with organic ligands was modelled. The largest Al_{13} concentration calculated under these conditions in streamwaters was as low as 0.2% of Al_T, which corresponds to a negligible amount, given that Al_T in streamwaters was on the order of 10^{-5} mol l^{-1}. Adding HAS polymers to the previous modelling led to the same order of Al_{13} concentration.

3.2. Consequences for equilibrium between solids and the aqueous phase

Even if the possible formation of polymeric HAS and organo-Al complexes was not considered, i.e. Al_{13} concentrations were maximum (see Fig. 1), the saturation of the soil solutions with respect to any Al and Al–Si minerals tested was hardly influenced at all by the use of a monomeric versus a polymeric Al model to calculate aqueous Al distribution (Fig. 5). Adding the formation of Al_{13} polycation in the simulation only affected the most supersaturated soil solutions with respect to interlayer

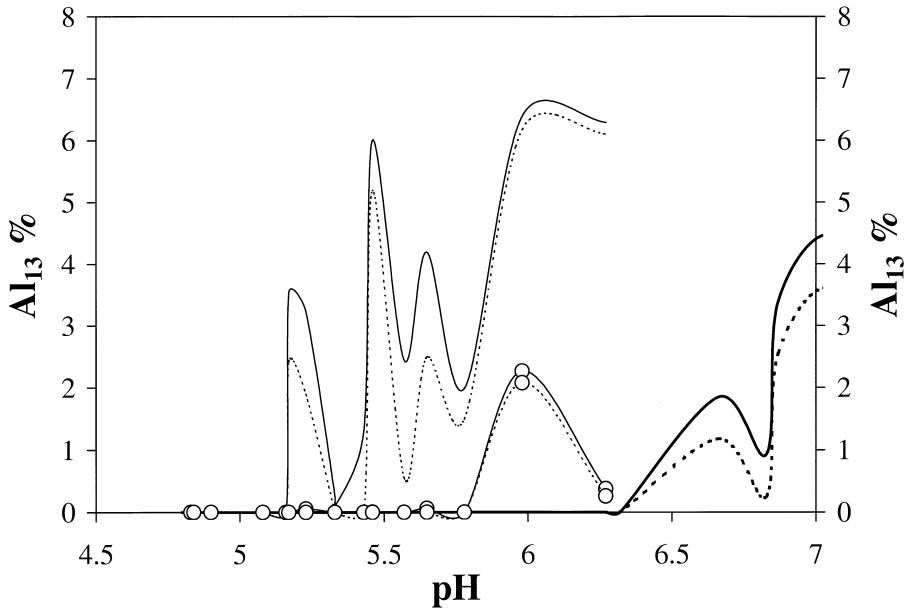

Fig. 4. Maximum and minimum calculated distribution of Al_{13} as a function of pH in upper and deep soil solutions. Calculations performed in deep soil solutions by accounting for the formation of organo-Al complexes only (narrow lines). Results obtained in deep soil solutions by simulating the formation of polymeric HAS species only (open circles). Calculations carried out in upper soil solutions by considering organo-Al complexes only (thick lines). The Al_{13} contribution to Al speciation in the upper soil solutions was insignificant when the formation of HAS polymers only was considered.

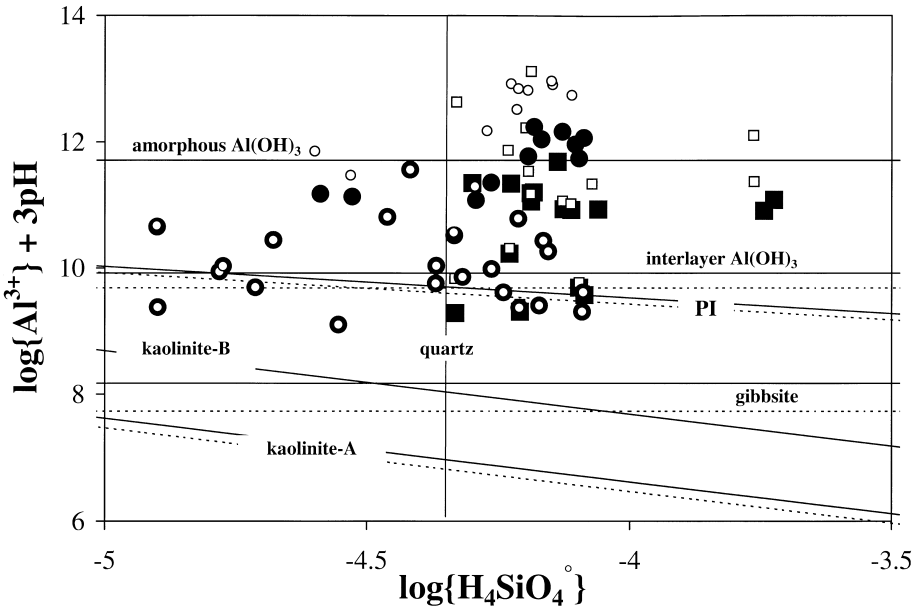

Fig. 5. Activity diagram for soil solutions (15 cm depth = squares; 120 cm depth = circles): activities calculated without considering the polymeric Al_{13} species (open symbols) and computed through the polymeric Al_{13} model (dark symbols). Stability fields for minerals accounting for uncertainties prevailing on their K constants, when known (Table 2). Stability fields are computed at 10°C, for simplicity, but activities used to plot the data are calculated at in situ temperature (see Appendix). Maximum solubility field: continuous line; minimum solubility field: shaded line.

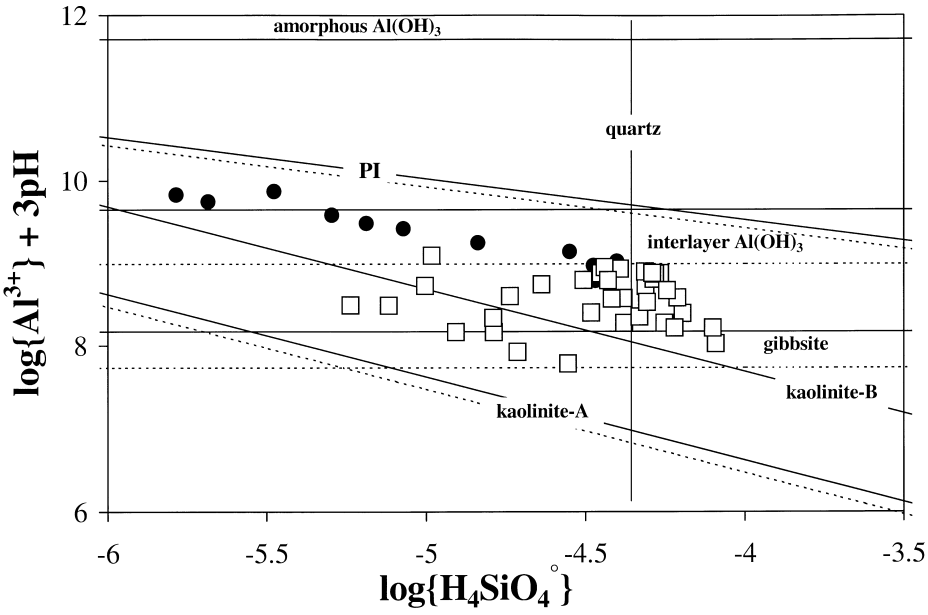

Fig. 6. Activity diagram for soil solutions (15 cm = open squares; 120 cm = dark circles): activities calculated by considering the polymeric Al_{13} species and the formation of both organo-Al complexes and HAS polymers. Stability fields for minerals accounting for the uncertainties prevailing on their K constants, when known (Table 2). Stability fields are computed at 10°C, for simplicity, but activities used to plot the data are calculated at in situ temperature (see Appendix). Maximum solubility fields: continuous lines; minimum solubility fields: shaded lines. Stability fields for interlayer $Al(OH)_3$ correspond to $\log K_{25°C} = 8.41 \pm 0.33$, as recalculated by considering the formation of HAS in the experiments made by Su et al. (1995).

$Al(OH)_3$, but those solutions remained largely supersaturated with respect to this phase.

Furthermore, most of the soil solutions studied in Fig. 5 were also supersaturated with respect to PI. Given that PI is known to precipitate easily even within an aqueous phase (i.e. by homogeneous nucleation), and therefore would be able to control dissolved Al (Lumsdom and Farmer, 1995), this weathering product may thus precipitate in the soil studied. This result disagreed with the fact that PI, imogolite or allophane products have not been identified in this soil (Ezzaïm et al., 1999). This conflicting result was solved when testing the formation of HAS in the calculations, with or without accounting for the formation of organo-Al complexes, as soil solutions became undersaturated with respect to PI under such conditions (Fig. 6). This result also supported the use of soluble HAS polymers in the speciation model, since only soluble precursors of PI may be stable when PI is thermodynamically unstable. Thermodynamic consistency in Fig. 6 was ensured by plotting stability fields for interlayer $Al(OH)_3$ corresponding to the recalculated K constant and uncertainty ($\log K_{25°C} = 8.41 \pm 0.33$) in the presence of soluble HAS polymers.

3.3. Maximum Al_{13} concentrations expected under different climates

This section is primarily devoted to the determination of the largest Al_{13} concentration that could be attained in natural waters in temperate and tropical environments. For that purpose, Al-complexing ligands were excluded from the calculations. Let us assume that Al_T is seldom higher than 10^{-3} mol l^{-1} in natural waters at low temperature (Eldhuset et al., 1987), which is already twice as large as the maximum observed in the natural soil solutions and surface waters previously studied.

The speciation calculations conducted at $T = 25$ and 0°C indicated that under such ideal conditions the Al_{13} polymer cannot contribute more than 7.5% of Al_T (Fig. 7). The maximum contribution of Al_{13} to Al speciation at $Al_T \leqslant 10^{-4}$ mol l^{-1} was slightly altered by changing the temperature. Disregarding pH, Al_{13} exhibited a larger stability with decreasing temperature compared to monomeric hydroxy-Al species. At $Al_T = 10^{-4}$ mol l^{-1}, the Al_{13} polycation reaches a maximum of 6.8% (6.8 μmol l^{-1}) and 7.2% (7.2 μmol l^{-1}) of Al_T at $T = 25°$ and 0°C, respectively. The temperature effect was larger in decreasing Al_T. The largest contribution of Al_{13} to Al speciation was 2.9% at $T = 25$°C and 6% at 0°C, at $Al_T = 10^{-5}$ mol l^{-1}. Moreover, temperature had a marked effect on the pH range wherein Al_{13} may be thermodynamically stable. At $T = 25$°C Al_{13} may be present at pH < 4.5 provided that Al_T is larger than 10^{-4} mol l^{-1}, in the absence of sufficient quantities of complexing ions other than OH^-. To compare, Al_T larger than 10^{-3} mol l^{-1} would be required if $T = 0$°C.

4. Discussion and conclusions

The Al_{13} content and contribution to Al speciation as calculated under equilibrium conditions in natural

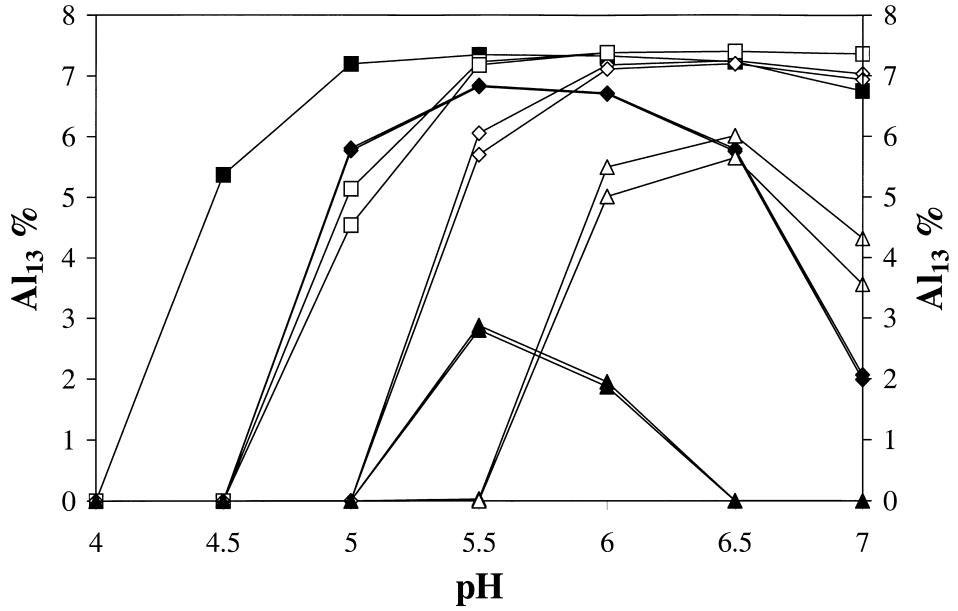

Fig. 7. Maximum and minimum contribution of Al_{13} to total dissolved Al in simulated surface waters as a function of pH, at $T = 0$°C (open symbols) and T = 25°C (dark symbols). $Al_T = 10^{-3}$ mol l^{-1} (squares), 10^{-4} mol l^{-1} (diamonds) and 10^{-5} mol l^{-1} (triangles).

waters at Al_T ranging from 10^{-5} to 5.10^{-4} mol l^{-1} were much lower than previously expected from modelling studies (Bourrié et al., 1989; Bourrié, 1990; Furrer et al., 1992, 1993). It was found that the Al_{13} polycation may not exceed about 7.2±0.1% of Al_T between pH 5.5 and 7 and that maximum was seldom attained although Al speciation was performed in a number of natural soil solutions and streamwaters collected over a period of several years. This investigation also demonstrated that the dimeric and trimeric hydroxy-Al species were always in negligible amounts in natural waters. The latter may therefore be ignored in dealing with Al speciation in low temperature environments (0–25°C). These noteworthy differences compared to the literature largely stemmed from the ignorance of Al–SO_4, Al–F, organo-Al complexes and hydroxyaluminosilicate polymers (HAS) when calculating Al speciation, along with the lack of information concerning the temperature dependence of the stability constant of the Al_{13} polymer. None of the monomeric Al–Si species may efficiently compete with Al_{13} in moderately acidic to near neutral waters (pH = 5.5–7), where the Al_{13} polycation reached a maximum concentration of a few μmol l^{-1} in natural waters. In contrast, HAS polymers may easily form in place of the Al_{13} polycation. Furthermore, when either HAS polymers or organo-Al complexes were considered, the maximum Al_{13} concentration may be reached at pH > 6, only. Under such conditions, the presence of Al_{13} in natural waters is uncertain, since this polymer is known to become unstable between pH 6 and 7 (Furrer et al., 1992).

The scarcity of Al_{13} in soil and surface waters was further confirmed between 0 and 25°C when modelling Al speciation in simplified solutions, i.e. without Al complexing species and at Al_T ranging up to 10^{-3} mol l^{-1}. Moreover, it should be noted that the occurrence of polymeric HAS and Al ligands other than those handled here may further impede the formation of Al_{13} in soil solutions. For example, Dietzel (1998) has shown that polysilicic acids are generated directly upon the dissolution of silicates in acid environments. Polysilicic acids are relatively stable and slowly convert to orthosilicic acid (Iler, 1979). Therefore, in agreement with Farmer and Lumsdom (1994), some of the conditions prevailing in natural soil solutions may have been unreadily met by Browne and Driscoll (1992) when observing the formation of dimeric HAS. However, further investigations are required under controlled polysilicic acid concentrations before considering such dimeric HAS species to calculate aqueous Al speciation.

The low concentration of Al_{13} in natural waters supports the theory in which $Al(OH)_3$ precipitation kinetics would be rate-limited by some reactions occurring in relation with the solid phase (surface reactions, heterogeneous growth, precursor formation and Ostwald ripening), instead of proceeding within the aqueous phase, for example by Al_{13} depolymerisation (Bourrié et al., 1989; Bourrié, 1990). This finding is consistent with the latest experimental evidence for heterogeneous growth kinetics of Al-trihydroxides (Nagy et al., 1999). It also follows from this study that the metastable reservoir or pool of Al that Al_{13} may constitute is much smaller than previously considered (Bottero et al., 1987; Bourrié, 1990). That Al pool may therefore be negligible under most natural conditions and the role of Al_{13} in buffering Al^{3+} activity appears highly uncertain. Furthermore, by considering the formation of polymeric HAS with or without accounting for organic Al complexation (Fig. 6), equilibrium relationships were in better agreement with the soil mineralogy at the Vauxrenard site (Ezzaïm et al., 1999) than without taking account of their formation (see Fig. 5). If so, soil solutions appeared to be undersaturated with respect to proto-imogolite and imogolite-like material, which were not detected in the studied soil system. Moreover, deep soil solutions at pH > 4.7 were within the equilibrium range of the $Al(OH)_3$ compound in vermiculite interlayers, as recalculated in order to be consistent with the use of HAS polymeric species in the calculations. Conversely, those collected at the upper horizon were clearly undersaturated with respect to this phase, and thus may be dissolving. This agrees with the observation that the clay fraction collected at the upper soil horizon had a much larger cation exchange capacity and a much lower Al content as extracted by Na-citrate than in the deep horizon (Ezzaïm et al., 1999).

Several findings regarding Al_{13} toxicity to plants can be inferred from this study. The toxicity level of Al_{13} to several plant species ranged between 3 and 5 μmol l^{-1} (Parker et al., 1989; Shann and Bertsch, 1993). Accordingly, it seemed that at the Vauxrenard site and in the long-term (5 a), no Al_{13} toxicity should occur in leaching solutions collected in the upper soil horizon. The Al_{13} content did not exceed 3.9±0.1 μmol l^{-1}, without including organo-Al complexes nor HAS polymers in the calculations. When organic Al was considered, the Al_{13} concentration did not exceed 2.4±0.3 μmol l^{-1} and its stability domain shifted to the near neutral pH range, where it is known to transform (Furrer et al., 1992). When HAS were considered, the Al_{13} polycation mostly disappeared in the upper leaching solutions. In the deep soil horizon, Al_T increased up to 5×10^{-4} mol l^{-1} and the Al_{13} concentration reached a maximum of about 25±2 μmol l^{-1} if HAS polymers were not considered in the speciation calculations. However, HAS formation had a profound impact on Al_{13} stability and lowered its maximum concentration below the toxicity level, at a pH range marked by Al_{13} instability (pH > 6). In the streamwaters studied, Al_{13} did not exceed 0.31±0.4 μmol l^{-1} and could not be considered as toxic for any living organism.

The calculations conducted for simulated waters at 0 and 25°C indicated that phytotoxicity of Al_{13} cannot be

encountered if Al_T is on the order of 10^{-5} mol l^{-1} and must be very weak at Al_T as large as 10^{-4} mol l^{-1}. It is well-known that capillary solutions play a major role in plant nutrition (e.g. Marques et al., 1996; Marques and Ranger, 1997). The Al_{13} concentration may be estimated in the capillary solutions of the soil studied by considering their pH (< 5.5) and their Al, SO_4 and F^- contents, which are similar to those measured in the leaching waters. Meanwhile, DOC and silica concentrations were also significantly larger than in the leaching solutions (Marques et al., 1996). One may thus reasonably forecast that the Al_{13} concentration was much lower in the capillary soil solutions, certainly on the order of a few μmol l^{-1} at most, and would not reach a toxic level.

As a conclusion, this study demonstrated that the Al_{13} content of natural waters is potentially very low, even if the formation reaction is equilibrium-controlled, due to the presence of Al ligands including dissolved silica. This implies that the role of Al_{13} for Al^{3+} concentration buffering and as rate-limiting agent for Al-trihydroxide precipitation should be minimised in natural environments. Moreover, Al_{13} toxicity to plants seems highly unlikely in natural soil solutions and streamwaters.

Acknowledgements

The ''Région Lorraine'' (France) is thanked for supporting this research, and Dr. E. Dambrine for fruitful discussions and data. The authors also wish to thank K.L. Nagy and an anonymous reviewer for improving the earlier version of the manuscript.

Appendix on next page

Appendix

Sample[a] (cm)	T (°C)	pH	Al	Si	SO_4^{2-}	F^-	DOC	Sample[a] (cm)	T (°C)	pH	Al	Si	SO_4^{2-}	F^-	DOC
15	7.4	4.86	1.72	3.47	21.47	0.10	33.90	120	5.8	4.77	4.81	4.31	26.55	0.20	5.70
15	8.6	4.96	1.19	1.17	7.02	0.10	62.71	120	7.4	4.74	0.59	2.43	13.20	0.04	20.68
15	13.6	5.27	1.06	1.27	8.80	0.10	45.52	120	11.6	4.77	3.71	4.40	23.68	0.21	7.13
15	13.6	5.07	2.55	2.85	16.55	0.10	74.60	120	9.4	5.98	4.22	3.02	23.49	0.10	5.37
15	3.8	4.78	1.78	3.77	9.51	0.10	19.79	120	5.8	5.16	3.31	3.56	23.86	0.18	4.54
15	8.6	5.29	1.42	3.72	9.42	0.10	21.06	Stream	7.0	6.96	0.17	3.84	6.55	0.10	2.5
15	8.6	4.79	1.92	4.41	11.60	0.10	19.12	Stream	7.0	6.77	0.05	3.58	3.34	0.00	5
15	8.6	5.97	1.16	3.28	8.23	0.10	25.66	Stream	7.0	6.67	0.07	5.46	6.13	0.10	1.7
15	13.6	5.02	1.27	2.60	10.09	0.10	26.91	Stream	7.0	6.57	0.09	2.68	2.18	0.54	1.87
15	13.6	6.19	0.90	1.56	10.18	0.10	29.78	Stream	7.0	6.47	0.11	2.77	4.57	0.06	1.87
15	13.6	5.43	0.61	0.76	6.74	0.10	27.48	Stream	7.0	6.36	0.17	3	3.34	1.11	2.5
15	13.6	4.80	2.13	2.60	6.61	0.10	55.30	Stream	7.0	6.3	0.05	4.23	7.52	0.08	0.25
15	13.6	4.80	2.40	2.94	5.69	0.10	55.30	Stream	7.0	6.25	0.23	3.67	2.25	0.04	7.47
15	7.4	4.71	1.98	3.07	12.39	0.14	55.90	Stream	7.0	6.2	0.15	2.18	2.58	0.44	2.5
15	3.8	4.89	2.06	4.92	10.25	0.10	54.40	Stream	7.0	6.08	0.09	1.63	4.89	0.00	5.62
15	3.8	6.87	1.61	5.05	12.55	0.15	27.80	Stream	7.0	5.94	0.08	2.85	3.59	0.00	0
15	3.8	4.95	1.55	4.05	13.37	0.14	21.40	Stream	7.0	5.89	0.04	3.2	7.66	0.08	7.82
15	3.8	5.08	1.56	3.29	9.82	0.10	24.40	Stream	7.0	5.81	0.21	3.33	3.3	0.32	1.25
15	3.8	6.27	1.57	4.83	17.39	0.15	41.60	Stream	7.0	5.8	0.15	3.43	4.41	0.00	5
15	3.8	4.92	1.74	4.89	15.79	0.14	32.30	Stream	7.0	5.77	0.13	3.1	9.99	0.07	2.39
15	3.8	4.76	1.71	5.11	13.53	0.14	21.90	Stream	7.0	5.6	0.11	4.31	8.95	0.09	0.59
15	3.8	6.83	1.56	4.17	14.52	0.17	43.10	Stream	7.0	5.56	0.14	2.14	2.2	0.10	2.57
15	3.8	6.32	1.56	3.87	13.85	0.15	37.80	Stream	7.0	5.48	0.16	2.47	2.86	0.10	1.96
15	3.8	6.66	1.55	4.80	13.91	0.15	20.60	Stream	7.0	5.47	0.29	3.48	2.71	0.18	5
15	3.8	5.28	1.18	4.21	11.68	0.14	18.50	Stream	7.0	5.46	0.12	3.45	4.52	0.09	2.73
15	3.8	4.81	1.91	1.68	17.72	0.39	74.16	Stream	7.0	5.45	0.04	2.78	10.59	0.06	2.69
15	3.8	4.73	1.69	3.17	11.56	0.13	29.71	Stream	7.0	5.35	0.03	3.61	2.23	0.00	0
15	8.6	5.50	1.46	3.08	9.09	0.10	33.36	Stream	7.0	5.32	0.17	3.37	3.81	0.21	2.76
15	8.6	5.15	2.02	4.15	12.04	0.10	33.14	Stream	7.0	5.3	0.17	2.96	2.52	0.21	4.6
15	8.6	4.89	1.31	3.71	12.43	0.13	29.65	Stream	7.0	5.28	0.27	3.49	4.46	0.28	0.83
15	8.6	5.03	1.02	1.00	5.84	0.10	40.96	Stream	7.0	5.26	0.20	3.09	3.51	0.22	1.79
15	8.6	5.04	0.90	1.02	4.70	0.10	36.86	Stream	7.0	5.23	0.19	2.84	9.41	0.06	2.34
15	8.6	5.42	0.34	0.38	2.11	0.10	17.38	Stream	7.0	5.2	0.16	2.88	4	0.19	0.1
15	8.6	5.34	0.51	0.50	2.52	0.10	21.81	Stream	7.0	5.16	0.21	2.84	3.39	0.30	2.81
15	13.6	4.88	0.65	0.76	3.25	0.10	14.74	Stream	7.0	5.15	0.16	3.27	8.35	0.10	1.41
15	7.4	4.79	2.13	3.52	7.88	0.17	41.86	Stream	7.0	5.13	0.22	3	3.53	0.25	0.37
15	7.4	4.76	1.27	2.03	6.73	0.14	31.10	Stream	7.0	5.12	0.17	2.92	9.46	0.08	12.39
15	7.4	5.60	1.18	1.79	6.44	0.16	56.78	Stream	7.0	5.11	0.29	2.89	2.91	0.39	2.5
15	3.8	5.29	1.44	2.10	6.00	0.18	71.94	Stream	7.0	5.09	0.44	3.52	9.73	0.07	4.73
120	11.6	4.79	2.35	1.97	16.33	0.10	8.35	Stream	7.0	5.07	0.32	3.54	3.07	0.05	6.65
120	9.4	5.17	11.45	11.10	28.06	0.10	5.14	Stream	7.0	5.04	0.18	1.93	6.44	0.06	2.12
120	9.4	5.46	11.52	11.42	28.41	0.10	6.18	Stream	7.0	5.03	0.12	3.67	15.05	0.09	2.58
120	9.4	5.23	8.37	5.34	25.87	0.10	5.80	Stream	7.0	5.02	0.22	3.32	3.42	0.14	2.5
120	5.8	5.33	5.43	4.53	27.68	0.10	9.03	Stream	7.0	5.01	0.38	2.67	3.23	0.43	6.87
120	7.4	5.08	1.83	2.80	22.09	0.10	16.99	Stream	7.0	5	0.23	3.48	4.53	0.24	0.55
120	11.6	4.83	5.23	4.86	31.33	0.10	6.88	Stream	7.0	4.98	0.26	3.61	5.22	0.12	0.18
120	9.4	4.90	4.04	4.95	34.13	0.10	5.19	Stream	7.0	4.95	0.16	3.11	2.43	0.04	3.75
120	5.8	5.65	4.37	3.59	26.60	0.10	6.32	Stream	7.0	4.89	0.27	3.48	5.3	0.11	0
120	7.4	5.43	4.21	3.93	30.83	0.10	6.53	Stream	7.0	4.85	0.18	3.23	4.71	0.05	1.87
120	9.4	5.78	3.80	3.96	21.83	0.10	26.32	Stream	7.0	4.83	0.39	4.85	6.94	0.09	1.86
120	5.8	4.84	4.28	3.72	29.65	0.10	8.20	Stream	7.0	4.79	0.40	3.96	4.76	0.15	3.33
120	5.8	4.75	4.09	3.38	25.08	0.10	7.10	Stream	7.0	4.77	0.52	2.99	13.26	0.09	2.82
120	7.4	5.57	3.78	3.91	29.88	0.10	10.38	Stream	7.0	4.75	0.33	2.59	9.69	0.08	2.06
120	5.8	6.27	4.36	4.41	27.40	0.15	7.40	Stream	7.0	4.72	0.52	4.19	3.7	0.10	5.2
120	5.8	5.33	4.89	4.69	27.48	0.17	6.40	Stream	7.0	4.71	0.65	2.08	7.14	0.10	1.87

[a] Concentrations are expressed in mg l^{-1}.

References

AFES, 1992. Principaux Sols d'Europe. Référentiel Pédologique. Association Française pour l'Etude des Sols. Institut National de Recherches Agronomique, Paris.

Alva, A.K., Edwards, D.G., Asher, C.J., Blamey, F.P.C., 1986. Effects of phosphorus/aluminum molar ratio and calcium concentration on plant response to aluminium toxicity. Soil Sci. Soc. Am. J. 50, 133–137.

Badora, A., Furrer, G., Grunwald, A., Schulin, R., 1998. Immobilization of zinc and cadmium in polluted soils by polynuclear Al_{13} and Al-montmorillonite. J. Soil Contam. 7, 573–588.

Bertsch, P.M., 1989. Aqueous polynuclear aluminium species. In: Sposito, G. (Ed.), The Environmental Chemistry of Aluminium. CRC Press, Bota Raton, Florida, pp. 87–115, (Chapter 4)..

Birchall, J.D., Exley, C., Chappell, J.S., Phillips, M.J., 1989. Acute toxicity of aluminium to fish eliminated in silicon-rich acid waters. Nature 338, 146–148.

Bottero, J.-Y., Axelos, M., Tschoubar, D., Cases, J.-M., Fripiat, J.-J., Fiessinger, F., 1987. Mechanism of formation of aluminum trihydroxide from Keggin Al_{13} polymers. J. Colloid. Interface Sci. 117, 47–57.

Boudot, J.-P., Becquer, T., Merlet, D., Rouiller, J., 1994. Aluminium toxicity in declining forests:a general overview with seasonal assessment in a silver fir forest in the Vosges mountains (France). Ann. Sci. For. 51, 27–51.

Boudot, J.-P., Maitat, O., Merlet, D., Rouiller, J., 1996. Occurrence of non-monomeric species of aluminium in undersaturated soil and surface waters: consequences for the determination of mineral saturation indices. J. Hydrol 177, 47–63.

Bourrié, G., 1990. Conséquences de l'existence de complexes polynucléaires de Al(III) sur la stabilité des minéraux alumineux: une reconsidération du système gibbsite-kaolinite-quartz. C.R. Acad. Sci. Paris 310, 765–770.

Bourrié, G., Grimaldi, C., Régeard, A., 1989. Monomeric versus mixed monomeric-polymeric models for aqueous aluminium species:constraints from low-temperature natural waters in equilibrium with gibbsite under temperate and tropical climate. Chem. Geol 76, 403–417.

Browne, B.A., Driscoll, C.T., 1992. Soluble aluminium silicates:stoichiometry, stability, and implications for environmental geochemistry. Science 256, 1667–1670.

Bryzgalin, O.V., Rafal'skiy, R.P., 1982. Estimation of the instability constants for ore-elements complexes at elevated temperature. Geochem. International 19, 839–849.

Cronan, C.S., Walker, W.J., Bloom, P.R., 1989. Predicting aqueous aluminium concentrations in natural waters. Nature 324, 140–143.

Dambrine, E., Pollier, B., Poszwa, A., Ranger, J., Probst, A., Viville, D. et al., 1998. Evidence of current soil acidification in spruce stands (Strengbach catchment, Vosges Mts, N-E France). Water, Air, Soil Pollut. 105, 43–52.

Devidal, J.-L., Dandurand, J.-L., Gout, R., 1996. Gibbs free energy of formation of kaolinite from solubility measurement in basic solution between 60 and 170°C. Geochim. Cosmochim. Acta 60, 553–564.

Dietzel, M., 1998. Polysilicic acid and the dissolution of silicates. Mineral Mag 62A, 385–386.

Drever, J.I., Stillings, L.L., 1997. The role of organic acids in mineral weathering. Colloids and Surfaces. A:Physicochemical and Engineering Aspects 120, 167–181.

Driscoll, C.T., Lehtinen, M.D., Sullivan, T.J., 1994. Modeling of acid-base chemistry of organic solutes in Adirondack, New-York lakes. Water Resour. Res. 30, 297–306.

Eldhuset, T., Göransson, A., Ingestad, T., 1987. Aluminium toxicity in forest tree seedlings. In: Hutchinson, T.C., Meema, K.M. (Eds.), Effects of Atmospheric Pollutants on Forests, Wetlands and Agricultural Ecosystems, NATO ASI Ser. G16. Springer-Verlag, Berlin, Heidelberg, pp. 401–409.

Exley, C., Birchall, J.D., 1995. Comment on "An assessment of complex formation between aluminium and silicic acid in acidic solutions" by V.C. Farmer and D.G. Lumsdon. Geochim. Cosmochim. Acta. 59, 1017.

Exley, C., Birchall, J.D., 1996. Letter to the Editor: Silicic acid and the biological availability of aluminium. Eur. J. Soil Sci. 47, 137.

Ezzaïm, A., Turpault, M.-P., Ranger, J., 1999. Quantification of weathering processes in an acid brown soil developed from tuff (Beaujolais, France). Part II. Soil formation. Geoderma 87, 155–177.

Farmer, V.C., 1979. Possible role of a mobile hydroxyaluminium orthosilicate complex (proto-imogolite) and other hydroxyaluminium and hydroxy-iron species in podzolization. In: Colloques Internationaux du CNRS. Migrations Organo-Minérales dans les Sols Tempérés. 303, pp. 275–279.

Farmer, V.C., Lumsdon, D.G., 1994. An assessment of complex formation between aluminium and silicic acid in acidic solutions. Geochim. Cosmochim. Acta 58, 3331–3334.

Farmer, V.C., Lumsdon, D.G., 1995. Reply to the Comment by C. Exeley and J.D. Birchall on "An assessment of complex formation between aluminium and silicic acid in acidic solutions". Geochim. Cosmochim. Acta 59, 1019.

Faust, B.C., Labiosa, W.B., Dai, K'o H., MacFall, J.S., Browne, B.A., Ribiero, A.A. et al., 1995. Speciation of aqueous mononuclear Al(III)-hydroxo and other Al(III) complexes at concentrations of geochemical relevance by aluminium-27 nuclear magnetic resonance spectroscopy. Geochim. Cosmochim. Acta. 59, 2651–2661.

Furrer, G., Ludwig, Chr., Schindler, P.W., 1992. On the chemistry of the Keggin Al_{13} polymer. I. Acid-base properties. J. Colloid Interface Sci. 149, 56–67.

Furrer, G., Trusch, B., Müller, C., 1993. The formation of polynuclear Al_{13} under simulated natural conditions. Geochim. Cosmochim. Acta 56, 3831–3838.

Gruaer, U.E., 1993. Modeling anion amelioration of aluminum phytotoxicity. Plant and Soil 157, 319–331.

Grzyb, K.R., 1995. NOAEM (natural organic anion equilibrium model): A data analysis algorithm for estimating functional properties of dissolved organic matter in aqueous environments: part 1. Ionic component speciation and metal association. Org. Geochem. 23, 379–390.

Helgeson, H.C., Delany, J.M., Nesbitt, H.W., Bird, D.K., 1978. Summary and critique of the thermodynamic properties of rock-forming minerals. Am. J. Sci. 278a, 1–229.

Hem, J.D. and Roberson, C.E., 1990. Aluminium hydrolysis reactions and products in mildly acidic aqueous systems. In: Melchior, D. C., Bassett, R.L. (Eds.), Chemical Modeling of Aqueous Systems II. ACS Symp. Ser. 416;, pp. 426–446.

Huang, P.M., 1991. Ionic factors affecting the formation of short-range ordered aluminosilicates. Soil Sci. Soc. Am. J. 55, 1172–1180.

Iler, R.K., 1979. The Chemistry of Silica — Solubility, Polymerization, Colloid and Surface Properties, and Biochemistry. Wiley-Interscience, New York.

Johnson, J.W., Oelkers, E.H., Helgeson, H.C., 1992. SUPCRT92: a software package for calculating the standard molal thermodynamic of minerals, gases, aqueous species, and reactions from 1 to 5000 bars and 0° to 1000°C. Computer Geosci. 18, 899–947.

Kittrick, J.A., 1966. Free energy of formation of kaolinite from solubility measurements. Amer. Mineral. 51, 1457–1466.

LaZerte, B.D., Loon, G., van Anderson, B., 1997. Aluminium in water. In: Yokel, R.A., Golub, M.S. (Eds.), Research Issues in Aluminium Toxicity. Taylor & Francis, Bristol, USA, pp. 17–45.

Lou, G., Huang, P.M., 1988. Hydroxy-aluminosilicate interlayers in montmorillonite:implications for acidic environments. Nature 335, 625–627.

Lumsdon, D.G., Farmer, V.C., 1995. Solubility characteristics of proto-imogolite sols: how silicic acid can de-toxify aluminum solutions. Eur. J. Soil. Sci. 46, 179–186.

Lumsdon, D.G., Farmer, V.C., 1996. Response to: 'Silicic acid and biological availability of aluminium' by C. Exley and J.D. Birchall. . Eur. J. Soil. Sci. 47, 139–140.

Marques, R., Ranger, J., 1997. Nutrient dynamics in a chronosequence of Douglas-fir (Pseudotsuga menziesii (Mirb) Franco) stands on the Beaujolais Mounts (France). 1: qualitative approach. For. Ecol. Manage. 91, 255–277.

Marques, R., Ranger, J., Gelhaye, D., Pollier, B., Ponette, Q., Gobert, O., 1996. Comparison of chemical composition of soil solutions collected by zero-tension plate lysimeters with those from ceramic cup lysimeters in a forest soil. Eur. J. Soil. Sci. 47, 407–417.

Nagy, K.L., Cygan, R.T., Hanchar, J.M., Sturchio, N.C., 1999. Gibbsite growth kinetics on gibbsite, kaolinite, and muscovite substrates: AFM evidence for epitaxy and an assessment of reactive surface area. Geochim. Cosmochim. Acta 63, 2337–2351.

Nordstrom, D.K., May, H.M., 1989. Aqueous equilibrium data for mononuclear aluminium species. In: Sposito, G. (Ed.), The Environmental Chemistry of Aluminium, CRC Press. CRC Press, Boca Raton, FL, pp. 29–55, (Chapter 2).

Parker, D.R., Kinraide, T.B., Zelazny, L.W., 1989. On the phytotoxicity of polynuclear hydroxy-aluminum complexes. Soil Sci. Soc. Am. J. 53, 789–796.

Party, J.-P., Probst, A., Dambrine, E., Thomas, A.-L., 1995. Critical loads of acidity to surface waters in the Vosges Massif. Water, Air, Soil Pollut. 85, 2407–2412.

Plyasunov, A.V., Grenthe, I., 1994. The temperature dependence of stability constants for the formation of polynuclear cationic complexes. Geochim. Cosmochim. Acta 58, 3561–3582.

Pokrovski, V.A., Helgeson, H.C., 1995. Thermodynamic properties of aqueous species and the solubilities of minerals at high pressures and temperatures: the system Al_2O_3–H_2O–NaCl. Amer. J. Sci. 295, 1255–1342.

Pokrovski, G.S., Schott, J., Harrichoury, J.-C., Sergeyev, A.S., 1996. The stability of alumino-silica complexes in acidic solutions from 25 to 150°C. Geochim. Cosmochim. Acta 60, 2495–2501.

Pokrovski, G.S., Schott, J., Salvi, S., Gout, R., 1998. Structure and stability of aluminum-silica complexes in neutral to basic solutions. Experimental study and molecular orbital. Mineral. Mag. 62a, 1194.

Probst, A., Dambrine, E., Viville, D., Fritz, B., 1990. Influence of acid atmospheric inputs on surface water chemistry and mineral fluxes in a declining spruce stand within a small granitic catchment (Vosges massif-France). J. Hydrol. 116, 101–124.

Probst, A., Party, J.-P., Fevrier, C., Dambrine, E., Thomas, A.-L., Stussi, J.-M., 1999. Evidence of springwater acidification in the Vosges mountains (north-east of France): influence of bedrock buffering capacity. Water, Air, Soil Pollut. 114, 395–411.

Ranger, J., Marques, R., Colin-Belgrand, M., Flammang, N., 1995. The dynamics of biomass and nutrient accumulation in a Douglas-fir (*Pseudotsuga menziesii* Franco) stand studied using a chronosequence approach. For. Ecol. Manage. 72, 167–183.

Ridley, M.K., Wesolowski, D.J., Palmer, D.A., Kettler, R.M., 1999. Association quotients of aluminum sulphate complexes in NaCl media from 50 to 125°C:results of a potentiometric and solubility study. Geochim. Cosmochim. Acta 63, 459–472.

Rimstidt, J.D., 1997. Quartz solubility at low temperatures. Geochim. Cosmochim. Acta 61, 2553–2558.

Salvi, S., Pokrovski, G.S., Schott, J., 1998. Experimental investigation of aluminium-silica aqueous complexing at 300°C. Chem. Geol. 151, 51–67.

Schecher, W.D., Driscoll, C.T., 1993. ALCHEMI: a chemical equilibrium model to assess the acid-base chemistry and speciation of aluminum in dilute solutions. In: Loeppert, R., Schwab, A.P., Goldberg, S. (Eds.), Chemical Equilibrium and Reaction Models. Soil Science Society of America, Div. S-1 V, SSSA special publication 42, USA, pp. 325–356 (Chapter 16).

Schecher, W.D., McAvoy, D., 1992. MINEQL+: a software environment for chemical equilibrium modeling. Comput. Environ. Systems 16, 65–76.

Shann, J.R., Bertsch, P.M., 1993. Differential cultivar response to polynuclear hydroxo-aluminium complexes. Soil Sci. Soc. Am. J. 57, 116–120.

Shock, E.L., Helgeson, H.C., 1988. Calculation of the thermodynamic and transport properties of aqueous species at high pressures and temperatures: correlation algorithms for ionic species and equation of state predictions to 5kb and 1000°C. Geochim. Cosmochim. Acta 53, 2009–2036.

Shock, E.L., Sassani, D.C., Willis, M., Sverjensky, D.A., 1997. Inorganic species in geologic fluids:correlations among standard molal thermodynamic properties of aqueous ions and hydroxide complexes. Geochim. Cosmochim. Acta 61, 907–950.

Stumm, W., Morgan, J.J., 1981. Aquatic Chemistry. An Introduction Emphasizing Chemical Equilibria in Natural Waters. John Wiley & Sons, New York.

Su, C., Harsh, J.B., Boyle, J.S., 1995. Solubility of hydroxy-aluminum interlayers and imogolite in a spodosol. Soil Sci. Am. J. 59, 373–379.

Thomas, A.-L., Dambrine, E., King, D., Party, J.-P., Probst, A.A., 1999. A spatial study of the relationships between streamwater acidity and geology, soil and relief (Vosges, north-eastern France). J. Hydrol. 217, 35–45.

Tipping, E., 1994. WHAM — a chemical equilibrium model and computer code for waters, sediments, and soils incorporating a discrete site/electrostatic model of ion-binding by humic substances. Computer and Geosci. 20, 973–1023.

USDA, 1994. Keys for soil taxonomy, 6th Edition. Soil Conservation Service.

Wada, S.-I., Wada, K., 1980. Formation, composition and structure of hydroxy-aluminosilicate ions. J. Soil. Sci. 31, 457–467.

Wolery, T.J., 1992. EQ3NR, a Computer Program for Geochemical Aqueous Speciation-solubility Calculations: Theoretical Manual. User's Guide, and Related Documentation (UCR-MA-110662 PT III). Lawrence Livermore National Lab.

Silice dans les solutions gravitaires et capillaires faiblement liées

Gérard F., François M., et Ranger J. (2002) Processes controlling silica concentration in leaching and capillary soil solutions of an acidic brown forest soil (Rhône, France). *Geoderma* **107**, 197-226.

ELSEVIER

Geoderma 107 (2002) 197–226

GEODERMA

www.elsevier.com/locate/geoderma

Processes controlling silica concentration in leaching and capillary soil solutions of an acidic brown forest soil (Rhône, France)

F. Gérard*, M. François, J. Ranger

Institut National de la Recherche Agronomique, Centre de Recherches Forestières, Unité Biogéochimie des Ecosystèmes Forestiers, 54280 Champenoux, France

Received 1 September 2000; accepted 17 October 2001

Abstract

Chemical analysis of leaching and capillary soil solutions collected at different soil depths was performed on a monthly basis for several years at the Vauxrenard site (Rhône, France). The seasonal variations in dissolved silica (Si) indicated considerable differences whether contained in leaching or capillary soil solutions. In capillary solutions, the maximum and minimum Si concentrations occurred in the summer and winter, respectively, while the opposite trend was observed with leaching soil solutions. In both solutions types, significant relationships may be obtained between Si concentration and soil temperature (T) and, to a lesser extent, H^+ concentration. Evaporation or evapotranspiration had little effect on Si in capillary solutions, limited to the upper soil layers. An inverse relationship between Si and T found in leaching solutions indicated that weathering did not control Si concentration. In contrast, a positive relationship between Si and T found in capillary solutions was consistent with this process. This was reinforced by a significant relationship obtained between logSi and pH, which was consistent with surface-controlled and proton-promoted weathering. Calculated apparent activation energy and reaction order with respect to pH were both consistent with muscovite at the laboratory scale. It is suggested that Si concentration in leaching solutions was controlled mainly by diffusion of aqueous silica (essentially orthosilicic acid) from capillary solutions in relation to soil drainage. Thermodynamic calculations showed that the temperature-dependence of the solubility of Si-containing secondary phases did not significantly control Si concentration in both soil solution types. However, it was calculated that the reversible formation of some hypothetical siliceous phases ($Si/Al > 1$) proceeded at relatively slow rates, thus limiting their impact on Si concentration. Kinetic calculations showed excellent results by correlating Si concentration in capillary solutions to specific weathering rate for primary soil silicates. In

* Corresponding author. Tel.: +33-8339-4146; fax: +33-8339-4069.
E-mail address: gerard@nancy.inra.fr (F. Gérard).

PII: S0016-7061(01)00149-5

agreement with most of the statistical analysis, soil temperature appeared to be the main driving force for chemical weathering. Protons (H^+) had a significant influence in the deeper soil horizons as well as in the seasons corresponding to lesser soil temperature variations. An important effect of organic ligands and particularly of low molecular weight compounds on weathering may explain larger Si concentration observed in the upper soil layers.

Keywords: Acidic soil; Soil solution; Silica; Weathering; Mechanism; Modelling

1. Introduction

It is important to understand the processes controlling dissolved silica (Si) concentration in soil solutions for a number of reasons. Dissolved Si can control aluminium (A1) mobility in soils through the formation of solid phases exhibiting a large range of Si and A1 contents, ranging from kaolinite to allophane-type and imogolite-type materials. Silica may also be important in higher plants' nutrition in contrasting climates (Bartoli, 1983; Sangster and Hodson, 1986). Moreover, dissolved Si may alleviate A1 toxicity in soil solutions and surface waters through the formation of proto-imogolite (PI) and soluble hydroxyaluminosilicate (HAS) species (Farmer, 1979; Lumsdon and Farmer, 1995; Exley and Birchall, 1995, 1996; Gérard et al., 2001). Several studies carried out on the watershed scale have shown relationships between Si concentration in surface waters and temperature (Meybeck, 1986; Drever and Zobrist, 1992; White and Blum, 1995; White et al., 1999). These studies supported the notion that Si concentration is controlled by mineral weathering on this scale. They outlined the role of Si concentration as a temperature and weathering rate indicator as well. Similar studies carried out at the soil scale are scarce. Moreover, there appears to be a lack of research focusing on the influence of soil temperature (i.e. season) on dissolved Si in both leaching and capillary soil solutions collected at different soil depths. For instance, Berner et al. (1998) have studied the seasonal variability of Si in leaching solutions disregarding soil depth. Given that leaching and capillary solutions have different residence times, different processes may control the amount of dissolved Si. Basically, capillary solutions are almost immobile, whereas leaching solutions flow through the soil and thus have a much shorter residence time. Therefore, Si concentration in capillary solutions may better reflect interactions with soil silicates and the chemistry of leaching and capillary solutions may be different (Giesler et al., 1996; Marques et al., 1996).

The aim of this paper is to discuss the processes that control the temporal and spatial variations in dissolved silica in both capillary and leaching soil solutions. A long-term survey of a forested acidic brown soil in a temperate climate has provided a comprehensive set of solution chemistry data, measured on a monthly basis for almost 5 years from the summer of 1995 to the winter of 1999–2000. This large time scale was particularly adapted to the scope of this study. Particular attention was first placed on the variations in a few measured variables, mainly soil temperature and H^+ concentration (estimated from the pH), and their relationship with Si concentration in both solution types. These variables were chosen essentially because of their relevance to processes likely to control Si concentration, specifically the interactions between soil silicates and

solutions. In a second step, thermodynamic and kinetic geochemical modelling was used as a tool to aid in understanding the importance of different Si-controlling processes.

2. Materials and methods

The soil studied is an acidic brown soil, classified as a 'Typic Dystrochrept' (USDA, 1994) or an Alocrisol (AFES, 1992). A 40-years-old plantation of Douglas-fir covered the soil. The study site is in the 'Montagne des Aiguilettes' in the Beaujolais (Rhône, France) at an altitude of about 750 m. The mean annual temperature is 7 °C and mean annual precipitation is 1000 mm. Chemical properties of the soil, stand characteristics, ecology and nutrient dynamics have been discussed in several studies (Ranger et al., 1995; Marques et al., 1996; Marques and Ranger, 1997; Ezzaïm et al., 1997, 1999b).

2.1. Soil mineralogy

The mineralogy of both the soil and bedrock at the Vauxrenard site, from which the soil solutions were collected, has been studied extensively (Ezzaïm et al., 1999a,b). The bedrock is an Upper Visean volcanic tuff that has undergone hydrothermal alteration. It is composed of approximately even proportions of phenocrysts and devitrified groundmass both made of quartz, K-feldspar, albite, andesine, white mica, biotite and minor apatite. The weathering gradient inferred by a quantitative study of the soil mineralogy compared to the unweathered tuff was: quartz<K-feldspar<white mica<biotite<albite<andesine. Kaolinite, hydroxy-Al interlayered vermiculites and interstratified vermiculite–biotite have been identified as the main weathering products. The presence of both allophane-type and imogolite-type materials (hereafter referred to as ATM and ITM, respectively) has not been observed. Moreover, the low quantities of Al and Si extracted by oxalate (Alo and Sio, respectively) consistently suggested that such poorly crystallised to amorphous siliceous phases were almost absent from this soil (see Ezzaïm et al., 1999b for more details).

2.2. Soil solutions

We studied the seasonality of Si concentration in solutions collected from the soil by zero-tension plate lysimeters (ZTL) and cup lysimeters connected to a constant suction (600 hPa), which are commonly called tension lysimeters (TL). Leaching and capillary soil solutions were collected at 15, 30, 60 and 120 cm depth below the organic layer, corresponding to the Al/Ap, A/(B), B and C horizons, respectively. Several replicates per depth were used in order to encompass, as comprehensively as possible, the effect of soil heterogeneity on the chemistry of soil solutions. Eight TL replicates per depth were available for the collection of capillary solutions at 15, 30, and 60 cm depth and four at 120 cm depth. Each was connected to an individual collection bottle, sampled and cleaned with bidistilled water on a monthly basis. Five ZTL replicates per depth were used but they were connected to the same collection bottle for practical reasons. Sampling and cleaning was performed monthly as well. After sampling, solutions were taken to the laboratory, filtered at 0.45 μm, maintained at 4 °C and analysed as quickly as possible (within 48 h).

The pH was measured with a single-rod pH electrode (INGOLD-XEROLIT®) connected to a Mettler DL21 pH-meter. ICP emission spectroscopy (JY 38+spectrometer) was used to measure the total concentrations of Si, Al, Ca, Mg, K, Na, Mn and Fe. Dissolved organic carbon (DOC) was measured with a SHIMDZU TOC 5050. Sulphate and flouride were analysed by ion chromatography.

2.3. Computer program and thermodynamic data

The EQ3NR computer program (Wolery, 1992) was used for calculating the distribution of aqueous species at the in situ temperatures of the soil (using monthly averages). The thermodynamic database considered for Al species has been thoroughly discussed in Gérard et al. (2001). The entire set of Al–Si aqueous species was taken into account in these calculations. It ranged from monomeric (Si/Al=1) to polymeric HAS species (Si/Al=0.5). Polymeric HAS species served to simulate ITM and ATM precursors. The same database was applied for the stability of secondary mineral phases. However, natural imogolite (Zysset et al., 1999) was added to the database to encompass the wide range of log$K$ proposed in the literature for imogolite. Upper and lower solubility boundaries for imogolite were defined by the maximum and minimum log$K$ (i.e. log$K$ plus and minus the standard deviation, respectively) for proto-imogolite (PI) and natural imogolite, respectively. The temperature-dependence of the log$K$ for natural imogolite was calculated with the Van't Hoff's equation. For the purpose of internal consistency of the database, the enthalpy of the formation reaction per mole of mineral (ΔH_r^0=187.5 kJ mol^{-1}) was recalculated according to Lumsdon and Farmer (1995) by considering the formation enthalpies for aqueous and mineral species included in our database. This value was also used for PI. Vermiculite was absent from the database, owing to the structural and compositional complexity and variability of this secondary sheet-silicate in addition to its interstratified nature with biotite and the lack of information concerning the distribution of Al in this phase between interlayer, octahedral and tetrahedral sites. For these reasons, no attempt was made to calculate mean structural formulae for vermiculite in Ezzaïm et al. (1999b).

The standard database of the EQ3NR computer program was used for other aqueous species and soil primary minerals (albite, K-feldspar and white mica). The thermodynamic equilibrium constant for white mica, $K_{0.94}(Mg_{0.19}Fe(II)_{0.14}Al_{1.71})Al_{0.73}Si_{3.27}O_{10}(OH)_2$ (see Ezzaïm et al., 1999b), was estimated with an ideal solid solution model (Tardy and Fritz, 1981) according to Eq. (1).

$$\ln K_m = \sum_j x_i \ln K_i + \sum_j x_i \ln x_i \quad (1)$$

where K_m is the equilibrium constant of the ideal solid solution m, j is the number of end-members i required to model the solid solution, x_i is the mole fraction of the end-member i in the solid solution m, and K_i is the thermodynamic equilibrium constant for the end-member i. Three end-members available in the EQ3NR database (muscovite, annite and Mg-phlogopite) were used. The primary mineral biotite was not considered in this study. Our choice was supported by the very great extent of the biotite transformation reaction to

secondary clays (pure vermiculite and interstratified vermiculite-biotite), compared to the relatively low amount of biotite within the unaltered tuff (Ezzaïm et al., 1999a,b).

2.4. Kinetic dissolution rate laws

The dissolution rate of primary soil silicates increases as a function of temperature. The Arrhenius law (Eq. (2)), from which Van't Hoff's equation (see previous section) may be derived, is widely used to represent these variations:

$$k_d(T) = k_d^0 \exp\left(-\frac{E_a}{RT}\right) \tag{2}$$

in which k_d is the dissolution rate constant (mol m^{-2} s^{-1}), k_d^0 is its value at a given reference temperature, E_a is the apparent activation energy of the dissolution reaction (kJ mol^{-1}), R is the gas constant (8.32×10^{-3} kJ mol^{-1} K^{-1}), T is the temperature in Kelvin.

It is known that E_a differs according to the rate-limiting mechanism of the overall reaction (Guy and Schott, 1989; Lasaga, 1998). The rate-limiting mechanism may be either the molecular diffusion of the reactants or products throughout different diffusion barriers (coatings at the mineral surface, leached layer, mineral micropores), or a surface reaction involving the reversible formation of an activated complex. Surface reactions are widely recognized as limiting the overall silicate dissolution rate under laboratory conditions and especially under temperature conditions consistent with weathering. Under natural conditions, the role of surface reactions relative to molecular diffusion is still the subject of active research (Velbel, 1993; Nugent et al., 1998; Turpault et al., 1998). Regardless of the rate-limiting mechanism, the main driving force for mineral dissolution is the chemical affinity (A_r) of the reacting solution. When A_r is equal to zero, the reaction reaches its equilibrium and the dissolution process stops. Dissolution rate (r_d) is exponentially related to A_r and, in case of a surface-controlled dissolution, provisions for the inhibitor or catalytic effect of the solution pH are commonly taken into account by means of the activity of H^+:

$$r_d = k_d S \{H^+\}^n \left(1 - \exp\left(-\frac{A_r}{RT}\right)\right) \tag{3}$$

with

$$A_r = -RT \ln\left(\frac{Q}{K}\right) \tag{4}$$

where r_d is the dissolution rate, S the reactive surface of the mineral (m^2 $kg_{H2O}{}^{-1}$), $\{H^+\}$ represents the activity of the protons in the reacting solution, n is an experimental exponent and Q represents the ionic activity product of the reaction.

The aluminium speciation-dependent kinetic expression (Schott and Oelkers, 1995; Gérard et al., 1998), in which the formation of a siliceous activated complex would be the rate-limiting mechanism of the bulk dissolution reaction and would involve a greater influence of the chemical affinity, was not considered in this study. According to Chen and

Brantley (1997), the validity of this theory seemed to be limited to higher temperature conditions (T>50 °C).

Therefore, it may be calculated that the chemical affinity term in Eq. (3) does not decrease r_d by more than 5% (that is, in an insignificant way) if the ratio A_r/RT is approximately greater than 3. If so, the dissolution is said to proceed under "far-from-equilibrium" conditions and Eq. (3) may be approximated by:

$$r_d = k_d S\{H^+\}^n \tag{5}$$

The rate constant, k_d, exponent, n, and activation energy, E_a, usually have different values depending on the pH. There are three pH regions for most silicates wherein far-from-equilibrium dissolution rates are influenced differently by pH. These are the acidic, neutral and basic regions leading to the well-known U-shape function (see, for example, the review in Drever and Stillings, 1997). For the primary silicates of the soil studied (albite, K-feldspars and white mica, considered by default as muscovite), the transition pHs typically range from 4.5 to 5 for the boundary between the acidic and neutral regions and from pH=7.5 to about 8 for the boundary between the neutral and the basic regions.

3. Results

3.1. Variations in dissolved silica concentration

In leaching soil solutions (Fig. 1a), a variance analysis (ANOVA) of the dependent variable Si as function of time showed the seasonal variability of dissolved silica at each soil depth. Time was expressed in terms of the season, that is, each month was associated with the relevant season (Table 1). The P-values ranged from <0.001 at 30 cm depth to 0.030 at 120 cm depth. The number of samples (N) ranged from 53 at 60 cm depth to 47 at 120 cm depth. Multiple comparisons (Student–Newman–Keuls test) then were performed at the different collection depths. Results indicated that the minimum mean Si concentration was always attained in the summer and the maximum in the winter (P<0.050). Depending on soil depth, mean Si concentration measured in the autumn and the spring may not be significantly different from the summer (minimum Si) or the winter (maximum Si). In a second step, ANOVA was done over soil depths at the different seasons. Results showed an effect of soil depth on Si concentration in leaching solutions. The P-values ranged from <0.001 in both the winter and the spring to 0.005 in the autumn. Sample numbers ranged from 41 to 61 in the spring and the winter, respectively. Multiple comparisons indicated significant differences in Si concentration at each season between 15, 60, 120 cm depth and 30 cm depth, where Si was much less concentrated (Fig. 1b). It thus seemed that there was a silica sink at 30 cm depth for leaching solutions, which prevailed over the seasons and the years.

In capillary soil solutions (Fig. 2), a variance analysis done for all the replicates showed very significant seasonal variations in Si concentration (N=335–316 and P<0.001 at 15, 30, and 60 cm depth; N=133, P=0.002 at 120 cm). However, contrary to leaching soil solutions, multiple comparisons indicated that the maximum Si concentration in capillary solutions was observed in the summer and the minimum was observed in the winter

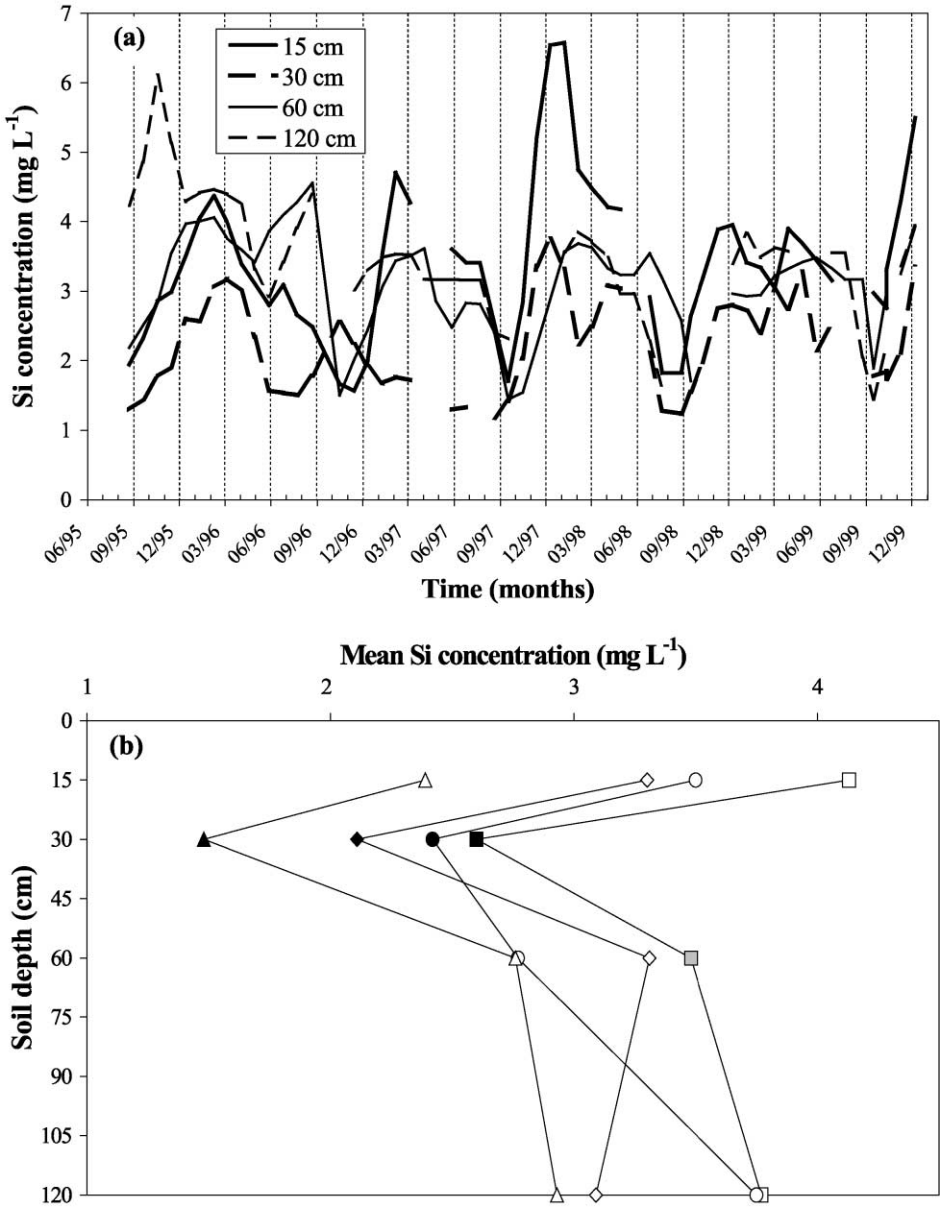

Fig. 1. (a) Dissolved silica (Si) concentration according to time in leaching soil solutions collected by zero-tension lysimeters (ZTL) at different soil depths (15, 30, 60, 120 cm) and (b) corresponding mean seasonal values for dissolved Si as a function of soil depth. Triangle symbols: summer; circle symbols: autumn; diamond symbols: spring; square symbols: winter. Symbols of different colours represent significantly different values according to soil depth.

Table 1
Sampling dates and the corresponding seasons considered in the study

Date	Season	Date	Season
25/07/95	1	09/12/97	2
22/08/95	1	06/01/98	3
19/09/95	1	03/02/98	3
18/10/95	2	02/03/98	3
14/11/95	2	03/04/98	3
13/12/95	2	28/04/98	4
09/01/96	3	25/05/98	4
07/02/96	3	25/06/98	4
05/03/96	3	20/07/98	1
03/04/96	3	27/08/98	1
29/04/96	4	09/10/98	2
28/05/96	4	09/11/98	2
25/06/96	4	08/12/98	2
22/07/96	1	05/01/99	3
22/08/96	1	02/02/99	3
17/09/96	1	02/03/99	3
10/12/96	2	29/03/99	3
09/01/97	3	26/04/99	4
04/02/97	3	24/05/99	4
05/03/97	3	24/06/99	4
02/04/97	3	20/07/99	1
25/04/97	4	24/08/99	1
27/05/97	4	15/09/99	1
24/06/97	4	11/10/99	2
22/07/97	1	08/11/99	2
19/08/97	1	01/12/99	2
16/09/97	1		

Seasons from 1 through 4: summer, autumn, spring and winter, respectively.

(P<0.050). Analysis of variance for each season at the profile scale showed that dissolved Si in capillary soil solutions also varied with soil depth (P<0.001 with N ranging from 198 to 411 in the autumn and the winter, respectively). Significant differences (P<0.050) were calculated by multiple comparisons, regardless of the season, between surface layers (15 and 30 cm depth) and deep soil layers (60 and 120 cm depth), where Si concentration was much lower (Fig. 3). Lastly, the standard deviation for Si concentrations measured in capillary solutions over all the replicates was clearly larger in surface soil layers (15 and 30 cm depth) than in deep soil layers, implying a greater spatial variability of the processes controlling Si in capillary solutions (Table 2).

3.2. Variations in soil temperature and relationships with Si concentration

Soil temperatures were measured almost continuously with in situ temperature probes at the four soil solution sampling depths. Daily in situ soil temperatures (T) were averaged over each period of soil solution collection. Marked seasonal variations in T were obtained (Fig. 4). Analysis of variance for the different soil depths confirmed the seasonality of T (N=53, P<0.001). Multiple comparisons showed a maximum in the summer (T=12.8 °C)

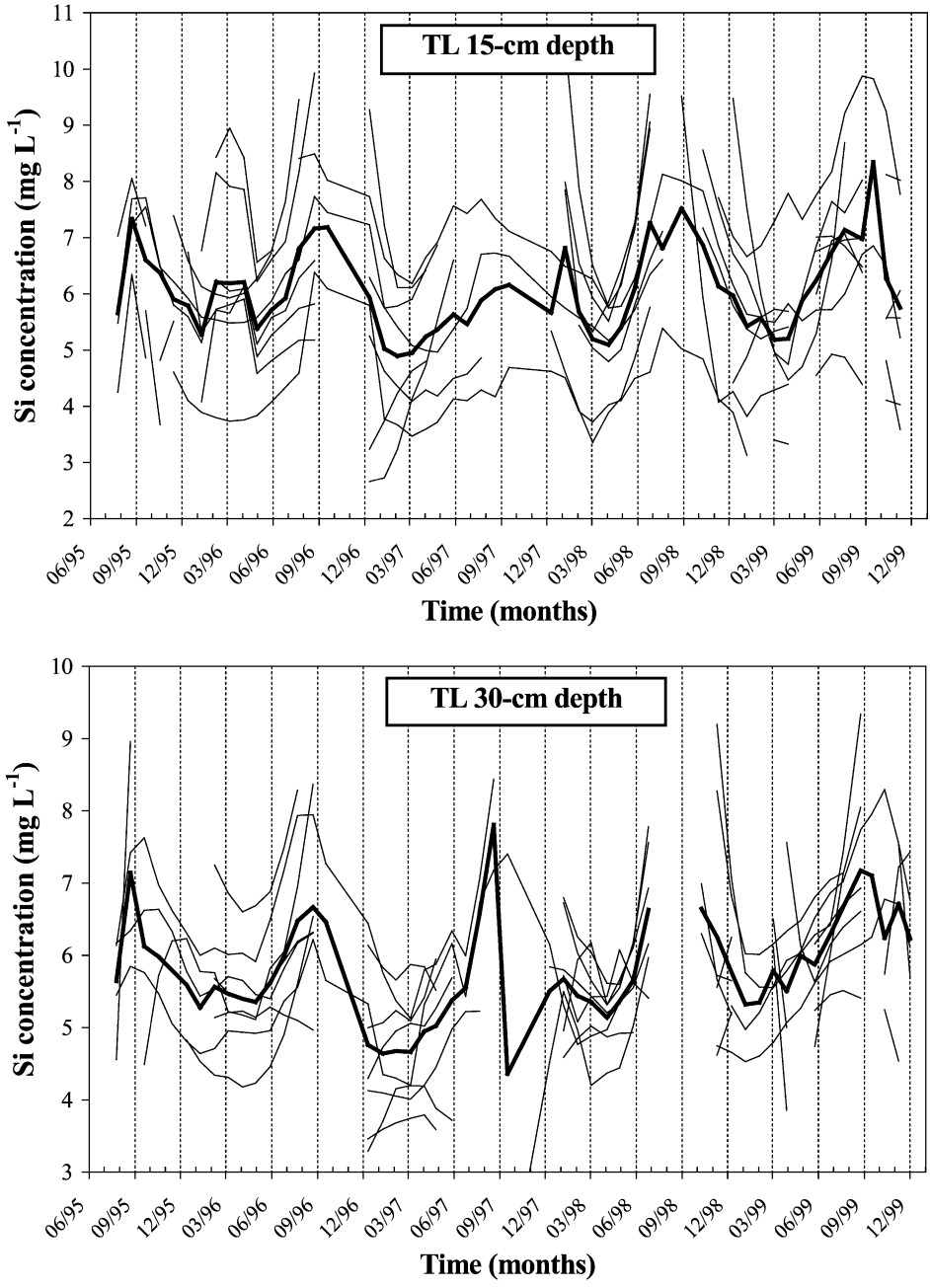

Fig. 2. Dissolved silica (Si) concentration according to time in capillary soil solutions collected by tension lysimeters (TL) at different soil depths (15, 30, 60, 120 cm).

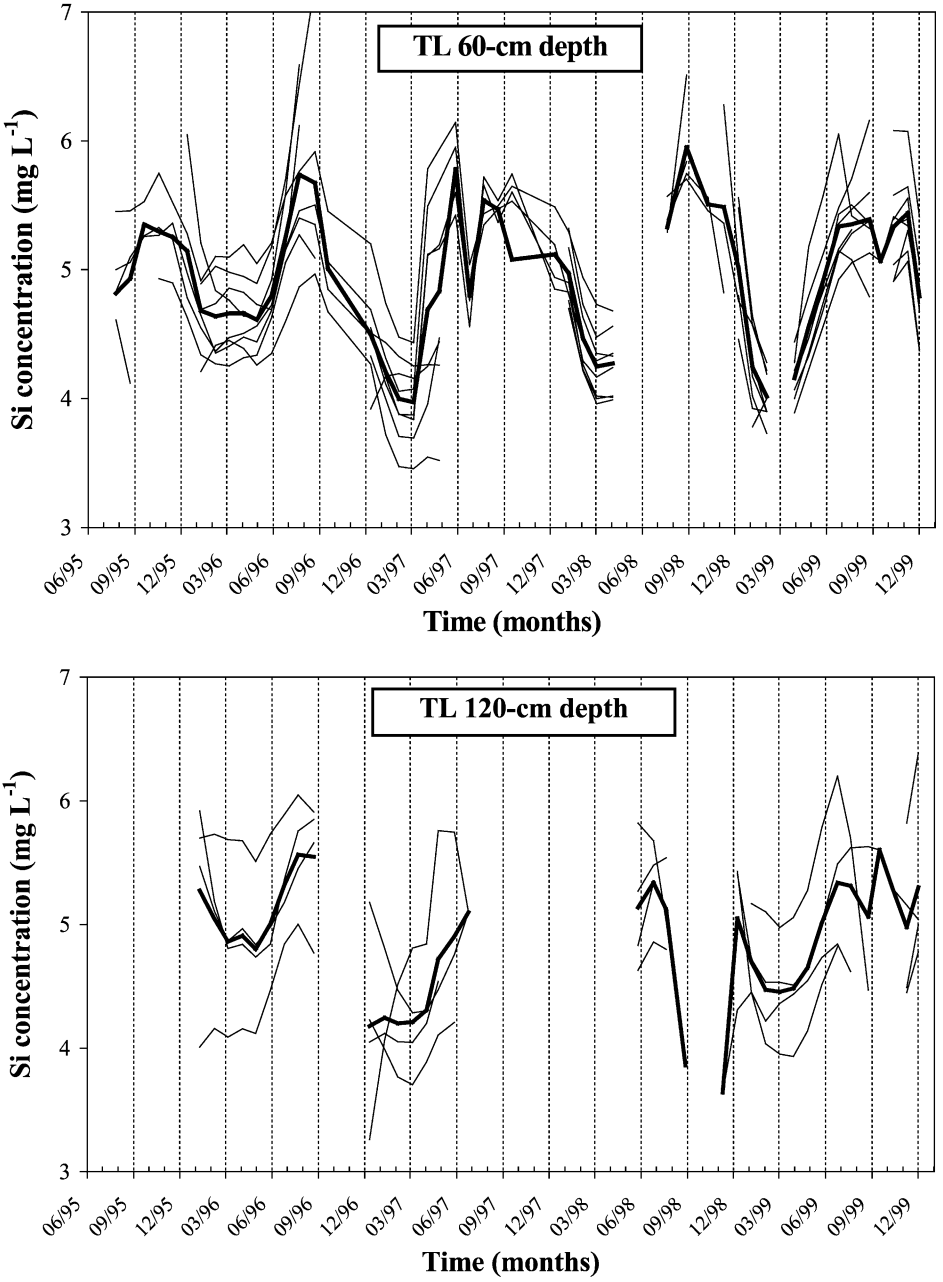

Fig. 2 (*continued*).

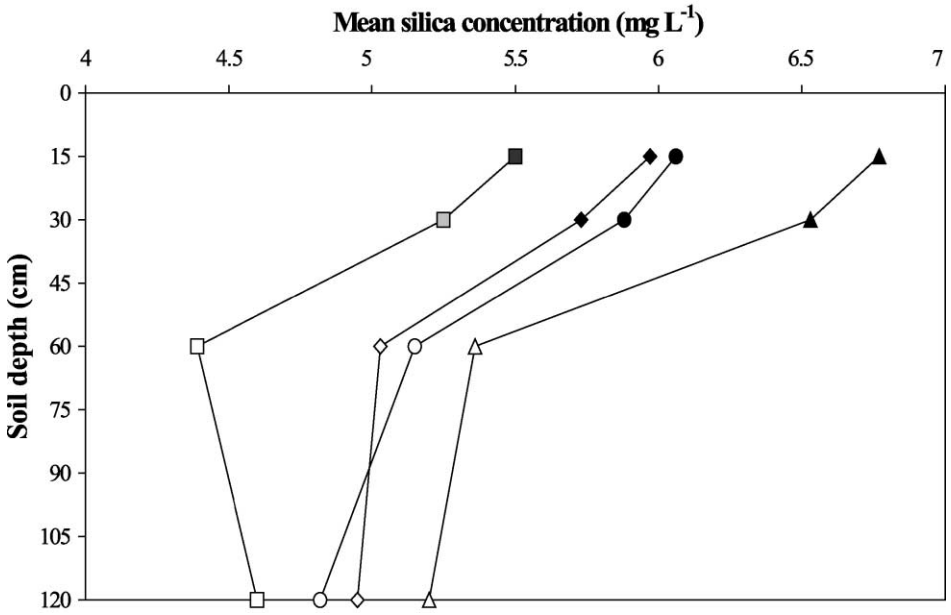

Fig. 3. Mean seasonal values for dissolved silica (Si) concentration in capillary solutions as a function of soil depth. Triangle symbols: summer; circle symbols: autumn; diamond symbols: spring; square symbols: winter. Symbols of different colours represent significantly different values according to soil depth.

and a minimum in the winter (T=4.8 °C), as observed with Si concentrations in capillary solutions. Depending on the season, significant temperature differences were obtained as a function of soil depth (Fig. 4). In the summer (N=55, P<0.001), multiple comparisons showed that the maximum temperature was attained at 15 and 30 cm depth (T=14.5 °C) and the minimum at 120 cm depth ($T\sim$ 11.7 °C). Conversely, there was apparently no significant influence of soil depth on T in both the spring and in the autumn (N=47 and 43, respectively). A slightly different result was obtained in the winter as the soil at 120 cm depth was significantly warmer (N=63, P<0.001).

In what follows, statistical analysis of the relationships between Si and T were not performed with the average concentration in Si made over all the replicates to ensure a similar number of data for each variables, because the degree of freedom would decrease.

Table 2
Mean Si concentrations and standard deviation (brackets) in capillary solutions calculated over all the replicates at the different seasons and soil depths

Soil depth (cm)	Si concentration (mg l^{-1})			
	Summer	Autumn	Winter	Spring
15	6.77 (1.50)	6.06 (1.65)	5.50 (1.35)	5.97 (1.25)
30	6.53 (1.30)	5.88 (1.16)	5.25 (0.79)	5.73 (0.81)
60	5.36 (0.58)	5.11 (0.47)	4.39 (0.44)	5.03 (0.49)
120	5.20 (0.60)	4.82 (0.79)	4.60 (0.56)	4.94 (0.54)

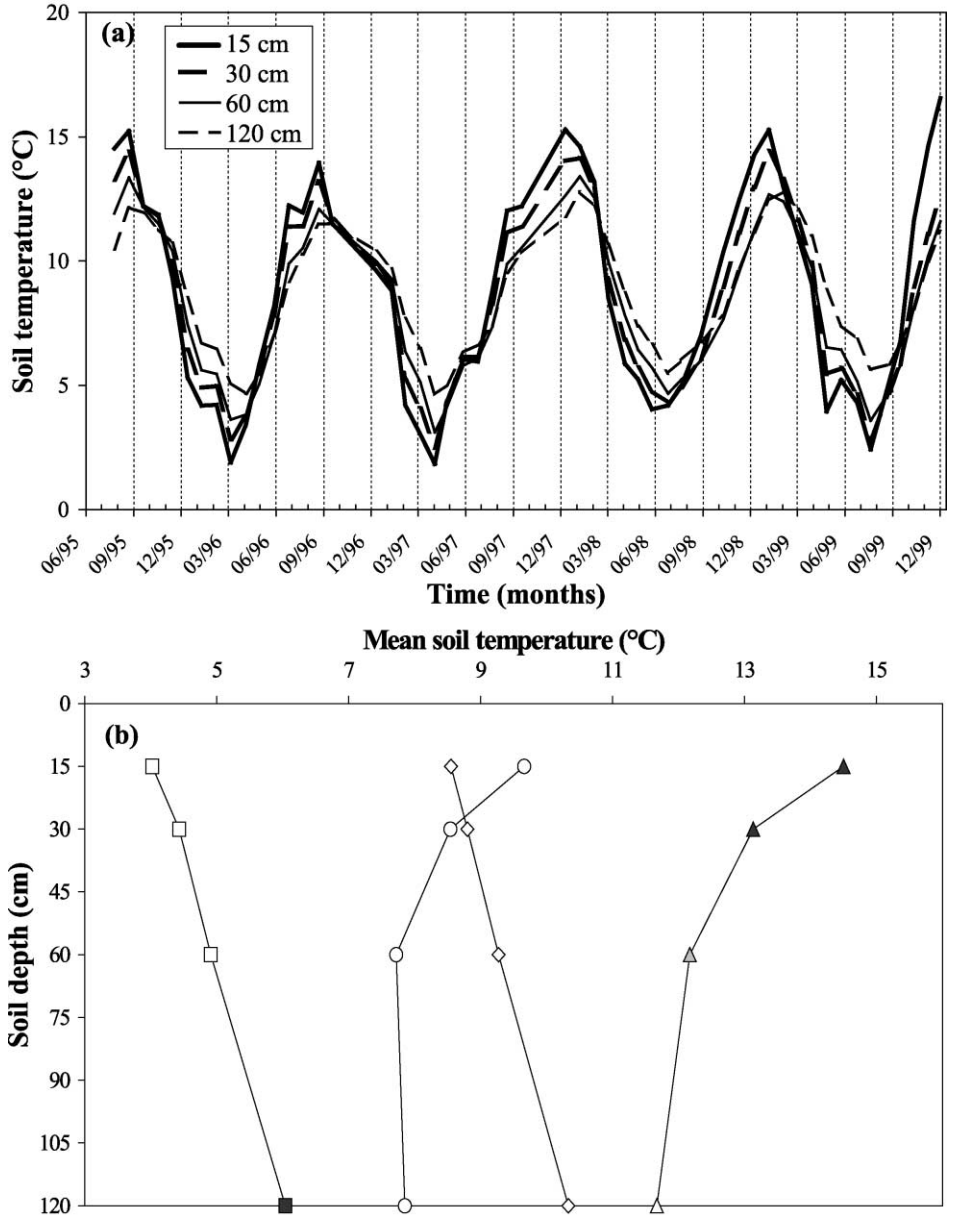

Fig. 4. (a) Soil temperature (T) according to time at 15, 30, 60 and 120 cm depth and (b) corresponding mean seasonal values for soil temperature as a function of soil depth. Triangle symbols: summer; circle symbols: autumn; diamond symbols: spring; square symbols: winter. Symbols of different colours represent significantly different values according to soil depth.

So, at a given date and soil depth, the same soil temperature was considered for the different concentrations in Si measured in the replicates. Relationships between soil temperature (T) and Si were first studied at each soil depth for both water types using ANOVA performed as a function of the season (main factor) with T as a covariate. In capillary solutions, Si and T were tightly related regardless of soil depth ($P<0.001$). In leaching soil solutions, an excellent relationship was found at 30 cm depth and to a lesser extent elsewhere. In a second step, the influence of soil depth on the relationship between Si and T was studied for each season. In capillary solutions, highly significant relationships between Si and T were obtained regardless of the season. In the spring and the summer, the P-value was <0.001. In the autumn and winter, the P-value was equal to 0.040 and 0.001, respectively. In leaching solutions as well, significant relationships were found, irrespective of the season. Lastly, ANOVA of the dependent variable Si relative to T was done for datasets corresponding to a given season and soil depth. In capillary solutions, significant relationships were found for each season at 60 cm depth. A significant results was sporadically obtained in the spring at 30 cm depth. There were no significant relationships at 15 and 120 cm depth in any case. Note that at 120 cm depth, sample numbers were always much lower than elsewhere, since only four TL replicates against eight were available at this soil depth (Section 2.2). This may render the variability of data that was not related to the variations in T more acute and thus may prevent the establishment of significant relationships. The same explanation may be valid for the lack of significant relationships between Si and T observed at the same scale for leaching solutions. However, low sample size does not explain the persisting lack of significance at 15 cm depth for capillary solutions, since N was as large as in the other datasets.

Relationships between T and Si in both leaching and capillary soil solutions were also studied using least-squares linear regressions with lnSi as a response and $1/T$ as an independent variable. By doing so, we considered that the Si concentration was proportional to the silica flux generated by a hypothetical temperature-dependent process and all the other factors were held constant. Therefore, the Arrhenius law (Eq. (2)) would give linear relationships between lnSi and $1/T$ and the slopes would be equal to the ratio $-E_a/R$. Most significant results for lnSi and $1/T$ may be expected at the yearly scale (i.e. separate regressions at each soil depth, disregarding the season) or at the profile scale (i.e. separate regressions for each season, disregarding soil depth), given that larger temperature variations were observed as a function of the season and soil depth (see above). For these reasons, linear regressions of lnSi on $1/T$ were not performed for datasets corresponding to a given season and soil depth.

In capillary solutions, results calculated at the yearly scale showed highly significant ($P<0.01$) linear trends. Negative slopes were obtained (Fig. 5) as expected by the seasonal variability of Si and T. Coefficient of determination (R^2) increased with soil depth, from 0.10 at 15 cm depth, 0.26 at 30 cm depth and 0.40 at 60 cm depth (N=335, 316 and 323, respectively). However, R^2 value was only 0.13 at 120 cm depth (N=133). The apparent activation energy ranged from 12.1 ± 3.8 to 17.7 ± 2.4 kJ mol^{-1} and showed no difference as a function of soil depth, outside the upper and lower boundaries given by the standard deviation.

In leaching solutions, significant results were also calculated at each soil depth, but Si concentration was inversely correlated to T, giving positive slopes for lnSi vs. $1/T$ (Fig. 6).

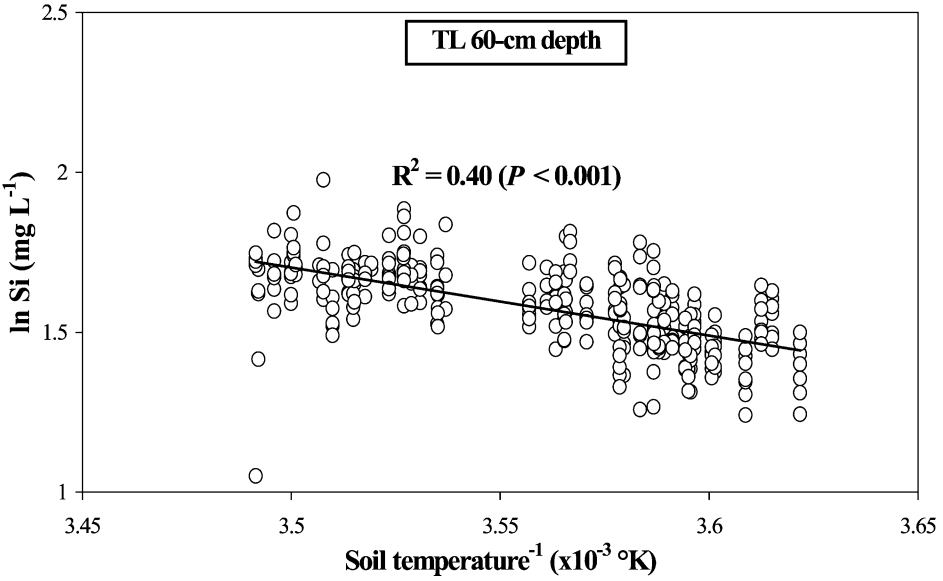

Fig. 5. Example of the linear relationship between the logarithm of silica concentration (lnSi) in capillary solutions and the inverse of soil temperature (1/*T*) expressed in Kelvin.

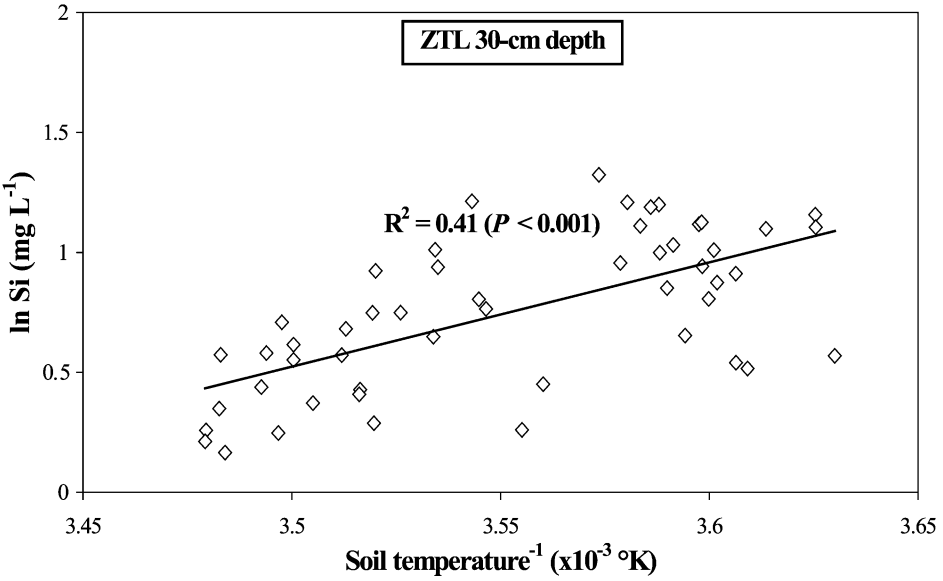

Fig. 6. Example of the linear relationship between the logarithm of silica concentration (lnSi) in leaching solutions and the inverse of soil temperature (1/*T*) expressed in Kelvin.

Negative values for E_a were also expected in leaching solutions, because of the seasonal variability of Si in regard to the variations in *T*. The apparent activation energy ranged from -26.7 ± 11.6 to -36.2 ± 12.2 kJ mol^{-1} regardless of soil depth. R^2 values ranged from 0.41 to 0.16, calculated at 30 and 120 cm depth (N=51 and 47), respectively. The corresponding *P*-values were <0.001 and equal to 0.005.

At the soil profile scale, significant relationships were obtained with capillary solutions regardless of the season. R^2 values ranged from 0.21 (N=279) in the spring to only 0.02 (N=412) obtained in the winter. The corresponding *P*-values ranged from 0.008 to <0.001. The apparent activation energy ranged from 25.6 ± 11.6 to 7.2 ± 6.8 kJ mol^{-1} calculated for the summer and the autumn, respectively. In leaching solutions, significant results prevailed only in the spring and the summer (R^2=0.11 and 0.22, respectively), still with inverse relationships between Si and *T*. The corresponding *P*-values were 0.028 and 0.002 (N=41 and 43). The calculated apparent activation energies were -27.2 ± 11.9 and -85.8 ± 25.3 kJ mol^{-1}, respectively.

3.3. Variations in solution pH and relationships with Si concentration

In capillary solutions, H^+ concentration was apparently not influenced by the season (ANOVA) at 15 and 30 cm depth. At both soil depths, mean pH was roughly equal to 4.30. At 60 and 120 cm depth, a significantly more acidic pH in the summer was observed. Mean corresponding pHs were equal to 4.22 and 4.25, in contrast to 4.3 in the other seasons. Note that slightly more acidic pHs calculated in the summer at 60 and 120 cm were not significantly different. A lack of influence of soil depth on H^+ concentration was found with ANOVA at the profile scale. In leaching soil solutions, there was a lack of seasonal variability of H^+ concentration at each soil depth. By the same token, no influence of the soil depth was observed. The mean pH in leaching solutions was equal to about 4.3.

Following the study carried out with soil temperature, the relationships between Si and H^+ concentration were first studied using ANOVA. In capillary solutions, ANOVA performed as a function of the season (main factor) with H^+ as a covariate showed significant relationships between the dependent variable Si and H^+ concentrations at 60 and 120 cm depth only (P=0.001 and 0.007, respectively). Conversely, significant results were found at 15 and 30 cm depth only in leaching solutions (P=0.001 and P=0.041, respectively). By distinguishing the different seasons and by taking into account soil depth as the main factor, insignificant relationships between Si and H^+ were calculated in capillary solutions except in the spring (P=0.001). In leaching solutions, a significant result was obtained in the autumn only (P=0.003). Lastly, and contrary to relationships between Si and *T*, ANOVA for H^+ at each season and soil depth indicated insignificant effects on Si concentration.

The quantitative relationships between H^+ and Si concentrations were also studied by means of least-squares linear regressions of logSi on pH. The possibility that Si concentration was controlled by silicate weathering limited by a surface reaction involving H^+ was thus tested here, since Eq. (5) reveals a linear relationship between logSi and pH. This has been widely observed at the laboratory by dissolving silicates under far-from-equilibrium conditions (see Section 2.4). Consistently, the slope corresponded to *n*, the

order of the overall reaction with respect to H^+ activity. A base assumption was proportionality between the Si concentration in capillary solutions and the silica flux generated by weathering. Moreover, the effect of other variables such as T on relationships between logSi and pH were considered to be insignificant. These two assumptions were already made in Section 3.2, wherein inverse relationships between Si and T and negative values taken by E_a in leaching solutions were obviously in conflict with a direct control of Si by weathering in this type of soil solution. Therefore, attempts to linearly relate logSi to pH were restricted to capillary solutions. Furthermore, linear regressions of logSi on pH were performed with data corresponding to the acidic region (pH<5), since the effect of H^+ on weathering of soil silicates may not have an important influence at greater pH (see Section 2.4). Lastly, contrary to the relationships between lnSi and $1/T$ (see Section 3.2), most significant regressions of logSi on pH may be expected from data corresponding to different seasons and soil depths given that T varied to a much lesser extent.

The large variations in T observed at the yearly scale did not obscure the highly significant linear trends observed at each soil depth for logSi vs. pH (Fig. 7). Calculated values for n were always negative, in agreement with our current understanding of silicate weathering in the laboratory (see Section 2.4). Most significant results were obtained at 30, 60 and 120 cm depth (R^2=0.06, 0.05, 0.13, respectively, and P<0.001). At 15 cm depth, the relationship was weaker (R^2=0.015, P=0.040, N=335) although the number of samples was a little larger than at 30 and 60 cm depth (N=316 and 323, respectively) and considerably larger than at 120 cm depth (N=133). Corresponding slopes ranged from −0.06 to −0.08 at 15, 30 and 60 cm depth with a high degree of uncertainty (about ±0.05) because of the very low values taken by R^2. A slightly steeper slope was obtained at 120

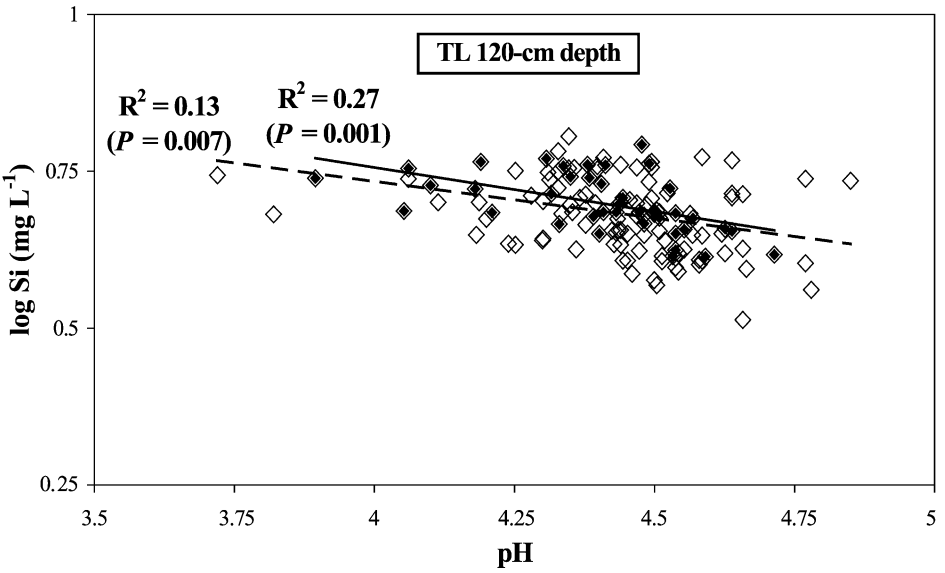

Fig. 7. Example of linear relationship between the logarithm of silica concentration (logSi) in capillary solutions and the pH. Results calculated at 120 cm depth at the yearly scale (R^2=0.13) and in the spring (R^2=0.27).

cm depth (n=−0.12±0.05). At the soil profile scale, linear regressions exhibited significant linear trends in the autumn and the spring only (P<0.001). R^2 value was equal to 0.09 (N=197) and 0.04 (N=279), respectively. Corresponding slopes were −0.10 and −0.06. Linear regressions done for each season and soil depth gave significant results for the summer at 15 cm depth, and the autumn at 30 cm depth (P=0.014 and P=0.004, respectively). Corresponding R^2 values were equal to 0.10 and 0.14 (N=64 and 58) and slopes were roughly equal to −0.08 and −0.09. Less variable results were calculated in the other seasons, especially in the spring where there was no significant relationship between logSi and pH at 15 cm depth. This particular lack of significance may be an artefact of low sample size. Interestingly, R^2, P-value and n increased in the spring with soil depth, ranging from R^2=0.06 and P=0.030 (N=84) at 30 cm, R^2=0.09 and P=0.006 (N=72) at 60 cm, to as much as R^2=0.27 and P<0.001 (N=43) at 120 cm depth (Fig. 7). Corresponding slopes were equal to −0.05, −0.08 and −0.14. In the winter, significant relationships were only obtained at 30 and 60 cm depth (P<0.001). R^2 values were equal to 0.11 (N=115) and 0.09 (N=121), respectively. Corresponding slopes were −0.09 and −0.07. The low sample size may explain the lack of significance at 120 cm, but not at 15 cm depth.

3.4. Si vs. chloride concentrations

Following Berner et al. (1998), we attempted to relate the chloride concentration to Si concentration to assess the influence of evaporation and evapotranspiration processes on sinusoidal patterns determined here for Si concentration in capillary solutions (see Fig. 2, Section 3.1). The explanation was based on the fact that evaporation and evapotranspira-

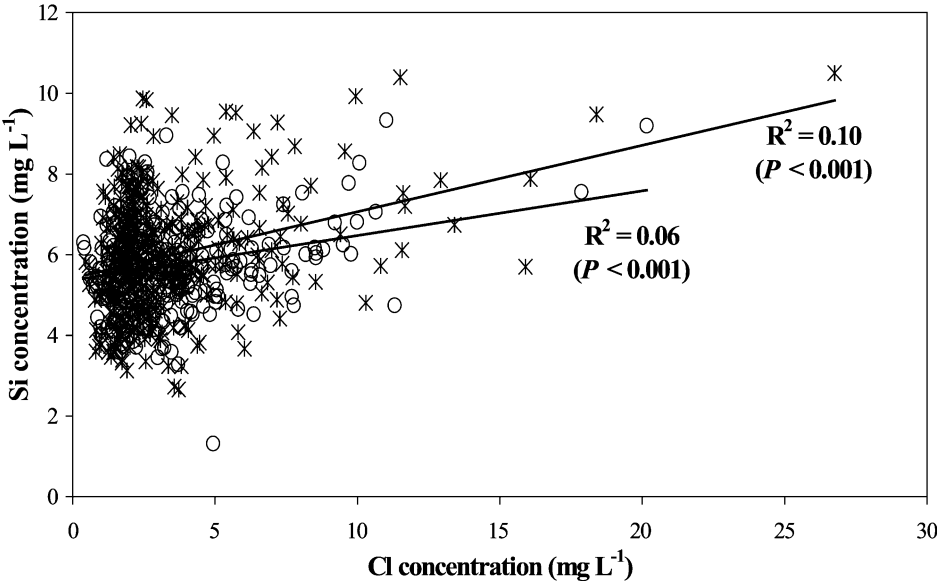

Fig. 8. Linear relationships between chloride (Cl) and silica (Si) concentrations in capillary solutions collected at 15 cm depth (cross symbols) and 30 cm depth (circle symbols).

tion typically attained a maximum in the summer and a minimum in the winter, because of vegetative dormancy along with higher mean precipitation levels in the winter (including colder and cloudier weather). Thus, these processes may increase Si concentration by water loss in the summer and decrease Si by dilution in the winter. This may lead to the build up in Si concentration observed in capillary solutions.

Linear regressions between chloride and Si concentrations (Fig. 8) indicated highly significant relationships at 15 and 30 cm depth only (N=335–316, P<0.001). Nevertheless, R^2 values were very low and indicated that only 10% and 6% of the variability of Si in capillary solutions may be explained by the influenced of evaporation and evapotranspiration processes. In other words, it appeared that these processes may only weakly control the silica concentration in capillary solutions in the upper soil layers, but did not influence the sinusoidal patterns established at 60 and 120 cm depth.

4. Discussion

4.1. Control of dissolved silica in leaching soil solutions

The seasonal variability of Si in leaching solutions (see Section 3.1) suggested that the controlling process may be related to the seasonal variability of precipitation and soil drainage. At the Vauxrenard site, as certainly anywhere else in a temperature climate, the amount of rain was more important in the winter than in the summer. Soil drainage may be reinforced in the winter by reduced evaporation and evapotranspiration. The collected volume of water by ZTL (quoted *V*) demonstrated such seasonal variations, but there was no significant relationship between Si in leaching solutions in *V.* This lack of relationship does not necessarily invalidate the suggested correlation between Si concentration and soil drainage, because it is known that the amount of intercepted water is typically a poor surrogate for the actual volume of gravity-driven water in soils. This is mostly caused by the so-called "wall effects" associated with the presence of the lysimeter that severely disturbs the flow paths (i.e. by-passed flow or preferential flow within the plate lysimeter). Sound calculation of the quantity of leaching water as a function both time and soil depth requires the use of a hydrological program for the unsaturated zone that allows for evaporation and evapotranspiration, as well as the knowledge of the hydraulic properties of the soil. This was well beyond the scope of this study.

It is likewise important to note that Berner et al. (1998) observed in leaching soil solutions a marked seasonal variability of Si similar to that established here in capillary solutions and thus the opposite of that found in leaching solutions. These authors suggested that Si concentration was controlled by temperature variations through the temperature-dependence of a hypothetical exchange constant for aqueous silica. However, aqueous silica species in acidic solutions are recognized as being dominated by neutral species, mostly orthosilicic acid ($H_4SiO_4^\circ$) (see, for example van Hees et al., 2000). That was clearly in contradiction to a control of Si concentration by ion exchange processes.

Alternatively, we propose that the fast reequilibration of the system (sandboxes) noted by Berner et al. (1998) was due to the rapid aqueous diffusion of Si between capillary solutions, mostly contained in micropores, and leaching solutions, mostly contained in

macropores. Therefore, if capillary solutions in sandboxes would have been collected in parallel to leaching solutions, Si concentration would have shown the same seasonal variability. This hypothesis naturally led to questions about the nature of the process responsible for the seasonality of Si observed here in leaching solutions. These opposed seasonal variations may stem from differences between our soil and the system studied in Berner et al. (1998). In our case, the soil contained a significant amount of clays (from ~ 22 to 9 wt.% increasing depth) and other fine soil fractions (see Ezzaïm et al., 1999b for further details). The bulk sand fraction (i.e. fine and coarse) did not constitute more than 40 wt.% of the soil material. Conversely, the sandboxes considered in Berner et al. (1998) were filled by an apparently clay-free quartz and feldspar-rich sand. In addition, we studied a natural acidic soil comprised of microporous aggregates of various sizes, made of a mixing of clays, organic matter and (oxy-)hydroxides. Therefore, it seems reasonable to assert that effective molecular diffusion rates from capillary to leaching waters were certainly much slower in our soil than in Berner et al.'s (1998) sandboxes, because of the greater tortuosity of the porous network filled by capillary solutions and may be the lesser contact surface between macropores and micropores. It follows that a major process in the control of Si concentration in leaching soil solutions studied herein may be the diffusion of aqueous silica, mostly in the form of orthosilicic acid, from capillary to leaching solutions. Higher drainage in the winter would thus imply a larger overall contact time between leaching solutions and capillary solutions, enabling aqueous silica to diffuse to a larger extent and to significantly increase Si concentration measured in leaching solutions.

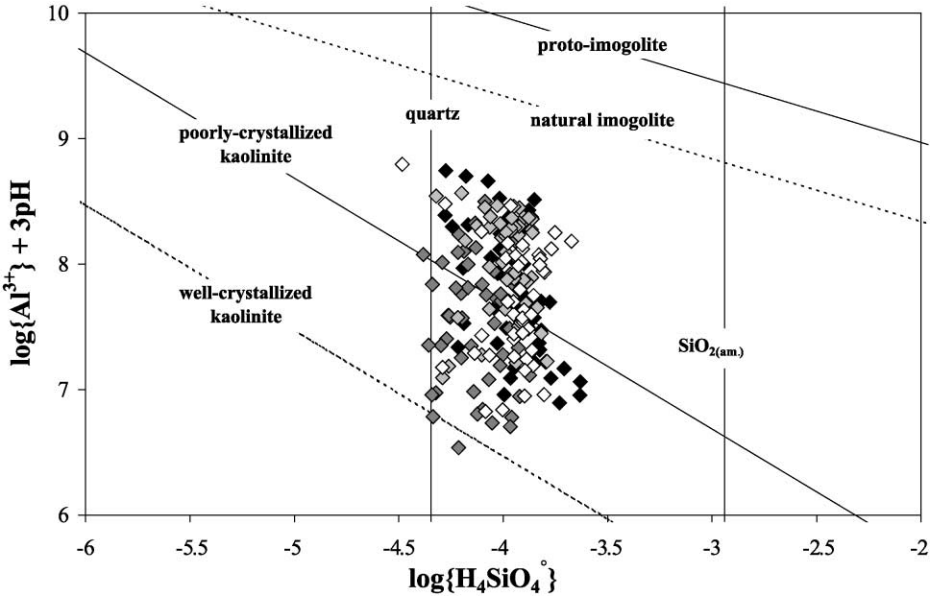

Fig. 9. Activity diagram for leaching soil solutions. From filled symbols through open symbols: results at 15, 30, 60 and 120 cm depth. Stability fields for minerals were computed at 10 °C for simplicity, but activities used to plot the data were calculated at in situ mean soil temperatures (see text for further details).

A parallel process may at least partially control the seasonality of Si in leaching solutions. A clue to this may be in the silica sink observed at 30 cm depth in any season (see Section 3.1), which may be attributed to the preferential formation of Si-containing secondary phases. Negative values of E_a calculated for leaching solutions at different scales (see Section 3.2) further led to propose that the seasonal variability of Si may also be caused by the temperature-dependence of the solubility of an Si-containing secondary phase. Speciation calculations were needed, together with an activity diagram relevant to the Al–Si system, to test this hypothesis. The activity diagram was drawn at a temperature of 10 °C from thermodynamic data for mineral equilibrium (Fig. 9). This temperature constraint was chosen for simplicity and it corresponded to the mean temperature of the bulk soil. Leaching solutions were considerably supersaturated and undersaturated with respect to well-crystallized kaolinite and ITM (i.e. from PI to natural imogolite), respectively. This was consistent with soil mineralogy since ITM were not detected in this soil (see Section 2.1). Concerning poorly crystallized kaolinite, which was surely the best surrogate for the form detected in this soil, results were more variable given that solutions were either supersaturated or undersaturated with respect to this phase. A significant linear regression for $\log\{Al^{3+}\}+3$ pH on $\log\{H_4SiO_4^\circ\}$ was obtained only at 15 cm depth, at the yearly scale (Fig. 10). The lack of a linear relationship noted elsewhere demonstrated that the formation of Si-containing phases may not, even partially, be responsible for either the silica sink at 30 cm depth and the seasonal variability of Si at 30, 60 and 120 cm depth.

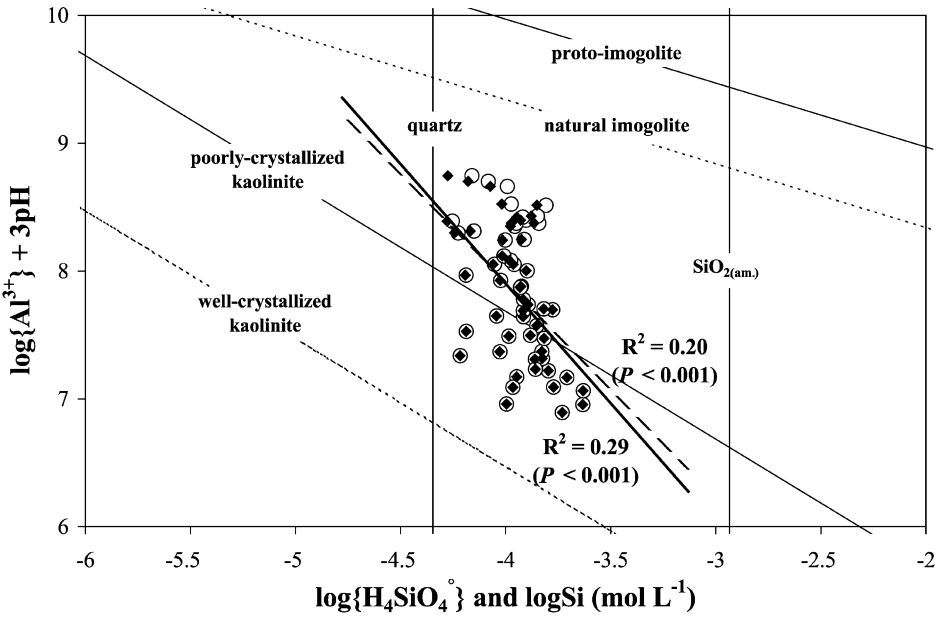

Fig. 10. Activity diagram for leaching soil solutions collected at 15 cm depth showing linear relationships as a function of either the activity of orthosilicic acid, $H_4SiO_4^\circ$, or the total dissolved silica concentration (Si).

The sole significant linear relationship gave a Si/Al molar ratio equal to 1.87 ± 0.80, which was problematic as significantly greater than kaolinite (Si/Al=1). The R^2 value was equal to 0.29 ($P<0.001$) and indicated that only about 29% of the variability in $\{H_4SiO_4^\circ\}$ at this scale may be controlled by the reversible formation of a secondary phase. Such a low R^2 value suggested that its formation proceeded at a relatively slow rate (i.e. kinetically controlled), since a ''pure'' equilibrium-controlled reaction (i.e. infinite rate) would certainly give a much greater R^2 value as it would buffer the activity of H_4SiO_4 along a given stability field. Nevertheless, the formation rate of this hypothetical compound must be deeply influenced by the chemical affinity (i.e. its solubility) in order to give a negative value of E_a (see Section 3.2).

The extent to which variations in $\{H_4SiO_4^\circ\}$ may be related to variations in Si needs to be studied at this point. Linear regressions of Si vs. $\{H_4SiO_4^\circ\}$ at the different soil depths for gave R^2 values ranging from 0.96 to 0.99. Thus, in agreement with the measurements performed in acidic soil solutions (van Hees et al., 2000), aqueous silica in our calculations was mostly in the form of orthosilicic acid even through few HAS species were considered in the thermodynamic database (Section 2.3). The role of the hypothetical secondary Al–Si phase in the control of Si concentration was assessed by making a linear regression of $\log\{Al^{3+}\}+3$ pH on log Si (Fig. 10). A significant linear relationship prevailed but R^2 decreased to 0.20, implying that the relatively slow reversible formation of the Si-secondary phase may not control more than 20% of the seasonal variability of Si in leaching solutions collected at 15 cm depth. Therefore, at 15 cm depth, the effect of this process on Si concentration was certainly minor compared to the diffusion of Si from capillary solutions.

Among the number of alternative explanations for the silica sink observed at 30 cm depth, the most likely involved the lateral heterogeneity of the soil. Actually, the effects of soil heterogeneities on soil solution chemistry may be less well integrated within the composition of leaching solutions than within capillary solutions, wherein Si concentration monotonously decreased with soil depth. As mentioned above (see Section 2.2), only five replicates of ZTL per soil depth were installed for the collection of leaching solutions compared to eight replicates of TL for capillary solutions. Above all, each collection depth for leaching solutions corresponded to a given soil profile. This design was necessary to prevent interactions between successive ZTL at increasing depth. Accordingly, the distance between different soil profiles containing five ZTL replicates disposed at a given depth was on the order of a few meters. A very different design was adopted for capillary solutions. We believe that the expected influence of the lateral heterogeneity of the soil on solution chemistry was better integrated as each TL replicate was inserted at 15, 30, 60 and 120 cm depth along the same vertical line within a unique soil profile and this was repeated up to eight times at different locations throughout the site.

4.2. Processes controlling silica concentration in capillary soil solutions

It was seen (Section 3.4) that evaporation and evapotranspiration may only control a small portion of the variability of Si in capillary solutions (see Fig. 2). Moreover, the effect of these processes was limited to the upper soil layers (see Fig. 5), because evapotranspiration process is a function of soil depth via decreasing root density (Ezzaïm et al., 1999b) and

evaporation decreases with soil depth. Therefore, different processes controlled the seasonal variability of Si in capillary solutions at 60 and 120 cm depth and the most important portion of the variability of Si at 15 and 30 cm depth. Significant relationships obtained between Si concentration and other measured variables, such as T, pH and H^+ concentration (see Sections 3.2 and 3.3), clearly suggested that these variables may control Si in capillary solutions to some extent through their influence on other Si-controlling processes.

The control of Si concentration in capillary soil solutions by the reversible formation of a secondary Si-containing phase through the influence of temperature on its solubility appeared plausible. However, only opals, silica gels, and silica polymorphs can exhibit a solubility increase with temperature (see, for example Bartoli and Wilding, 1980), as opposed to secondary aluminosilicates such as kaolinite and ITM. The question remains open regarding ATM behaviour because of the lack of data concerning the effect of temperature on solubility, together with the wide range of potential Si/Al ratios for such short-range ordered to amorphous products (Wada, 1989).

Speciation calculations produced overall results similar to those obtained for leaching solutions (see previous section). Briefly, capillary solutions were quite dispersed in the activity diagram (Fig. 11), indicating the equilibrium-controlled formation of a secondary siliceous phase may not control Si in capillary solutions. Linear regressions of log-$\{Al^{3+}\}$+3 pH vs. log$\{H_4SiO_4^\circ\}$ done at the yearly scale revealed significant relationships, except at 15 cm depth. Regardless of soil depth, R^2 values were roughly equal to 0.18 and Si/Al molar ratios ranged from 1.49 to as much as 3.74. Regressions of log$\{Al^{3+}\}$+3 pH

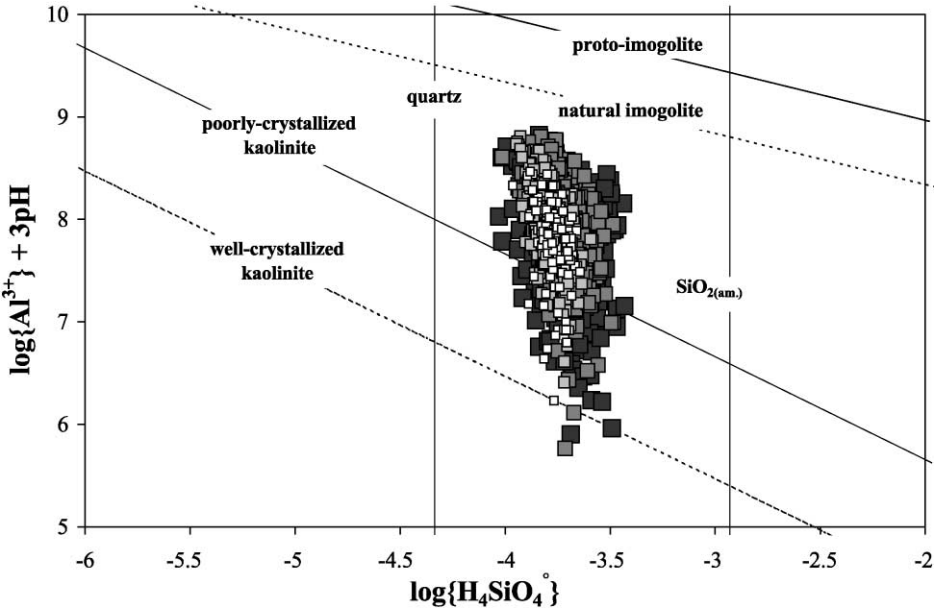

Fig. 11. Activity diagram for capillary soil solutions. From filled symbols through open symbols: results at 15, 30, 60 and 120 cm depth. Stability fields for minerals were computed at 10 °C for simplicity, but activities used to plot the data were calculated at in situ mean soil temperatures (see text for further details).

vs. logSi revealed lower R^2 values, ranging from 0.08 at both 60 and 120 cm depth and to as low as 0.03 at 30 cm depth. Therefore, formation of secondary siliceous phases may only explain a little percent of the seasonal variability of Si in capillary solutions collected at 30, 60 and 120 cm depth at the yearly scale. Weaker results were obtained with additional linear regressions done for datasets corresponding to the other scales. These results further suggested that Si in capillary solutions was almost uncontrolled by the formation of secondary siliceous phases.

Contrary to leaching solutions, a potential process for the control of Si concentration in capillary solutions is the chemical weathering of primary soil silicates, driven by soil temperature and pH variations (see Section 2.4). Temperature accelerates chemical weathering and thus furnishes positive values for E_a, as those calculated in this study with lnSi vs. $1/T$ (see Section 3.2).

Before any attempt to relate silicate weathering rates to Si concentration in capillary solutions, it was noteworthy to observe that significant relationships between logSi and pH established in the acidic region (see Section 3.3) were indicative of a surface-controlled and proton-promoted weathering of primary silicates under far-from-equilibrium conditions. Speciation calculations indicated that soil primary silicates dissolved under far-from-equilibrium conditions (Fig. 12). The reaction for K-feldspar was found to be closer to the equilibrium, but the range of its ratio A_r/RT was larger than 3, implying that K-feldspar dissolved under far-from-equilibrium conditions as well (see Section 2.4). The values taken by the slope, n, were similar to this recently reported for muscovite under temperature conditions consistent with weathering ($n=-0.14$, see Kalinowski and Schweda, 1996).

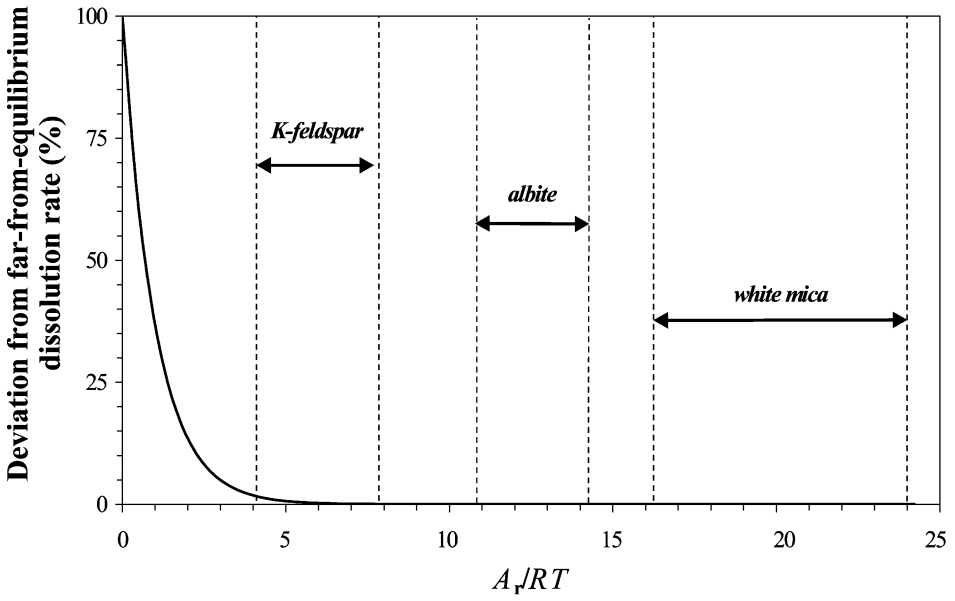

Fig. 12. Percentage of deviation of primary soil silicate dissolution rates from far-from-equilibrium conditions attributable to the effect of the chemical affinity for the reaction, A_r.

These results would thus indicate that white mica was being dissolved much faster than alkali-feldspars, which typically exhibit n values of −0.5 (see review by Blum and Stillings, 1995). The values of E_a confirm this important finding. It appeared that E_a determined in the laboratory for muscovite in the acidic region is equal to 22 kJ mol^{-1} (Nagy, 1995) compared to about 50–60 kJ mol^{-1} for alkali-feldspars (Blum and Stillings, 1995). Therefore, the measurement of both Si concentration and pH in capillary solutions may be an indirect method to study ongoing mechanisms limiting soil silicate weathering rates in their natural context.

The scope of these important findings may be greatly limited by low R^2 values associated with lnSi vs. $1/T$ and logSi vs. pH. Another limitation was the absence of significant results for certain datasets, whereas the sample size was not excessively low. We believe that such a large unexplained dispersion of the data arose from the confounding influence of undetermined variables such as mineral reactive surfaces, S, which are certainly the most difficult parameters to constrain in natural systems for a number of reasons. Contamination of capillary solutions from the transfer and mixing of a portion of leaching solutions driven by capillary forces may be an important source of dispersion in the data. The influence of organic ligands on weathering may also be significant (e.g. Drever and Stillings, 1997). Lastly, the validity of the assumptions underlying the establishment of linear relationships (see Sections 3.2 and 3.3) may be weak in some cases.

Primary silicate dissolution rates were calculated with Eq. (3) and kinetic parameters listed in Table 3. We calculated dissolution rates per unit of reactive surface area, usually quoted as specific dissolution rates and denoted here by r_d*. Results indicated that r_d* for the three primary silicates was subject to the same seasonal variations as Si concentration in capillary solutions (Fig. 13). Accordingly, Si and r_d* were found very well correlated (P<0.001). Larger R^2 values obtained for the relationships of r_d* vs. Si concentration at 30, 60 and 120 cm depth (Table 4) may be self-consistent with the faster weathering rate for white mica previously inferred from slopes for logSi vs. pH and lnSi vs. $1/T$ (n and E_a), compared to literature data used here to calculate r_d* (see Table 3).

It can be determined that soil temperature was the main driving force for r_d*. Consistently, H^+ concentration played a minor role in the overall seasonal variability of r_d*. Nevertheless, as can be seen by comparing k_d to r_d* (Fig. 14), H^+ concentration had

Table 3
Kinetic parameters for albite, K-feldspar, and white mica dissolution used in Eqs. (2) and (3)

Mineral	log k_d^{ac} (mol m^{-2} s^{-1})	log k_d^{ne} (mol m^{-2} s^{-1})	pH$_1$	n	E_a^{ac} (kJ mol^{-1})	E_a^{ne} (kJ mol^{-1})
Albite[a]	−9.5	−11.8	5	0.5	60[b]	67.7
K-feldspar[a]	−9.6	−11.8[c]	5	0.5	51.7	60[b]
White mica[d]	−11.8[d]	−13.0[e]	5	0.14	22[e]	60[b]

Dissolution rate constants at T=25 °C, k_d^{ac} and k_d^{ne}, refer to acidic (pH<pH$_1$) and neutral regions (pH$_1$<pH), respectively. Apparent activation energies, E_a^{ac} and E_a^{ne}, refer to acidic and neutral regions, respectively.

[a] Selected from the review in Blum and Stillings (1995).

[b] Default value for surface-controlled reaction (see, e.g. Gérard et al., 1998).

[c] Considered as being identical to albite.

[d] Parameters for muscovite, from Kalinowski and Schweda (1996).

[e] Nagy (1995).

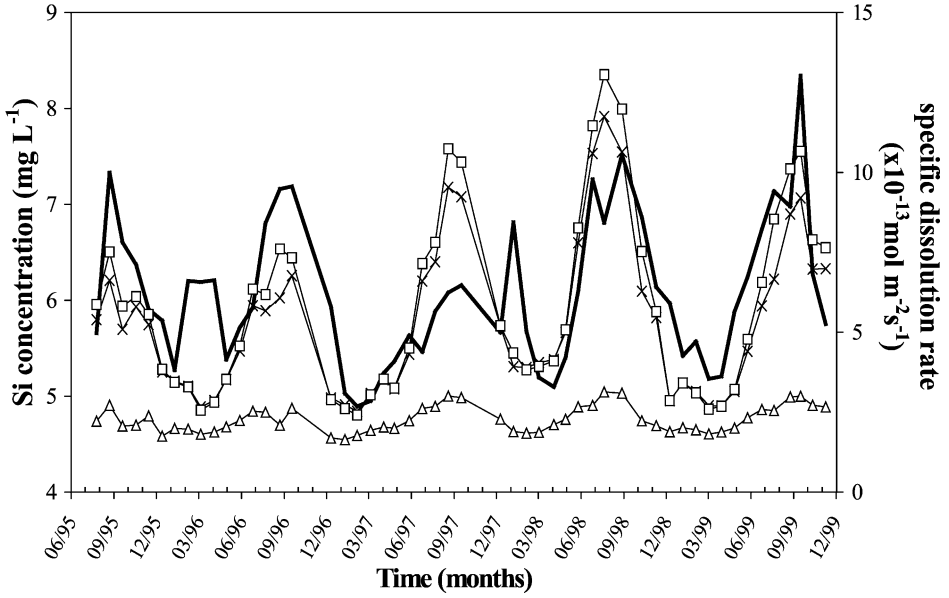

Fig. 13. Specific dissolution rates (r_d*) for K-feldspar (cross symbols), albite (square symbols) and white mica (triangle symbols) vs. silica (Si) concentration in capillary solutions. Example given at 15 cm depth.

an important effect on the absolute value of r_d*. Such a profound influence of T on the seasonal variability of both r_d* and Si concentration in capillary solutions supported the highly significant relationships between Si and T obtained by ANOVA (see Section 3.2). Conversely, Si concentration was much less well-correlated (ANOVA) with H^+ as significant relationships were only obtained at 60 and 120 cm depth (yearly scale) and in the spring, at the profile scale (see Section 3.3). In a consistent way, it was shown that seasonal variations in T were attenuated at 60 and 120 cm depth and that T was not significantly altered by soil depth in the spring (see Fig. 4). In addition, ANOVA done for each season and soil depth still sporadically indicated significant relationships between Si and T, whereas Si was never significantly related to H^+ concentrations. Consistent results were also observed in comparing linear relationships for logSi vs. pH to lnSi vs. $1/T$. In particular, significant linear trends for logSi vs. pH were found not only in the spring, but also in the autumn, which was also associated with an absence of a significant influence of

Table 4
Coefficient of determination (R^2) obtained by correlating (Pearson's correlation) dissolved silica concentrations (Si) in capillary solutions with specific dissolution rates for primary soil silicates (r_d*) at the yearly scale

Soil depth (cm)	Sample number (N)	Albite	K-feldspar	White mica
15	335	0.11	0.07	0.03
30	316	0.14	0.11	0.19
60	323	0.29	0.27	0.30
120	133	0.16	0.16	0.20

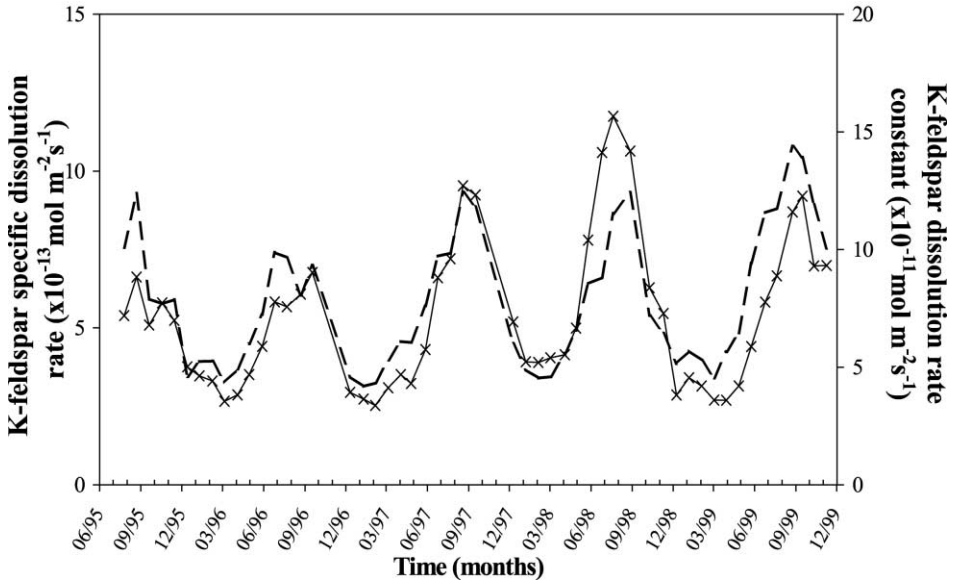

Fig. 14. Specific dissolution rates (r_d*) (cross symbols) vs. dissolution rate constants (k_d) (dashed line). Example given at 15 cm depth for K-feldspar.

soil depth on *T*. Significant relationships for logSi vs. pH were also obtained at 60 and 120 cm depth, whereas the relationships for lnSi vs. $1/T$ always gave significant linear trends.

Interestingly, R^2 values for each primary silicate increased from 15 to 60 cm depth (see Table 4). The R^2 value for 120 cm depth was intermediate compared to values for 30 and 60 cm depth, but *N* was more than two times lower. Such a variation in the value of R^2 as a function of soil depth was inconsistent with a predominant control of Si by temperature-dependent weathering, as *T* varied to a lesser extent as soil depth increased. We believe also that neither evapotranspiration nor evaporation are responsible for this trend, given the low R^2 values obtained by correlating Si concentration to chloride (Cl) concentration at 15 and 30 cm depth (see Section 3.4). In the same way, variations in either *T* or H^+ may not entirely elucidate variations in Si concentration at the soil profile scale. In particular, *T* was not significantly altered by soil depth in both the spring and the autumn, whereas Si showed larger concentrations in the upper soil layers (see Figs. 3 and 4). Moreover, *T* was larger in the winter at 120 cm depth but Si still exhibited a greater concentration at 15 and 30 cm depth.

Such unexplained trends appeared consistent with a smaller positive influence of organic ligands on chemical weathering when the density of roots decreased as soil depth increased (Drever and Stillings, 1997). These findings suggested that rock-eating ectomychorrhizal fungi play a major role in this soil (see van Breemen et al., 2000 and references therein), through the intensive exudation of low molecular weight (LMW) organic acids by fungal hyphae. Furthermore, van Hees et al. (2000) showed that citric acid, which is recognized for its marked influence on silicate weathering rates, may be more concentrated in the upper soil horizons of acidic soils, regardless of the season. Giesler et al. (2000) also suggested a greater influence of mycorrhizal hyphae on larger Si concentrations in capillary solutions

collected in the E horizon of some Podzols. Incidentally, it may be interesting to observe the similarities between acidic brown soils and Podzols in terms of Si concentration in capillary solutions vs. soil depth and biologically mediated weathering.

Lastly, it follows that the greater variability of Si concentrations between each replicate observed in the upper soil layers (see Table 2) may be ascribed to a larger spatial variability of the effect of either organic ligands or temperature, or both, on soil silicate weathering.

4.3. Role of plant phytoliths

Phytoliths, constituted of opal-A, are a minor but nearly ubiquitous constituent of soils (Drees et al., 1989). It appears doubtful that Si concentrations in capillary solutions may be controlled by the solubility variations of biogenic opal. Such constituents are formed within plant tissues (mostly leaves) and thus may not react reversibly in a soil, as this implies that their precipitation occurs at a very fast rate. Opal-CT may be formed in some soils from the transformation of opal-A, primarily by means of dissolution–reprecipitation reactions (Drees et al., 1989), but was not detected in this soil (see Section 2.1). Furthermore, Douglas-fir phytoliths were found to dissolve at a rate similar to quartz in acidic solutions, thus very slowly, and could not be expected to support Si concentrations commonly found in soil environments under a temperate climate (Bartoli and Wilding, 1980). Their relatively great stability was also consistent with their presence down to 50 cm depth in such brown acidic soils (Bartoli and Souchier, 1978). We are aware that a controversy may arise regarding to the role of plant phytoliths in the silica cycling in tropical rainforest (Alexandre et al., 1994, 1997). For instance, Alexandre et al. (1994) found a half-life of only 1 to 1.5 month in the tropical rainforest soil. This result contrasts with these proposed by Bartoli and Souchier (1978) for acidic forested soils under a temperature climate, ranging from 1 to 300 years. Possibly, the greater degradation rate of organic matter in a warm and wet climate compared to a temperature climate may explain this discrepancy, as well as the larger efficiency of the vegetation type to recycle Si (Sangster and Hodson, 1986; Alexandre et al., 1997 and references therein).

4.4. Nature of the secondary Si–Al phases

Calculated Si/Al ratios for secondary Si-containing phases in leaching solutions at 15 cm depth and at the other soil depths for capillary solutions (see Sections 4.1 and 4.2) were always found to be significantly larger than one. Such secondary phases were not observed in the soil (see Section 2.1). Therefore, their identification is uncertain. Nevertheless, according to Wada (1989), siliceous ATM (Si/Al>1) may exist in soils even if they have not been isolated and, logically, the temperature-dependence of their solubility constant has not been documented. Their relatively slow reversible formation rate, inferred from the low R^2 values associated with linear regressions of $\log\{Al^{3+}\}+3$ pH vs. $\log\{H_4SiO_4\}$, seemed consistent with the very weak amounts of Sio and Alo.

In terms of Si/Al ratios, it seemed also plausible that such the hypothetical secondary siliceous phases may be Si–Al colloidal species less than 0.45 μm in size as observed in acidic forest soil solutions (e.g. Goenaga et al., 1989; Xu and Harsh, 1993). Their presence may be consistent with the release of relatively stable polysilicic acid directly upon silicate

weathering in acidic environments (Dietzel, 2000). Polysilicic acids can promote the formation of polymeric HAS (Farmer and Lumsdon, 1994) that could further combine with each other to form colloids. However, their stability in soil solutions has not been studied.

5. Conclusion

Different processes controlled dissolved silica (Si) concentrations depending on the type of soil solution, producing marked differences in the seasonal variability of Si. Surface-controlled weathering of white mica appeared to be the primary Si-controlling process in capillary solutions. In leaching solutions, the main process may be the slow diffusion of aqueous silica from capillary solutions, in relation to soil drainage. The reversible formation of Si-containing phases may be considered to be a minor process in the control of Si concentrations in both solution types. Soil temperature appeared to deeply effect chemical weathering rates and may be considered as the dominant factor for seasonal variations in Si concentration. The influence of pH appeared tenuous, but became more acute in deep soil horizons over years and over the soil profile, depending on the season, when temperature variations as a function of soil depth were insignificant. Organic ligands apparently promoted chemical weathering and thus increased Si concentrations in the upper soil layers.

These findings were particularly useful as a fist step toward the use of a sophisticated reactive-transfer program to model solution chemistry on a mechanistic or process-oriented basis. The most relevant processes and minerals to consider in a model may be determined along with, at least for silicate dissolution, the rate-limiting mechanism. Clearly, additional study is needed to more thoroughly understand Si-controlling processes in acidic soils. For example, future research may demonstrate the influence of LMW organic ligands on in situ weathering, thus on Si concentration in capillary solutions, by determining their concentrations vs. soil depth and time. Furthermore, the presence of siliceous colloids and their partial equilibrium in acidic soil solutions needs to be established.

Acknowledgements

The Lorraine regional authorities (France) and the French Ministry for the Environment (MATE, GIP-ECOFOR program) are thanked for supporting this research. Many thanks also go to E. Gerson for revising the English. E. Dambrine, D. Gelhaye, J.G. Genon and C. Uterano are also thanked for fruitful scientific and technical discussions. The manuscript was improved by F. Bartoli, J.L. Drever and an anonymous reviewer.

References

AFES, 1992. Principaux sols d'Europe. Référentiel pédologique. INRA Edition, Paris.

Alexandre, A., Colin, F., Meunier, J.-D., 1994. Phytoliths as indicators of the biogeochemical turnover of silicon in equatorial rainforest. C. R. Acad. Sci. Paris 319 II, 453–458.

Alexandre, A., Meunier, J.-D., Colin, F., Koud, J.-M., 1997. Plant impact on the biogeochemical cycle of silicon and related weathering processes. Geochim. Cosmochim. Acta 61, 677–682.

Bartoli, F., 1983. The biogeochemical cycle of silicon in two temperate forest ecosystems. Environ. Biogeochem. Ecol. Bull. 35, 469–476.

Bartoli, F., Souchier, B., 1978. Cycle et rôle du silicium d'origine végétale dans les écosystèmes tempérés. Ann. Sci. For. 35, 187–202.

Bartoli, F., Wilding, L.P., 1980. Dissolution of biogenic opal as function of its physical and chemical properties. Soil Sci. Soc. Am. J. 44, 873–878.

Berner, R.A., Rao, J.-L., Chang, S., O'Brien, R., Keller, C.K., 1998. Seasonal variability of adsorption and exchange equilibria in soil waters. Aquat. Geochem. 4, 279–290.

Blum, A.E., Stillings, L.L., 1995. Feldspar dissolution kinetics. In: White, A.F., Brantley, S.L. (Eds.), Chemical Weathering Rates of Silicate Minerals. Reviews in Mineralogy, vol. 31. MSA, Washington, DC, pp. 291–351.

Chen, Y., Brantley, S., 1997. Temperature and pH dependence of albite dissolution rate at acid pH. Chem. Geol. 135, 275–290.

Dietzel, M., 2000. Dissolution of silicates and the stability of polysilicic acid. Geochim. Cosmochim. Acta 19, 3275–3281.

Drees, L.R., Wilding, L.P., Smeck, N.E., Senkayi, A.L., 1989. Silica in soils: quartz and disordered silica polymorphs. In: Dixon, J.B., Weed, S.B. (Eds.), Mineral in Soil Environments, 2nd edn. SSSA, Madison, WI, pp. 913–974.

Drever, J.I., Stillings, L.L., 1997. The role of organic acids in mineral weathering. Colloids Surf., A 120, 167–181.

Drever, J.I., Zobrist, J., 1992. Chemical weathering of silicate rocks as a function of elevation in the southern Swiss Alps. Geochim. Cosmochim. Acta 56, 3209–3216.

Exley, C., Birchall, J.D., 1995. Comment on "An assessment of complex formation between aluminium and silicic acid in acidic solutions" by V.C. Farmer and D.G. Lumsdon. Geochim. Cosmochim. Acta 59, 1017.

Exley, C., Birchall, J.D., 1996. Letter to the Editor, Silicic acid and the biological availability of aluminium. Eur. J. Soil Sci. 47, 137.

Ezzaïm, A., Turpault, M.-P., Ranger, J., 1997. Répartition des nutriments dans un sol brun acide développé sur tuff (Beaujolais, France). Conséquences pour l'évolution de la fertilité minérale à long terme. Ann. Sci. For. 54, 371–387.

Ezzaïm, A., Turpault, M.-P., Ranger, J., 1999a. Quantification of weathering processes in an acid brown soil developed from tuff (Beaujolais, France): Part I. Formation of weathered rind. Geoderma 87, 137–154.

Ezzaïm, A., Turpault, M.-P., Ranger, J., 1999b. Quantification of weathering processes in an acid brown soil developed from tuff (Beaujolais, France): Part II. Soil formation. Geoderma 87, 155–177.

Farmer, V.C., 1979. Possible role of a mobile hydroxyaluminium orthosilicate complex (proto-imogolite) and other hydroxyaluminium and hydroxy-iron species in podzolization. Colloq. Int. C. N. R. S., Migr. Organo-Miner. Sols Temperees 303, 275–279.

Farmer, V.C., Lumsdon, D.G., 1994. An assessment of complex formation between aluminium and silicic acid in acidic solutions. Geochim. Cosmochim. Acta 58, 3331–3334.

Gérard, F., Fritz, B., Clément, A., Crovisier, J.-L., 1998. General implications of aluminium speciation-dependent kinetic dissolution rate law in water–rock modelling. Chem. Geol. 151, 247–258.

Gérard, F., Boudot, J.-P., Ranger, J., 2001. Consideration on the occurrence of the Al_{13} polycation in natural soil solutions and surface waters. Appl. Geochem. 16, 513–529.

Giesler, R., Lundström, U.S., Grip, H., 1996. Comparison of soil solution chemistry assessment using zero-tension lysimeters or centrifugation. Eur. J. Soil Sci. 47, 395–405.

Giesler, R., Ilvesniemi, H., Nyberg, L., van Hees, P.A.W., Starr, M., Bishop, K., Kareinen, T., Lumström, U.S., 2000. Distribution and mobilization of Al, Fe and Si in three podzolic soil profiles in relation to the humus layer. Geoderma 94, 249–263.

Goenaga, X., Bryant, R., Williams, D.J.A., 1989. Influence of sorption processes on aluminum determinations in acidic waters. Anal. Chem. 59, 2673–2678.

Guy, C., Schott, J., 1989. Multisite surface reaction versus transport control during the hydrolysis of a complex oxide. Chem. Geol. 78, 181–204.

Kalinowski, B.G., Schweda, P., 1996. Kinetics of muscovite, phlogopite and biotite dissolution and alteration at pH 1–4, room temperature. Geochim. Cosmochim. Acta 60, 367–385.

Lasaga, A.C., 1998. Kinetic Theory in the Earth Sciences. Princeton Univ. Press, New Jersey.
Lumsdon, D.G., Farmer, V.C., 1995. Solubility characteristics of proto-imogolite sols, how silicic acid can detoxify aluminum solutions. Eur. J. Soil. Sci. 46, 179–186.
Marques, R., Ranger, J., 1997. Nutrient dynamics in a chronosequence of Douglas-fir (*Pseudotsuga menziesii* (Mirb.) Franco) stands on the Beaujolais Mounts (France): 1. Qualitative approach. For. Ecol. Manage. 91, 255–277.
Marques, R., Ranger, J., Gelhaye, D., Pollier, B., Ponette, Q., Gobert, O., 1996. Comparison of chemical composition of soil solutions collected by zero-tension plate lysimeters with those from ceramic cup lysimeters in a forest soil. Eur. J. Soil. Sci. 47, 407–417.
Meybeck, M., 1986. Composition chimique des ruisseaux non pollués de France. Sci. Geol., Bull. 39, 3–77.
Nagy, K.L., 1995. Dissolution and precipitation kinetics of sheet silicates. In: White, A.F., Brantley, S.L. (Eds.), Chemical Weathering Rates of Silicate Minerals. Reviews in Mineralogy, vol. 31. MSA, Washington, DC, pp. 173–233.
Nugent, M.A., Brantley, S.L., Pantano, C.G., Maurice, P.A., 1998. The influence of natural mineral coatings on feldspar weathering. Nature 395, 588–591.
Ranger, J., Marques, R., Colin-Belgrand, M., Flammang, N., 1995. The dynamics of biomass and nutrient accumulation in a Douglas-fir (*Pseudotsuga menziesii* Franco) stand studied using a chronosequence approach. For. Ecol. Manage. 72, 167–183.
Schott, J., Oelkers, H., 1995. Dissolution and crystallisation rates of silicate minerals as a function of chemical affinity. Pure Appl. Chem. 67, 903–910.
Sangster, A.G., Hodson, M.J., 1986. Silica in higher plants. Silicon Biogeochemistry. Ciba Foundation Symposium, vol. 121. Wiley, Chichester, pp. 90–111.
Tardy, Y., Fritz, B., 1981. An ideal solid solution model for calculating solubility of clay minerals. Clay Miner. 16, 361–373.
Turpault, M.-P., Augusto, L., Bonnaud, P., Ranger, J., 1998. Evolution of the weathering rate of a labradorite feldspar introduced in acid soils over nine years. Mineral. Mag. 62A, 1555–1556.
USDA, 1994. Keys for Soil Taxonomy, 6th edn. Soil Conservation Service, Washington, DC.
van Breemen, N., Lundström, U.S., Jongmans, A.G., 2000. Do plants drive podzolization via rock-eating mycorrhizal fungi? Geoderma 94, 163–171.
van Hees, P.A.W., Lundström, U.S., Giesler, R., 2000. Low molecular weight organic acids and their Al-complexes in soil solution-composition, distribution and seasonal variation in three podzolized soils. Geoderma 94, 173–200.
Velbel, M.A., 1993. Formation of protective surface layers during silicate-mineral weathering under well-leached, oxidizing conditions. Am. Mineral. 78, 405–414.
Wada, K., 1989. Allophane and imogolite. In: Dixon, J.B., Weed, S.B. (Eds.), Mineral in Soil Environments, 2nd edn. SSSA, Madison, WI, pp. 1051–1087.
White, A.F., Blum, A.E., 1995. Effects of climate on chemical weathering in watersheds. Geochim. Cosmochim. Acta 59, 1729–1747.
White, A.F., Blum, A.E., Bullen, T.D., Vivit, D.V., Schulz, M., Fitzpatrick, J., 1999. The effect of temperature on experimental and natural chemical weathering rates of granitoid rocks. Geochim. Cosmochim. Acta 63, 3277–3291.
Wolery, T.J., 1992. EQ3NR, a computer program for geochemical aqueous speciation–solubility calculations, Theoretical manual, User's guide, and related documentation. Lawrence Livermore National Lab., UCR-MA-110662 PT III, California.
Xu, S., Harsh, J.B., 1993. Labile and nonlabile aqueous silica in acid solutions, relation to the colloidal fraction. Soil Sci. Am. J. 57, 1271–1277.
Zysset, M., Blaser, P., Luster, J., Gehring, A.U., 1999. Aluminum solubility control in different horizons of a podzol. Soil Sci. Soc. Am. J. 63, 110–1115.

Silice et solutions extraites par centrifugation

Gérard F., Ranger J., Ménétrier C., et Bonnaud P. (2003) Silicate weathering mechanisms determined using soil solutions held at high matric potential. *Chemical Geology* **202**, 443-460.

ELSEVIER

Chemical Geology 202 (2003) 443–460

CHEMICAL GEOLOGY
INCLUDING
ISOTOPE GEOSCIENCE

www.elsevier.com/locate/chemgeo

Silicate weathering mechanisms determined using soil solutions held at high matric potential

F. Gérard*, J. Ranger, C. Ménétrier, P. Bonnaud

Institut National de la Recherche Agronomique (INRA), Unité Biogéochimie des Ecosystèmes Forestiers, Centre de Nancy, 54280 Champenoux, France

Received 26 September 2001; received in revised form 16 September 2002; accepted 19 December 2002

Abstract

We present evidence of surface-controlled and proton-promoted chemical weathering of primary silicates in a brown acidic soil (Vauxrenard, Rhône, France). We used aqueous silica (Si) in soil solutions held at high matric potential (180–1600 kPa), which are representative of solutions reacting with soil solids. Si concentration was well correlated with H^+ concentration and to a lesser extent with dissolved organic carbon (DOC), which showed a significant affect ($P<0.05$) only in the surface layer (0–15 cm). Significant negative linear relationships were obtained between log(Si) and pH at the profile scale, at each soil depth and for most sampling dates. We found no significant influence of soil temperature ($P>0.05$). Geochemical modelling showed that primary silicates dissolved under far-from-equilibrium conditions, and that organic ligands (modelled with a triprotic analogue) may have a weak but significant effect on the variations in log(Si) at the profile scale and at both 15–30 and 30–45 cm depths. Comparison of Si/Al ratios to literature data and observed soil mineralogy demonstrated that significant linear relationships found in the activity diagram between $\log[Al^{3+}]+3pH$ and $\log[H_4SiO_4^\circ]$ may not have been caused by the reversible formation of secondary Al–Si phases in the soil. Instead, the apparent trends may arise from relationships between log(Si) and pH and the control of Al-mobility by the reversible formation of Al-hydroxides in the vermiculite interlayer. All these results indicated that active, in situ chemical weathering of silicates may be surface-controlled and mostly proton-promoted. Mineralogy suggested that K-feldspar weathered much faster than albite and white mica, in contrast to the weathering gradient inferred from the mass balance between unweathered and soil material. This was certainly caused by differential changes in mineral reactive surfaces with time.

Keywords: Weathering; Silicates; Soil; Solutions; Matric potential; Modelling

1. Introduction

Knowledge of the mechanism controlling the chemical weathering rates of silicates in the field is important for several environmental issues. Acidification of soils and surface waters is closely connected to weathering, and this process also constitutes an important source of nutrients for plants over the long-term. The hydrolysis of silicates during rock weathering occurs via a sequence of mechanisms. The form of the kinetic expression depends on the nature of the rate-limiting mechanism. Thus, knowledge of the present-day, in

* Corresponding author. Tel.: +33-3-83-39-41-46; fax: +33-3-83-39-40-69.
E-mail address: gerard@nancy.inra.fr (F. Gérard).

0009-2541/$ - see front matter © 2003 Elsevier B.V. All rights reserved.
doi:10.1016/j.chemgeo.2002.12.001

situ rate-limiting mechanism is the first step toward the accurate calculation of chemical weathering rates using a reactive-transfer model.

It is well established that surface reactions control silicate weathering (i.e. surface-controlled dissolution) under laboratory conditions. One line of evidence is the decline in dissolution rates when the pH of the reacting solution increases (e.g. Nagy, 1995; Blum and Stillings, 1995; Drever and Stillings, 1997). Surface-controlled silicate dissolution rates become almost pH-independent at a pH greater than about 5 units. Below pH ~ 5, hereafter termed the acidic region, silicate dissolution mostly involves protons (H^+) as the reacting species and is said to be proton-promoted. Organic acids ranging from low molecular weight acid to humic substances may promote silicate weathering, depending on the pH and on the nature and concentration of organic substances (Bennett and Casey, 1994; Welch and Ullman, 1993, 1996; Ochs, 1996; Stillings et al., 1996; Drever and Stillings, 1997; Zhang and Bloom, 1999). Most of these authors report an increase in the promoting effect of low molecular weight organic acids with the pH of the reacting solution, as proton-promoted dissolution rate decreases and deprotonation of organic acids increases. Low molecular weight organic acids are typically more effective in accelerating silicate dissolution than larger molecules, such as fulvic acids (Zhang and Bloom, 1999) and humic acids (Ochs, 1996), possibly due to differences of carboxylic site densities and chelation efficiency (Drever and Vance, 1994). Furthermore, high molecular weight acids may even decrease the rate of silicate dissolution as pH increases (Ochs, 1996; Drever and Stillings, 1997). However, dissolved organic carbon (DOC) was generally found to enhance silicate dissolution under acidic conditions (Lundström and Öhman, 1990; Raulund-Rasmussen et al., 1998). This reveals the nature of the net effect on silicate weathering rates of the range of organic compounds present in natural samples.

Nevertheless, the exact nature of the rate-limiting mechanism remains unclear in the field. Weathering rates can be controlled by the diffusion of reacting or product species through microporous residual layers, amorphous or crystalline coatings stuck to mineral surfaces, and mineral micropores and mesopores (<50 nm) (e.g. Anbeek et al., 1994; Hochella and Banfield, 1995; White et al., 1996; Brantley, 1998; Nugent et al., 1998; Hodson, 1999). Soil minerals have generally been subjected to weathering agents over geological time spans, enabling residual layers and coatings to develop to a much greater extent than in the laboratory. The surface reactivity of minerals may decrease with exposure to weathering (Anbeek, 1993; Augusto et al., 2000). The well-known discrepancy between field and laboratory dissolution rate constants (e.g. Paces, 1983; Brantley et al., 1993; Swoboda-Colberg and Drever, 1993; White, 1995; White et al., 2001) gives further reason to wonder whether these differences are due to our inability to characterise the complexity of the dissolution mechanisms operating in natural systems or if dissolution mechanisms differ fundamentally between field and laboratory (White et al., 1996; Nugent et al., 1998).

The chemistry of soil solutions depends on the nature and intensity of active and in situ soil processes/mechanisms, and vice versa. Aqueous silica may be used as weathering rate indicator, as in the laboratory during experimental dissolution of silicates (e.g. Hellmann, 1994; Frogner and Schweda, 1998) and in some stream and river waters wherein its role as weathering rate indicator has also been pointed out when the stoichiometry of the overall weathering reactions is known (Meybeck, 1986; Drever and Zobrist, 1992; White and Blum, 1995; White et al., 1999). This research is aimed at investigating the active mechanisms controlling chemical weathering rates of soil silicates, using a certain type of soil solution collected from field samples. One may distinguish two main types of soil solutions according to the energy with which they are retained by solids, generally termed the matric potential (ψ). Leaching solutions circulate into interconnected macropores driven by the gravitational force, and solute species are transferred downward by advection. The remaining portion of the bulk soil water corresponds to "capillary" soil solutions, which are almost immobile as they are retained by capillary forces in narrower interconnected pores. Soil scientists used the field capacity to define the ψ value below which gravitational transfers may occur. The GRIZZLY database (Havenkamp et al., 1998) may be used to demonstrate that field capacity varies from about $\psi = 3-30$ kPa in most soils, depending on their texture and structure. Mass transfers between leaching and capillary solutions correspond to mixing processes, as they

occur via molecular diffusion and eventually via capillarity if ψ exceeds field capacity due to water loss by evaporation and evapotranspiration. Accordingly, the chemical properties of capillary and leaching solutions generally differ because of the differences in their residence time, implying different contact times with soil solids and some variations in the nature and intensity of the physical and biological processes. Capillary solutions are generally more concentrated in most solutes than leaching waters and their chemistry shows seasonal variations (Zabowski and Ugolini, 1990; Marques et al., 1996; Giesler et al., 1996; Ranger et al., 2001; Gérard et al., 2002). In our conceptual model, capillary solutions form a continuum in chemical terms because the impact of the evaporation and evapotranspiration processes is attenuated as ψ increases and, conversely, the influence of water–solid interactions on the chemical properties of capillary solutions increases with ψ (Fig. 1). Note that this is not only caused by the weakness of biological and physical processes but also by a weaker influence of molecular diffusion, since the diffusion distance for solutes released by water–solid interactions gets smaller as ψ increases. Therefore, we shall consider capillary solutions held at greater ψ values as most representative of the solution reacting with soil-forming minerals.

2. Materials and method

2.1. Field site and soil mineralogy

The soil studied is an acidic brown soil, classified as a 'Typic Dystrochrept' (USDA, 1998) or an Alocrisol (AFES, 1992), covered by a 45-year-old Douglas fir plantation (*Pseudotsuga menziesii* (Mirb.) Franco). The area studied is located in the Montagne des Aiguilettes in the Beaujolais (Rhône, France), at an altitude of about 750 m. The mean annual temperature is 7 °C and mean annual precipitation is ~ 1000 mm. Chemical properties of the soil, stand characteristics, ecological situation and nutrient dynamics have been discussed by Ranger et al. (1995), Marques et al. (1996) and Marques and Ranger (1997).

The mineralogy and chemical properties of the soil have also been comprehensively studied (Ezzaïm et al., 1997, 1999a,b). The bedrock is an Upper Visean volcanic tuff that has undergone hydrothermal alteration. Unweathered material contained about 45% quartz, andesine, albite and biotite phenocrysts (< 2 mm) and 55% devitrified groundmass. The devitrified volcanic glass consists of an association of quartz, andesine, albite, K-feldspar spherolites and biotite microcrysts (1–10 μm). The weathering gradient inferred from the mass balance between soil material (0–

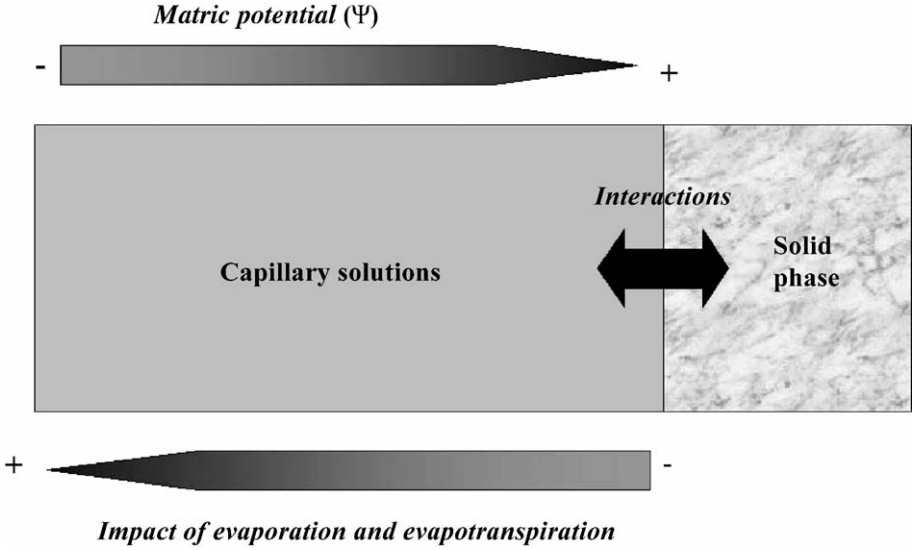

Fig. 1. Conceptual model used for the chemistry of capillary solutions.

1 cm) and the unweathered tuff was: quartz < K-feldspar < white mica < biotite < albite < andesine. Extensive Ca and Na depletion was observed in the soil material, corresponding to the almost complete dissolution of andesine and of ~ 77% albite (see Fig. 5 in Ezzaïm et al., 1999b). Meanwhile, the relative abundance of K-feldspar and white mica slightly increased by about 64% and 43%, respectively.

Scanning and transmission electron spectroscopy (SEM and TEM, respectively), and X-ray diffraction (XRD) have led us to identify kaolinite, hydroxy-Al interlayered vermiculites and interstratified vermiculite–biotite as secondary minerals. Small amounts of Si and Al were extracted by oxalate (Si_o and Al_o, respectively) from the fine earth fraction. Both oxalate and pyrophosphate released similar amounts of Al, proving that extractable Al was essentially organically bound. The very small value taken by the $(Al_p - Al_o)/Si_o$ ratio, with Al_p standing for Al extracted by pyrophosphate, further suggested that allophane or ITM were either absent or present in very weak quantities in the soil material (see Ezzaïm et al., 1999b).

2.2. Solution collecting technique

The centrifuge drainage method made it possible to collect capillary solutions corresponding to high matric potential (ψ) from soil samples collected in the field (e.g. Giesler and Lundström, 1993; Giesler et al., 1996). Here, a JOUAN KR4 22 centrifuge was used at room temperature ($T \sim 20$ °C). This apparatus permits the centrifugation of six soil samples of approximately 1600 cm^3 each placed in double bottomed polycarbonate tubes, consisting of an upper soil holding cup with a perforated base and a lower solution collecting cup. A stepwise procedure was adopted to extract the portion of capillary solutions corresponding to the highest matric potential. A first extraction was performed at 1000 rpm for 20 min, yielding capillary solutions corresponding to $\psi < 180$ kPa. The second step consisted of centrifuging the same soil samples for an additional 20-min period at 3000 rpm. Capillary solutions corresponding to a matric potential range of 180–1600 kPa were thereby obtained. In agreement with the above conceptual model for soil solutions, only capillary solutions corresponding to the higher matric potential range were retained in the present study and considered as the best representing of solutions reacting with soil minerals.

2.3. Soil sampling and solution chemistry

The soil samples were collected during five field campaigns from 1999 to 2000, in October and November 1999, February, May and October 2000. Extraction of capillary solutions in quantities commensurate with chemical analysis of major solutes (see below) is often prevented in the summer, because of excessively dry conditions. Thus, no sampling occurred in this season. Soil samples were collected at least two days after the last rainfall or snowmelt in order to minimise the replenishment of capillary solutions with new meteoritic water. Otherwise, the chemistry of capillary solutions could be misleadingly altered by leaching solutions given their different chemical properties, as discussed in Section 1.

Sampling points were selected to deal as well as possible with spatial variations in parameters controlling chemical weathering rates, especially mineral reactive surfaces. Samples were taken within three tree-free circular areas of approximately 2-m radius about 15 m apart. Three soil samples were taken from each collecting zone at three depth intervals (0–15, 15–30 and 30–45 cm) below the litter layer, corresponding to the A_1/A_P, A_P and A/(B) horizons, respectively. A stainless steel tube (length = 15 cm, diameter = 8 cm) was used and samples were immediately stored in plastic bags. The hole was partly refilled with litter, gravel, pebbles and uncollected soil material. Soil sampling locations were then marked to avoid being sampled at a later date. On average, about 72 h elapsed between field sampling and centrifugation in the laboratory. Samples were not refrigerated during transport. This time period covered field sampling, sample transportation and their centrifugation in the laboratory. Then, capillary solutions were immediately filtered after extraction through a 0.45-μm filter (GN-6 Metricel®, Pall) and pH was determined using a combination pH electrode (INGOLD-XEROLIT®) with a Mettler DL21 pH-meter. Total Si, Al, Ca, Mg, K, Na, Mn and Fe were analysed by ICP emission spectroscopy (JY 38+ spectrometer). DOC was measured with a SHIMADZU TOC 5050. Sulphate and fluoride were both analysed by ion chromatography (DIONEX DX 300).

Nitrate, ammonium and chloride were measured by colorimetry (TRAACS 2000). Soil temperature was measured at different depths with either in situ or portable temperature probes, depending on equipment availability.

2.4. Surface-controlled weathering rate equation

According to Lasaga (1995), a general surface-controlled rate expression as a function of the activity of reacting species in a non-isothermal system may be described by:

$$r = S\prod_i k_i[i]^{n_i} A\exp\left(\frac{-E_a}{RT}\right) \quad (1)$$

where r is the mineral dissolution rate (mol s^{-1} $kg_{H_2O}^{-1}$), S is the reactive surface of the mineral (cm^2 $kg_{H_2O}^{-1}$), k_i is the rate constant for the reaction involving the reacting species i (mol cm^{-2} s^{-1}), $[i]$ is the aqueous activity of reacting species i involved in the rate-limiting surface reactions, n_i is an experimental exponent, A is the pre-exponential factor, E_a is the apparent activation energy of the overall reaction (J mol^{-1}), R is the universal gas constant (8.31451 J mol^{-1} K^{-1}) and T is the Kelvin temperature.

By taking the logarithm of r with only H^+ and a given organic ligand (noted L) as the reacting species and by considering dissolved silica (Si) as weathering rate indicator, Eq. (1) becomes:

$$\log(\mathrm{Si}) = \log(Sk_{H^+}k_L A) + n_{H^+}\mathrm{pH} + n_L\log[\mathrm{L}] - \left(\frac{E_a}{2.303RT}\right) \quad (2)$$

Eq. (2) is valid if there is no change in the reaction mechanism with temperature and if species concentrations are not significantly altered by other reactions. It shows that log(Si) may be expressed as a linear function of pH, log[L] and T^{-1}, with slopes n_{H^+}, n_L and $-E_a/2.303R$, respectively. The slope n_{H^+} should have a negative value, in order to reproduce the decrease of the dissolution rate in the acidic range as pH increases. In contrast, the slope n_L can have either a negative or positive value depending on whether the given organic ligand slows or accelerates the dissolution rate.

2.5. Geochemical modelling

A number of variables and processes may obscure or yield spurious linear relationships between log(Si) and pH because of excessive dispersion of the data. Their influence may be identified by means of geochemical modelling, such as chemical affinity, A_r (with $A_r = -RT\ln[Q/K]$ with Q the ion activity product and K the thermodynamic equilibrium constant). Eq. (2) will be linear with respect to pH when $A_r \gg 0$ and therefore the influence of A_r on chemical weathering rates is weak. Note that this condition, generally termed as far-from-equilibrium, is also maintained in laboratory dissolution experiments in order to limit secondary phase precipitation. The standard Transition State Theory was used in this study to check whether soil silicates dissolved under far-from-equilibrium conditions or not when in contact with capillary solutions. Accordingly, the dissolution rate exhibits first order dependency with respect to A_r and may not be significantly altered if the A_r/RT ratio is greater than 3.

The formation of secondary aluminosilicates in soils can also affect silica mobility. Secondary aluminosilicates such as allophane and imogolite type materials (ITM) may form at relatively fast rates in acidic soils (hence their short range ordered nature) and may be kaolinite precursors (Steefel et al., 1990; Su et al., 1995; Lumsdon and Farmer, 1995). Accordingly, their formation occurs close to equilibrium and is thus influenced by their solubility (i.e. equilibrium-controlled reaction). It follows that this process can lead to mistaken linear relationships between log(Si) and pH because of the Al content of these phases (Si/Al ~ 0.5). The solubility of these phases depends directly and indirectly (i.e. through the activity of Al^{3+}) on the pH and should therefore increase non-linearly when the pH decreases. Because of the expected variability in the data, an apparent linear relationship between log(Si) and pH may be found, with a negative slope n_{H^+} as it would be with surface-controlled and proton-promoted silicate weathering (Eq. (2)).

Temperature changes induce solubility variations as well. The Van't Hoff expression (Eq. (3)) represents the influence of T on the equilibrium constant:

$$K = K_0\exp\left(\frac{-\Delta H_r}{RT}\right) \quad (3)$$

where ΔH_r is the standard enthalpy change for the reaction (or heat of reaction) over a given temperature range (J mol^{-1} K), K and K_0 are the equilibrium constants at a given temperature and at a reference temperature, respectively. A linear function of T^{-1} may be obtained by taking the logarithm of the Van't Hoff expression:

$$\log(K) = \log(K_0) - \left(\frac{\Delta H_r}{2.303RT}\right) \quad (4)$$

Assuming that the Si concentration was controlled by the equilibrium-controlled formation of ITM, log(Si) would be proportional to log(K). Since log(Si) may be falsely linearly related to the pH due to its effect on the solubility of ITM, as discussed above, one can write:

$$\log(\mathrm{Si}) \equiv \log(K_0) + n_{H^+}\mathrm{pH} - \left(\frac{\Delta H_r}{2.303RT}\right) \quad (5)$$

Comparison of Eq. (5) with Eq. (2) for the case of $n_L = 0$ clearly shows that a linear relationship might be obtained with the same dataset, though due to different Si-controlling processes. This demonstration can be extended to organic ligands as well, because Al speciation and thus the solubility of ITM may also be influenced by the organic ligand concentration through the formation of organo-Al complexes. A greater complexing influence of organic ligands would lower the activity of Al^{3+} and would thus increase the Si concentration needed to maintain an equilibrium with ITM, giving a positive value of n_L as expected in Eq. (2) should organic ligands significantly promote silicate weathering.

We have seen in the introduction that DOC in soil solutions encompasses a huge range of organic compounds of different molecular weight and functionality, which may have contrasting effects on silicate dissolution kinetics. DOC speciation is not yet readily determined and provisions for minimising the potential influence of organic ligands on field silicate weathering rates (i.e. $n_L[L] \rightarrow 0$ in Eq. (2)) were made to improve linear relationships between log(Si) and pH and T^{-1}. Studying mineral layers of an acidic forest soil where solution pH is mostly below 5, by definition, may satisfy this condition as data corresponding only to the acidic region wherein surface-controlled weathering may be mostly proton-promoted would be obtained. Nevertheless, since the influence of organic ligands may not be negligible, some simple models exist in the literature and may be used profitably to assess the organic ligand concentration for test purposes.

We incorporated one of these in the PHREEQC 2.0 hydrochemical computer program (Parkhurst and Appelo, 1999) used for calculating the equilibrium distribution of the aqueous species in capillary solutions and their chemical affinity for the dissolution of the primary silicates. We considered the triprotic analogue representation of the acid–base properties of the DOC collected in the Hubbard Brook Experimental Forest (Driscoll et al., 1994; Schecher and Driscoll, 1995). This approach permits the simulation of the complexation between dissolved Al and an analogue organic ligand, L, having a mean site density, m, equal to 0.055 mol site/mol carbon (Driscoll et al., 1994). Boudot et al. (1994) obtained acceptable agreement between this model and experimental values of Al speciation in solutions collected from forested acidic soils located in the Vosges mountains (N.E. France). More recently, Boudot et al. (2000), Maitat et al. (2000) and Gérard et al. (2001) used this model to simulate Al speciation in acidic soil porewaters collected from a number of other forested acidic soils. The question of the relative validity of the triprotic analogue representation of the acid–base properties of DOC was raised by a recent research showing that low molecular weight and higher molecular weight-acids in acidic forest soils exhibited similar acid–base properties (Bergelin et al., 2000).

The origin the thermodynamic data used in PHREEQC 2.0 for mineral and inorganic aqueous species has been thoroughly discussed in Gérard et al. (2001). Natural imogolite (Zysset et al., 1999) was added to the initial database in order to encompass the wide range of log(K) values proposed in the literature for ITM. Upper and lower solubility boundaries for ITM were defined by the maximum and the minimum log(K) values (i.e. log(K) plus and minus the standard deviation) for proto-imogolite sol (PI) and natural imogolite. Soil vermiculites were not considered in the thermodynamic database because of the uncertainties with respect to the stability of interstratified clays. Furthermore, there was a lack of data on the distribution of Al between interlayer, octahedral and tetrahedral sites, which meant that it was not possible to

calculate a mean structural formula (see Ezzaïm et al., 1999b). Conversely, the thermodynamic equilibrium constant for white mica, $K_{0.94}(Mg_{0.19}Fe(II)_{0.14}Al_{1.71})Al_{0.73}Si_{3.27}O_{10}(OH)_2$ (see Ezzaïm et al., 1999b), was estimated using an ideal solid solution model (Tardy and Fritz, 1981) according to Eq (6).

$$\log(K_m) = \sum_j x_i \log(K_i) + \sum_j x_i \log(x_i) \quad (6)$$

where K_m is the equilibrium constant of the ideal solid solution m, j is the number of end-members i required to model the solid solution, x_i is the mole fraction of the end-member i in the solid solution m and K_i is the thermodynamic equilibrium constant for the end-member i. Three end-members available in the database were used (muscovite, annite and Mg-phlogopite).

The primary mineral biotite was not considered in this study. Our choice was supported by the very great extent of the transformation of biotite to secondary clays (vermiculite and interstratified vermiculite–biotite), compared to the relatively small amount of biotite within the unaltered tuff (Ezzaïm et al., 1999a,b).

2.6. Statistics

All the statistics were computed using the program SAS version X81 for UNIX (SAS Institute). The first set of tests concerned general statistics of the measured variables relevant to the present work, i.e. Si and H^+ concentrations, DOC and soil temperature. A preliminary study of correlations between these variables was made by means of a factor analysis (PCA, two factors). Then variance analysis (ANOVA), followed by multiple comparisons (Student–Neumann–Keuls) whether necessary (i.e. null hypothesis rejected), were used in order to get the statistical significance of the previous correlations and to study the influence of soil depth and sampling depth on Si concentration. In a second step, attempts to obtain significant relationships between log(Si), pH and T^{-1} and the organic ligand term in Eq. (2) were made by multiple linear regression analysis. In a first step, statistical analysis was made between measured variables only, i.e. between log(Si), pH and T^{-1}. Thereafter, the organic ligand term was included in the multiple linear regression analysis for test purposes.

3. Results

3.1. General statistics, factor analysis and ANOVA

Capillary solutions were extracted from more than 100 soil samples by centrifugation and analysed ($N=114$). Measured pH never exceeded 5 units and ranged from 3.8 to 4.9 exhibiting a standard deviation (S.D.) of 0.21. Si concentrations ranged from 4.2 to 19.3 mg l^{-1}. Soil temperatures ranging from $T=2$–12 °C were measured when soil samples were collected. DOC ranged from 10 to 74 mg l^{-1}.

Factor analysis done with the variables DOC, Si and H^+ concentrations, and T showed that Si concentration was tightly correlated with H^+ concentration, through the first principal component (Fig. 2). Soil temperature was poorly correlated with the other variables, especially Si concentration. A better correlation was found between Si concentration and DOC. The statistical significance (i.e. P-value) of such correlations was studied by means of variance analysis (ANOVA), by taking into account the plausible influence soil depth and sampling date on Si concentration (taken as factors). The variables H^+ concentration, DOC and T were considered/tested as covariates of Si concentration. The relationships between Si and both H^+ and DOC were highly significant ($P<0.0001$), while there was a lack of significant influence of T. Sampling date, unlike soil depth, exhibited a significant influence on Si concentration but we also obtained a highly significant interaction between soil depth and sampling date. This required additional ANOVA using data subsets corresponding to the different sampling dates (regardless of soil depth) and to the different soil depths (regardless of sampling date). By doing so, a unique factor may be considered in ANOVA, either soil depth or sampling date. In the first case, soil depth significantly affected Si concentration except for the subset of data corresponding to February 2000. A significant correlation between Si and H^+ concentrations prevailed for all sampling dates. In contrast, there was a lack of significant affect of T on Si concentration in all the cases (i.e. whatever the sampling date), as well as for DOC with an exception in October 2000. Multiple comparisons showed that the maximum Si concentration was reached in the surface layer (0–15 cm), corresponding to Si ~ 15 mg l^{-1} compared to an average of about 8 mg l^{-1} at the other depths. Within

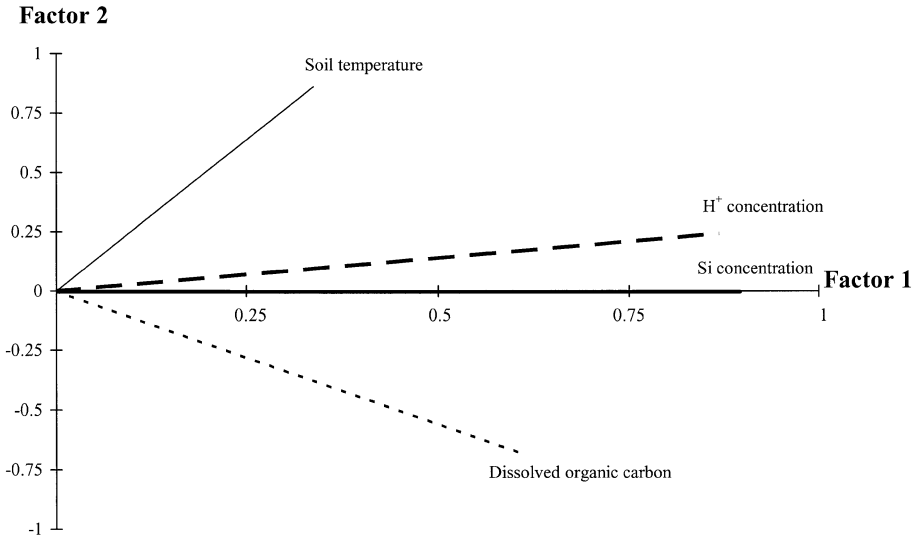

Fig. 2. Result of the factor analysis (PCA, two factors) using the measured silica, H^+, dissolved organic carbon concentrations and soil temperature.

data subsets corresponding to the different soil depths, sampling date always significantly affected Si concentration. The maximum Si concentration was reached in May and/or October 2000 ($\sim 15-10\ mg\ l^{-1}$), depending on the soil depth. Meanwhile, Si concentration was well correlated with H^+ at each soil depth (i.e. in all the data subsets), while the correlation with DOC was only significant in the surface soil layer.

3.2. Log(Si)–pH–T^{-1} relationships

Attempts to establish significant relationships between log(Si) and pH and T^{-1} were first made by multiple linear regression analysis of Eq. (2), without the term representing organic ligands. The whole set of data was first used regardless of the soil depth interval and sampling date. Such a scale (hereafter referred to as the profile scale) appeared the most suitable to minimise the distorting influence of data variability due to uncontrolled variables and processes (reactive surfaces, mass transfers, organic ligands, etc.) as it provided the greatest number of data. Moreover, results may be indicative of the Si-controlling process at the soil profile scale. By doing so, a highly significant linear relationship ($P<0.0001$) was established between log(Si) and pH at the profile scale (Fig. 3), whereas no significant influence of the temperature term (i.e. T^{-1}) was found. This was consistent with the absence of significant correlation between soil temperature and Si concentration found in the previous section. The slope, n_{H^+}, of the relationship between log(Si) and pH was equal to -0.47 (S.E. = 0.05). The coefficient of determination, R^2, indicated that about 43% of the variability in log(Si) concentration was controlled by pH.

Then, multiple linear regression analysis was done with the same data subsets defined in the previous section. First, data from the different soil depth intervals were considered. A highly significant linear relationship between log(Si) and pH prevailed at 0–15 cm depth ($N=39$) and there was still no significant influence of the temperature term (Table 1). Beneath the upper soil mineral layer, at the 15–30 and 30–45 cm depths, there was a persistent lack of influence of the temperature term in Eq. (2) on log(Si). Significant linear relationships between log(Si) and pH were still calculated (see Table 1), though to a lesser extent than at either the profile scale or surface layer interval, suggesting that the control of log(Si) by pH was apparently weaker than in the upper soil layer.

Multiple linear regressions for data subsets corresponding to each sampling date also showed a lack of significant influence of soil temperature on log(Si). Significant relationships between log(Si) and pH were

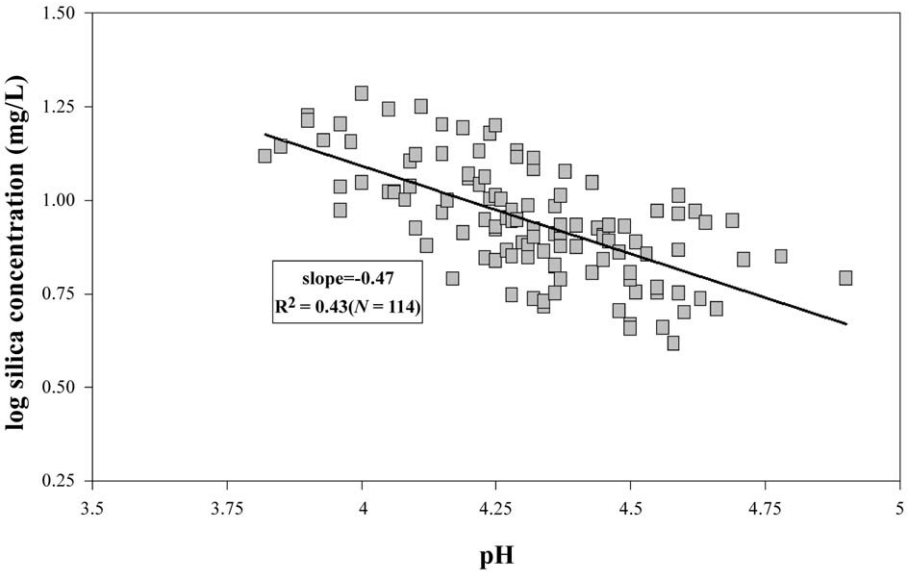

Fig. 3. Linear relationship between the logarithm of the silica concentration and the pH of capillary solutions at the soil profile scale.

obtained for all sampling dates except for October 2000 (Table 2).

3.3. Modelling

A temperature constraint is required for geochemical modelling since this variable affects the stability of aqueous species and minerals. Statistical analysis failed to reveal a significant effect of T on Si concentration (note that plausible explanations for this result are discussed in Section 4.4). The absence of correlation between Si concentration and T suggests that a single temperature value could be reasonably used to calculate aqueous speciation and chemical affinities of capillary solutions. In the absence of an obvious and relevant single temperature value, the following calculations were done at $T = 25$ °C because it corresponds to the standard condition at which thermodynamic parameters used by the model are better known. Therefore, setting $T = 25$ °C should minimize modelling errors.

It can be seen in Fig. (4) that the A_r/RT ratio in capillary solutions for the dissolution of albite and white mica was mostly higher than the threshold value

Table 1
Slope (n_{H^+}), coefficient of determination (R^2), significance (P) and number of data (N) for the relationships between log(Si) and pH calculated with the data subsets corresponding to each soil depth interval

Soil depth interval (cm)	n_{H^+}	R^2	P	N
0–15	−0.54 (0.09)	0.49	****	39
15–30	−0.30 (0.09)	0.24	**	39
30–45	−0.46 (0.12)	0.29	***	36

****$P < 0.0001$, ***$0.0001 < P < 0.001$, **$0.001 < P < 0.01$, *$0.01 < P < 0.05$, ns = $P > 0.05$.
Values in parentheses are the standard error (S.E.) associated with the slope.

Table 2
Slope (n_{H^+}), coefficient of determination (R^2), significance (P) and number of data (N) for the relationships between log(Si) and pH calculated with the data subsets corresponding to each sampling date

Sampling date (month–year)	n_{H^+}	R^2	P	N
10–99	−0.42 (0.12)	0.41	****	19
11–99	−0.73 (0.09)	0.71	****	27
02–00	−0.25 (0.12)	0.16	*	25
05–00	−0.35 (0.08)	0.48	***	23
10–00	ns	0.15	ns	20

****$P < 0.0001$, ***$0.0001 < P < 0.001$, **$0.001 < P < 0.01$, *$0.01 < P < 0.05$, ns = $P > 0.05$.
Values in parentheses are the standard error (S.E.) associated with the slope.

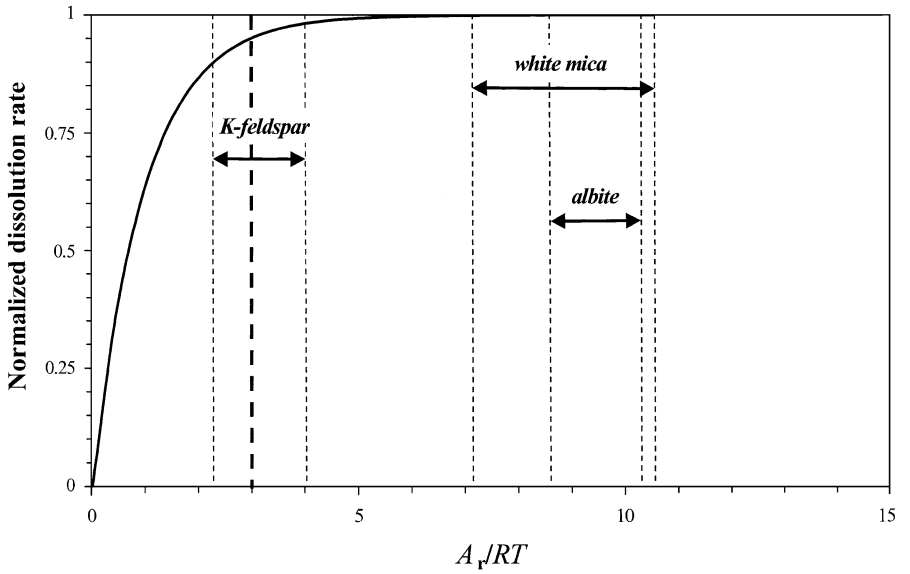

Fig. 4. Normalized dissolution rate (i.e. dissolution rate divided by far-from-equilibrium dissolution rate) plotted as a function of the chemical affinity term (A_r/RT), at $T=25$ °C. Thin dashed lines correspond to the range of A_r/RT ratios calculated for primary minerals (mean value ± standard deviation). The thick dashed line stands for the threshold value of 3 for the A_r/RT ratio given by a first order dependency of the dissolution rate, according to the standard Transition State Theory. Below this limit ($A_r/RT<3$), the dissolution rate is significantly reduced (i.e. by over 5%) by the chemical affinity of the reaction.

of 3 specified by the Transition State Theory. Mean A_r/RT values for albite and white mica were 9.42 (S.E. = 0.08) and 8.80 (S.E. = 0.16), respectively, implying that their dissolution is unaltered by chemical affinity (i.e. normalized rate equal to 1). The mean value of the A_r/RT ratio for K-feldspar was 3.11 (S.E. = 0.08) and thus overlaps the threshold value. Accordingly, K-feldspar dissolution rate may be decreased by 10% (i.e. normalized rate of 0.9) due to the effect of chemical affinity.

The thermodynamic state of capillary solutions regarding equilibrium with secondary phases in the Al–Si system was studied by means of the relevant activity plot of $\log[Al^{3+}]+3pH$ vs. $\log[H_4SiO_4^\circ]$ (Fig. 5). Capillary solutions were greatly over-saturated with respect to poorly crystallized kaolinite, certainly the best proxy for the kaolinite identified in this soil (Section 2.1). Solutions were close to equilibrium with respect to natural imogolite at low activities in orthosilicic acid (lower than about $10^{-3.5}$), but this phase has not been observed in this soil. A linear regression analysis of all the data gave a slope of −1.45 (S.E. = 0.14), corresponding to the Si/Al ratio of a hypothetical secondary phase, with an R^2 coefficient equal to 0.47 ($P<0.0001$). Speciation calculations indicated that most (~ 99%) dissolved Si was present as $H_4SiO_4^\circ$, in agreement with measurements done by van Hees et al. (2000) in acidic soil solutions. Accordingly, the linear regression between $\log[Al^{3+}]+3pH$ and log(Si) gave an R^2 coefficient almost unchanged, equal to 0.40, indicating that about 40% of the variability in log(Si) may be controlled by the relatively fast and reversible formation (i.e. equilibrium-controlled) of a hypothetical Al–Si compound. The same calculations were made with data subsets for each soil depth interval and sampling date (Table 3). Significant linear relationships were obtained except for data from October 1999. Significant calculated values of the slope were scattered and indicated that a hypothetical compound with a Si/Al ratio ranging from about 0.5 to 2.34 may control from 79% of the variability in log(Si) at most (in October 2000) to 17% at least (at 30–45 cm depth).

The second step of the multiple linear regression analysis of the data using Eq. (2) in its full form was to test the influence of organic ligands on aqueous silica mobility. As discussed previously, a very simplified approach was adopted, based on a triprotic analogue representation of the acid–base properties of DOC.

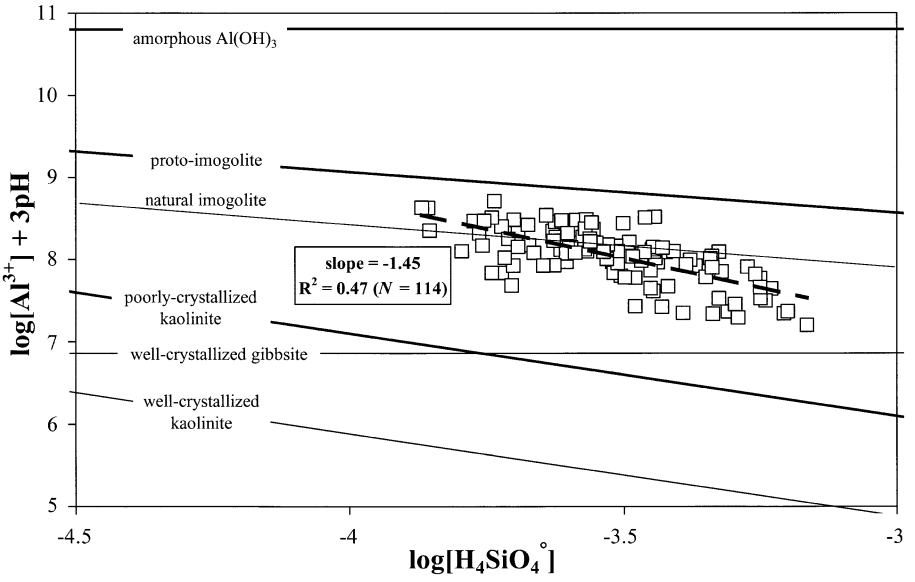

Fig. 5. Activity diagram for capillary solutions at the profile scale (T=25 °C) showing a significant linear relationship between the logarithm of the activity of orthosilicic acid, log[H_4SiO_4°], and the activity term for Al^{3+}(log[Al^{3+}]+3pH).

The outputs of the calculation were used to generate an organic ligand concentration as follows:

$$(L) = (H_2L^-) + 2(HL^{2-}) + 3(L^{3-}) \quad (7)$$

where the species L stands for the triprotic organic analogue, expressed in terms of molar concentration (mol l^{-1}), and (L) is the equivalent organic ligand concentration (mol l^{-1}).

Table 3
Absolute value of the slope (Si/Al), coefficient of determination (R^2), statistical significance (P) and number of data (N) for the linear relationships between log[Al^{3+}]+3pH and log[H_4SiO_4°] calculated with different subsets of data corresponding to the different soil depth intervals and sampling dates (values in parentheses are the standard error (S.E.) associated with the slope)

Data subsets	Si/Al	R^2	P	N	$R^{2a}_{tot.}$	$P^{b}_{tot.}$
0–15 cm	1.52 (0.24)	0.51	****	39	0.48	****
15–30 cm	1.18 (0.26)	0.36	****	39	0.23	**
30–45 cm	0.72 (0.21)	0.25	**	36	0.17	*
Oct. 1999	ns.	0.12	ns	19	0.05	ns
Nov. 1999	1.14 (0.29)	0.37	***	27	0.27	**
Feb. 2000	0.81 (0.32)	0.22	*	25	0.20	*
May 2000	1.70 (0.46)	0.40	**	23	0.38	**
Oct. 2000	2.09 (0.25)	0.80	****	20	0.79	****

****$P<0.0001$, ***$0.0001<P<0.001$, **$0.001<P<0.01$, *$0.01<P<0.05$, ns=$P>0.05$.

[a] Coefficient of determination of the linear relationships between log[Al^{3+}]+3pH and log(Si).

[b] Significance of the linear relationships between log[Al^{3+}]+3pH and log(Si).

Accounting for the organic ligand term confirmed the lack of influence of the temperature term. Organic ligands were found to have a significant effect on log(Si) at the profile scale. The corresponding partial R^2 coefficient was equal to 0.09 ($P<0.0001$) and the regression parameter (n_L) took a positive value equal to 0.16 (S.E.=0.03). The regression parameter of the pH term, n_{H^+}, was then equal to −0.50 (S.E.=0.05). The partial R^2 value for the relationship between log(Si) and pH was unaltered compared to the statistical analysis first made without taking into account the organic ligand term (see Section 3.2). The model R^2 coefficient (i.e. the sum of the partial R^2 value for pH and organic ligand terms) was equal to 0.52.

Making distinction between each soil depth interval, there was a lack of significant effect of organic ligands on log(Si) in capillary solutions from the surface layer (0–15 cm). However, a significant influence was found in the deeper soil depth intervals. At 15–30 cm depth, a partial coefficient of determination of about 0.19 (P=0.0015) was obtained for the organic ligand term, with n_L=0.23 (S.E.=0.07). The regression parameter n_{H^+} became equal to −0.52 (S.E.=0.10). At 30–45 cm depth, the influence of

organic ligands appeared to be weaker but was still significant ($P = 0.01$), with $n_L = 0.27$ (S.E. = 0.10) and a partial R^2 value of 0.12. The newly calculated value of n_{H^+} was -0.76 (S.E. = 0.16). Multiple linear regressions applied to data subsets corresponding to the different sampling dates regardless of soil depth did not show a significant influence of organic ligands.

4. Discussion and conclusions

4.1. Possibility of control by secondary phases

Several results showed a great deal of uncertainty whether there is a significant control of Si concentrations by the fast reversible formation of secondary phases, inferred from the establishment of linear relationships between $\log[Al^{3+}] + pH$ and log(Si) (see Section 3.3). In particular, Si/Al ratios of the hypothetical Si-controlling solids were generally inconsistent with these reported for allophane and ITM. ITM, which are well-defined allophane compounds, typically exhibit a Si/Al ratio of 0.5 (Wada, 1989; Su et al., 1995; Lumsdon and Farmer, 1995). According to Wada (1989), siliceous allophane-type compounds with a Si/Al ratio greater than one have not been isolated in soils. Consistent with this, soil mineralogy did not reveal the presence of such secondary phases, either by direct measurement (XRD, SEM and TEM observations) or by chemical extraction of short range ordered to amorphous products present in the soil material (see Section 2.1). Note that the role of Si–Al colloid species observed in acidic forest soil solutions and exhibiting a wide composition range (Xu and Harsh, 1993 and references cited therein) do not seem very persuasive to date, because of the uncertainty surrounding the possibility of these species being in or close to a thermodynamic equilibrium state with soil solutions. Dietzel (2000, 2001) measured the occurrence of relatively stable polysilicic acids released by dissolving silicates, which further combined with soluble Al to form Al–Si polymers of greater stability. This appeared to be inconsistent with their reversible formation in natural soil solutions.

We believe that significant relationships between $\log[Al^{3+}] + 3pH$ and either $\log[H_4SiO_4^\circ]$ or log(Si) stem from the concomitant effect of the control of Si by surface-controlled chemical weathering of silicates and two other processes widely recognized as controlling Al-mobility in forest soils, notably in the absence of allophane-type materials. The mixing up of these processes may explain why relationships drawn up over the activity diagram closely mapped linear relationships between log(Si) and pH (see Section 3.2). For example, the best fit was obtained with both relationships at the surface soil depth interval and became markedly weaker as soil depth increased.

It is widely recognised that the major Al-controlling processes in acidic soils are the reversible formation of hydroxy-Al compounds and the adsorption of soluble Al on soil organic matter (Bloom et al., 1979; Cronan et al., 1986; Dalghren and Walker, 1993; Berggren and Mulder, 1995; Simonsson and Berggren, 1998, Monterroso and Macías, 1998). The control of soluble Al by exchange reactions with soil organic matter convincingly explained linear relationships between $-\log[Al^{3+}]$ (i.e. pAl) and pH in solutions undersaturated with respect to the type of Al-hydroxide identified in the soil material. The relative importance of these two Al-controlling processes depends on both the pH and the organic matter content of the soil. In organic horizons, exchange reactions with soil humic substances may exert an influence at pH < 5.2 (Cronan et al., 1986). In mineral organic horizons, wherein organic matter content ranged from 1.9 to 0.68 wt.% (Rosenlund soils, in southernmost Sweden), Berggren and Mulder (1995) found a limit at about pH = 4.1.

Consistent results were found in this study regarding the presence of Al-hydroxides in the interlayer of soil vermiculites and the very low organic carbon content of this soil at the studied depth intervals (see Ezzaïm et al., 1999b). Solutions at the profile scale were supersaturated and under-saturated with respect to well-crystallized gibbsite and amorphous $Al(OH)_3$, respectively (Fig. 6). Throughout the measured pH range, most of the data were found to be close to equilibrium with respect to interlayered Al-hydroxides in vermiculites determined by Dalghren and Walker (1993). A highly significant linear relationship was found between pAl and pH over the entire pH range ($R^2 = 0.72$, $P < 0.0001$, $N = 114$), with a slope (ratio Al/OH) of 2.21 (S.E. = 0.13). Although significantly below the value of 2.7 reported by Dalghren and Walker (1993), this value was consistent with the Al/OH ratio determined for Al-hydroxides formed in vermiculite interlayers, which ranges from 2 to 2.8 (Barhisel and

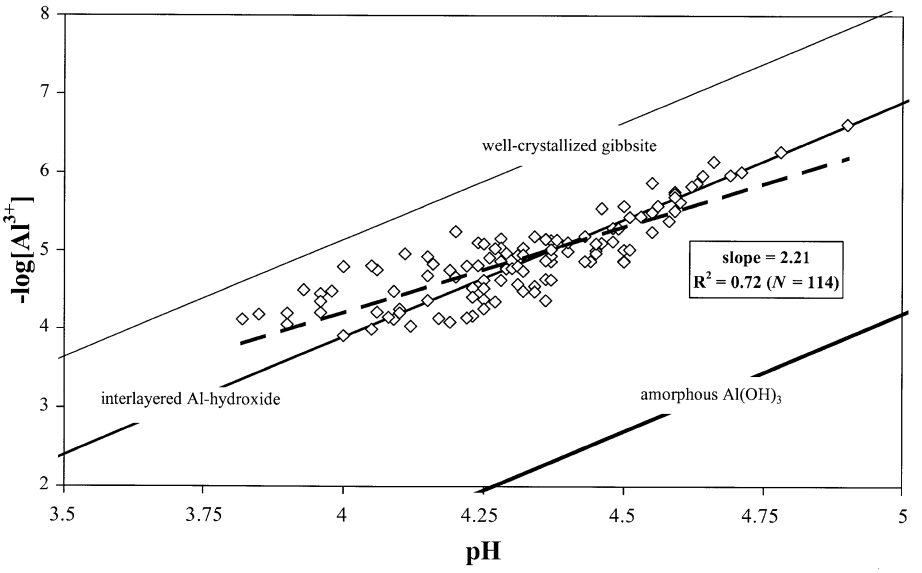

Fig. 6. Activity diagram for capillary solutions at the profile scale ($T = 25$ °C) showing a significant linear relationship between the negative of the logarithm of the activity of Al^{3+}, $-\log[Al^{3+}]$, and the pH.

Bertsch, 1989; Monterroso and Macías, 1998). Using only data at pH>4.1 would give better results regarding the control of Al mobility by Al-hydroxides (Berggren and Mulder, 1995). By doing so, the coefficient of determination slightly increases to 0.73 ($P < 0.0001$) and the slope increases (Al/OH = 2.70 ± 0.17) to the value determined by Dalghren and Walker (1993). Note that the consistency of our results with those in the literature also support the relatively good validity of our thermodynamic database for acidic forest soils.

4.2. Surface-controlled and dominating proton-promoted chemical weathering

If the previous arguments for the absence of significant Si-controlling phases are correct, significant relationships between log(Si) and pH may therefore be indicative of active surface-controlled chemical weathering of soil silicates. Geochemical modelling indicated that soil capillary solutions are far-from-equilibrium with respect to primary silicates, which is a prerequisite for the establishment of linear relationships between log(Si) and pH involved in the chemical weathering of primary silicates. Furthermore, our results also suggest that chemical weathering in this soil is weakly enhanced by organic ligands and is promoted by H^+. If this were not the case, it is uncertain whether significant relationships between Si and H^+ (see Section 3.1) and log(Si) and pH (see Section 3.2) could be obtained while disregarding the influence of organic ligands on chemical weathering. Consistent with this, multiple linear regression analysis with a term representing organic ligands (by means of an analogue organic ligand, L) gave partial R^2 coefficients that were either too low to ensure significant results or much lower than the pH term (see Section 3.3). In addition, it was calculated that the analogue organic ligand only had a significant affect on the variability in log(Si) below the surface soil layer. Additional ANOVA focusing on the variations in H^+ concentration as a function of soil depth indicated that capillary solutions collected at 15–30 and 30–45 cm depth were less acidic than in the surface soil layer (mean pH ~ 4.14 compared to ~ 4.32 units beneath). This result supports the validity of the triprotic analogue model for studying the relative contribution of low molecular weight organic acids vs. protons in the mechanisms of silicate weathering in acidic forest soils (see Section 1). It is interesting to outline the divergence between the apparent influences of the analogue ligand on Si concentration, calculated with Eq. (2), and that of DOC unravelled by a factor

analysis and ANOVA. Possibly DOC may be a better proxy for the effect on silicate dissolution of larger organic molecules, such as fulvic acids, which usually constitute the major fraction of DOC (van Hees et al., 2001 and references therein) and have been recognized in the laboratory for their greater accelerating effect as pH decreases (see Section 1).

4.3. Assessing the active weathering sequence

As our results indicated that Si mobility in capillary solutions may be controlled by surface-controlled and mostly proton-promoted weathering, the calculated n_{H^+} value corresponded to the order of the overall weathering rate of soil primary silicates with respect to pH. In the laboratory, the pH dependency of silicate weathering is studied by utilizing dissolution rates normalized to a surface area, S, as it can be measured unlike in natural systems. Nevertheless, an analogy between values of n_{H^+} measured in the laboratory and those calculated here from field samples seemed to be reasonably valid. Actually, one must assume that variations in S in this soil did not show a systematic trend with the solution pH. Variations in S are most likely contributing to data dispersion.

Both albite and K-feldspar typically exhibit pH dependency of about -0.5 in the acidic region (see review by Blum and Stillings, 1995). The pH dependency for the white mica present in our soil has not been studied in the laboratory. Therefore, we compare with muscovite as a proxy. Muscovite typically exhibits much lower pH dependency than alkali-feldspars. Kalinowski and Schweda (1996) obtained $n_{H^+} = -0.14$ to -0.20 at $T = 25$ °C. Nagy (1995) reported n_{H^+} values for muscovite that range from -0.10 to -0.08 under similar temperature conditions and pH. We have seen previously that biotite was extensively transformed to secondary products and was almost absent in the soil material. Therefore, this sheet silicate was excluded from the list of potential Si-controlling primary silicates. Comparisons between calculated n_{H^+} values, including error bars spanning a symmetric confidence interval of 95% (Webster, 2001), and those measured in the laboratory under similar conditions suggest that alkali-feldspars weathered significantly faster than white mica (Fig. 7). Values of n_{H^+} corresponding to the different groups of data were markedly outside the range of laboratory values for muscovite and overlapped the laboratory value for alkali-feldspars, whether the weak simulated influence

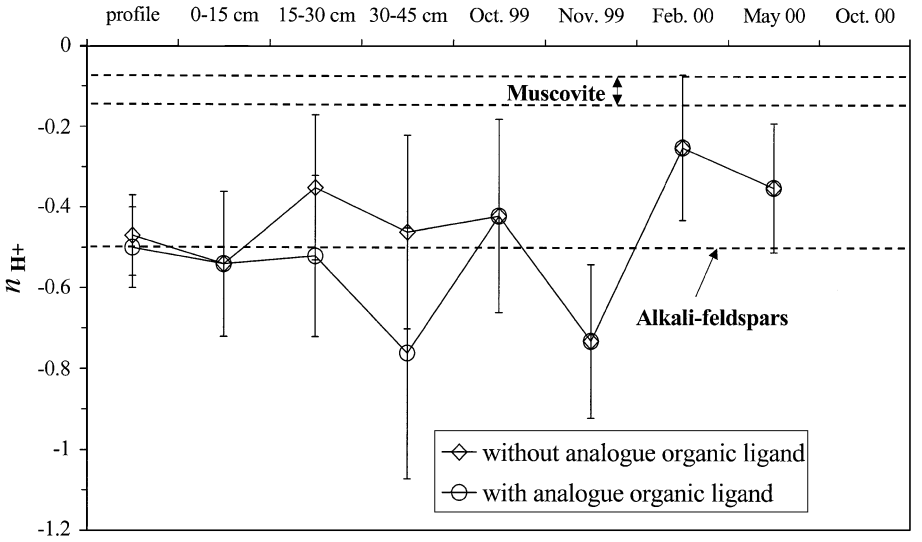

Fig. 7. Values of the linear regression parameter n_{H^+} (i.e. the slope of relationships between log(Si) and pH) calculated with different sets of data either considering the influence of organic ligands (open circles) or not (open diamonds). Error bars span a symmetric confidence interval of 95% of the mean value. Thick dashed lines represent the n_{H^+} values measured in the laboratory for primary minerals.

of organic ligands was taken into account or not. More variable results were obtained by distinguishing each collecting date (see Fig. 7), certainly due to the smaller number of samples involving a larger hindering influence of uncontrolled variables and processes. For example, error bars in February 2000 suggest that the control of Si concentration by white mica is possible, and the range of n_{H^+} corresponding to November 1999 was inconsistent with both alkali-feldspar and white mica weathering. But, at the profile scale, where the larger number of samples furnished a better statistical definition of the relationship between log(Si) and pH (i.e. smaller SE and confidence interval), the calculated n_{H^+} value was clearly consistent with alkali-feldspar dissolution in the laboratory.

This approach clearly suggest that the historical weathering sequence may still prevail, as it was found that albite should have been weathered much more intensively than muscovite (see Section 2.1). However, Ezzaïm et al. (1999b) found that the relative abundance of albite has decreased by about 77% in the soil material compared to the unweathered tuff, whereas that of K-feldspar has increased by 63%. Such an intensive reaction over the long term has certainly led to a greater decrease in the reactive surface (S) for albite than for K-feldspar and perhaps a proportional change in relative weathering rates. The possibility of a higher weathering rate for K-feldspar compared to albite seems reasonable, as the dissolution rate constants in the acidic region (k_{H^+}) are similar (see review in Blum and Stillings, 1995). Estimating the reactive surface area of weathered silicates in the soil material can confirm such an important finding. Besides, attempts to establish significant linear relationships between Si concentration and potassium concentration, for K-feldspar, and sodium concentration for albite, proved to be unsuccessful. This indicated that processes other than weathering controlled alkaline element concentration, perhaps ion exchanges and solute uptake by roots or litter degradation.

The empirical equation for mineral reactive surfaces included in the PROFILE computer programme (Sverdrup and Warfvinge, 1995) may be used for this purpose. This function gives the total reactive surface of a soil per unit of bulk soil volume ($S_{tot.}$ in $m^2\ m^{-3}$). Input parameters are the main size fractions of the soil material, soil density and density of the solid phase. Using data from Ezzaïm et al. (1999b) for size fractions with a soil density of 0.8 g cm^{-3} and a solid phase density of 2.7 g cm^{-3}, we obtained $S_{tot.} \sim 0.75\ m^2\ m^{-3}$, regardless of the soil depth interval, from which we calculated $S \sim 60\ cm^2\ m^{-3}$ for albite compared with up to 420 $cm^2\ m^{-3}$ for K-feldspar.

4.4. On the absence of a temperature effect on Si concentration

The time elapsed at $T = 20$ °C, from the moment at which samples were collected in the field to when solutions were extracted in the laboratory, may be long enough to allow a fast reaction to equilibrate with the new temperature conditions. Accordingly, the unrecognised occurrence of a fast reacting Si-containing product may explain the temperature independency of Si concentration. However, we have shown that a predominant effect of this process over a control by silicate dissolution was very uncertain, based on geochemical modelling, mineralogical observations, and finally reinforced by statistical analysis of the data compared to silicate dissolution experiments as a function of pH. Alternatively, and perhaps more likely, the absence of a significant relationship between Si concentration and T may reflect the limited data available and the small temperature range. In addition, this lack may also stem from the use of T values of a mixed origin, from either direct measurement in soil samples using a portable temperature probe or from in situ temperature probes located thorough the field site.

Acknowledgements

This research was funded by the Lorraine regional authorities (France). The authors thank our technical staff (especially S. Bienaimée, L. Gelhaye, B. Pollier), who performed the chemical analysis of soil solutions, A.-M. Wall (UCD, Translation Service, INRA Jouy-en-Josas, France) for revising the English and Dr. P. Montpied for his help in statistics. The authors also thank Drs. S. P. Anderson, A. E. Blum, J. Chorover

and an anonymous reviewer for their constructive comments and criticisms. **[EO]**

References

AFES, 1992. Principaux sols d'Europe. Référentiel pédologique. INRA (Ed.), Paris.

Anbeek, C., 1993. The effect of natural weathering on dissolution rates. Geochim. Cosmochim. Acta 57, 4963–4975.

Anbeek, C., van Breemen, N., Meijer, E.L., van der Plas, L., 1994. The dissolution of naturally weathered feldspar and quartz. Geochim. Cosmochim. Acta 58, 4601–4613.

Augusto, L., Turpault, M.-P., Ranger, J., 2000. Impact of forest tree species on feldspar weathering rates. Geoderma 96, 215–237.

Barhisel, R.I, Bertsch, P.M., 1989. Chlorites and hydroxy-interlayered vermiculites and smectites. In: Dixon, J.B., Weed, S.B. (Eds.), Mineral in Soil Environments. SSSA, Madison, WI, pp. 729–788.

Bennett, P.C., Casey, W., 1994. Chemistry and mechanisms of low-temperature dissolution of silicates by organic acids. In: Pittman, E.D., Lewan, M.D. (Eds.), Organic Acids in Geological Processes. Springer-Verlag, Berlin, Germany, pp. 162–200.

Bergelin, A., van Hees, P.A.W., Wahlberg, O., Lumdström, U.S., 2000. The acid–base properties of high and low molecular weight organic acids in soil solutions of podzolic soils. Geoderma 94, 223–235.

Berggren, D., Mulder, J., 1995. The role of organic matter in controlling aluminium solubility in acidic mineral soil horizons. Geochim. Cosmochim. Acta 59, 4167–4180.

Bloom, P.R., McBride, M.B., Weaver, R.M., 1979. Aluminum organic matter in acid soils: buffering and solution aluminum activity. Soil Sci. Soc. Am. J. 48, 488–493.

Blum, A.E., Stillings, L.L., 1995. Feldspar dissolution kinetics. In: White, A.F., Brantley, S.L. (Eds.), Chemical Weathering Rates of Silicate Minerals. Reviews in Mineralogy, vol. 31. MSA, Washington, DC, pp. 291–351.

Boudot, J.-P., Merlet, D., Rouiller, J., Maitat, O., 1994. Validation of an experimental procedure for aluminium speciation in soil solutions and surface waters. Sci. Total Environ. 158, 237–252.

Boudot, J.P., Maitat, O., Merlet, D., Rouiller, J., 2000. Soil solutions and surface water analysis in two contrasted watersheds impacted by acid deposition, Vosges mountains, N.E. France: interpretation in terms of Al impact and nutrient imbalance. Chemosphere 41, 1419–1429.

Brantley, S.L., 1998. Surface area and porosity of primary silicate minerals. Mineral. Mag. 62A, 229–230.

Brantley, S.L., Blai, A.C., Cremeen, D.L., MacInnis, I., Darmody, R.G., 1993. Natural etching rates of feldspar and hornblende. Aquat. Sci. 55, 262–272.

Cronan, C.S., Walker, W.J., Bloom, P.R., 1986. Predicting aqueous aluminium concentrations in natural waters. Nature 324, 140–143.

Dalghren, R.A., Walker, W.J., 1993. Aluminum release rates from selected Spodosol Bs horizons: effect of pH and solid-phase aluminum pools. Geochim. Cosmochim. Acta 57, 57–66.

Dietzel, M., 2000. Dissolution of silicates and the stability of polysilicic acid. Geochim. Cosmochim. Acta 19, 3275–3281.

Dietzel, M., 2001. Formation and stability of polymeric Al–Si complexes. Proc. 11th Goldschmidt Conference. Lunar and Planetary Inst., Houston.

Drever, J.I., Stillings, L.L., 1997. The role of organic acids in mineral weathering. Colloids and Surface: A. Physicochemical and Engineering Aspects 120, 167–181.

Drever, J.I., Vance, G.F., 1994. Role of soil organic acids in mineral weathering processes. In: Pittman, E.D., Lewan, M.D. (Eds.), Organic Acids in Geological Processes. Springer-Verlag, Berlin, Germany, pp. 138–161.

Drever, J.I., Zobrist, J., 1992. Chemical weathering of silicate rocks as a function of elevation in the southern Swiss Alps. Geochim. Cosmochim. Acta 56, 3209–3216.

Driscoll, C.T., Lehtinen, M.D., Sullivan, T.J., 1994. Modeling of acid–base chemistry of organic solutes in Adirondack, New-York lakes. Water Resour. Res. 30, 297–306.

Ezzaïm, A., Turpault, M.-P., Ranger, J., 1997. Répartition des nutriments dans un sol brun acide développé sur tuf (Beaujolais, France). Conséquences pour l'évolution de la fertilité minérale à long terme. Ann. Sci. For. 54, 371–387.

Ezzaïm, A., Turpault, M.-P., Ranger, J., 1999a. Quantification of weathering processes in an acid brown soil developed from tuff (Beaujolais, France): Part I. Formation of weathered rind. Geoderma 87, 137–154.

Ezzaïm, A., Turpault, M.-P., Ranger, J., 1999b. Quantification of weathering processes in an acid brown soil developed from tuff (Beaujolais, France): Part II. Soil formation. Geoderma 87, 155–177.

Frogner, P., Schweda, P., 1998. Hornblende dissolution kinetics at 25 °C. Chem. Geol. 151, 169–179.

Gérard, F., Boudot, J.-P., Ranger, J., 2001. Consideration on the occurrence of the Al_{13} polycation in natural soil solutions and surface waters. Appl. Geochem. 16, 513–529.

Gérard, F., Franҫois, M., Ranger, J., 2002. Processes controlling silica concentration in leaching and capillary soil solutions of an acidic brown forest soil (Rhône, France). Geoderma 107, 197–226.

Giesler, R., Lundström, U.S., 1993. Soil solution chemistry: effects of bulking soil samples. Soil Sci. Soc. Am. J. 57, 1283–1288.

Giesler, R., Lundström, U.S., Grip, H., 1996. Comparison of soil solution chemistry assessment using zero-tension lysimeters or centrifugation. Eur. J. Soil Sci. 47, 395–405.

Havenkamp, R., Zammit, C., Bouraoui, F., 1998. Grizzly soil data base, http://www.lthe.hmg.inpg.fr/Grizzly/.

Hellmann, R., 1994. The albite–water system: Part I. The kinetics of dissolution as a function of pH at 100, 200, and 300 °C. Geochim. Cosmochim. Acta 58, 595–611.

Hochella, M.F., Banfield, J.F., 1995. Chemical weathering of silicates in nature: a microscopic perspectives with theoretical considerations. In: White, A.F., Brantley, S.L. (Eds.), Chemical Weathering Rates of Silicate Minerals. Reviews in Mineralogy, vol. 31. MSA, Washington, DC, pp. 352–406.

Hodson, M.E., 1999. Micropore surface area variation with grain size in unweathered alkali feldspars: implications for surface roughness and dissolution studies. Geochim. Cosmochim. Acta 62, 3429–3435.

Kalinowski, B.G., Schweda, P., 1996. Kinetics of muscovite, phlogopite and biotite dissolution and alteration at pH 1–4, room temperature. Geochim. Cosmochim. Acta 60, 367–385.

Lasaga, A.C., 1995. Fundamental approaches in describing mineral dissolution and precipitation rates. In: White, A.F., Brantley, S.L. (Eds.), Chemical Weathering Rates of Silicate Minerals. Reviews in Mineralogy, vol. 31. MSA, Washington, DC, pp. 173–233.

Lundström, U., Öhman, L.O., 1990. Dissolution of feldspars in the presence of natural solutes. J. Soil Sci. 41, 359–369.

Lumsdon, D.G., Farmer, V.C., 1995. Solubility characteristics of proto-imogolite sols: how silicic acid can de-toxify aluminum solutions. Eur. J. Soil Sci. 46, 179–186.

Maitat, O., Boudot, J.-P., Merlet, D., Rouiller, J., 2000. Aluminium chemistry in two contrasted acid forest soils and headwater streams impacted by acid deposition, Vosges mountains, N.E. France. Water Air Soil Pollut. 117, 217–243.

Marques, R., Ranger, J., 1997. Nutrient dynamics in a chronosequence of Douglas-fir (*Pseudotsuga menziesii* (Mirb.) Franco) stands on the Beaujolais Mounts (France): 1. Qualitative approach. For. Ecol. Manag. 91, 255–277.

Marques, R., Ranger, J., Gelhaye, D., Pollier, B., Ponette, Q., Gobert, O., 1996. Comparison of chemical composition of soil solutions collected by zero-tension plate lysimeters with those from ceramic cup lysimeters in a forest soil. Eur. J. Soil Sci. 47, 407–417.

Meybeck, M., 1986. Composition chimique des ruisseaux non pollués de France. Sci. Géol. Bull. 39, 3–77.

Monterroso, C., Macías, F., 1998. Evaluation of the test-mineral method for studying minesoil geochemistry. Soil Sci. Soc. Am. J. 62, 1741–1748.

Nagy, K.L., 1995. Dissolution and precipitation kinetics of sheet silicates. In: White, A.F., Brantley, S.L. (Eds.), Chemical Weathering Rates of Silicate Minerals. Reviews in Mineralogy, vol. 31. MSA, Washington, DC, pp. 173–233.

Nugent, M.A., Brantley, S.L., Pantano, C.G., Maurice, P.A., 1998. The influence of natural mineral coatings on feldspar weathering. Nature 395, 588–591.

Ochs, M., 1996. Influence of humified and non-humified natural organic compounds on mineral dissolution. Chem. Geol. 132, 119–124.

Paces, T., 1983. Rate constants of dissolution derived from the measurement of mass balance in hydrologic catchments. Geochim. Cosmochim. Acta 47, 1855–1863.

Parkhurst, D.L., Appelo, C.A.J., 1999. User's guide to PHREEQC (Version 2). U.S. Geol. Surv., Water Resour. Inv. Rep. 95-4227.

Ranger, J., Marques, R., Colin-Belgrand, M., Flammang, N., 1995. The dynamics of biomass and nutrient accumulation in a Douglas-fir (*Pseudotsuga menziesii* Franco) stand studied using a chronosequence approach. For. Ecol. Manag. 72, 167–183.

Ranger, J., Marques, R., Jussy, J.-H., 2001. Forest dynamics during stand development assessed by lysimeter and centrifuge solutions. For. Ecol. Manag. 144, 129–145.

Raulund-Rasmussen, K., Borgaard, O.K., Hansen, H.C.B., Olsson, M., 1998. Effect of natural organic soil solutes on weathering rates of soil minerals. Eur. J. Soil Sci. 49, 397–406.

Schecher, W.D., Driscoll, C.T., 1995. ALCHEMI: a chemical equilibrium model to assess the acid–base chemistry and speciation of aluminum in dilute solutions. In: Leoppart, R.H., Schwab, A.P., Goldberg, S. (Eds.), Chemical Equilibrium and Reaction Models. SSSA Special Publication, vol. 42, pp. 325–356.

Simonsson, M., Berggren, D., 1998. Aluminium solubility related to secondary phases in upper B horizons with spodic characteristics. Eur. J. Soil Sci. 49, 317–326.

Steefel, C.I., van Cappellen, P., Nagy, K.L., Lasaga, A.C., 1990. Modeling water–rock interactions in the surficial environment: the role of precursors, nucleation, and Ostwald ripening. Chem. Geol. 84, 322–325.

Stillings, L.L., Drever, J.I., Brantley, S.L., Sun, Y., Oxburgh, R., 1996. Rates of feldspar dissolution at pH 3–7 with 0–8 mM oxalic acid. Chem. Geol. 132, 79–89.

Su, C., Harsh, J.B., Boyle, J.S., 1995. Solubility of hydroxy-aluminum interlayers and imogolite in a spodosol. Soil Sci. Soc. Am. J. 59, 373–379.

Sverdrup, H., Warfvinge, P., 1995. Estimating field weathering rates using laboratory kinetics. In: White, A.F., Brantley, S.L. (Eds.), Chemical Weathering Rates of Silicate Minerals. Reviews in Mineralogy, vol. 31. MSA, Washington, DC, pp. 485–541.

Swoboda-Colberg, N., Drever, J., 1993. Mineral dissolution rates in plot-scale field and laboratory experiments. Chem. Geol. 105, 51–69.

Tardy, Y., Fritz, B., 1981. An ideal solid solution model for calculating solubility of clay minerals. Clay Miner. 16, 361–373.

USDA, 1998. Keys for Soil Taxonomy, 8th ed. Soil Conservation Service, Pocahontas Press, Blacksburg, Virginia, USA.

van Hees, P.A.W., Lundström, U.S., Giesler, R., 2000. Low molecular weight organic acids and their Al-complexes in soil solution-composition, distribution and seasonal variation in three podzolized soils. Geoderma 94, 173–200.

van Hees, P.A.W., Tipping, E., Lundström, U.S., 2001. Aluminium speciation in forest soil solution—modelling the contribution of low molecular weight organic acids. Sci. Total Environ. 278, 215–229.

Wada, K., 1989. Allophane and imogolite. In: Dixon, J.B., Weed, S.B. (Eds.), Mineral in Soil Environments. SSSA, Madison, WI, pp. 1051–1087.

Webster, R., 2001. Statistics to support soil research and their presentation. Eur. J. Soil Sci. 52, 331–340.

Welch, S.A., Ullman, W.J., 1993. The effect of organic acids on plagioclase dissolution rates and stoechiometry. Geochim. Cosmochim. Acta 57, 2725–2736.

Welch, S.A., Ullman, W.J., 1996. Feldspar dissolution in acidic and organic solutions: compositional and pH dependence of dissolution rate. Geochim. Cosmochim. Acta 60, 2939–2948.

White, A.F., 1995. Chemical weathering rates of silicate minerals in soils. In: White, A.F., Brantley, S.L. (Eds.), Chemical Weathering Rates of Silicate Minerals. Reviews in Mineralogy, vol. 31. MSA, Washington, DC, pp. 407–459.

White, A.F., Blum, A.E., 1995. Effects of climate on chemical weathering in watersheds. Geochim. Cosmochim. Acta 59, 1729–1747.

White, A.F., Blum, A.E., Schulz, M., Bullen, T.D., Harden, J.W., Peterson, M.L., 1996. Chemical weathering rates of a soil chronosequence on granitic alluvium: I. Quantification of mineralog-

ical and surface area changes and calculation of primary silicate reaction rates. Geochim. Cosmochim. Acta 60, 2533–2550.

White, A.F., Blum, A.E., Bullen, T.D., Vivit, D.V., Schulz, M., Fitzpatrick, J., 1999. The effect of temperature on experimental and natural chemical weathering rates of granitoid rocks. Geochim. Cosmochim. Acta 63, 3277–3291.

White, A.F., Bullen, T.D., Schulz, M., Blum, A.E., Huntington, T.G., Peters, N.E., 2001. Differential rates of feldspar weathering in granitic regoliths. Geochim. Cosmochim. Acta 65, 847–869.

Xu, S., Harsh, J.B., 1993. Labile and nonlabile aqueous silica in acid solutions, relation to the colloidal fraction. Soil Sci. Soc. Am. J. 57, 1271–1277.

Zabowski, D., Ugolini, F.C., 1990. Lysimeter and centrifuge soil solutions: Seasonal differences between methods. Soil Sci. Soc. Am. J. 54, 1130–1135.

Zhang, H., Bloom, P.R., 1999. Dissolution kinetics of hornblende in organic acid solutions. Soil Sci. Soc. Am. J. 63, 815–822.

Zysset, M., Blaser, P., Luster, J., Gehring, A.U., 1999. Aluminum solubility control in different horizons of a podzol. Soil Sci. Soc. Am. J. 63, 1106–1115.

Transferts hydriques : pédotransfert et écoulements préférentiels

Gérard F., Tinsley M., et Mayer K. U. (2004) Preferential flow revealed by hydrologic modeling based on predicted hydraulic properties. *Soil Science Society of America Journal* **68**, 1526-1538. + Errata **70**, 305.

Preferential Flow Revealed by Hydrologic Modeling Based on Predicted Hydraulic Properties

Frédéric Gérard,* Mark Tinsley, and K. Ulrich Mayer

ABSTRACT

Pedotransfer functions have shown a reasonable reliability and accuracy for predicting soil hydraulic properties. However, the contribution of the range of macroscopic features leading to preferential water flow is not readily taken into account. We modified and used the hydrological component of the reactive transport model MIN3P and the neural network-based code ROSETTA in an attempt to simulate 4 yr of daily measurements of the soil water content in a forest soil covered by Douglas-fir (*Pseudotsuga menziessii* Franco). A good fit of the mean measured water contents was obtained during periods of low soil moisture, while the model tended to overpredict water contents during periods of high soil moisture. This behavior is typical for the presence of significant preferential flow. Slightly better results were obtained by using predicted values of the saturated hydraulic conductivity, while the assumption of a water table located at shallow depth increased discrepancies. A good match was obtained by calibration of a simple preferential flow scheme, which was based on the assumption that the retention properties of the porous network control preferential flow. Accordingly, preferential flow seemed to initiate within the capillary pore domain. This causes a much greater sensitivity of the results to the position of the water table than with other schemes that consider pure gravity-driven flow in large macropores. Knowledge of the functional pore size is needed to ascertain the type of preferential flow scheme to be used.

Knowledge of soil hydraulic properties is crucial for the modeling of flow in unsaturated soils. The accurate estimation of the water flux is of importance for environmental issues such as metal mobility and nutrient cycling. Two of the key properties of an unsaturated soil are the soil water retention curve (WRC) and the hydraulic conductivity (HC). Measurements of the soil HC and/or WRC are costly, time-consuming, and sometimes unreliable because of soil heterogeneity and experimental errors. Methods have been developed to estimate soil hydraulic properties from more easily measured soil properties. These methods involve the use of pedotransfer functions (PTFs). A number of PTFs can be found in the literature and can be classified according to the nature of the basic input soil properties and the method adopted to generate predictions (Wösten et al., 2001). Recent publications focus on comparing PTF predictions with independent data sets of hydraulic properties measured in the laboratory. Results of the comparisons vary; good agreement was found in several studies (Schaap and Leij, 2000; Cornelius et al., 2001; Rawls et al., 2001; Wagner et al., 2001) whereas significant discrepancies were observed by others (Chen and Payne, 2001; Pachepsky and Rawls, 2003; Soet and Stricker, 2003). The evaluation of the PTFs performance in various field situations has also been addressed in several publications (e.g., see review by Wösten et al., 2001). A set of on-site measured pressure heads and/or volumetric moisture contents at different soil depths are generally considered as functional variables (FV) to evaluate the predictive performance of the PTFs (e.g., Espino et al., 1996; Hack-ten Broeke and Hegmans, 1996; van Alphen et al., 2001; Nemes et al., 2003). Actual hydraulic properties were measured and served to preevaluate the predictive accuracy of PTFs (Nemes et al., 2003; Soet and Stricker, 2003) and, more frequently, to run numerical simulations in addition to those parameterized with PTF predictions (Wösten et al., 1990; Hack-ten Broeke and Hegmans, 1996; van Alphen et al., 2001). The accuracy of the predictions can vary appreciably according to the PTF used and the number of input data considered (e.g., van Alphen et al., 2001; Wösten et al., 2001; Nemes et al., 2003). Overall, however, the performance of PTFs for prediction can be described as reasonably good given the inherent complexity of the hydraulic behavior of soils at the field scale.

We would like to emphasize two general limitations in the past studies targeting the functional evaluation of PTFs. First, the widespread occurrence of preferential flow in soils has never been considered. Furthermore, functional evaluation has not been performed in a forest soil and there is ample evidence for fast preferential flow of water and solutes in such soils (e.g., Feyen et al. [1999] and references therein). A number of macroscopic features cause preferential flow to occur in soils in general, and in forest soils in particular. These include cracks produced by shrinkage of clay soils and biotic pores formed by the decay of dead plant roots and fauna (e.g., Larsson et al. [1999] and references therein). Second, in previous functional evaluation studies, the number of FV data points used was rather small compared with the duration of the simulated time series (typically 1–2 yr). Therefore, knowing that the accurate prediction of high water contents is difficult due to the presence of preferential flow channels (e.g., Simunek et al., 2003), we believe that the relative lack of FV data corresponding to these periods could preclude the detection of preferential flow while testing the performance of PTFs at the field scale. Furthermore, provis-

F. Gérard and M. Tinsley, INRA, Centre de Nancy, Unité Biogéochimie des Ecosystèmes Forestiers, Forêt d'Amance, 54280 Champenoux, France; K.U. Mayer, Univ. of British Colombia, Dep. of Earth and Ocean Sciences, 6339 Stores Road, V6T 1Z4 Vancouver, BC, Canada; M. Tinsley, present address: Chemistry School, Clark Hall, West Virginia Univ., Morgantown, WV 26506. Received 20 Aug. 2003. *Corresponding author (gerard@nancy.inra.fr).

Published in Soil Sci. Soc. Am. J. 68:1526–1538 (2004).

677 S. Segoe Rd., Madison, WI 53711 USA

Abbreviations: FV, functional variable; HC, hydraulic conductivity; MRE, mean residual error; PTF, pedotransfer function; REW, reserve of extractable water; RMSE, root mean square error; TDR, time-domain reflectometry; WRC, water retention curve.

ions are generally taken to avoid macroscopic heterogeneities in soil samples studied in the laboratory. In other words, samples often better reflect the hydraulic properties of the soil matrix rather than field-scale values that include a range of structural features potentially causing preferential flow to occur. This fundamental bias, often referred to as scaling effect, is well recognized in studies involving the use of PTFs at various spatial scales (e.g., Inskeep et al., 1996; Chen and Payne, 2001; Wagner et al., 2001). Researchers are attempting to overcome this issue (Lin et al., 1999; Jarvis et al., 2002; Pachepsky and Rawls, 2003). The PTFs proposed by Lin et al. (1999) gave reasonable predictions of some of the hydraulic properties controlling preferential flow, especially the HC at water saturation, but these PTFs also require a rather large number of predictors. Moreover, some of these, such as the macropore porosity, can be difficult to measure in the field. Jarvis et al. (2002) tentatively established a PTF for the prediction of the near-saturated soil HC involving a fewer number of predictors, but they obtained a poor match with measurements.

Concerns regarding forest decline and sustainable land management have motivated research on ecosystems evolution since the 1970s. Nowadays networks of forested sites are subjected to various degrees of monitoring of soil physical and chemical properties and many other ecological variables. One of these, the Vauxrenard field site (Rhône, France), was managed by INRA, FMN department (Institut National de la Recherche Agronomique, Forêts et Milieux Naturels), from April 1992 to January 2000. Among other instruments progressively implemented on-site, replicated time-domain reflectometry (TDR) probes have provided 4-yr records of hourly measurements of the soil volumetric water content at different soil depths. Clearly, this survey has led to an extraordinary database of FV data, which is thus particularly well suitable to a functional evaluation of PTFs in a forest soil with a special focus on preferential flow. The objectives of the present paper are twofold: (i) to perform a functional evaluation of a selected PTF for a forest soil; (ii) to study whether significant preferential flow is occurring in this forested soil, and to determine the prediction errors made in terms of soil moisture when preferential flow is ignored.

MATERIALS AND METHODS

Study Field Site

The field site was situated on a gentle slope (<10°) nearby the summit of a small mountain (Montagne des Aiguillettes, Rhône, France) within the Beaujolais Hills. Site elevation is about 60 m at the foot of the hill and reaching an 842-m altitude at the top. A mean annual temperature of 7°C and a mean annual precipitation of roughly 1000 mm characterize the climate. The soil is of brown acidic type, classified as Typic Dystrochrept according to USDA (Soil Survey Staff, 1994), or as an Alocrisol (AFES, 1992). A 40-yr old douglas-fir forest covers the field site. The parent material from which the soil is derived consists of a volcanic tuff dating from the upper Visean. Regional metamorphism has led to its intensive recrystallization (Ezzaïm et al., 1999). Many other aspects of the site have been discussed in several studies, such as stand characteristics, nutrient dynamics, and silicate weathering mechanisms (e.g., Ranger et al., 1995; Marques and Ranger, 1997; Ranger et al., 2001; Gérard et al., 2003). Soil texture is loamy, organic matter is rather high (6–7% down to 20 cm), and most roots are located in the top 50 cm but some have been observed down to a depth of 100 cm (Ranger et al., 2001). Root diameter distribution according to soil depth is given in Table 1. Four soil horizons can be distinguished in a representative soil profile: the A11 (0- to 12-cm depth), the A12 (12- to 35-cm depth), the B (35- to 55-cm depth), and the C (55- to 120-cm depth).

Functional Variable Dataset and Evaluation Criteria

Soil water content were measured hourly at three soil depths (15, 30, and 60 cm) during 4 yr by means of TDR probes (Trase System, Soil Moisture Equipment Core, Goleta, CA). Six replicates per depth were installed to evaluate the influence of spatial heterogeneity. Data is available from January 1996 to December 1999, with some time gaps caused by the temporary breakdown of the monitoring system. Time domain reflectometry probes were internally calibrated and tested in free water and in dry sand for the maximum and minimum moisture values before installation. Onsite control tests have also been completed in June 1999 (Fig. 1). Control values of the soil water content were measured nearby (approximately 0.5 m) in soil samples (gravimetric measurements) and in situ by means of a portable TDR probe (Delta-T Devices, Theta Probe, Thermo Electron Corp., Waltham, MA) installed in holes excavated with an Edelman auger. The auger diameter was marginally smaller than the probe to ensure good contact between the probe and the soil material. A statistical test (ANOVA, Unistat 5.0 software, Unistat Ltd., England) showed a lack of significance differences in the measured soil water contents.

Two statistical criteria were used for model evaluation purposes. The first is the root mean square error (RMSE):

$$\mathrm{RMSE} = \left[\frac{\sum_{i=1}^{n}(P_i - O_i)^2}{N}\right]^{\frac{1}{2}} \quad [1]$$

Table 1. Root diameter distribution, expressed in number of roots per square meter and per soil depth interval (from Vilette, 1994).

Depth interval	Root count per diameter class				
	$\phi < 0.03$	$0.03 < \phi < 0.05$	$0.05 < \phi < 0.10$	$0.10 < \phi < 0.20$	$0.20 < \phi$
	m				
0.1–0.2	1078	31	0	9	12
0.2–0.3	919	34	19	6	19
0.3–0.4	762	19	9	22	6
0.4–0.5	693	38	10	4	0
0.5–0.6	562	12	3	3	0
0.6–0.7	584	3	9	0	0
0.7–0.8	379	6	0	0	0
0.8–0.9	125	0	0	0	0
0.9–1.0	144	4	4	0	0

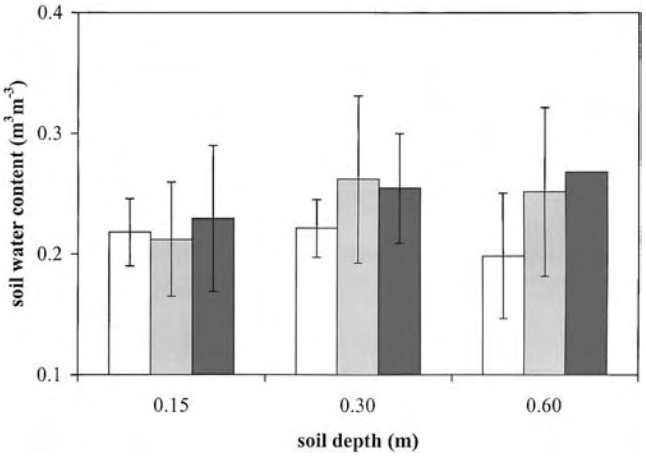

Fig. 1. Comparison of on-site control measurements of the soil water content at different soil depths. Error bars correspond to the standard deviation. White bars: mean value measured with the trase-system Soil Moisure time domain reflectometry (TDR) probes; light-gray colored bars: mean value measured with the Theta Probe Delta-T Devices; dark-gray colored bars: gravimetric measurements.

where P_i is the model prediction, O_i the observed value, and N is the number of observation.

This RMSE is a measure for the scatter around the observed mean water content between measured and simulated values. The mean residual error (MRE) was also used to evaluate the direction of the error:

$$\mathrm{MRE} = \frac{\sum_{i=1}^{N}(P_i - O_i)}{N} \qquad [2]$$

Values of the MRE close to zero indicate that measured and simulated moisture contents do not differ systematically from each other.

Model and Parameters

The hydrological component of the reactive-transport model MIN3P was used for the simulations. The MIN3P model is a coupled multicomponent reactive transport model (e.g., Mayer, 1999; Mayer et al., 2002). Richards equation is solved for pressure head using Eq. [3] to describe the relationship between pressure head and soil water content.

$$S = S_r + \frac{1 - S_r}{[1 + (\alpha|h|)^n]^m} \qquad \text{for } h \le 0 \qquad [3]$$

where h is the pressure head, n and m are experimental exponents, S is the saturation given by the ratio θ/θ_s, and S_r is the residual saturation given by the ratio θ_r/θ_s, where θ, θ_r, and θ_s are the volumetric water content, the residual water content, and the saturated water content, respectively. The van Genuchten–Mualem relation (Eq. [4]) is used for unsaturated hydraulic conductivity (van Genuchten, 1980).

$$k_{rel} = S_e^L [1 - (1 - S_e^{1/m})^m]^2 \qquad [4]$$

where k_{rel} is the relative hydraulic conductivity, L is an empirical pore tortuosity/connectivity parameter, and S_e is the effective saturation given by:

$$S_e = \frac{S - S_r}{1 - S_r} \qquad [5]$$

The unsaturated HC is calculated using:

$$K = K_0 k_{rel} \qquad [6]$$

where K_0 (m s^{-1}) corresponds to the matching point at saturation. The empirical exponent L is commonly assumed to be 0.5, as recommended by Mualem (1976). However, different values (mostly negative ones) have also been widely used to improve the fit to experimental data under unsaturated conditions (e.g., Wösten et al., 1999; Schaap et al., 2001). This often corresponds to values of K_0 one order of magnitude lower than the measured hydraulic conductivity at saturation, K_s (Schaap and Leij, 2000).

In MIN3P, the solution of Richards equation is obtained using integrated finite differences in space and implicit time weighting. The equations are linearized using a modified Newton's method and solved using a sparse iterative matrix solver (Vanderkwaak et al., 1997). For the present application the model has been extended in two ways; first, to account for the influence of evapotranspiration on the soil water content, and second to introduce functions that allow the simulation of preferential flow. Several numerical verification tests were conducted to ensure proper behavior of the model including single soil layer simulations and comparison with single permeability simulations. Also trends in soil water content were examined as various parameters of the system were varied to ensure that the model was behaving qualitatively reasonably.

The rate of water uptake and loss is calculated at each time step by adopting a method similar to the one used in the soil water module SWIF of the FORHYD model (Tiktak and Bouten, 1992; Tiktak and Bouten, 1994; Bouten, 1995). The mass balance equation for water in the forest ecosystem can be expressed as:

$$\mathrm{PET} = (T - f_i I) + E_u + f_i I \qquad [7]$$

where PET is the potential evapotranspiration (mm d^{-1}), T is the actual tree transpiration rate (mm d^{-1}), E_u corresponds to the sum of understory plus soil evaporation (mm d^{-1}), and I is the amount of intercepted water by the tree canopy (mm). Intercepted water is evaporated at a certain rate, hence the f_i factor is introduced (d^{-1}). The correction of T by the $f_i I$ term serves to take account of the tree transpiration reduction by the evaporative demand of a wet canopy on days with precipitation.

Daily PET values (Penman), rainfall (P), and throughfall (Th) used in the simulations can be seen in Fig. 2. Potential evapotranspiration and P were obtained from a nearby meteorological station (Météo France Co., Tarrare Station, Rhône). The daily amounts of throughfall were calculated with the process-oriented regression model of Vilette (1994), where parameters were obtained from the best fit between monthly throughfall measured onsite and monthly rainfall measured in a field located nearby. Consistent with the work of Vilette (1994), E_u was set to 8% of PET. This proportion was determined from the mean ratio between solar radiation above and below the canopy measured on-site. In agreement with most of the previous studies on water balance modeling in a forest soil, water uptake was arbitrarily limited to the topsoil layer. The generic value of $f_i = 0.2$ from Granier et al. (1999) was used. Tiktak and Bouten (1994) used a similar value (f_i = 0.141) for the simulation of the long-term water balance in a douglas-fir stand in the Netherlands.

The actual tree transpiration is distributed in each i^{th} discretization control volume according to the root length density of the j^{th} soil layer and weighted by the local soil moisture content:

$$Q_{i,j} = \left(\frac{V_{i,j} R_j S_{i,j}}{\sum_{j=1}^{nj} \sum_{i=1}^{ni} V_{i,j} R_j S_{i,j}} \right) T \qquad [8]$$

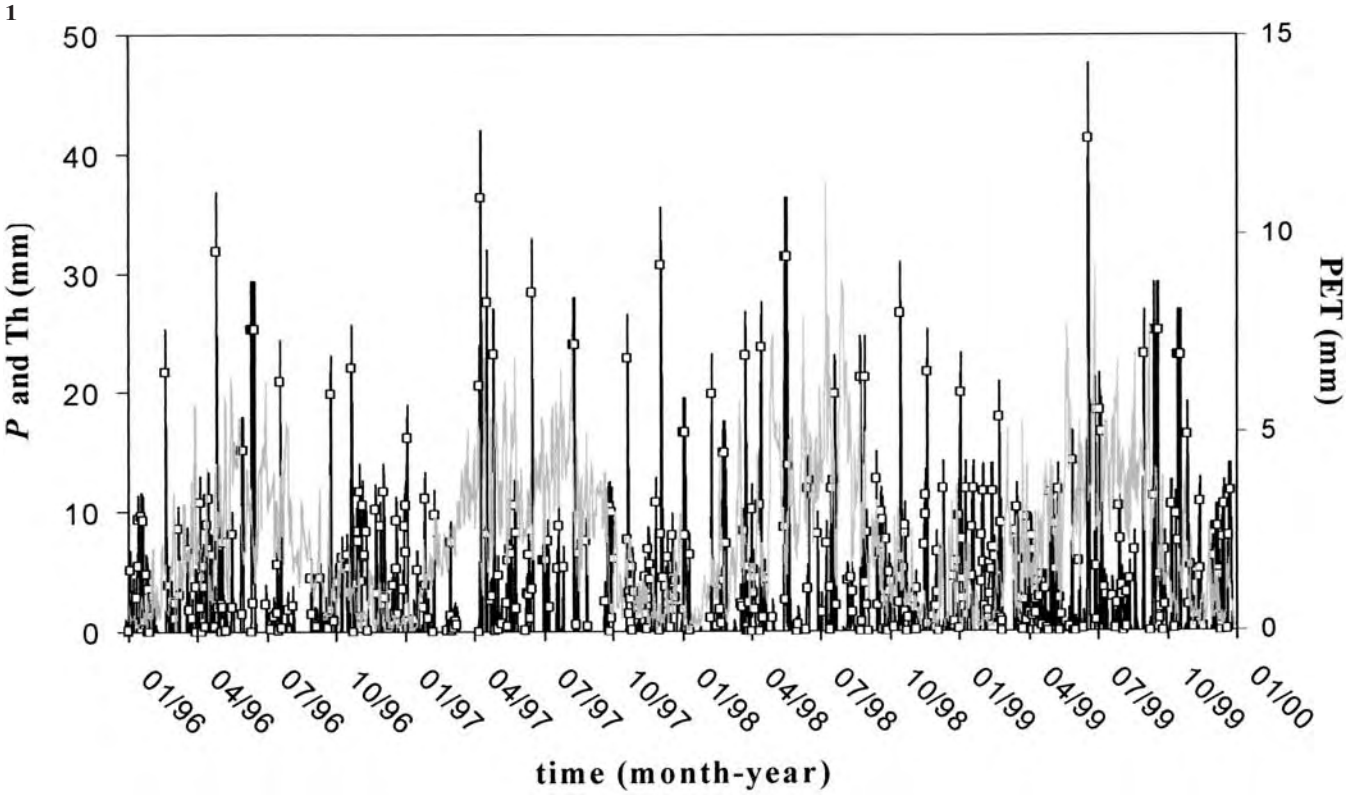

Fig. 2. Variations in precipitation (*P*, dark solid line), throughfall (Th, square symbols), and potential evapotranspiration (PET, light solid line).

where $Q_{i,j}$ ($m^3\ s^{-1}$) is the water uptake rate by trees in the i^{th} control volume of the j^{th} soil layer, $V_{i,j}$ is the volume of the control volume, R_j ($m^2\ m^{-3}$) is root length density in the j^{th} soil layer (i.e., the ratio of the root surface per volume of soil), $S_{i,j}$ is the water saturation in the i^{th} control volume of the j^{th} soil layer.

The decrease in the water uptake at low water content is also taken into account in the model. However, the use of an implicit numerical scheme in the model for solving mass balance equations did not allow the implementation of the common discontinuous reduction function. Instead, the continuous function used by Battaglia and Sands (1997) was implemented into MIN3P:

$$\alpha_{i,j} = \frac{\mathrm{REW}_{i,j}^2 \exp(p_1 \mathrm{REW}_{i,j})}{\mathrm{REW}_0^2 \exp(p_1 \mathrm{REW}_0) + \mathrm{REW}_{i,j}^2 \exp(p_1 \mathrm{REW}_{i,j})} \quad [9]$$

where $\alpha_{i,j}$ is the dimensionless reduction factor, $\mathrm{REW}_{i,j}$ is the reserve of extractable water, REW_0 and p_1 are fitting parameters. $\mathrm{REW}_{i,j}$ is defined as:

$$\mathrm{REW}_{i,j} = \frac{S_{i,j} - S_j^{\lim}}{S_j^{\mathrm{f}} - S_j^{\lim}} \quad [10]$$

where $S_j^{\lim}$ is the water saturation at wilting point (i.e., no water uptake below this critical value), and S_j^{f} is the water saturation at field capacity.

Measurements of the ratio between *T* and PET as a function of REW given by Granier et al. (1999) was fitted with Eq. [10] using the nonlinear fitting procedure of the Unistat 5.0 software (Unistat Ltd, England). We considered data corresponding to a leaf area index equal to 6 $m^2\ m^{-2}$, which is close to the generic value proposed for coniferous trees in a recent review article (Breuer et al., 2003). The same leaf area index was used by Vilette (1994).

Values of the soil-related transpiration parameters; that is, *R*, the root length density, and REW, the reserve of extractable water, were obtained during calibration of the model (e.g., Musters and Bouten, 2000; Vrugt et al., 2001; Hupet et al., 2003). It is necessary to stress that parameter optimization is often required for practical reasons during model calibration. While the maximum rooting depth was fixed to 1.2 m based on measurements (see Table 1); in the present study *R* could not be easily measured in a 45-yr-old douglas-fir stand (i.e., trees of about 20 m high). Similar considerations can be made with respect to the definition of the reserve of extractable water, REW, except that the likely range of values for the parameters in Eq. [10] is better bounded. Typically, the water saturation at wilting point, $S^{\lim}$, is assumed as $\log|h(\mathrm{cm})|$or pF = 4.2 in agronomy. Slightly greater values have been frequently reported depending on a variety of factors such as soil texture and plant species (e.g., Volaire and Lelièvre, 2001). The saturation at field capacity, S^{f}, defines the upper limit of available water for roots. This maximum again may vary according to a number of factors including plant species. In theory, S^{f} can range from close to saturation to some value greater than $S^{\lim}$.

Numerous techniques have been developed for the implementation of preferential flow (see Simunek et al. [2003] for a review). Briefly these techniques may be subdivided into two types; equilibrium and nonequilibrium formulations (i.e., instantaneous and slow transfer between macroporosity and the matrix, respectively). Both types of preferential flow schemes have been implemented in MIN3P. The equilibrium formulation involves a composite HC function to allow for divergences from the standard unsaturated HC behavior at higher water content (Mohanty et al., 1997). The calculated HC is an average property of the two pore systems. Below a certain pressure head, noted h_{pf}, the standard van Genuchten–Mualem relationship is used to calculate the HC. Above that head the HC is assumed to increase exponentially according to:

$$K(h) = K(h) + \kappa[\exp(h - h_{\mathrm{pf}}) - 1] \quad [11]$$

Table 2. Basic soil properties used as input in ROSETTA.

Soil layer	Sand	Silt	Clay	Bulk density
	%			g cm^{-3}
A11	32.3	44.2	23.5	1.05
A12	32	44.9	23.1	1.10
B	36.9	41.2	21.9	1.36
C	53.5	34.7	11.8	1.46

where κ is a scaling factor that determines the magnitude of preferential flow.

The nonequilibrium preferential flow scheme implemented in MIN3P is based on the work of Gerke and van Genuchten (1993a, 1993b). The water flux evolution is calculated by solving Richards equation in both the macropore and micropore system (using Eq. [3] and [4]), and a first-order process-based expression is used to calculate interstitial flow between micro and macropore regions. However, such a scheme requires an increased number of input parameters for simulating preferential flow. Since the present application would require calibration of poorly constrained preferential flow parameters to improve the fit between simulated and measured water contents, only the equilibrium formulation is considered here.

The PTF available in the ROSETTA software (Schaap et al., 2001) was used in this study to predict the soil hydraulic parameters. This PTF is based on an artificial neural network and constitutes one of the most recent PTFs that overall has shown reasonable predictions evaluation studies. For example, Nemes et al. (2003) recently showed that the functional performance of the ROSETTA model with different sets of input data was reasonably good for simulating soil moisture variations in the field. An advantage of neural network approaches resides in the fact that no a priori model concept is required to convert basic soil properties to hydraulic parameters. The ROSETTA model is flexible as its hierarchical structure enables the input of limited and more extended sets of predictors. A trend of improvement was observed with an increasing number of predictors (Nemes et al., 2003). This behavior has been frequently found in other evaluation studies of PTFs (Rawls et al., 2001; van Alphen et al., 2001; Wösten et al., 2001). It is unfortunate that soil hydraulic properties were never measured at the Vauxrenard field site, and are not measurable today because the storm on 27 Dec. 1999 destroyed the 45-yr-old douglas-fir stand (like millions of hectares throughout Western Europe) and the soil was deeply tilled by falling trees. Therefore, contrary to past studies only a blind-functional evaluation could be undertaken; that is, without any possible reference to measured hydraulic properties. However, this presented an opportunity to evaluate the reliability of a PTF already recognized for its predicting capacity in the context of great scarcity of information on soil properties. Available predictors for the present application are sand, silt and clay content, and bulk density data for each soil layer. Basic soil properties had been measured for various purposes in each soil layer at a number of locations randomly distributed throughout the site. For simplicity, we used the mean values of the basic soil layer properties (Table 2) as input for ROSETTA. Another interesting aspect of the ROSETTA model lies in the use of the bootstrap method to provide uncertainty estimates of the predicted hydraulic parameters, which can then be considered in the simulations. Also, the common relationship $m = 1 - 1/n$ is used in ROSETTA and predicted values of both K_s (with $L = 0.5$) and K_0 (with $L \neq 0.5$) are generated. Uncertainties exist in the reliability of either K_0 or K_s values to model field water content. Besides the order of magnitude of difference typically encountered between these two soil parameters, Schaap et al. (2001) also outlined that using $K_0 < K_s$ leads to an untenable situation near saturation because the HC should be equal to K_s while Eq. [4] provides K_0.

In addition to the lack of measured hydraulic parameters, the position of the water table was not determined. However, the local situation of the Vauxrenard field site (i.e., hill slope, crystalline bed rock presumably fractured, moderate soil thickness) suggests that if a perched aquifer were present or not beneath the field site it should be very deep. Moreover, the soil is recognized to be well aerated and hydromorphic features have never been observed in this soil to a depth of 2.5 m (i.e., the greatest depth reached by trenches excavated for various purposes). Accordingly, the total Fe concentration in soil solutions collected down to 1.20 m was always found to be very low, on the order of a few micromoles, as controlled by formation of low solubility Fe(III) hydroxides (Bourrié et al., 1999).

Modeling Procedure

All simulations are performed for a one-dimensional soil profile. The top 120 cm of soil are subdivided into 120 control volumes of equal size. Each soil horizon is defined in the simulation by a property layer having its own set of hydraulic and soil-dependent transpiration parameters with the upper boundary open to throughfall. In a first step, we use the outputs of ROSETTA to simulate daily variations in soil moisture during the 4-yr period of TDR measurements. The reliability of the two types of predictions for the K_0 and L parameters was studied. Values of the soil-related transpiration parameters (i.e., R and REW) were manually optimized in each soil layer to obtain the best fit during the drought events of the January 1996 and December 1997 time series; that is, in the summer when their influence is greater due to the low water content and the maximum transpiration demand. Then, the calibrated values were kept constant for the simulation of the following 2-yr period of TDR measurements, that is, from January 1998 to December 1999. The influence of the position of the water table on the simulations was minimized at this stage by setting it to 100 m below the bottom of the soil profile (i.e., lower boundary condition $h = -100$ m). In a second step, the influence of prediction uncertainties and of the position of the water table is examined using the best simulation found previously. Lastly, the equilibrium preferential flow scheme and manual parameter estimation were used to improve the fit. In all the simulations, the steady-state solution was calculated to give the initial conditions in the soil column, with the mean value of PET, I, and Th been used to generate the

Table 3. Hydraulic parameters predicted by ROSETTA. Prediction uncertainties provided in parentheses.

Soil layer	θ_s	θ_r	α	n	L	K_s	K_0
	%		cm^{-1}			cm d^{-1}	
A11	50.2 (±1.0)	7.8 (±0.8)	0.0071 (±0.076)†	1.58 (±0.016)†	0.21 (±1.43)	75.06 (±0.12)†	2.43 (±0.30)†
A12	48.7 (±0.9)	7.6 (±0.8)	0.0069 (±0.074)†	1.59 (±0.015)†	0.20 (±1.38)	60.37 (±0.13)†	2.31 (±0.29)†
B	41.7 (±0.8)	6.7 (±0.8)	0.0085 (±0.072)†	1.55 (±0.013)†	−0.13 (±0.98)	15.17 (±0.12)†	2.66 (±0.22)†
C	37.5 (±0.8)	4.4 (±0.5)	0.0176 (±0.062)†	1.45 (±0.011)†	−0.65 (±0.73)	28.02 (±0.10)†	8.07 (±0.21)†

† log uncertainty.

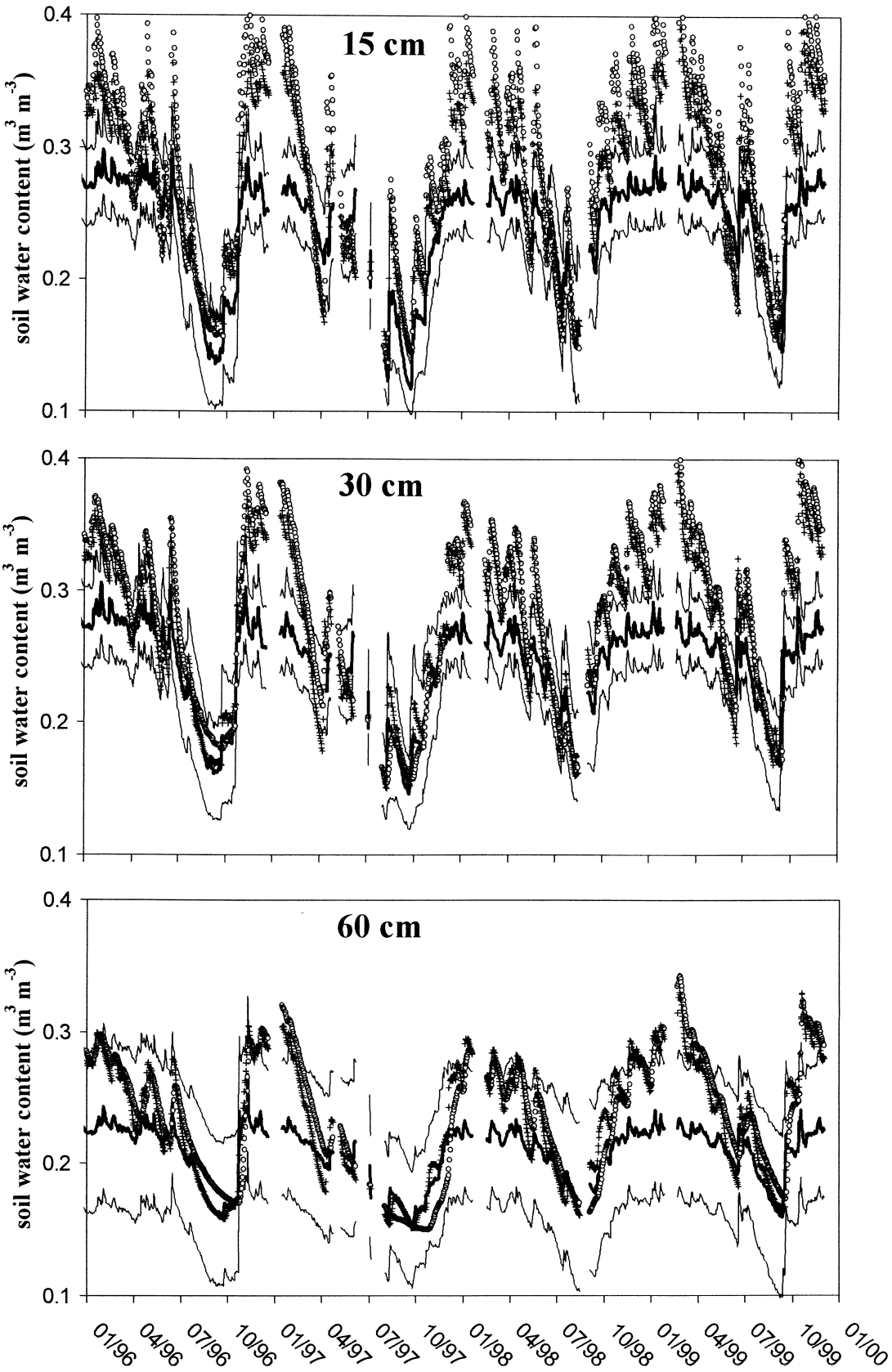

Fig. 3. Result of the simulations made with predicted hydraulic parameters and using the two types of prediction for hydraulic conductivity: K_s with $L = 0.5$ (cross), and K_0 with $L \neq 0.5$ (circles). Mean and spread of the soil moisture content as measured by means of six time domain reflectometry probe replicates are shown (thick line: mean; thin lines: mean ± sd).

Table 4. Statistical criteria at the 15-, 30-, and 60-cm depth for simulations using the two types of prediction for the hydraulic conductivity (K_s with $L = 0.5$, and K_0 with $L \neq 0.5$). Statistics are provided for the total simulation period (from January 1996 to December 1999) and for each season.

		15 cm					30 cm					60 cm				
		Total	Summer	Fall	Winter	Spring	Total	Summer	Fall	Winter	Spring	Total	Summer	Fall	Winter	Spring
		$m^3\ m^{-3}$														
K_s	MRE	0.036	0.033	0.047	0.066	0.022	0.031	0.025	0.038	0.062	0.021	0.027	0.021	0.028	0.056	0.023
	RMSE	0.068	0.044	0.052	0.068	0.037	0.063	0.039	0.048	0.064	0.035	0.049	0.032	0.040	0.058	0.031
K_0	MRE	0.052	0.046	0.068	0.089	0.035	0.040	0.031	0.039	0.078	0.036	0.028	0.021	0.015	0.058	0.033
	RMSE	0.086	0.064	0.077	0.092	0.054	0.072	0.048	0.058	0.081	0.045	0.051	0.032	0.040	0.062	0.038

steady- state solutions. Also, each simulation was started three months before January 1996. This initial period was ignored in data treatments to suppress any influence of the different initial conditions.

RESULTS AND DISCUSSION

Hydraulic parameters and uncertainties predicted with ROSETTA are presented in Table 3. As reported by Schaap and Leij (2000), the difference between K_0 and K_s reached about one order of magnitude. Results of the simulations made by using the values of K_0 (with $L \neq 0.5$) and K_s (with $L = 0.5$) are illustrated in Fig. 3. For comparison purposes, the same values of the soil-dependent evapotranspiration parameters were used in both cases. In each soil layer S^f was set to saturation and S^{lim} corresponds to $|h| = 160$ m (pF = 4.2), which corresponds to the theoretical wilting point (see above). Results were found to be very similar. Whether K_s or K_0 were used in MIN3P, results clearly exhibited an overestimation of the soil water content during periods of high soil moisture. Simulated water contents even exceeded the measured maximum as given by the mean measured soil water content plus the standard deviation. Also, calculated water contents were slightly less overestimated within the high soil moisture periods when using K_s (i.e., smaller MRE and RMSE—see Table 4). The value obtained from these statistic criteria decreased from 0.052 at the 15-cm depth to 0.028 at the 60-cm depth when K_0 was considered, in comparison with 0.036 and 0.027, respectively, when using K_s. Consistently, the calculated RMSE follow the same trends with soil depth. By distinguishing the seasons on a calendar-basis, the MRE reaches its maximum in the winter and its minimum during the spring or in the summer. The maximum

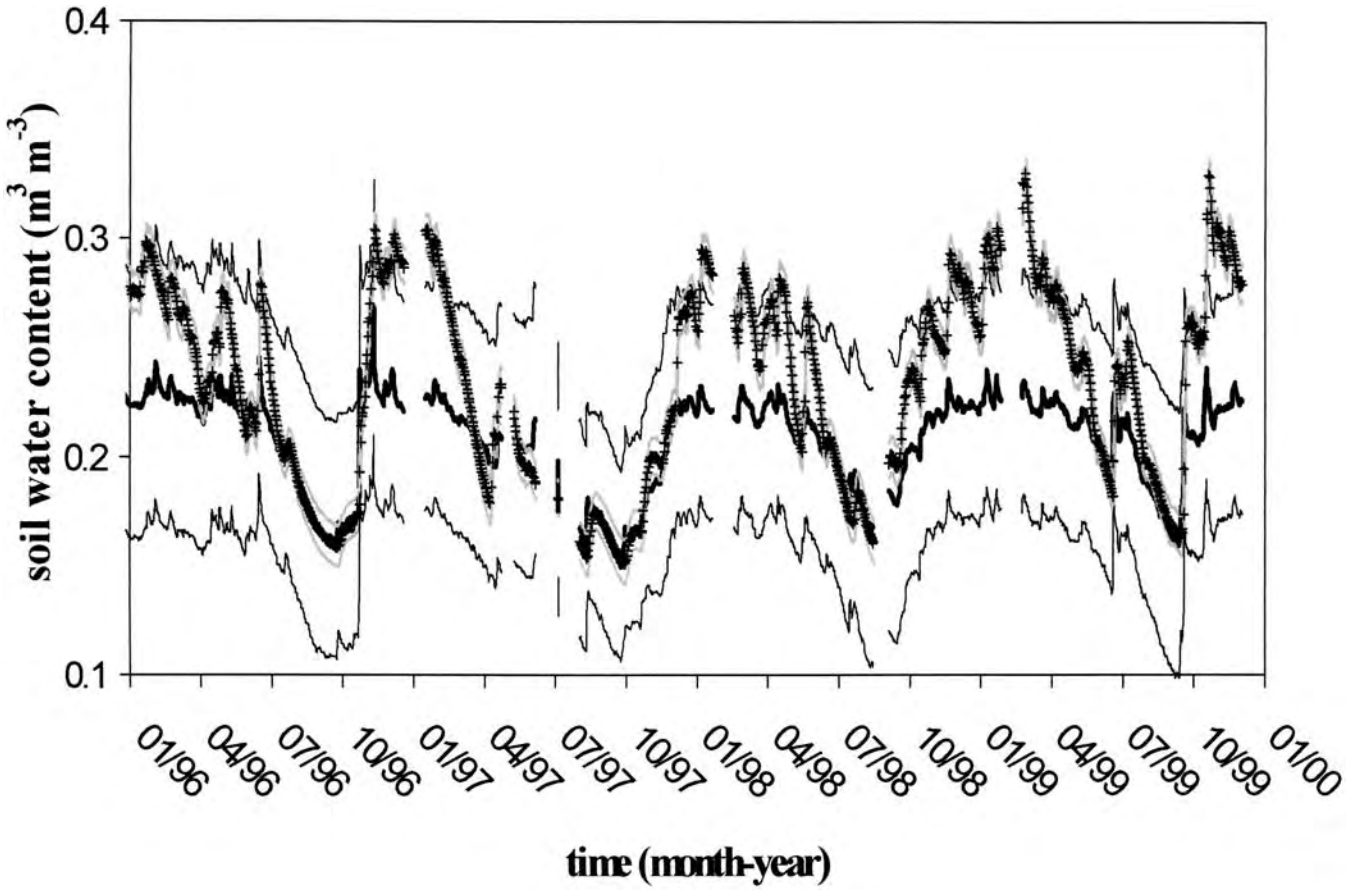

Fig. 4. Simulated water content at 60 cm by taking into account the prediction uncertainties given by ROSETTA (light curves) and using K_s and $L = 0.5$. Cross: simulation with the mean values of hydraulic parameters. Mean and spread of the measured soil moisture content are shown (thick line: mean; thin lines: mean ± sd).

MRE value was 0.089 at the 15-cm depth with K_0 in comparison to 0.066 when using K_s. In each season a tendency to decrease was found for the values of both statistical criteria with increasing soil depth. These results, and particularly the overpredictions of the water content during periods of high soil moisture and the such systematic decrease in discrepancy with increasing soil depth, strongly suggest the occurrence of preferential flow, which appears to be related to the root density distribution (see Table 1). Better results obtained by using K_s instead of K_0, and the corresponding values of L, were likely caused by the much smaller value determined for K when K_0 was considered and the soil water content was high. The same conclusions can be drawn to a lesser extent with respect to results obtained for the other seasons, notably in the summer and spring when the model becomes very sensitive toward the values of the evapotranspiration parameters. Readjusting the values taken by REW and R did not bring significant improvements. Improving the fit of the mean measured water content locally caused the predictions to become poorer elsewhere. Therefore, it appears that for the present application the K_s approach provides better results, and will be considered hereafter.

Predictions showed little variations in the simulated water contents within the range of uncertainty given by ROSETTA. An example at the 60-cm depth is shown in Fig. 4, where the effect of uncertainties was large enough to warrant graphical presentation. The range of the uncertainty effects on the simulated water contents was established by testing all the combinations of the van Genuchten–Mualem parameters plus or minus uncertainties.

The mean values of the predicted hydraulic parameters were used for testing the influence of a hypothetical water table. Given the uncertainty in the location of the water table and the potential for water table fluctuations (see above), several test simulations were conducted by setting a fixed water table at various depths during the wet periods (winter and fall), while a deep water table (i.e., water table set at the 100-m depth) was still assumed during the dry periods (spring and summer). Results showed that the impact of the water table becomes significant at the 60-cm depth when specified at a depth of about 3.5 m or shallower. As shown in Fig. 5, discrepancies during the periods of high soil moisture become larger when the water table is closer to the surface while no significant change was observed during the periods of low water content (i.e., dry periods). Additional tests were performed, in which case the water table was kept at the same level during the entire course of the simulation. Under such conditions, simulated water contents markedly increased during dry periods as well, but could be compensated by readjusting

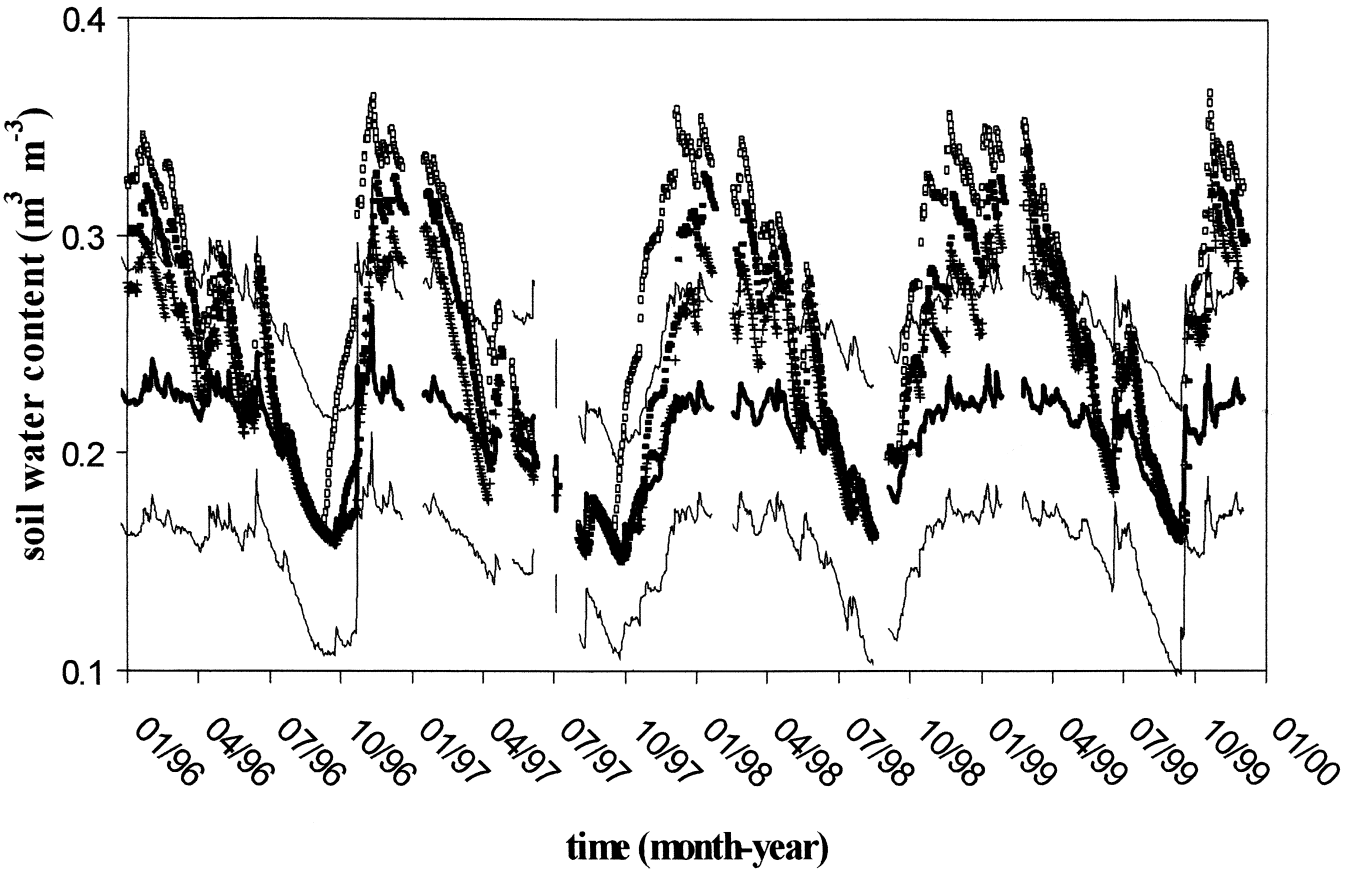

Fig. 5. Simulated water content at 60 cm using K_s and L = 0.5 and by setting the water table during the wet periods (i.e., winter and fall) at the 2-m depth (open squares) and at the 3-m depth (filled squares). For comparison purposes, results calculated by neglecting the influence of the water table are given (cross). Mean and spread of the measured soil moisture content are shown (thick line: mean; thin lines: mean ± sd).

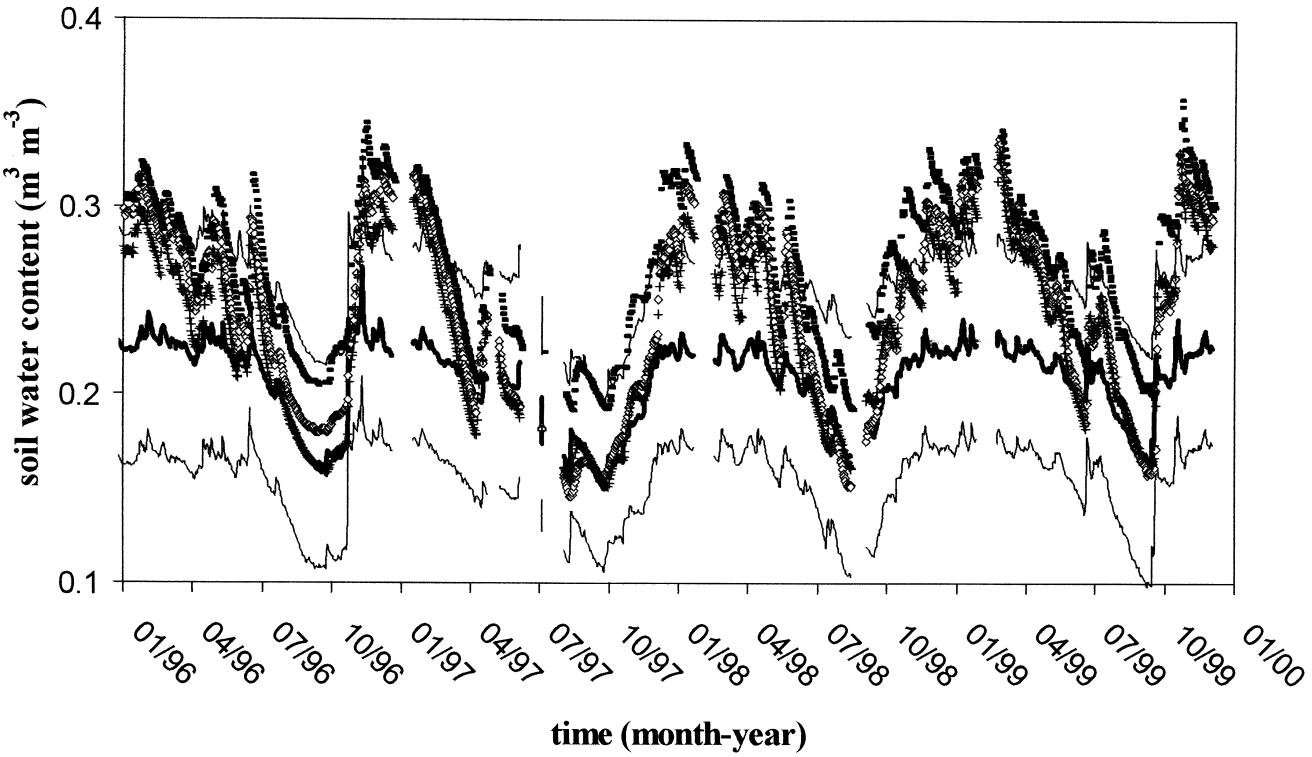

Fig. 6. Simulated water content at 60 cm using K_s and $L = 0.5$ and by setting the water table at the 3-m depth, without readjusting the soil-dependent transpiration parameters (filled squares), after readjustment (open diamonds). For comparison purpose, results calculated by neglecting the influence of the water table are given (cross). Mean and spread of the measured soil moisture content are shown (thick line: mean; thin lines: mean ± sd).

the soil-dependent transpiration parameters. In the example shown in Fig. 6, the water table was set to a 3-m depth, and a reasonable fit was obtained by setting S^f to the value given at $|h| = 10$ m (S^{lim} unchanged, given by $|h| = 160$ m) in each soil layer. Values of the root length density needed to be readjusted as well. The overprediction during the periods of high soil moisture were even greater than previously calculated by minimizing the influence of the water table (i.e., position set at the 100-m depth).

The preferential flow scheme proposed by Mohanty et al. (1997) was used in an attempt to correct for the overpredictions of calculated soil water content. As expected, accounting for preferential flow drastically improved predictions (Fig. 7). Statistics presented in Table 5 confirm this result. Corresponding fitted values of parameters in Eq. [11] are $\kappa = 100$ m d^{-1} in each horizon, and $|h_{pf}| = 8.3$ and 4 m in the top three horizons and in the bottom soil horizon, respectively. The value of the HC associated with preferential flow, κ, is about two orders of magnitude larger than K_s predicted by ROSETTA. Such a difference was not surprising considering that, for example, Feyen et al. (1999) reported a decrease of travel time for a tracer of about three orders of magnitude in a forest soil in comparison to travel times estimated from saturated HC of the soil matrix. By application of the Jurin's law, values taken by h_{pf} yield an equivalent pore diameter of about 4 μm at the 15- and 30-cm depths, and of 8 μm at the 60-cm depth, which are within the range of the capillary soil porous system. Such a low pore diameter limit can be viewed as evidence for the occurrence of a bimodal porosity distribution in this soil (Othmer et al., 1991), which was not considered by the ROSETTA PTF. However, such pore diameter values are theoretical since the complexity of the porous network is not considered (i.e., pore roughness, tortuosity, heterogeneity of the surrounding solids). This implies that the effective pore diameter corresponding h_{pf} should be larger. Furthermore, we believe that the above limits are uncertain in the absence of physical measurements. These values may be caused by the type of preferential flow scheme used since the WRC predicted by the PTF is being considered together with the extra term accounting for preferential flow (see Eq. [11]). Any of the other modeling approaches for preferential flow also attempt to correct overestimations during periods of high soil moisture through parameter optimization. For example, the approach available in the MACRO model (e.g., Roulier and Jarvis, 2003) which considers preferential flow driven by gravity only; that is, occurring within macropores large enough to neglect the influence of capillary forces. Knowledge of the active pore diameters wherein preferential flow occurs could guide modelers in the selection of the preferential flow schemes (i.e., only gravity-driven flow in large macropores, gravity and capillary-driven flow in case of smaller macropores, or the need for the co-consideration of both formulations). In practice, comprehensive measurements of the soil hydraulic properties (i.e., WRC and HC function) especially at large water contents and at the field-scale should be considered.

The type of preferential flow scheme is also of rele-

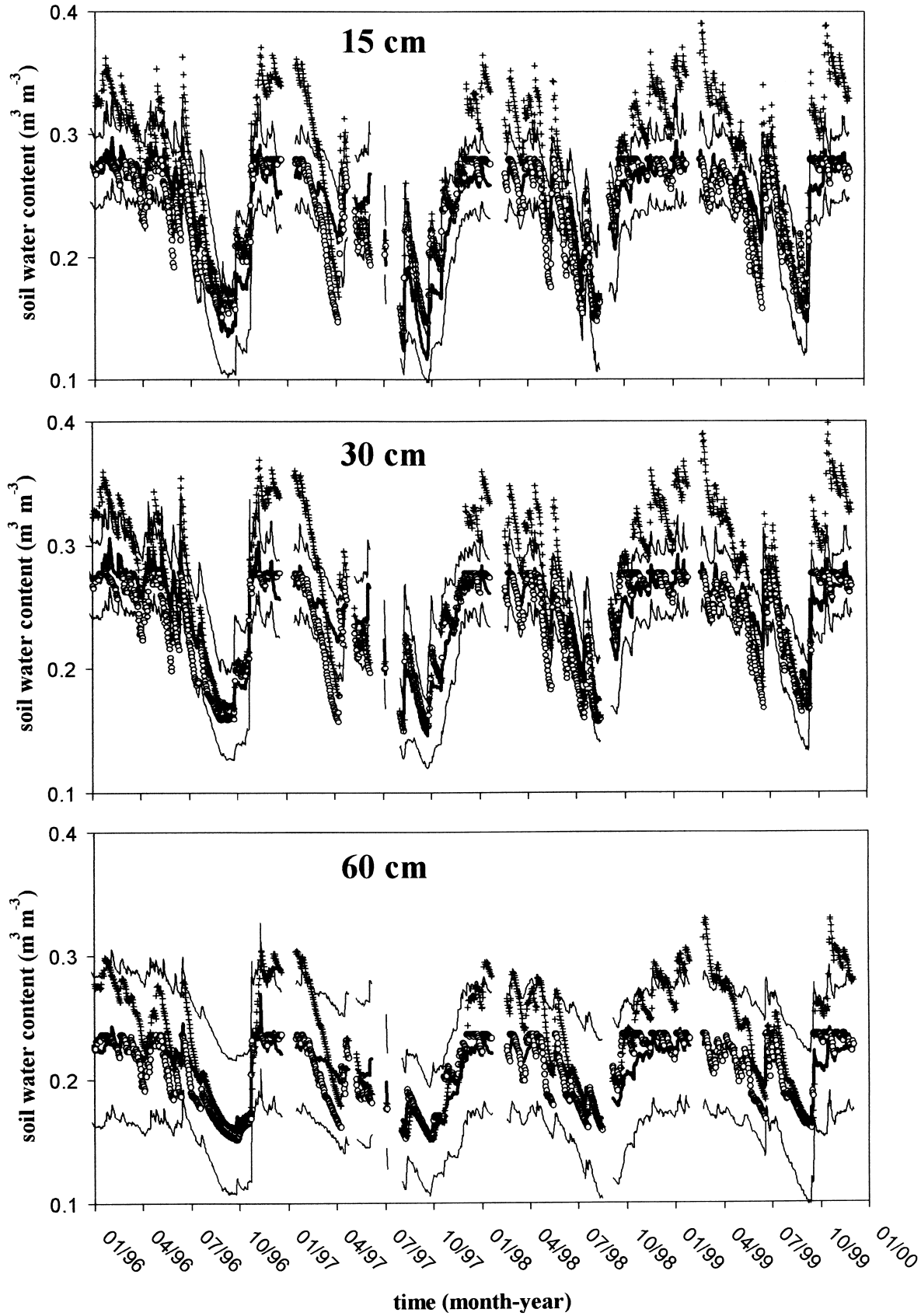

Fig. 7. Simulated water content with preferential flow (circles), after calibration of the parameters involving in Eq. [11]. For comparison purposes, results calculated without preferential flow and using K_s and $L = 0.5$ are shown (cross). Mean and spread of the measured soil moisture content are shown (thick line: mean; thin lines: mean ± sd).

Table 5. Statistical criteria at the 15-, 30-, and 60-cm depth for the simulations performed including preferential flow. Statistics are provided for the total simulation period (from January 1996 to December 1999) and for each season.

	15 cm					30 cm					60 cm				
	Total	Summer	Fall	Winter	Spring	Total	Summer	Fall	Winter	Spring	Total	Summer	Fall	Winter	Spring
	$m^3\ m^{-3}$														
MRE	0.001	0.003	0.016	0.003	0.017	0.006	0.004	0.008	0.002	0.020	0.001	0.001	0.009	0.004	0.010
RMSE	0.045	0.017	0.020	0.011	0.026	0.041	0.015	0.014	0.010	0.026	0.028	0.010	0.015	0.008	0.016

vance considering that the preferential flow schemes used here led to a much greater sensitivity of the results with respect to the position of the water table. The influence of the water table was minimized in the above calculations by setting it at the 100-m depth. By assuming a water table closer to the bottom of the simulated soil profile, capillary- driven upward preferential flow led to much larger discrepancies. This observation is illustrated in Fig. 8, where the water table was set to a depth of 3 m during winter and fall, similar to the simulations shown in Fig. 5. It can be seen that the upward water movements became so significant that simulated water contents mirrored the stepwise adjustment of the water table. Clearly, such a large sensitivity to the water table level would not be obtained when using a gravity-driven preferential flow scheme. Future development of a more comprehensive scheme in MIN3P enabling the simulation of preferential flow in both macropores (i.e., gravity-driven flow) and in smaller pores (capillary-driven flow) would also be of advantage; as such processes are very likely to be present in a natural system.

CONCLUSIONS

We presented an investigation of evapotranspiration and preferential water flow in the vadose zone of a forest soil using an extended version of the reactive-transport model MIN3P. With the exception for periods of high soil moisture, during which significant and systematic overpredictions were observed, the neural network-based PTF implemented in the ROSETTA model showed good predictive ability for simulating daily average values of the measured water content over a 4-yr period. Various sensitivity tests were performed and showed their inability to correct for such overestimates. As expected from these results and the literature, a good fit was obtained by considering the occurrence

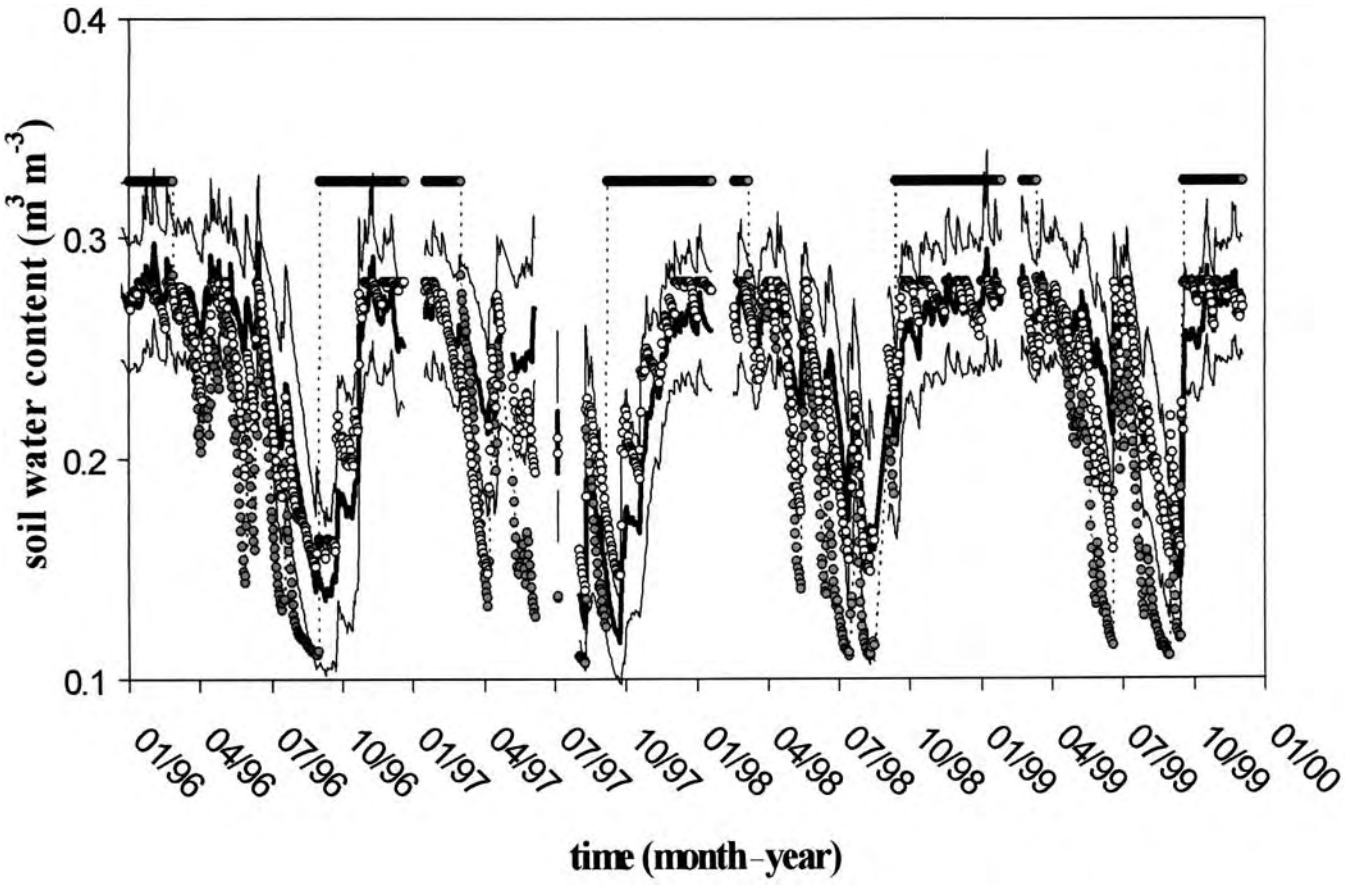

Fig. 8. Influence of the position of the water table on the results of simulations performed with preferential flow at the 15-cm depth (Gray circles: water table set at the 3-m depth in winter and fall, and at the 100-m depth in summer and spring). For comparison purposes, results calculated by setting no influence of the water table are shown (open circles).

of preferential flow in this soil. Thus, it appears the ROSETTA PTF can give reasonable predictions of the hydraulic properties corresponding to the soil matrix of the present study field site. We further demonstrated the limited physical meaning of the preferential flow parameters obtained by calibration. These parameters are model-dependent in the absence of measured soil hydraulic properties at high water content. Process understanding can be enhanced by studying the corresponding size and nature of the active pores, as well as by means of comprehensive on-site measurements of the soil hydraulic properties. Results of such measurements should also help to determine the type of preferential flow formulation to be used in a model. Such findings should be of further practical relevance, because the use of preferential flow schemes that include capillary-controlled flow may lead to massive upward capillary-driven preferential flow.

ACKNOWLEDGMENTS

The authors gratefully acknowledge financial support for this cooperative research from the French Canada Research Foundation, the French Embassy in Ottawa, the INRA FMN department (Institut National de la Recherche Agronomique, Forêts et Milieux Naturels), and NSERC (Natural Sciences and Engineering Research Council of Canada). Many thanks also go to the GIP-ECOFOR Program for funding TDR instrumentation and measurements. The authors are grateful to D. Gelhaye for supervising the TDR system, and to the scientific manager of the field site, J. Ranger.

REFERENCES

AFES. 1992. Principaux sols d'Europe. Référentiel pédologique Association Française pour l'Etude des Sols. Institut National de Recherches Agronomique, Paris.

Battaglia, M., and P. Sands. 1997. Modelling site productivity of Eucalyptus Globulus in response to climatic and site factors. Aust. J. Plant Physiol. 24:831–850.

Bourrié, G., F. Trolard, J.-M.R. Génin, A. Jaffrezic, V. Maître, and M. Abdelmoula. 1999. Iron control by equilibria between hydroxygreen rusts and solutions in hydromorphic soils. Geochim. Cosmochim. Acta 63:3417–3427.

Bouten, W. 1995. Soil water dynamics of the Solling spruce stand, calculated with the FORHYD simulation package. Ecol. Modell. 83:67–75.

Breuer, L., K. Eckhardt, and H.-G. Frede. 2003. Plant parameter values for models in temperature climates. Ecol. Modell. 169:237–293.

Chen, C., and W.A. Payne. 2001. Measured and modeled unsaturated hydraulic conductivity of a Walla Walla silt loam. Soil Sci. Soc. Am. J. 65:1385–1391.

Cornelius, W.M., J. Ronsyn, M. Van Meirvenne, and R. Hartmann. 2001. Evaluation of Pedotransfer functions for predicting soil moisture retention curve. Soil Sci. Soc. Am. J. 65:638–648.

Espino, A., D. Mallants, M. Vanclooster, and J. Feyen. 1996. Cautionary notes on the use of pedotransfer functions for estimating soil hydraulic properties. Agric. Water Manage. 29:235–253.

Ezzaïm, A., M.-P. Turpault, and J. Ranger. 1999. Quantification of weathering processes in an acid brown soil developed from tuff (Beaujolais, France). Part I. Formation of weathered rind. Geoderma 87:137–154.

Feyen, H., H. Wunderli, H. Wydler, and A. Papritz. 1999. A tracer experiment to study flow paths of water in a forest soil. J. Hydrol. (Amsterdam) 225:155–167.

Gérard, F., J. Ranger, C. Ménétrier, and P. Bonnaud. 2003. Silicate weathering mechanisms determined using soil solutions held at high matric potential. Chem. Geol. 202:443–460.

Gerke, H.H., and M.Th. van Genuchten. 1993a. Evaluation of a first order water transfer term for variably saturated dual-porosity models. Water Resour. Res. 29:1225–1238.

Gerke, H.H., and M.Th. van Genuchten. 1993b. A dual porosity model for simulating the preferential movement of water and solutes in structure porous media. Water Resour. Res. 29:305–319.

Granier, A., N. Bréda, P. Biron, and S. Vilette. 1999. A lumped water balance model to evaluate duration and intensity of drought constraints in forest stands. Ecol. Modell. 116:269–283.

Hack-ten Broeke, M.J.D., and J.H.B.M. Hegmans. 1996. Use of soil physical characteristics from laboratory measurements or standard series for modelling unsaturated water flow. Agric. Water Manage. 29:201–213.

Hupet, F., S. Lambot, R.A. Feddes, J.C. van Dam, and M. Vanclooster. 2003. Estimation of root water uptake parameters by inverse modeling with soil water content data. Water Resour. Res. 39:1312–1328.

Inskeep, W.P., J.M. Wraith, J.P. Wilson, R.D. Snyder, R.E. Macur, and H.M. Gaber. 1996. Input parameter and model resolution effects on predictions of solute transport. J. Environ. Qual. 25:453–462.

Jarvis, N.J., L. Zavattaro, K. Rajkai, W.D. Reynolds, P.-A. Olsen, M. McGechan, M. Mecke, B. Mohanty, P.B. Leeds-Harrison, and B. Jacques. 2002. Indirect estimation of near-saturated hydraulic conductivity from readily available soil formation. Geoderma 108:1–17.

Larsson, M.H., N.J. Jarvis, G. Torstensson, and R. Kasteel. 1999. Quantifying the impact of preferential flow on solute transport to tile drains in a sandy field soil. J. Hydrol. (Amsterdam) 215:116–134.

Lin, H.S., K.J. McInnes, L.P. Wilding, and C.T. Hallmark. 1999. Effect of soil morphology on hydraulic properties: II. Hydraulic pedotransfer functions. Soil Sci. Soc. Am. J. 63:955–961.

Marques, R., and J. Ranger. 1997. Nutrient dynamics in a chronosequence of Douglas-fir (Pseudotsuga menziesii (Mirb.) Franco) stands on the Beaujolais Mounts (France). 1: Qualitative approach. For. Ecol. Manage. 91:255–277.

Mayer, K.U. 1999. A numerical model for multicomponent reactive transport in variably saturated porous media. University of Waterloo, Waterloo, Canada.

Mayer, K.U., E.O. Frind, and D.W. Blowes. 2002. A numerical model for the investigation of reactive transport in variably saturated media using a generalized formulation for kinetically controlled reactions. Water Resour. Res. 38:1174–1194.

Mohanty, B.P., R.S. Bowman, J.M.H. Hendrick, and M.Th. van Genuchten. 1997. New piecewise-continuous hydraulic functions for modelling preferential flow in an intermittent flood-irrigated field. Water Resour. Res. 33:2049–2063.

Mualem, Y. 1976. A new model predicting the hydraulic conductivity of unsaturated porous media. Water Resour. Res. 12:513–522.

Musters, P.A.D., and W. Bouten. 2000. A method for identifying optimum strategies of measuring soil water contents for calibrating a root water uptake model. J. Hydrol. (Amsterdam) 227:273–286.

Nemes, A., M.G. Schaap, and J.H.M. Wösten. 2003. Functional evaluation of pedotransfer functions derived from different scales of data collection. Soil Sci. Soc. Am. J. 67:1093–1102.

Othmer, H., B. Diekkrüger, and M. Kutilek. 1991. Bimodal porosity and unsaturated hydraulic conductivity. Soil Sci. 152:139–149.

Pachepsky, Y.A., and W.J. Rawls. 2003. Soil structure and pedotransfer functions. Eur. J. Soil Sci. 54:443–451.

Ranger, J., R. Marques, M. Colin-Belgrand, and N. Flammang. 1995. The dynamics of biomass and nutrient accumulation in a Douglas-fir (Pseudotsuga menziesii Franco) stand studied using a chronosequence approach. For. Ecol. Manage. 72:167–183.

Ranger, J., R. Marques, and J.-H. Jussy. 2001. Forest dynamics during stand development assessed by lysimeter and centrifuge solutions. For. Ecol. Manage. 144:129–145.

Rawls, W.J., Y. Pachepsky, and M.H. Shen. 2001. Testing soil water retention estimation with the MUUF pedotransfer model using data from the southern United States. J. Hydrol. (Amsterdam) 251: 177–185.

Roulier, S., and N. Jarvis. 2003. Analysis of inverse procedures for estimating parameters controlling macropore flow and solute transport in the dual-permeability model MACRO. Vadose Zone J. 2: 349–357.

Schaap, M.G., and F.J. Leij. 2000. Improved prediction of unsaturated

hydraulic conductivity with the Mualem–van Genuchten. Soil Sci. Soc. Am. J. 64:843–851.
Schaap, M.G., F.J. Leij, and M.Th. van Genuchten. 2001. ROSETTA: A computer program for estimating soil hydraulic parameters with hierarchical pedotransfer functions. J. Hydrol. (Amsterdam) 251: 163–176.
Simunek, J., N.J. Jarvis, M.Th. van Genuchten, and A. Gärdenäs. 2003. Review and comparison of models for describing non-equilibrium and preferential flow and transport in the vadose zone. J. Hydrol. (Amsterdam) 272:14–35.
Soet, M., and J.N.M. Stricker. 2003. Functional behaviour of pedotransfer functions in soil water flow simulation. Hydrol. Process. 17: 1659–1670.
Soil Survey Staff. 1994. Keys for soil taxonomy. 6th ed. USDA-SCS, Washington, DC.
Tiktak, A., and W. Bouten. 1992. Modelling soil water dynamics in a forested ecosystem. III: Model description and evaluation of discretization. Hydrol. Process. 6:455–465.
Tiktak, A., and W. Bouten. 1994. Soil water dynamics and long-term water balances of a Douglas fir stand in the Netherlands. J. Hydrol. (Amsterdam) 156:265–283.
van Alphen, B.J., H.W.G. Booltink, and J. Bouma. 2001. Combining pedotransfer functions with physical measurements to improve the estimation of soil hydraulic properties. Geoderma 103:133–147.
van Genuchten, M.Th. 1980. A closed-form equation for predicting the hydraulic conductivity of unsaturated soils. Soil Sci. Soc. Am. J. 44:892–898.
Vanderkwaak, J.E., P.A. Forsyth, K.T.B. MacQuarrie, and E.A. Sudicky. 1997. WatSolv- sparse matrix interative solver, user's guide for version 2.16. University of Waterloo, Waterloo, Canada.
Vilette, S. 1994. Etablissement du bilan hydrique sur une chronosequence de peuplement de Douglas (*Pseudotsuga menziesii* (Mirb.) Franco). (In French.) ENESA-ENITA/INRA, Dijon.
Volaire, F., and F. Lelièvre. 2001. Drought survival in Dactylis glomerata and Festuca arundinacea under similar rooting conditions in tubes. Plant Soil 229:225–234.
Vrugt, J.A., J.W. Hopmans, and J. Simunek. 2001. Calibration of a two-dimensional root water uptake model. Soil Sci. Soc. Am. J. 65:1027–1037.
Wagner, B., V.R. Tarnawski, V. Hennings, U. Muller, G. Wessolek, and R. Plagge. 2001. Evaluation of pedo-transfer functions for unsaturated soil hydraulic conductivity using an independent data set. Geoderma 102:275–297.
Wösten, J.H.M., C.H.J.E. Schuren, J. Bouma, and A. Stein. 1990. Functional sensitivity analysis of four methods to generate soil hydraulic functions. Soil Sci. Soc. Am. J. 54:832–836.
Wösten, J.H.M., A. Lilly, A. Nemes, and C. Le Bas. 1999. Development and use of a database of hydraulic properties of European soils. Geoderma 90:169–185.
Wösten, J.H.M., Ya. A. Pachepsky, and W.J. Rawls. 2001. Pedotransfer functions: Bridging the gap between available basic soil data and missing soil hydraulic characteristics. J. Hydrol. (Amsterdam) 251:123–150.

ERRATA

Preferential Flow Revealed by Hydrologic Modeling Based on Predicted Hydraulic Properties

FRÉDÉRIC GÉRARD, MARK TINSLEY, AND K. ULRICH MAYER

Soil Sci. Soc. Am. J. 68:1526–1538.

On page 1528, Eq. [7] is incorrect. Equation [7] should read as follows:

$$\mathrm{PET} = T + E_u + f_i I$$

Amelioration of Degraded Rain Forest Soils by Plantations of Native Trees

R. F. FISHER

Soil Sci. Soc. Am. J. 59:544–549.

Table 3 (p. 546) gave incorrect data. The correct table is printed below.

Table 3. Soil organic matter in the upper 15 cm of soil before and after 3 yr of occupancy by various species

	Soil Organic Matter	
	1987	1992
Species	g kg^{-1}	
Control (pasture)	77	70*
Virola koschnyi	74	76
Stryphnodendron microstachyum	75	76
Vochysia guatemalensis	74	82*
Pithecellobium macradenium	76	77
Pinus tecunumanii	77	75
Hieronyma alchorneoides	78	80
Gmelina arborea	78	76
Vochysia ferruginea	74	81*
Inga edulis	74	74
Acacia mangium	73	77*
Pentaclethra macroloba	73	72

* Significantly different at the 0.05 probability level.

Characterizing Water Dependent Soil Repellency with Minimal Parameter Requirement

C. M. REGALADO AND A. RITTER

Soil Sci. Soc. Am. J. 69:1955–1966.

The acknowledgments section was incomplete. The authors acknowledge additional funding for their research. Their work was financed with funds of the INIA-Programa Nacional de Recursos y Tecnologas Agroalimentarias (Projects RTA2005-228 and RTA01-097).

Insect Infestations Linked to Shifts in Microclimate: Important Climate Change Implications

A. T. CLASSEN, S. C. HART, T. G. WHITMAN, N. S. COBB, AND G. W. KOCH

Soil Sci. Soc. Am. J. 2005 69: 2049–2057

T. G. Whitman is incorrectly spelled in the author list. The correct spelling is T. G. Whitham.

Synthèse : prise en compte de la matière organique naturelle dans les modèles de spéciation et applications

Dudal Y. et Gérard F. (2004) Accounting for natural organic matter in aqueous chemical equilibrium models: a review of the theories and applications. *Earth-Science Reviews* **66**, 199-216.

Available online at www.sciencedirect.com
SCIENCE DIRECT®
Earth-Science Reviews 66 (2004) 199–216
EARTH-SCIENCE REVIEWS
www.elsevier.com/locate/earscirev

Accounting for natural organic matter in aqueous chemical equilibrium models: a review of the theories and applications

Yves Dudal[a,*], Frédéric Gérard[b,1]

[a] INRA, Unité Climat, Sol et Environnement, Domaine Saint-Paul, Site Agroparc, 84914 Avignon Cedex 9, France
[b] INRA, Unité Biogéochimie des Ecosystèmes Forestiers, Forêt d'Amance, 54280 Champenoux, France

Received 7 May 2003; accepted 21 January 2004

Abstract

Soil organic matter consists of a highly complex and diversified blend of organic molecules, ranging from low molecular weight organic acids (LMWOAs), sugars, amines, alcohols, etc., to high apparent molecular weight fulvic and humic acids. The presence of a wide range of functional groups on these molecules makes them very reactive and influential in soil chemistry, in regards to acid–base chemistry, metal complexation, precipitation and dissolution of minerals and microbial reactions. Out of these functional groups, the carboxylic and phenolic ones are the most abundant and most influential in regards to metal complexation. Therefore, chemical equilibrium models have progressively dealt with organic matter in their calculations.

This paper presents a review of six chemical equilibrium models, namely NICA-Donnan, EQ3/6, GEOCHEM, MINTEQA2, PHREEQC and WHAM, in light of the account they make of natural organic matter (NOM) with the objective of helping potential users in choosing a modelling approach. The account has taken various faces, mainly by adding specific molecules within the existing model databases (EQ3/6, GEOCHEM, and PHREEQC) or by using either a discrete (WHAM) or a continuous (NICA-Donnan and MINTEQA2) distribution of the deprotonated carboxylic and phenolic groups.

The different ways in which soil organic matter has been integrated into these models are discussed in regards to the model-experiment comparisons that were found in the literature, concerning applications to either laboratory or natural systems. Much of the attention has been focused on the two most advanced models, WHAM and NICA-Donnan, which are able to reasonably describe most of the experimental results. Nevertheless, a better knowledge of the humic substances metal-binding properties is needed to better constrain model inputs with site-specific parameter values. This represents the main axis of research that needs to be carried out to improve the models. In addition to humic substances, more non-humic compounds should also be introduced in model databases, notably the ones that readily interact with the soil microorganisms. Thermodynamic data are generally available for most of these compounds, such as low molecular-weight organic acids. However, the more complex non-humic substances, exhibiting a ratio of hydrophobic versus hydrophilic bonds lower than humic substances, need to be further characterised for a comprehensive implementation in chemical equilibrium models.

Keywords: Modelling; Metal complexing; Organic acids; Humic acids; Soils; Aqueous solutions

1. Introduction

The 1960s were the birth of geochemical models based on the recent development of both computing

* Corresponding author. Fax: +33-4-32-72-22-12.
E-mail addresses: Yves.Dudal@avignon.inra.fr (Y. Dudal), gerard@nancy.inra.fr (F. Gérard).
[1] Fax: +33-3-83-39-40-69.

0012-8252/$ - see front matter © 2004 Elsevier B.V. All rights reserved.
doi:10.1016/j.earscirev.2004.01.002

capacities and aqueous geochemistry (Garrels and Thompson, 1962; Helgeson, 1968, 1969; Helgeson et al., 1969; Stumm and Morgan, 1970). Their first objective was to predict chemical speciation in water from thermodynamic laws, and the reaction-path followed by a water–mineral system toward a thermodynamic equilibrium state (i.e. the feasibility and the extent of mass transfers between water and reacting solids). Most of the chemical entities included in the calculations were of inorganic nature, although the metal-complexing capacities were known for a number of organic compounds (Chaberek and Martell, 1959). However, difficulties associated with their detection and quantification in aqueous media as well as their behaviour in solutions prevented their introduction within model databases. In a thorough review of the existing geochemical models, Bassett and Melchior (1990) already underlined the need for further research regarding thermodynamic and kinetic data advancements, coupled hydrology and chemistry, and the introduction of organic compounds (natural organic matter and anthropogenic organic compounds). Considerable improvements on the first topics have been carried out until recently (Sparks and Suarez, 1991; Johnson et al., 1992; McNab and Narasimhan, 1993; Suarez and Simunek, 1996; Gérard et al., 1998; Mayer et al., 2002).

The research on organic compounds has been enriched in this last decade through the development of analytical techniques (Piccolo and Conte, 1998; Hatcher et al., 2001). However, the NOM present in soil solutions and surface waters consists of an incredibly complex mixture of compounds, ranging from simple low molecular weight organic acids (LMWOAs) or sugars to high apparent molecular weight humic acids, and the humin fraction (Hayes and Clapp, 2001). The chemical properties of NOM and its role in most soil processes, such as metal complexation, cation exchange capacity and chemical weathering, have been well identified (Stevenson, 1994). These improvements have led to the development of aqueous equilibrium models that include new concepts or new molecules.

The present study aims at reviewing the science underlying these concepts as well as the real cases on which the new models are being applied in order to help potential users in choosing a modelling approach. The paper is organised along four consecutive questions: why should we account for NOM in chemical equilibrium models? How do the existing models take it into account? Is it enough based on comparisons between model and experiments? And how could they be improved? In the following sections, these questions are addressed in light of several chemical equilibrium models considered to be the most comprehensive, as they can describe a wide range of aqueous chemical equilibrium reactions of different nature. We have selected six models that consider natural organic matter; these are Eq3/6 (Wolery, 1992), Geochem progenies' such as Geochem-PC and Soilchem (Parker et al., 1995; Sposito and Coves, 1995), Minteqa2 (Allison and Brown, 1995), Nica-Donnan (Keiser and Van Riemsdijk, 2002), Phreeqc (Parkhurst and Appelo, 1999) and Wham (Tipping, 1998).

2. Main chemical equilibrium processes

The core of chemical equilibrium models resides in the use of the ion-association approach, also called the Debye–Hückel model, to calculate the activity coefficient of charged aqueous species in dilute waters. The corresponding equation can take slightly different forms, as proposed by Davies (1962) and Helgeson (1969), referred to as the Davies and B-dot equations, respectively. Two selected aqueous chemical equilibrium models (Eq3/6 and Phreeqc as Phreeqpitz) also propose the ion-interaction approach developed by Pitzer (1979), which relies on empirical coefficients to describe ion complexing at high ionic strength (I>0.3 M) as the ion-association description looses accuracy (Pitzer and Kim, 1974).

2.1. Basic speciation and phase equilibrium

Acid–base and oxydo-reduction reactions, metal complexation and mineral dissolution/precipitation are described in the six models as aqueous phase equilibrium. Some of these models can also consider these reactions by using various kinetic expressions. However, this topic is beyond the scope of the present study. The input value of the solution pH in conjunction with the thermodynamic equilibrium constants registered in the database for acid–base reactions (pK_a) is used to calculate the speciation of acids and bases. Similarly, the redox potential (Eh) is used to

distribute the members of redox couples according to the thermodynamic constants of half reactions. Complexation and chelation, as ion pairing, are also treated as aqueous phase equilibrium between a ligand and a free metal ion, or simply between two ions present in the solution. After the speciation of the initial solution, an ion activity product (IAP) is calculated for each mineral registered in the database (with possible exclusions by the user) and compared to its equilibrium constant (K) through a saturation index, SI (with SI = IAP/K). The saturation index is indicative of the direction of the reaction that can spontaneously proceed in order to attain an equilibrium condition. As a convention, precipitation or dissolution can occur if SI>1 or SI < 1, respectively. If mass transfer from the mineral to the solution (dissolution) or vice versa (precipitation) is required to reach an equilibrium, the aqueous speciation is recalculated in response to corresponding variations in total concentrations.

2.2. Surface interaction equilibrium

Most chemical equilibrium models take into account some of the interactions occurring between the aqueous phase ions and the surface species. Sorption of aqueous ions onto specific surface sites can be described using non-electrostatic or electrostatic models. Non-electrostatic sorption is described using either a simple equilibrium distribution coefficient (K_D) of the component between the aqueous phase and the solid phase or the Langmuir or Freundlich models (Stumm and Morgan, 1996). This quantification of sorption phenomena does not consider any charge involvement in the surface attraction forces. In contrast, the electrostatic sorption models describe the charge-based attraction of anions and cations by positively and negatively charged surface sites, respectively. The widely used double-layer model considers a first layer of counter ions covering the surface and a second diffuse layer of ions balancing the charge difference created by the first layer.

Ion-exchange reactions between aqueous phase cations and exchanger organic or mineral phases can also be modelled using various selectivity coefficient descriptions for the major cations. In this case, knowledge of selectivity coefficients for each cation as well as the charge fraction (Gaines–Thomas convention) or the molar fraction (Vanselow convention) or the concentration (Gapon convention) in exchangeable cations of the exchanger allows the calculation of their activity in the aqueous phase (Appelo and Postma, 1996).

3. Why should NOM be accounted for in chemical equilibrium speciation models?

3.1. The nature of NOM

A great diversity of organic molecules of both humic and non-humic nature constitutes NOM in soils and sediments. They originate from the partial decomposition of plant and animal litter by microorganisms and they undergo abiotic transformations in soils (Stevenson, 1994). Non-humic substances, which can be called biochemical compounds, are mainly carbohydrates, amino-acids, peptides or proteins, lipids and a wide range of organic acids (Sposito, 1989). As a source of nitrogen and phosphorous, they can be part of the microbial metabolism and they sustain a lot of the "easily mineralisable" fraction of SOM (Stevenson, 1994). In contrast, our knowledge about humic substances is still partially hypothetical in terms of structure and focuses a lot of attention and debate (Burdon, 2001; MacCarthy, 2001). These organic substances include fulvic acids (FA) and humic acids (HA) with apparent molecular weights of a few hundred and a few thousand daltons, respectively, and humin (Stevenson, 1994; Derenne and Largeau, 2001; Piccolo, 2001; Rice, 2001). This fractionation of HS originates from the separation protocol based on the use of aqueous solvents, bases and acids (Hayes et al., 1996). It has long been considered that these apparent high molecular weight organic compounds exhibited a complex tridimensional structure either as coil or as micelles, based on covalent associations (Ghosh and Schnitzer, 1980; Wershaw, 1999; Hayes and Clapp, 2001). However, recent strong evidence have been gathered for a supramolecular structure of HS, where smaller bio-molecules are associated through weak dispersive forces (hydrophobic or hydrogen bonds), responsible for the apparent large molecular size (Piccolo, 2001; Buurman et al., 2002; Kim et al., 2003). This supramolecular structure can explain some of the reactivity of these

molecules (Lopez et al., 2003; Piccolo et al., 2003). Also included in the HS, the humin fraction may be considered as a mixture of organic matter and clay, linked by covalent or strong hydrogen bonds (Derenne and Largeau, 2001). The complete knowledge of the structure and composition of NOM is made almost impossible by all these aspects (MacCarthy, 2001). Therefore, further understanding of organic matter is gained by studying its properties and functions in soils.

3.2. The properties of NOM

Three general properties represent the major characteristics of NOM and can explain its fundamental behaviour in soils; polyfunctionality, macromolecular charge and hydrophilicity.

NOM owns a wide range of different functional groups, which are responsible for its reactivity. One key element in these groups is oxygen (Steelink, 1985). Thus, the oxygen content of organic matter or more precisely the oxygen to carbon ratio gives a good estimate of organic matter affinities for proton and metal binding. The O/C ratio of FA is stronger (0.7) than the one for HA (0.5) partially explaining its greater reactivity (Steelink, 1985). The oxygen-containing functional groups, mostly carboxylic and phenolic groups, are ubiquitous in organic matter. Their distribution can be seen from the derivatives of the titration curves (Fig. 1a) of purified humic materials where no distinct breaks in the curves are visible (Sposito et al., 1982b). The analysis of proton-binding curves measured over a wide pH range usually shows evidence for a bimodal distribution of the affinity sites. The observation of a continuous presence of a large number of functional groups combined to their closeness in a rather small volume leads to what has been called the delocalisation effect where the pK_a of two adjacent groups interfere (Perdue, 1985).

The deprotonation of carboxylic groups (pK_a's around 4) and phenolic groups (pK_a's around 10) induces the development of negative charges, responsible for the polyelectrolyte character of HS and for their macromolecular charge (Perdue, 1985; Stevenson, 1994). The occurrence of negative charges gives NOM the ability to bind dissolved cations and to be adsorbed at reactive sites of a positive charge at the surface of clays and (oxy)hydroxides (Stevenson, 1994; Cheshire et al., 2000). Metal binding by NOM, and more specifically by HS, also occurs within the diffuse layer by means of electrostatic interactions. The diffuse layer is responsible for the effect of the ionic strength on the charging behaviour of HS and thus on their capacity to bind metals. Once deprotonated, the oxygen-containing functional groups can form hydrogen bonds with the surrounding water molecules and become solvated. This property allows an important fraction of NOM to become soluble and to be further transferred from soils to groundwater and surface waters (Currie et al., 1996; Oste et al., 2002).

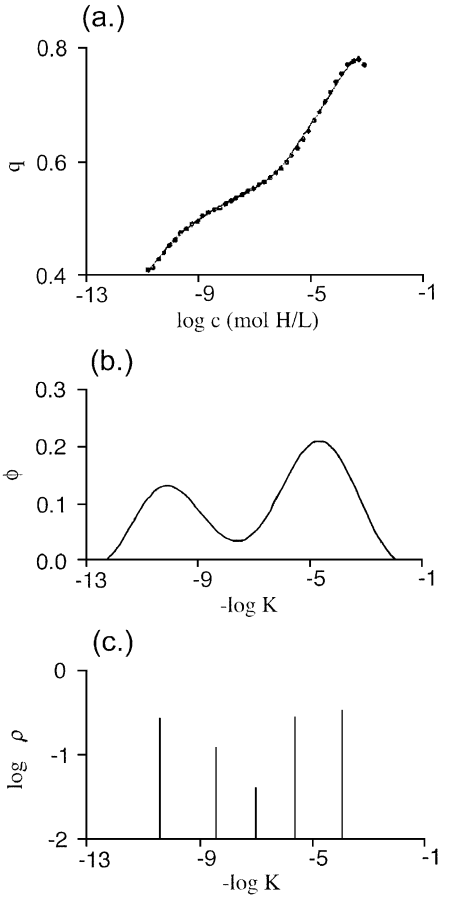

Fig. 1. Acid–base titration of an aquatic humus as a function of pH (a) Discrete model (b) and continuous model (c) fit to the experimental titration data (adapted from Warren and Haack, 2001, initially adapted from Černick et al., 1995).

3.3. The functions of NOM

The intrinsic properties of NOM are responsible for its functions in natural environments such as soils, when in contact with other soil constituents like the inorganic matrix (clay, iron or aluminium oxyhydroxides, sand), metals in various forms and the biological matrix (microorganisms, roots). These functions can be classified into three broad categories: physical (soil aggregation), chemical (cation exchange capacity, acidity and metal reservoir) and biological (detoxification, micronutrient carrier, source of mineralisable C and N). In particular, microorganisms, which are prolific in most soils, are very reactive towards NOM. Heterotrophic bacteria use a wide range of organic molecules present in the soil as a source of energy. The catabolism of these organic substrates leads to metabolites that have great implications in the soil chemistry (Dassonville and Renault, 2002). Under aerobic conditions, the major product of organic decomposition is CO_2, which mostly acts on the acid–base equilibrium of the soil. However, under anaerobic conditions, which can be found in water-saturated soils or in some micro-sites where soil aggregation has limited the oxygen transfer, bacteria metabolise organic substrates by reducing different terminal electron acceptors (nitrate, sulfate, iron or manganese in oxides). Such reactions play an important role in the soil redox environment and lead to a wide variety of stable organic metabolites, mostly LMWOAs like acetate, lactate, pyruvate, etc. (Küsel and Drake, 1999). These compounds are metal ligands but their appearance is not taken into account in chemical equilibrium models. Similarly, the microbially driven increase in the CO_2 pressure is usually not considered in the models, despite the potential implications regarding metal binding through pH variations and the formation of metal–carbonate complexes. Furthermore, it has recently been shown that bacteria are also responsible for the production of refractory dissolved organic matter, from simple labile compounds such as glucose and glutamate (Ogawa et al., 2001). Finally, it has to be noticed that microorganisms can act as binding sites for macromolecular organic compounds and metals, and therefore can influence in another way the soil chemistry (Fein et al., 2002; Frost et al., 2003; Kaiser, 2003).

Thus, organic matter acts as a major constituent of soils in terms of its physical, chemical and biological functions and any realistic reconstitution of what is happening in a soil will have to integrate these organic matter functions. Similarly, aqueous chemical equilibrium models should ultimately be able to cope with the functions of NOM in soils. Section 4 takes a closer look at how the present-day models listed earlier account for the great diversity of the functions of NOM.

4. How do the existing models cope with NOM?

4.1. Non-humic substances

The family of non-humic substances most accounted for in the geochemical models is the LMWOAs. These organic acids play a major role in the functioning of the bulk soil (Lundström, 1993) and in microenvironments such as the rhizosphere (Jones, 1998). Their ligand properties are responsible for the formation of metal–ligand complexes, and thus lead to diminish the bio-toxicity of metals, to increase the solubility of minerals and to enhance their dissolution rate. LMWOAs are ubiquitous in soil solutions, but may also be sorbed onto the mineral matrix (Jones and Brassington, 1998). Malate, citrate, acetate and oxalate have been shown to be the most abundant LMWOAs found in the soil solution (Jones and Brassington, 1998). These acids are degradation products of the original organic matter but also originate from the Krebs cycle of the microbial metabolism and therefore exhibit both abiotic and biological origins. Two different approaches have been developed to describe the LMWOAs contribution to aqueous geochemistry. First, they have been considered as bulk participants to the overall soil solution acidity and metal-complexing capacity, and therefore are described with the other acidic components (humic and fulvic acids; see Section 5). Secondly, the default database of some geochemical models, such as MINTEQA2 (Allison and Brown, 1995), GEOCHEM-PC (Parker et al., 1995) and EQ3/6 (Wolery, 1992), contains a number of LMWOAs as master species. The first 2 models and their default thermodynamic database appear the richest in this domain as about 20 LMWOAs have been registered.

In contrast, the formation of complexes between organic ligands and some metal cations may be insufficiently described. For example, the database of the EQ3/6 model registers 2 organic acids only, acetic and phthalic, but has critical equilibrium values for up to 105 complexes between cations and acetate, covering most of the periodic chart of elements. In comparison, 38 metal–acetate complexes are registered in the GEOCHEM-PC model and 41 in MINTEQA2. The second family of non-humic substances found in the databases of some geochemical models (MINTEQA2 and GEOCHEM-PC) is made of amines. These compounds, contrary to organic acids, can be positively charged and therefore have the property to bind anions. Nevertheless, they can also be implicated in complex formations with metal cations (Martell and Smith, 1975). Methylamine, ethylenediamine, trimethylamine, isopropylamine, hexylamine and others have been listed in MINTEQA2, but only for their interactions with protons and metal cations. Similarly, hydroxylamine is registered in GEOCHEM-PC for its interactions with metal cations.

In addition to the low molecular weight organic acids already mentioned, the databases of some geochemical models (MINTEQA2 and GEOCHEM-PC) list some polyprotic organic acids of higher molecular weight, such as ethylenediamine-tetraacetate (EDTA), nitrilotriacetate (NTA) or cyclohexyldiaminetetraacetate (CDTA). These molecules are very strong ligands for metal cations with stability constants for their complex formation orders of magnitude greater than those of LMWOAs (Chaberek and Martell, 1959). Amino acids represent another family of organic compounds usually found in soils (Stevenson, 1994; Senwo and Tabatabai, 1998) and are partially taken into account in geochemical models, as seen in GEOCHEM-PC, but also in MINTEQA2. The former lists most of the 20 amino acids and their interactions with some metal cations, such as iron, manganese, copper, zinc and nickel.

One should observe that the values of the complexation and protonation constants can also vary from one database to another. Generally, these values are mostly based on the works of Martell and Smith (1974, 1975, 1976, 1977). Improvements in analytical techniques have led to corrections for some equilibrium constant values as well as values for additional metal–ligand complexes (Martell and Smith, 1982, 1989; Serkiz et al., 1996). Therefore, care has to be taken in the choice of a model to describe complex formation between non-humic substances and metal cations, not only according to the number of metal–ligand complexes but also to the accuracy of the stability constants introduced in databases (Smith and Martell, 1995). Nevertheless, enlightened model users will update the default database with the latest refined values of protonation and metal–ligand stability constants available in the most recent literature (see for example Smith and Martell, 2001). It clearly comes from this that the accessibility of the model thermodynamic database to change the value of a given equilibrium constant and to add new species has to be a criterion to be considered.

From the above list of non-humic substances introduced in the databases of geochemical models, it can be seen that proton and metal binding is the major function of the organic matter that is taken into account. The same observation can be made for humic substances.

4.2. Humic substances

Two main types of geochemical models have been developed to describe the distribution of proton and metal binding to HS and are referred to as humic ion-binding models.

4.2.1. Continuous site distribution—the NICA-Donnan model

The first one is based on a continuous site distribution (Fig. 1b) and states that the distribution of the metal-binding functional groups follows statistical rules, and that the p*K*'s are distributed normally along the molecule (Perdue et al., 1984; Susetyo et al., 1990; Grimm et al., 1991). This approach has been introduced in the MINTEQA2 model, where both carboxylic and the weaker phenolic functional groups may be considered for proton binding using two mean stability constants and the corresponding standard deviation (Allison and Brown, 1995). Nevertheless, this model appears limited by using a mean binding constant to represent metal binding. A random approach of the issue has been proposed by Grzyb (1995), wherein the ionic balance of the solution is used to estimate the binding parameters. A normal log distribution of proton-binding sites is also considered. However,

the distribution of binding sites is limited to carboxylic sites only and, as in the MINTEQA2 model, there is no explicit consideration of electrostatic cation binding. A much more mechanistic formulation has been developed by Van Riemsdijk and co-workers (Benedetti et al., 1995; Kinniburgh et al., 1996) and incorporated in the more comprehensive ECOSAT model (Keiser and Van Riemsdijk, 2002). It describes specific binding of ions to carboxylic and phenolic sites (named A-type sites and B-type sites, respectively) with a non-ideal competitive adsorption model (NICA). Electrostatic interactions are represented by means of a simple Donnan model comprehensively discussed in Benedetti et al. (1996a). The first version of the corresponding NICA-Donnan model assumes only monodentate binding of metals to proton-binding sites. This led to the release, at most, of one proton per metal ion bound, but did not fit well some experimental data. For example, the ratio of proton release by HS caused by the binding of Cu^{2+} should be two in case of monodentate association, but measured values were invariably less. This was also the case for other divalent cations such as Ca^{2+} and Cd^{2+}. To allow the reduction of the positive correlation between the binding site distributions of the proton and the metal cation, Kinniburgh et al. (1999) developed a new version of the model allowing variable stoichiometry of metal-binding to proton-binding sites (from monodentate to tridentate). This was done by redefining a thermodynamically consistent NICA equation. The corresponding model, temporarily renamed NICA-Donnan to point out its consistency, requires seven parameters for each humic substance in order to simulate non-specific and specific proton binding at different ionic strengths. For each type of binding sites, input parameters correspond to the median value of the distribution of the proton-binding constants ($K_{H(A)}$ and $K_{H(B)}$), the proton-binding site density (Q_A and Q_B) and a normal distribution parameter ($m_{H(A)}$ and $m_{H(B)}$), which represents the heterogeneity of the relevant proton-binding constant centred on the median value. The Donnan volume, noted b, is the key parameter for non-electrostatic effects and has an influence on electrostatic interactions as well. Five additional parameters per metal cation are required to represent metal binding by HS. For a given metal cation m, parameters are a median intrinsic stability constant ($K_{m(A)}$ and $K_{m(B)}$) and a non-ideality coefficient measuring the apparent heterogeneity of the humic substance ($n_{m(A)}$ and $n_{m(B)}$) corresponding to each type of proton-binding sites (A and B). The fifth parameter is used in order to account for the variable stoichiometry of metal-binding to proton-binding sites.

4.2.2. Discrete site distribution—the WHAM model

The second type of model is based on a discrete distribution of binding sites (Fig. 1c) as opposed to a continuous one. This model type relies on the selection of a certain number of characteristic binding sites to represent the whole behaviour of the molecule. For instance, two fulvic acid sites, FULV1 and FULV2, and binding parameters regarding metal cations are listed in the shared database of the GEOCHEM-PC and SOILCHEM models. This feature is inherited from the precursor study done by Sposito et al. (1981), who fitted conditional stability constants for the binding of several metals by different FAs. However, such binding parameters may be only valid at pH = 5, because they result from experiments performed at a fixed pH (Lamy et al., 1994). In a similar manner, authors have come up with organic acid analogues, where analogue mono-, di- and triprotic carboxylic acids describe the acidity of surface waters and the formation of organic-Al species (Driscoll et al., 1994). Such an approach has also been successfully developed for acidic soil solutions (Lundström, 1993). It is obvious that such discrete site-type approaches do not satisfactorily account for the mechanisms leading to the binding of proton and metals to HS; hence, the apparent strength of the binding constants and the limited interest of these models. To illustrate this matter, Lundström (1993) estimated different values for the Al-binding constant depending on the season. As a matter of fact, these variations may be due to a number of causes, like some variations in the density of the binding sites, and are not necessarily due to seasonal variations in the properties of HS.

Alternatively, a mixture model has been proposed by Sposito et al. (1982a) in the GEOCHEM-PC model. This approach lies in the use of a set of simple organic acids with contrasting well-defined acid–base and metal-binding properties to simulate the behaviour of HS, and was applied to FA. A random approach to the problem has been developed to generate discrete artificial molecules representing the distribution

of specific metal-binding sites (Murray and Linder, 1983). The random molecular structures are generated from a number of parameters: the percentage of carbon, hydrogen and oxygen, the concentration of functional groups, the percentage of aromaticity and the molecular mass of HS. From these data, a mixture of ligands can be computed, for which the metal-binding stability constants are known. This approach has been developed for both FA and HA and takes into account cation binding by electrostatic effects. It has been used in conjunction with the PHREEQE speciation model (Mountney and Williams, 1992; Bryan et al., 1997), which is an older version of the PHREEQC model.

A more mechanistic development of the discrete binding sites approach has been proposed by Tipping and Hurley (1992) by means of the first version of the WHAM model (WHAM stands for Windemere Humic Aqueous Model). Successive versions of this simulator have been released, from model IV to model VI, according to the implementation of new features for a better representation of proton and metal binding to HS under different conditions (ionic strength, presence of competing cations). The WHAM model is centered on carboxylic and phenolic-type functional groups (A-type sites and B-type sites, respectively), where each type site is evenly divided into four different subsites. Electrostatic effects are accounted for via a Donnan-type expression to permit the simulation of counterion (metals) accumulation in the diffuse layer of HS. Tipping (1998) pointed out the great similarity between the WHAM model and the NICA-Donnan formulation implemented in the ECOSAT model (see above), although they are based on a discrete or continuous representation of the binding properties of HS, respectively. This similarity implies that the same number of parameters is required to characterise HS in both models. In summary, input parameters involved in the WHAM model for FA and HA are density parameters for carboxylic and phenolic sites ($n_{(A)}$ and $n_{(B)}$, respectively), two median intrinsic proton-binding constants ($pK_{(A)}$ and $pK_{(B)}$), two distribution parameters describing the spread of proton-binding constants around the median ($\Delta pK_{(A)}$ and $\Delta pK_{(B)}$) and an electrostatic term (p). In WHAM, however, the density of phenolic sites is not user-set but calculated from the density of carboxylic sites using the empirical relation $n_B = n_A/2$. Four parameters are needed to describe the complexation of metal cations with HS at carboxylic and phenolic sites as well as two median intrinsic stability constants ($pK_{m(A)}$ and $pK_{m(B)}$) and two heterogeneity values ($\Delta pK_{m(A)}$ and $\Delta pK_{m(B)}$). This model incorporates bidentate and tridentate complexation between metals and pairs and triplets of sites, and the occurrence of multidentate complexes depends on a theoretical proximity factor, noted f, which defines whether pairs of proton-binding sites are close enough or not to form multidentate sites for metals. Prior to the introduction of capabilities for a variable stoichiometry of metal-binding to proton-binding sites in the NICA-Donnan model (Kinniburgh et al., 1996), Tipping (1998) consistently showed that the WHAM model reproduced the displacement of protons by metals better than the NICA-Donnan model.

Both models can also simulate interactions between metals and undissolved HS. Metal and proton binding by this type of organic matter is represented by the mean of a standard HS taken separately from dissolved HS. A mixture with inorganic phases can also be considered to simulate the influence of suspended particulate matter (SPM). In WHAM, this is feasible by coupling the code with the SCAMP model (Lofts and Tipping, 1998). In the resulting simulator, called the WHAM-SCAMP model by Lofts and Tipping (2000), SPM can be constituted of HS, clay minerals and various oxides. A surface complexation submodel and an electrostatic submodel are used for proton and metal binding to oxides and cation exchange on clays, respectively.

Principal numerical models and the effect of NOM on major aqueous geochemical processes have been presented. In Section 5, their application and comparisons with experimental and field data will be discussed.

5. Has organic matter been well accounted for? Examples of model applications

Studies of metal-organic interactions in natural systems by using a chemical equilibrium model have become progressively more frequent and realistic in the recent years. The number of their applications to natural systems is even now comparable to those carried out under controlled and thus rather simple

systems, in the laboratory, which involve purified organic substances.

5.1. Laboratory applications

The laboratory applications are performed for various purposes; mainly for the determination of generic model parameter values by fitting simulations to measurements of proton or/and metal binding, and to test the robustness of database parameters to reproduce laboratory observations.

For example, Kerven et al. (1995) studied the interactions between dissolved aluminium and mixtures of oxalic and citric acids using GEOCHEM-PC (see above) and NMR spectroscopic measurements of Al-organic compounds. They found large discrepancies between computed and measured values, which were ascribed to unreliable equilibrium constants in the database.

In regards to the interactions between inorganic solutes and HS, which form the vast majority of the laboratory applications of chemical equilibrium models, Tipping et al. (1995b) have used the WHAM model to simulate proton and copper binding by HA at different ionic strengths. Discrepancies were assigned to differences in the binding properties of the given HA, and reasonable results have been found by adjusting intrinsic metal-binding parameters. Such optimised values have enriched the default database. The same approach has been used in Kinniburgh et al. (1996), who fitted the NICA-Donnan model to data for H, Ca, Cd, Cu and Pb non-competitive binding with peat HA. Model robustness was tested by Benedetti et al. (1996a) in comparing the results of the Donnan component of the NICA-Donnan model to six different HS data sets of proton-binding curves, representing a wide range of pH and salt level. Farmer and Lumsdon (2001) challenged the WHAM model for its ability to simulate the binding of Al in a mixture of Ca-fulvate and a proto-imogolite sol in order to study the podzolisation process. Rather large discrepancies between the simulation and measurements have been found and these divergences have been ascribed to the inadequacy of the WHAM model to reproduce Al-Ca-fulvate-proto-imogolite equilibria. A number of other examples of proton- and metal-HS-binding experiments, sometimes involving several metals (i.e. competition experiments), fit to WHAM or its competitor, the NICA-Donnan model can be found in the literature (Benedetti et al., 1995; Pinheiro et al., 1999).

In his presentation paper of the latest development of WHAM (i.e. model VI; see Section 4.2.2), Tipping (1998) obtained some ''best-average'' or generic parameter values by fitting to 19 sets of published data for proton binding and 110 sets for metal binding. As a result, intrinsic metal-binding parameters for 22 metal species have been derived (Table 1). Well-constrained experimental systems have also been studied in a goal of model comparisons in Christensen et al. (1998), who challenged the WHAM model and the NICA-Donnan model for their ability to fit proton-binding curves at different ionic strengths for purified FA of various origins, ages and structures. Based on the observation that the use

Table 1
List of metal cations for which a generic value of the binding parameters with humic substances are available in the WHAM and NICA-Donnan models

Metal ion
Al^{3+}
Am^{3+}
Ba^{2+}
Ca^{2+}
Cd^{2+}
Cm^{3+}
Co^{2+}
Cr^{3+}
Cu^{2+}
Dy^{3+}[a]
Eu^{3+}
Fe^{2+}
Fe^{3+}
Hg^{2+}[b]
Mg^{2+}
Mn^{2+}
Ni^{2+}
Pb^{2+}
Sr^{2+}
Th^{4+}
UO_2^{2+}
VO^{2+}[a]
Zn^{2+}

[a] Metal ion absent from WHAM default databases for metal-binding by humic substances, although model parameters have been derived by fitting to experimental data in Tipping (1998, Summary, Table 10, p. 34).

[b] Metal ion absent from the summary table in Tipping (1998, Table 10, p. 34), since binding parameters have been estimated from competition experiments by using generic parameter values for the other metals derived from separate experiments.

of default values for proton-binding properties compared to site-specific values gave more stable results in the WHAM model than the NICA-Donnan model, Christensen et al. (1998) concluded that the WHAM model was the most practical as it may be used in different fields by implementing default parameters without suspecting large deviations. However, serious improvements should be expected using generic parameter values consistent with the NICA-Donnan model recently derived by Milne et al. (2001) for proton-binding, and Milne et al. (2003) for 23 metal ions (see Table 1), since they fitted the model to a much greater number of experimental data than Tipping (1998). Further model comparisons involving more recent model versions will be discussed in the following subsections.

A more marginal use of chemical equilibrium models coping with organic matter in experimental systems concerns the validation of new methods to measure aqueous metal speciation. Excellent recent examples of this can be found in Göttlein (1998), Temminghoff et al. (2000), Oste et al. (2002) and Weng et al. (2001a, 2002b). The study accomplished by Weng et al. (2002b) reveals to be of particular interest to lead to Section 5.2, as together with experiments involving a HA purified from a forest soil, the authors used NICA-Donnan to test their method in natural systems.

5.2. Model applications to natural systems

A number of applications of chemical equilibrium models to problems involving inorganic and organic interactions have been performed in natural systems.

5.2.1. Analogue models

The simplest ones consisted in the use of the aforementioned analogue models (Lundström, 1993; Driscoll et al., 1994). The triprotic analogue model along with proton- and metal-binding parameters proposed by Driscoll et al. (1994) have been implemented in several geochemical models to study Al speciation in soil and stream waters (Boudot et al., 2000; Maitat et al., 2000; Gérard et al., 2001, 2002). The validity of the calculations was found to be relatively good, as evaluated in regards to log-log activity plots made for the analysis of the equilibrium relationships between the secondary minerals of the soils and the aqueous solutions. Such an agreement may be surprising because of the expected variability of the analogue model parameters, but was also certainly due to the log scale which makes results poorly sensitive to model uncertainties. An analogue model together with its site-specific parameters to simulate metal binding by NOM in another field site has been used by van Hees et al. (2000) in studying Al binding to LMWOAs and high molecular weight organic acids in solutions collected in a podzolised soil. These authors took the mean value of the apparent proton- and Al-binding constant of a monoprotic model proposed by Lundström (1993), which corresponds to a different location in the Svartberget research Park in Sweden, and exhibits a different vegetation (i.e. "pure" *Pinus sylvestris*, against a mixing of this tree species with *Picea abies*).

5.2.2. Humic ion-binding models

The more mechanistic MINTEQA2 model and, to a much larger extent, the WHAM and NICA-Donnan models described above have been intensively used in natural systems (at the field or at the laboratory scale) to study interactions between dissolved metal ions and NOM. Applications of such humic ion-binding models are more realistic owing to their mechanistic nature, but are also more generally characterized by the lack of knowledge about site-specific parameters for the organic phase.

5.2.2.1. On the need and difficulties to constrain field parameters. The proportions of FA and HA in NOM as well as their concentrations can vary from one site to another, and shall also depend on the type of organic matter (i.e. solid, particulate or dissolved organic matter). Binding affinities can also be subjected to temporal variations, and affected by the soil type and the nature of the vegetation (Guggenberger and Zech, 1999; Kaiser et al., 2001, 2002; Maie et al., 2002). However, cumbersome chemical pre-treatments are required to determine these parameters in natural solutions (i.e. the International Humic Substances Society procedure based on Amberlite XAD-8 resin), especially if one need to study purified FA and HA fractions in quantities proportionate with potentiometric titration (see for instance Christensen et al., 1998). Furthermore, the chemical fractionation

of NOM and purification of FA and HA may modify the number of reactive sites (e.g. Benedetti et al., 1996b), the affinity constant for proton binding (Benedetti et al., 2002), and may involve FA generation from more HA-like substances (Ritchie and Perdue, 2001). The supramolecular structure of humic substances proposed by Piccolo (2001) can certainly help to explain such observations of conformational changes and their implications on the acid-base properties of humic substances (Lopez et al., 2003).

Difficulties to apply humic ion-binding models under well-constrained conditions to natural systems, and the progressive emergence of model applications under increasingly well-constrained conditions, has led us to discuss hereafter model applications to the field according to the degree of knowledge regarding NOM speciation and binding properties. We also believe that such a presentation could be helpful to future users, as a guideline that would serve: (1) to legitimate hypothesis to be made to overcome the uncertainties regarding the actual NOM speciation and binding properties; (2) to support their choice of the calibration strategy to fit measured data.

5.2.2.2. Lack of knowledge of NOM speciation and binding properties. In such a case, generic values of the proton- and metal-binding parameters taken from the model database (see Section 5.1) are used as a surrogate for NOM. Also, the whole NOM is generally taken as pure FA or HA depending on whether NOM corresponds to dissolved or particulate/solid organic matter, respectively. These hypotheses enable first comparisons between modelled and experimental values of metal speciation, in almost all cases. A poor match leads to model calibration. Note that in the absence of measurements of metal speciation, model calibration can be driven by the charge balance constrain. However, no unique way to calibrate models has been found in the literature; therefore, the nature and the number of parameters subjected to calibration closely depends on the authors.

For example, Allison and Brown (1995) used the MINTEQA2 model to simulate Al binding by dissolved organic matter (DOM) in stream water. Large discrepancies between modelled and observed values were compensated by increasing carboxylic site density by a factor of 10, from 0.5 to 4.5 mol kg^{-1} DOM, in agreement with literature data. Similarly, Benedetti et al. (1996b) used the NICA-Donnan model to study Cu binding to DOM in a lake water and the binding of Cu and Cd to two sandy soils. Although a good fit was obtained for Cu binding to DOM in the lake water, discrepancies were observed for metal binding to SOM. Modelled values were fitted to metal speciation measurements by changing two parameters: the densities of carboxylic and phenolic sites for HA, which had to be increased or decreased depending on the field site. Similarly, Weng et al. (2001b, 2002a) adjusted the overall binding site density of the generic HA to various extents in studying the interactions between several dissolved trace metals (Cu, Cd, Zn, Ni and Pb) and NOM in a number of sandy soil samples exhibiting a range of chemical characteristics (i.e. pH, metal concentration, composition in metal-binding phases).

Single parameter calibration method was also adopted by Dwane and Tipping (1998), Vulkan et al. (2000) and Bryan et al. (2002) in using WHAM to model copper speciation in acidified and copper-amended surface waters and soil solutions. The goodness-of-fit was obtained by assuming that only a fraction of the DOC (from 40% to 80%, taken as FA) had the capacity to bind metals, the rest being inert with respect to this process. The underlying assumption is that NOM metal-binding properties are conferred by HS only. Another example of an "active" portion of HS with respect to cation complexation can be found in a study by Tipping et al. (2002), who looked at the competitive Al(III) and Fe(III) binding to NOM in freshwaters. The best fit of the values of organically bound Al was obtained by considering a proportion of "active" HS ranging from 61% to 70% of the NOM, depending on the equilibrium constant considered for the formation of Fe-hydroxides and the proportion of HA and FA in NOM. Such a notion of "active" fraction of HS has also been evoked in order to model the influence of soil organic matter on aluminium solubility and pH buffering in forest soils using WHAM (Lofts et al., 2001). Two additional examples can be found in Tipping et al. (2003a) for the simulation of the solid-solution partitioning of Cu, Zn, Cd, Pb in surface soil samples and in Tipping et al. (2003b), a study of the release of several potentially toxic metals from peat caused by drought-induced acidification. In

these studies, a charge balance constrain and the observed soil pH have been respectively considered to optimise the model.

Tipping et al. (1995a) and de Wit et al. (1999, 2001) have used the WHAM model to cope with sorption/desorption of HS by soil solids in order to predict aluminium and soil organic matter solubility in organic layers of acidic soils. Two fitting parameters are involved in addition to the "active" concentration in HS: a distribution parameter used to calculate a degree of hydrophobicity for a number of FA fractions and the "active" concentration of organically bound Al.

5.2.2.3. Applications supported by a better knowledge of HS-binding properties. Only a few studies have been supported by the measurements of the sites-specific binding properties of HS. Furthermore, in such studies calibration is still widely used to gain the best fit between simulations and metal speciation measurements. If so, the values of the metal-binding constants are optimised and one can readily assume that results would reinforce the reliability of the generic metal-binding constants. An example application of humic ion-binding model falling within the present classification can be found in Benedetti et al. (2002). These authors studied Pb and Al competitive binding by particulate and colloidal organic matter present in river waters using the NICA-Donnan model. They derived proton-binding parameters directly from the titration of the different purified fractions and compared them to generic ones in order to discuss whether they are HA- or FA-like compounds. Based on experimental evidences for the weakness of the contribution of phenolic-type sites, a good fit of the experimental values for Pb binding was obtained by using higher metal-binding constant for carboxylic sites. Another example can be found in Christensen et al. (1999), who used previously published data for the acid–base properties of DOM fractions (Christensen et al., 1998) to support their study of dissolved organically bound Cu and Pb in polluted groundwater.

Such a type of applications of humic ion-interaction models are not limited to the simulation of measured values in a natural system but also concern comparisons between models. Christensen and Christensen (1999) found better agreement with WHAM for Ni binding by DOC in groundwater, whereas the results obtained with WHAM and MINTEQA2 for Cd complexation were almost similar. However, a reasonable agreement was obtained with MINTEQA2 for Zn-DOC binding while the WHAM model still gave largely overestimated amounts. This discrepancy was balanced by changing the value of the metal-binding constant. Christensen and Christensen (2000) further observed that the MINTEQA2 model was unable to predict the pH-dependence of the complexation of Cd, Ni and Zn, in opposition to WHAM. To correct for this effect, empirical relations between the stability constants and pH had to be estimated and registered in the MINTEQA2 database.

An intermediate solution to the one relying on measurements of binding parameters would be to use some values inferred in past studies by calibration, as seen in Section 4. Tipping et al. (1995c) gave raise to this, as they simulated with reasonable success the solid-solution distribution coefficients for a set of radionuclides (Co, Sr and Am) in some acidic soils by considering the proportions of "active" HA and FA obtained by Tipping et al. (1995a) in a similar environment. A similar approach has been used in Lofts and Tipping (2000) for solid-solution partitioning of five trace metals (Co, Ni, Cu, Zn and Pb) in surface waters.

5.2.2.4. Applications with some consideration on non-humic substances. One has to stress that the restriction of organically bound metals to the influence of HS may be an oversimplification regarding the huge range of non-humic substances that can bind metals. Xue and Sigg (1999) gave a first evidence for that, by using both the NICA-Donnan and the WHAM models. They observed that stronger ligands than FA and HA may be present at low concentrations in the lakewaters, by comparison of the titrations of FA and HA with Cu and Cd with those of lakewater samples. They also observed that binding efficiency of such ligands may be related to the biological productivity of the lakes.

Although LMWOAs are ubiquitous in natural waters and are widely recognized for their metal-binding capacity, the concomitant influence of HS and LMWOAs has only been explicitly taken into account in a single study so far. The concentration in organically bound Al in solutions collected in organo-mineral layers of podzols has been studied

by van Hees et al. (2001) in using the WHAM model and the individual concentration in a number of LMWOAs determined by HPLC. Results pointed the moderate contribution of LMWOAs to overall metal binding by NOM, since they were found to complex on average up to 19% of Al. It should be noted that good agreement between calculated and experimental values of organic-Al was still obtained by considering an "active" fraction of the DOC (excluding LMWOAs) as FA (see Section 5.2.2.2). The charge balance constraint was considered to optimise the model.

6. How could organic matter be better accounted for in chemical equilibrium models? Some perspectives

The study of the current field applications of chemical equilibrium models incorporating organo-mineral interactions shows that there is still room for improvement in the incorporation of NOM.

First, we believe that improvements toward a better knowledge of the site-specific parameters for HS are needed. A research direction could be supported by the fact that the proportion of HS vs. non-humic substances in NOM could be estimated for a low cost by UV photometry, when supported by the potentially site-specific relationship linking the light absorption at 260 nm to a concentration in HS (Dilling and Kaiser, 2002). Improvements concerning HS substances themselves can be done as well. Indeed, the advanced WHAM and NICA-Donnan models have demonstrated their reasonable efficiency and reliability in simulating metal-binding to NOM through a number of applications in a range of natural and experimental systems, and for a number of competing metal cations and physico-chemical conditions. However, by considering a range of the degree of metal complexation with DOM and the corresponding variations between predictions and measurements, Weng et al. (2002a) showed that the latest version of NICA-Donnan needs to be further improved to better predict Zn, Ni and Pb speciation (whereas robustness for Cu and Cd is good). They proposed several ways or research directions to do so. These are many fold, and one can add to these a better implementation of the heterogeneity of binding sites and their expected influence on the overall binding properties (Leenheer et al., 2003), or by taking account of the kinetic of metal-HS dissociation reactions (Schmitt et al., 2003). Following Tipping (1998), a better understanding of the "active" metal-binding fraction of the NOM behaving as the "best default" HS of the WHAM model may also require further attention. For example, a cause may be the conditional conformation of HS (e.g. Piccolo, 2001). However, such an "active" fraction is typically issued from calibration, where an estimate of the actual HS fraction is used as initial guess. Thus, one can alternatively suggest that the concept of NOM fraction to be taken as HS regarding cation binding does not pose a conceptual problem since NOM does not solely contain HS. Furthermore, as we showed here by reviewing current model applications to the field, the need to define an "active" NOM fraction depends on the optimisation strategy assumed in fitting metal speciation data. For example, we have seen that the maximum density of the binding sites may also be optimised to fit metal speciation measurements (see Benedetti et al., 1996b), and doing so is consistent with the well-known variability of the density of the HS-binding sites.

A more comprehensive account of the NOM speciation should also be a priority, since most organic constituents have been reported to bind dissolved metals to various extents. Nevertheless, we have seen that the effectiveness of some small organic molecules (i.e. biochemical compounds) vs. HS in natural waters has been thoroughly established in a single study so far (van Hees et al., 2001). A specific effort should be placed in the microbial substrates and metabolites that readily interact with the soil chemistry, either at the acid–base and metal complexation levels (sugars, amino acids, LMWOAs under anaerobic conditions) or at the redox level (use of various terminal electron acceptors such as nitrate, sulfate, iron or manganese). Chromatographic techniques can be profitably used to quantify these compounds (e.g. Lombardi and Jardim, 1999), and to further integrate their concentrations into a geochemical model using a relevant thermodynamic database and a mechanistic approach for the effect of HS. Similarly, the capacity of chemical equilibrium models to deal with the range of macromolecules exhibiting a ratio of hydrophobic versus hydrophilic

bonds lower than humic and fulvic acids constitutes an important research direction. Such a research has been recently initiated by Croué et al. (2003) who used a two-column array of Amberlite XAD-8 and XAD-4 resins to study Cu binding to a transphilic neutral fraction (mostly proteinaceous) and a transphilic acid fraction (showing the highest proportion of polysaccharides) in addition to the hydrophobic fraction (i.e. HS by definition). The three fractions represented "only" 57% of the DOM. Promisingly, the authors have also derived binding parameters values consistent with NICA-Donnan for proton and copper binding for the three isolated fractions.

In parallel to adding more molecules, it would be enriching for the models to add more functions. Up to now, the acid–base chemistry, the metal cation binding and partially the surface chemistry of organic compounds have been addressed. However, one major property of organic molecules is their ability to be biodegraded by soil microorganisms. Therefore, biokinetic mechanisms have to be taken into account when studying the soil solution chemistry. Microorganisms exert a strong influence on the metal cation binding capacity of a sample, on a short time-scale, but also on a longer one by slowly modifying the structure of humic matter. These mechanisms still have to be taken into account in future development of chemical equilibrium models.

Finally, researchers should be encourage to use advanced chemical equilibrium models such as WHAM and NICA-Donnan (and accompanying codes; SCAMP and ECOSAT, respectively) for analysing, understanding and predicting their observations. A wider publishing effort in this field would provide materials for model improvements in the future and better embodiment of the great variety of NOM and its functions.

Acknowledgements

We thank Dr. Sherri Dudal for carefully reviewing the manuscript.

References

Allison, J.D., Brown, D.S., 1995. MINTEQA2/PRODEFA2. In: Loeppert, R.H., Schwab, A.P., Goldberg, S. (Eds.), A Geochemical Speciation Model and Interactive Preprocessor. Chemical Equilibrium and Reaction Models. Soil Sci. Soc. Am., and Am. Soc. Agronomy, Madison, WI, pp. 241–252.

Appelo, C.A.J., Postma, D., 1996. Geochemistry, Groundwater, and Pollution A.A. Balkema, Rotterdam, The Netherlands. 536 pp.

Bassett, R.L., Melchior, D.C., 1990. Chemical modeling of aqueous systems: an overview. In: Melchior, D.C., Bassett, R.L. (Eds.), Chemical Modeling of Aqueous Systems II, vol. 416. American Chemical Society, Washington, DC, pp. 1–14.

Benedetti, M.F., Milne, C.J., Kinniburgh, D.G., Van Riemsdijk, W.H., Koopal, L.K., 1995. Metal ion binding to humic substances: application of the non-ideal competitive adsorption model. Environ. Sci. Technol. 29, 446–457.

Benedetti, M.F., Van Riemsdijk, W.H., Koopal, L.K., 1996a. Humic substances considered as a heterogeneous Donnan gel phase. Environ. Sci. Technol. 30, 1805–1813.

Benedetti, M.F., et al., 1996b. Metal ion binding by natural organic matter: from the model to the field. Geochim. Cosmochim. Acta 60, 2503–2513.

Benedetti, M.F., Ranville, J.F., Ponthieu, M., Pinheiro, J.P., 2002. Field-flow fractionation characterization and binding properties of particulate and colloidal organic matter from the Rio Amazon and Rio Negro. Org. Geochem. 33, 269–279.

Boudot, J.-P., Maitat, O., Merlet, D., Rouiller, J., 2000. Soil solutions and surface water analysis in two contrasted watersheds impacted by acid deposition, Vosges mountains, N.E. France: interpretation in terms of Al impact and nutrient imbalance. Chemosphere 41, 1419–1429.

Bryan, N.D., et al., 1997. Metal-humic interactions: a random structural modelling approach. Geochim. Cosmochim. Acta 61, 805–820.

Bryan, S.E., Tipping, E., Hamilton-Taylor, J., 2002. Comparison of measured and modelled copper binding by natural organic matter in freshwaters. Comp. Biochem. Physiol. 133, 37–49.

Burdon, J., 2001. Are the tridimensional concepts of the structures of humic substances realistic? Soil Sci. 166, 752–769.

Buurman, P., van Lagen, B., Piccolo, A., 2002. Increase in stability against thermal oxidation of soil humic substances as a result of self-association. Org. Geochem. 33, 367–381.

Černick, M., Borkovec, M., Westall, J.C., 1995. Regularized least-squares methods for the calculation of discrete and continuous affinity distributions for heterogeneous sorbents. Environ. Sci. Technol. 29, 413–425.

Chaberek, S., Martell, A.E., 1959. Organic Sequestering Agents Wiley, New York, NY. 549 pp.

Cheshire, M.V., Dumat, C., Fraser, A.R., Hillier, S., Staunton, S., 2000. The interaction between soil organic matter and soil clay minerals by selective removal and controlled addition of organic matter. Eur. J. Soil Sci. 51, 497–509.

Christensen, J.B., Christensen, T.H., 1999. Complexation of Cd, Ni, and Zn by DOC in polluted groundwater: a comparison of approaches using resin exchange, aquifer material sorption and computer speciation models (WHAM and MINTEQA2). Environ. Sci. Technol. 33, 3857–3863.

Christensen, J.B., Christensen, T.H., 2000. The effect of pH on the complexation of Cd, Ni and Zn by dissolved organic carbon from leachate-polluted groundwater. Water Res. 34, 3743–3754.

Christensen, J.B., Tipping, E., Kinniburgh, D.G., Gron, C., Christensen, T.H., 1998. Proton binding by groundwater fulvic acids of different age, origins, and structure modeled with the Model V and NICA-Donnan model. Environ. Sci. Technol. 32, 3346–3355.

Christensen, J.B., Botma, J.J., Christensen, T.H., 1999. Complexation of Cu and Pb by DOC in polluted groundwater: a comparison of experimental data and predictions by computer speciation models (WHAM and MINTEQA2). Water Res. 33, 3231–3238.

Croué, J.-P., Benedetti, M.F., Violleau, D., Leenheer, J.A., 2003. Characterization and copper binding of humic and nonhumic organic matter isolated from the South Platte River: evidence for the presence of nitrogenous binding site. Environ. Sci. Technol. 37, 328–336.

Currie, W.S., Aber, J.D., McDowell, W.H., Boone, R.D., Magill, A.H., 1996. Vertical transport of dissolved organic C and N under long-term amendments in pine and hardwood forests. Biogeochemistry 35, 471–505.

Dassonville, F., Renault, P., 2002. Interactions between microbial processes and geochemical transformations in anaerobic conditions: a review. Agronomie 22, 51–68.

Davies, C.W., 1962. Ion Association Butterworths, London. 190 pp.

de Wit, H.A., Kotowski, M., Mulder, J., 1999. Modeling aluminium and organic matter solubility in the forest floor using WHAM. Soil Sci. Soc. Am. J. 63, 1141–1148.

de Wit, H.A., Groseth, T., Mulder, J., 2001. Predicting aluminium and soil organic matter solubility using the mechanistic equilibrium model WHAM. Soil Sci. Soc. Am. J. 65, 1089–1100.

Derenne, S., Largeau, C., 2001. A review of some important families of refractory macromolecules: composition, origin, and fate in soils and sediments. Soil Sci. 166, 833–847.

Dilling, J., Kaiser, K., 2002. Estimation of the hydrophobic fraction of dissolved organic matter in water samples using UV photometry. Water Res. 36, 5037–5044.

Driscoll, C.T., Lehtinen, M.D., Sullivan, T.J., 1994. Modeling the acid–base chemistry of organic solutes in Adirondack, New York, lakes. Water Resour. Res. 30, 297–306.

Dwane, G.C., Tipping, E., 1998. Testing a humic speciation model by titration of copper-amended natural waters. Environ. Int. 4, 609–616.

Farmer, V.C., Lumsdon, D.G., 2001. Interactions of fulvic acid with aluminium and a proto-imogolite sol: the contribution of E-horizon eluates to podzolization. Eur. J. Soil Sci. 52, 177–188.

Fein, J.B., Scott, S., Rivera, N., 2002. The effect of Fe on Si adsorption by *Bacillus subtilis* cell walls: insights into non-metabolic bacterial precipitation of silicate minerals. Chem. Geol. 182, 265–273.

Frost, P.C., Maurice, P.A., Fein, J.B., 2003. The effect of cadmium on fulvic acid adsorption to *Bacillus subtilis*. Chem. Geol. 200, 217–224.

Garrels, R.M., Thompson, M.E., 1962. A chemical model for sea water at 25 °C and one atmosphere total pressure. Am. J. Sci. 260, 57–66.

Gérard, F., Clément, A., Fritz, B., 1998. Numerical validation of a eularian hydrochemical code using a 1D multisolute mass transport system involving heterogeneous kinetically controlled reactions. J. Contam. Hydrol. 30, 201–216.

Gérard, F., Boudot, J.-P., Ranger, J., 2001. Consideration on the occurence of the Al_{13} polycation in natural soil solutions and surface waters. Appl. Geochem. 16, 513–529.

Gérard, F., François, M., Ranger, J., 2002. Processes controlling silica concentration in leaching and capillary soil solutions of an acidic brown forest soil (Rhône, France). Geoderma 107, 197–226.

Ghosh, K., Schnitzer, M., 1980. Macromolecular structures of humic substances. Soil Sci. 129, 266–276.

Göttlein, A., 1998. Determination of free Al^{3+} in soil solutions by capillary electrophoresis. Eur. J. Soil Sci. 49, 107–112.

Grimm, D.M., Azarraga, L.V., Carreira, L.A., Susetyo, W., 1991. Continuous multiligand distribution model used to predict the stability constant of Cu(II) metal complexation with humic material from fluorescence quenching data. Environ. Sci. Technol. 25, 1427–1431.

Grzyb, K.R., 1995. NOAEM (natural organic anion equilibrium model): a data analysis algorithm for estimating functional properties of dissolved organic matter in aqueous environments: Part I. Ionic component speciation and metal association. Org. Geochem. 23, 379–390.

Guggenberger, G., Zech, W., 1999. Soil organic matter composition under primary forest, pasture, and secondary forest succession, Región Huetar Norte, Costa Rica. For. Ecol. Manag. 124, 93–104.

Hatcher, P.G., Dria, K.J., Kim, S., Frazier, S.W., 2001. Modern analytical studies of humic substances. Soil Sci. 166, 770–794.

Hayes, M.H.B., Clapp, C.E., 2001. Humic substances: considerations of compositions, aspects of structure, and environmental influences. Soil Sci. 166, 723–737.

Hayes, T.M., Hayes, M.H.B., Skjemstad, J.O., Swift, R.S., Malcolm, R.L., 1996. Isolation of humic substances from soil using aqueous extractants of different pH and XAD resins, and their characterization by ^{13}C-NMR. In: Clapp, C.E., Hayes, M.H.B., Senesi, N., Griffith, S.M. (Eds.), Humic Substances and Organic Matter in Soil and Water Environments. IHSS, University of Minnesota, St. Paul, MN, pp. 13–24.

Helgeson, H.C., 1968. Evaluation of irreversible reactions in geochemical processes involving minerals and aqueous solutions: I. Thermodynamic relations. Geochim. Cosmochim. Acta 32, 853–877.

Helgeson, H.C., 1969. Thermodynamics of hydrothermal systems at elevated temperatures and pressures. Am. J. Sci. 267, 724–804.

Helgeson, H.C., Garrels, R.M., MacKenzie, F.T., 1969. Evaluation of irreversible reactions in geochemical processes involving minerals and aqueous solutions: II. Applications. Geochim. Cosmochim. Acta 34, 569–592.

Johnson, J.W., Oelkers, E.H., Helgeson, H.C., 1992. SUPCRT92: a software package for calculating the standard molar thermodynamic properties of minerals, gases, aqueous species, and reactions from 1 to 5000 bar and 0 to 1000 °C. Comput. Geosci. 18, 899–947.

Jones, D.L., 1998. Organic acids in the rhizosphere—a critical review. Plant Soil 205, 25–44.

Jones, D.L., Brassington, D.S., 1998. Sorption of organic acids in acid soils and its implications in the rhizosphere. Eur. J. Soil Sci. 49, 447–455.

Kaiser, K., 2003. Sorption of natural organic matter fractions to

goethite (α-FeOOH): effect of chemical composition as revealed by liquid-state ^{13}C NMR and wet chemical analysis. Org. Geochem. 34, 1569–1579.

Keiser, M.G., Van Riemsdijk, W.H., 2002. ECOSAT: a Computer Program for the Calculation of Speciation and Transport in Soil–Water Systems. Wageningen University, Wageningen, The Netherlands.

Kaiser, K., Kaupenjohann, M., Zech, W., 2001. Sorption of dissolved organic carbon in soils: effects of soil sample storage, soil-to-solution ratio, and temperature. Geoderma 99, 317–328.

Kaiser, K., Guggenberger, G., Haumaier, L., Zech, W., 2002. The composition of dissolved organic matter in forest soil solutions: changes induced by seasons and passage through the mineral soil. Org. Geochem. 33, 307–318.

Kerven, G.L., Larsen, P.L., Bell, L.C., Edwards, D.G., 1995. Quantitative ^{27}Al NMR spectroscopic studies of Al(III) complexes with organic ligands and their comparison with GEOCHEM predicted values. Plant Soil 171, 35–39.

Kim, S., Simpson, A.J., Kujawinski, E.B., Freitas, M.A., Hatcher, P.G., 2003. High resolution electrospray ionization mass spectrometry and 2D solution NMR for the analysis of DOM extracted by C_{18} solid phase disk. Org. Geochem. 34, 1325–1335.

Kinniburgh, D.G., et al., 1996. Metal ion binding by humic acid: application of the NICA-Donnan model. Environ. Sci. Technol. 30, 1687–1698.

Kinniburgh, D.G., et al., 1999. Ion binding to natural organic matter: competition, heterogeneity, stoichiometry and thermodynamic consistency. Colloids Surf. 151, 147–166.

Küsel, K., Drake, H.L., 1999. Microbial turnover of low molecular weight organic acids during leaf litter decomposition. Soil Biol. Biochem. 31, 107–118.

Lamy, I., Cambier, P., Bourgeois, S., 1994. Pb and Cd complexation with soluble organic carbon and speciation in alkaline soil leachates. Environ. Geochem. Health 16, 1–16.

Leenheer, J.A., Wershaw, R.L., Brown, G.K., Reddy, M.M., 2003. Characterization and diagenesis of strong-acid carboxyl groups in humic substances. Appl. Geochem. 18, 471–482.

Lofts, S., Tipping, E., 1998. An assemblage model for cation binding by natural particulate matter. Geochim. Cosmochim. Acta 62, 2609–2625.

Lofts, S., Tipping, E., 2000. Solid-solution metal partitioning in the humber rivers: application of wham and scamp. Sci. Total Environ. 251–52, 381–399.

Lofts, S., Woof, C., Tipping, E., Clarke, N., Mulder, J., 2001. Modelling pH buffering and aluminium solubility in European forest soils. Eur. J. Soil Sci. 52, 189–204.

Lombardi, A.T., Jardim, W.F., 1999. Fluorescence spectroscopy of high performance liquid chromatography fractionated marine and terrestrial organic materials. Water Res. 33, 512–520.

Lopez, R., Fiol, S., Antelo, J.M., Arce, F., 2003. Analysis of the effect of concentration on the acid–base properties of soil fulvic acid. Conformational changes. Colloids Surf. 226, 1–8.

Lundström, U.S., 1993. The role of organic acids in the soil solution chemistry of a podzolized soil. J. Soil Sci. 44, 121–133.

MacCarthy, P., 2001. The principles of humic substances. Soil Sci. 166, 738–751.

Maie, N., Watanabe, A., Hayamizu, K., Kimura, M., 2002. Comparison of chemical characteristics of type A humic acids extracted from subsoils of paddy fields and surface and soils. Geoderma 106, 1–19.

Maitat, O., Boudot, J.-P., Merlet, D., Rouiller, J., 2000. Aluminium chemistry in two contrasted acid forest soils and headwater streams impacted by acid deposition, Vosges mountains, N.E. France. Water Air Soil Pollut. 117, 217–243.

Martell, A.E., Smith, R.M., 1974. Critical stability constants. Amino Acids, vol. 1. Plenum, New York, NY.

Martell, A.E., Smith, R.M., 1975. Critical stability constants. Amines, vol. 2. Plenum, New York, NY.

Martell, A.E., Smith, R.M., 1976. Critical stability constants. Inorganic Complexes, vol. 4. Plenum, New York, NY.

Martell, A.E., Smith, R.M., 1977. Critical stability constants. Other Organic Ligands, vol. 3. Plenum Press, New York, NY.

Martell, A.E., Smith, R.M., 1982. Critical stability constants. First Supplement, vol. 5. Plenum, New York, NY.

Martell, A.E., Smith, R.M., 1989. Critical stability constants. Second Supplement, vol. 6. Plenum, New York, NY.

Mayer, K.U., Frind, E.O., Blowes, D.W., 2002. Multicomponent reactive transport modeling in variably saturated porous media using a generalized formulation for kinetically controlled reactions. Water Resour. Res. 38, 1174–1183.

McNab, W.W., Narasimhan, T.N., 1993. A multiple species transport model with sequential decay chain interactions in heterogeneous subsurface environments. Water Resour. Res. 29, 2737–2746.

Milne, C.J., Kinniburgh, D.G., Tipping, E., 2001. Generic NICA-Donnan model parameters for proton binding by humic substances. Environ. Sci. Technol. 35, 2049–2059.

Milne, C.J., Kinniburgh, D.G., van Riemsdijk, W.H., Tipping, E., 2003. Generic NICA-Donnan model parameters for metal-ion binding by humic substances. Environ. Sci. Technol. 37, 958–971.

Mountney, A.W., Williams, D.R., 1992. Computer simulation of metal ion-humic and fulvic acid interactions. J. Soil Sci. 43, 679–688.

Murray, K., Linder, P.W., 1983. Fulvic acids: structure and metal binding: I. A random molecular model. J. Soil Sci. 34, 511–523.

Ogawa, H., Amagai, Y., Koike, I., Kaiser, K., Benner, R., 2001. Production of refractory dissolved organic matter by bacteria. Science 292, 917–920.

Oste, L.A., Temminghoff, E.J.M., Van Riemsdijk, W.H., 2002. Solid-solution partitioning of organic matter in soils as influenced by an increase in pH or Ca concentration. Environ. Sci. Technol. 36, 208–214.

Parker, D.R., Norvell, W.A., Chaney, R.L., 1995. GEOCHEM-PC. A chemical speciation program for IBM and compatible personal computers. In: Loeppert, R.H., Schwab, A.P., Goldberg, S. (Eds.), Chemical Equilibrium and Reaction Models. Soil Sci. Soc. Am., and Am. Soc. Agronomy, Madison, WI, pp. 253–269.

Parkhurst, D.L., Appelo, C.A.J., 1999. PHREEQC. U.S. Geological Survey, Denver, CO.

Perdue, E.M., 1985. Acidic functional groups of humic substances.

In: Aiken, G.R., McKnight, D.M., Wershaw, R.L., MacCarthy, P. (Eds.), Humic Substances in Soil, Sediment, and Water. Wiley, New York, NY, pp. 493–526.

Perdue, E.M., Reuter, J.H., Parrish, R.S., 1984. A statistical model of proton binding by humus. Geochim. Cosmochim. Acta 48, 1257–1263.

Piccolo, A., 2001. The supramolecular structure of humic substances. Soil Sci. 166, 810–832.

Piccolo, A., Conte, P., 1998. Advances in nuclear magnetic resonance and infrared spectroscopies of soil organic particles. In: Huang, P.M., Senesi, N., Buffle, J. (Eds.), Structure and Surface Reactions of Soil Particles. Wiley, New York, NY, pp. 183–250.

Piccolo, A., Conte, P., Spaccini, R., Chiarella, M., 2003. Effects of some dicarboxylic acids on the association of dissolved humic substances. Biol. Fertil. Soils 37, 255–259.

Pinheiro, J.P., Mota, A.M., Van Leeuwen, H.P., 1999. On lability of chemically heterogeneous systems. Complexes between trace metals and humic matter. Colloids Surf. 151, 181–187.

Pitzer, K.S., 1979. Theory: ion interaction approach. In: Pytkowicz, R.M. (Ed.), Activity Coefficients in Electrolyte Solutions. CRC Press, Boca Raton, FL, pp. 157–208.

Pitzer, K.S., Kim, J.J., 1974. Thermodynamics of electrolytes: IV. Activity and osmotic coefficients for mixed electrolytes. J. Am. Chem. Soc. 96, 5701–5707.

Rice, J.A., 2001. Humin. Soil Sci. 166, 848–857.

Ritchie, J.D., Perdue, E.M., 2001. Proton-binding study of standard and reference fulvic acids, humic acids, and natural organic matter. Geochim. Cosmochim. Acta 67, 85–96.

Schmitt, D., Saravia, F., Frimmel, F.H., Schuessler, W., 2003. NOM-facilitated transport of metal ions in aquifers: importance of complex-dissociation kinetics and colloid formation. Water Res. 37, 3541–3550.

Senwo, Z.N., Tabatabai, M.A., 1998. Amino acid composition of soil organic matter. Biol. Fertil. Soils 26, 235–242.

Serkiz, S.M., Allison, J.D., Perdue, E.M., Allen, H.E., Brown, D.S., 1996. Correcting errors in the thermodynamic database for the equilibrium speciation model MINTEQA2. Water Res. 30, 1930–1933.

Smith, R.M., Martell, A.E., 1995. The selection of critical stability constants. In: Soil Science Society of America, American Society of Agronomy (Eds.), Chemical Equilibrium and Reaction Models. Soil Sci. Soc. Am., Madison, WI, pp. 7–29.

Smith, R.M., Martell, A.E., 2001. NIST Standard reference database 46. Critically selected stability constants of metal complexes database.

Sparks, D.L., Suarez, D.L. (Eds.), 1991. Rates of Soil Chemical ProcessesSSSA Spec. Publ., vol. 27. Soil Sci. Soc. Am., Madison, WI. 302 pp.

Sposito, G., 1989. The Chemistry of Soils. Oxford University Press, New York, NY.

Sposito, G., Coves, J., 1995. SOILCHEM on the Macintosh. In: Loeppert, R.H., Schwab, A.P., Goldberg, S. (Eds.), Chemical Equilibrium and Reaction Models. Soil Sci. Soc. Am., and Am. Soc. Agronomy, Madison, WI, pp. 271–287.

Sposito, G., Holtzclaw, K.M., LeVesque, C.S., 1981. Trace metal complexation by fulvic acid extracted from sewage sludge: I. Determination of stability constants and linear correlation analysis. Soil Sci. Soc. Am. J. 45, 465–468.

Sposito, G., Bingham, F.T., Yadav, S.S., Inouye, C.A., 1982a. Trace metal complexation by fulvic acid extracted from sewage sludge: II. Development of chemical models. Soil Sci. Soc. Am. J. 46, 51–56.

Sposito, G., Holtzclaw, K.M., LeVesque, C.S., Johnston, C.T., 1982b. Trace metal chemistry in arid-zone field soils amended with sewage sludge: II. Comparative study of the fulvic acid fraction. Soil Sci. Soc. Am. J. 46, 265–270.

Steelink, C., 1985. Ch. 18: implications of elemental characteristics of humic substances. In: Aiken, G.R., McKnight, R.L., Wershaw, R.L., MacCarthy, P. (Eds.), Humic Substances in Soil, Sediment, and Water. Wiley, New York, NY, pp. 457–475.

Stevenson, F.J., 1994. Humus Chemistry: Genesis, Composition, Reactions. Wiley, New York, NY. 512 pp.

Stumm, W., Morgan, J.J., 1970. Aquatic Chemistry Wiley-Interscience, New York, NY. 583 pp.

Stumm, W., Morgan, J.J., 1996. Aquatic Chemistry. Chemical Equilibria and Rates in Natural Waters. Wiley, New York, NY. 1040 pp.

Suarez, D.L., Simunek, J., 1996. Solute transport modeling under variably saturated water flow conditions. In: Lichtner, P.C., Steefel, C.I., Oelkers, E.H. (Eds.), Reactive Transport in Porous MediaReviews in Mineralogy. Mineralog. Soc. Am., Washington, DC, pp. 229–268.

Susetyo, W., Dobbs, J.C., Carreira, L.A., Azarraga, L.V., Grimm, D.M., 1990. Development of a statistical model for metal–humic interactions. Anal. Chem. 62, 1215–1221.

Temminghoff, E.J.M., Plette, A.C.C., van Eck, R., van Riemsdijk, W.H., 2000. Determination of the chemical speciation of trace metals in aqueous systems by the Wageningen Donnan membrane technique. Anal. Chim. Acta 417, 149–157.

Tipping, E., 1998. Humic ion-binding model: VI. An improved description of the interactions of protons and metal ions with humic substances. Aquat. Geochem. 4, 3–48.

Tipping, E., Hurley, M.A., 1992. A unifying model of cation binding by humic substances. Geochim. Cosmochim. Acta 56, 3627–3641.

Tipping, E., Berggren, D., Mulder, J., Woof, C., 1995a. Modelling the solid-solution distributions of protons, aluminium, base cations and humic substances in acid soils. Eur. J. Soil Sci. 46, 77–94.

Tipping, E., Fitch, A., Stevenson, F.J., 1995b. Proton and copper binding by humic acid: application of a discrete-site/electrostatic ion-binding model. Eur. J. Soil Sci. 46, 95–101.

Tipping, E., Woof, C., Kelly, M., Bradshaw, K., Rowe, J.E., 1995c. Solid-solution distributions of radionuclides in acid soils: application of the WHAM chemical speciation model. Environ. Sci. Technol. 29, 1365–1372.

Tipping, E., Rey-Castro, C., Bryan, S.E., Hamilton-Taylor, J., 2002. Al(III) and Fe(III) binding by humic substances in freshwaters, and implications for trace metal speciation. Geochim. Cosmochim. Acta 66, 3211–3224.

Tipping, E., Rieuwerts, J., Pan, G., Ashmore, M.R., Lofts, S., Hill, M.T.R., Farago, M.E., Thornton, I., 2003a. The solid-solution

partitioning of heavy metals (Cu, Zn, Cd, Pb) in upland soils of England and Wales. Environ. Pollut. 125, 213–225.

Tipping, E., Smith, E.J., Lawlor, A.J., Hugues, S., Stevens, P.A., 2003b. Predicting the release of metals from ombrotrophic peat due to drought-induced acidification. Environ. Pollut. 123, 239–253.

van Hees, P.A.W., Lundström, U.S., Giesler, R., 2000. Low molecular weight organic acids and their Al-complexes in soil solution—composition, distribution and seasonal variation in three podzolized soils. Geoderma 94, 173–200.

van Hees, P.A.W., Tipping, E., Lundström, U.S., 2001. Aluminium speciation in forest soil solution—modelling the contribution of low molecular weight organic acids. Sci. Total Environ. 278, 215–229.

Vulkan, R., et al., 2000. Copper speciation and impacts on bacterial biosensors in the pore water of copper-contaminated soils. Environ. Sci. Technol. 34, 5115–5121.

Warren, L.A., Haack, E.A., 2001. Biogeochemical controls on metal behaviour in freshwater environments. Earth-Sci. Rev. 54, 261–320.

Weng, L., Temminghoff, E.J.M., van Riemsdijk, W.H., 2001a. Contribution of individual sorbents to the control of heavy metal activity in sandy soil. Environ. Sci. Technol. 35, 4436–4443.

Weng, L., Temminghoff, E.J.M., van Riemsdijk, W.H., 2001b. Determination of the free ion concentration of trace metals in soil solution using a soil column Donnan membrane technique. Eur. J. Soil Sci. 52, 629–637.

Weng, L., Temminghoff, E.J.M., Lofts, S., Tipping, E., van Riemsdijk, W.H., 2002a. Complexation with dissolved organic matter and solubility control of heavy metals in a sandy soil. Environ. Sci. Technol. 36, 4804–4810.

Weng, L., Temminghoff, E.J.M., van Riemsdijk, W.H., 2002b. Aluminium speciation in natural waters: measurement using Donnan membrane technique and modeling using NICA-Donnan. Water Res. 36, 4215–4226.

Wershaw, R.L., 1999. Molecular aggregation of humic substances. Soil Sci. 164, 803–813.

Wolery, T.J., 1992. EQ3/6. Lawrence Livermore National Laboratory, Livermore, CA.

Xue, H., Sigg, L., 1999. Comparison of the complexation of Cu and Cd by humic or fulvic acids and by ligands observed in lake waters. Aquat. Geochem. 5, 313–335.

Spéciation du carbone organique dissous

Jaffrain J., Gérard F., Meyer M., et Ranger J. (2007) Assessing the quality of dissolved organic matter in forest soils using ultraviolet absorption spectrophotometry. *Soil Science Society of America Journal* **71**, 1851-1858.

Assessing the Quality of Dissolved Organic Matter in Forest Soils Using Ultraviolet Absorption Spectrophotometry

J. Jaffrain
Biogéochimie des Ecosystèmes Forestiers
UPR1138
INRA
F-54280 Champenoux
France

F. Gérard*
Biogéochimie des Ecosystèmes Forestiers
UPR1138
INRA
F-54280 Champenoux
France

current address:
Biogéochimie du Sol et de la Rhizosphère
UMR1222
INRA
SupAgro
Place Viala
F-34060 Montpellier
France

M. Meyer
LIMSAG
UMR5663 CNRS-Université de Bourgogne
UFR Sciences et Techniques
9 avenue Alain Savary
BP 47870
F-21078 Dijon
France

J. Ranger
Biogéochimie des Ecosystèmes Forestiers
UPR1138
INRA
F-54280 Champenoux
France

Ultraviolet spectrophotometry was used to investigate the effects, 30 yr after planting, of tree species substitution on the aromatic C content and related properties of dissolved organic carbon (DOC). Precautions were taken to correct measurements for the absorbance of NO_3 and dissolved Fe. In litter leachates, a significant reduction in the aromatic content of DOC was found in the Douglas-fir [*Pseudotsuga menziesii* (Mirb.) Franco] plantation but not in the beech (*Fagus sylvatica* L.) plantation. The disturbance of short-term C dynamics thus revealed agreed well with field observations. Significant differences in aromatic content were also found in capillary soil solutions from the two planted stands. Overall, these modifications, produced by the substitution of trees 30 yr previously, mostly concerned the beech plantation. Soil processes, and probably adsorption, played a central role in controlling the quality of DOC in this soil and appeared to be influenced by the species planted. In low-capillary solutions, located in larger pores, changes to the aromatic content were only detectable in the surface soil of the beech plantation. We found a more pronounced effect of tree substitution in high-capillary solutions filling soil micropores, where the aromatic content of DOC might be tightly controlled by soil organic matter. It is difficult to say, however, whether the planting of Douglas-fir had actually accelerated soil recovery, or whether there will be future changes to attain a completely new equilibrium.

Abbreviations: DOC, dissolved organic carbon; SUVA, specific ultraviolet absorbance; UV, ultraviolet.

The concentration and composition (i.e., quality) of natural organic matter are variables that have a significant effect on nutrient cycling. Because trees interact markedly with their environment, the common practice of tree species substitution or shifting usually leads to ecosystem modifications (e.g., Binkley, 1995). It is well established that the chemistry of soil solutions constitutes a good indicator of current ecosystem functioning (e.g., Zabowski and Ugolini, 1990; Smethurst, 2000; Ranger et al., 2001). Although the inorganic chemistry of soil solutions has been quite extensively studied, less attention has been paid to the quality of dissolved organic carbon (DOC) (Ströbel et al., 2001).

A broad range of chemical and physical methods are available to assess the different properties of DOC (Leenheer and Croué, 2003). Most of these techniques, however, are costly, time consuming, and invasive, and require a large sample volume even for a single analysis such as measuring the concentration in humic substances (Martin-Mousset et al., 1997; Simonsson et al., 2005). These analytical constraints generally constitute a limiting factor when it comes to studying soil solutions (Dilling and Kaiser, 2002). Ultraviolet (UV) absorption spectrophotometry is commonly used to study various properties of the DOC, such as its aromaticity, hydrophobic content, and biodegradability (e.g., Hautala et al., 2000; Dilling and Kaiser, 2002; Croué et al., 2003; Uyguner et al., 2004). The method is rapid, requires little sample preparation, is noninvasive, and only a small sample is necessary (Chen et al., 2002). Ultraviolet absorption spectrophotometry has been used extensively in a number of surface

Soil Sci. Soc. Am. J. 71:1851–1858
doi:10.2136/sssaj2006.0202
Received 26 May 2006.
*Corresponding author (gerard@supagro.inra.fr).

environments (e.g., McKnight et al., 1997; Maurice et al., 2002; O'Loughlin and Chin, 2004), including soil solutions sampled in fen areas and temperate forest ecosystems (Kalbitz, 2001; Simonsson et al., 2005). The UV properties of DOC derive from its aromatic C content. The π–π^* electronic transition absorbs the wavelength corresponding to the UV spectral domain. This molecular orbit is driven by the double-bond C of benzene-type material (Wieteska, 1986). Specific absorption at 254 nm (i.e., measured absorbance divided by the DOC concentration), referred to as specific ultraviolet absorbance (SUVA), has been used for many years to assess the aromaticity of DOC. Specific UV absorbance is used routinely as a criterion for water quality by the drinking water industry (see, e.g., Weishaar et al., 2003). Specific absorbance value, or absorptivity, measured at different key wavelengths has also been used to assess a variety of properties, such as aromaticity, hydrophobic content, apparent molecular weight and size, and biodegradability (e.g., Chin et al., 1994; Peuravuori and Pihlaja, 1997; Kalbitz et al., 2003; Simonsson et al., 2005). A review of the literature allowed us to select the most commonly used wavelengths (Table 1). Empirical relationships are usually established between absorptivity and various DOC properties using standard methods. Because of the heterogeneous nature of DOC and the expected spatial and temporal variability of its properties, however, its applicability to different field sites may be uncertain and could be misleading (Marschner and Kalbitz, 2003). We have therefore chosen to restrict our study to relative variations in specific absorbance that are indicative of relative differences in the aromatic C content and related properties of DOC (see Table 1).

This study thus aimed to use UV absorption spectrophotometry to study the effects of substituting certain tree species in a native forest (reference plot) on DOC properties in different types of soil solutions. Substitution had occurred about 30 yr previously. The influence of soil depth, water potential, and time was also investigated to broaden our view of the dynamics of organic matter in soils several decades after the substitution of a native forest by different tree species. The composition and dynamics of soil solutions may vary as a function of their matric potential because of differences in residence times, implying different contact times with soil solids and variations in the nature and intensity of physical and biological processes (Zabowski and Ugolini, 1990; Giesler et al., 1996; Ranger et al., 2001; Gérard et al., 2003). A relatively comprehensive view of the dynamics of organic matter can thus be achieved by studying soil solutions with different matric potentials.

MATERIALS AND METHODS

Materials

Soil solutions were sampled in the Breuil-Chenue forest (Morvan, France, 47°18′10″N and 4°4′44″E). This site is located on a south-tilted granite plateau with a mean elevation of approximately 650 m above sea level. The mean annual temperature is roughly 9°C and mean annual precipitation and potential evapotranspiration values reach approximately 1280 and 640 mm, respectively. The soil has been classified as a Typic Dystrochrept according to Soil Survey Staff (1994), and as an Alocrisol according to the AFES (1992). The soil is well aerated. The mean pH and organic C content are pH 4.4 and 60 g kg^{-1}, respectively. The soil cation exchange capacity is about 5.56 $cmol_c$ kg^{-1} with a base saturation of 18% (Levrel and Ranger, 2006). Vegetation cover corresponds to plantations of different tree species planted in 1976 to replace a 150-yr-old clear-cut native forest. The native forest is dominated by beech (*Fagus sylvatica L.*), with sessile oak (*Quercus sessiliflora* Smith) being found less frequently. In addition to the samples collected in a reference plot of native forest, we focused our study on soil solutions collected in two planted stands: beech, a deciduous species, and Douglas-fir [*Pseudotsuga menziesii* (Mirb.) Franco], a coniferous species. The difference in the thickness of the hol-organic horizon (hereinafter referred to as the *O horizon*) in the three forest stands was marked. We measured an O horizon of 6 to 8 cm in the two broad-leaved plots (native forest and beech plantation) vs. only about 1 cm in the Douglas-fir stand.

Methods

Ceramic suction-cup lysimeters maintained at a constant suction (~50 kPa) were used to collect solutions from the mineral soil. We also extracted solutions from the mineral soil by centrifuging fresh samples in the laboratory. The use of these two techniques enabled us to consider two types of solutions collected from the mineral soil, hereinafter referred to as *low-capillary* and *high-capillary solutions*, respectively. We also sampled litter leachates by means of zero-tension plate lysimeters installed immediately below the O horizon.

Low-capillary soil solutions are located in larger interconnected pores; given the suction applied, they correspond to a matric potential <50 kPa. As suction is continuously maintained, some gravitational flow is nonetheless collected after rain events. This type of capillary water is therefore composed of both mobile and weakly fixed capillary solutions. For reasons of convenience, we will use the term *low-capillary solutions* for this admixture of both mobile and capillary solutions. Conversely, high-capillary solutions constitute a good proxy for a solution that reacts with soil material, as they are retained by stronger capillary forces in narrower, interconnected pores (Zabowski and Ugolini, 1990; Giesler et al., 1996; Ranger et al., 2001; Gérard et al., 2003). Dissolved organic C properties in this type of soil solution may be more closely related to those of soil organic

Table 1. Key wavelengths selected in this study and corresponding reference works.

Wavelength	Property	Reference
nm		
250	aromaticity, apparent molecular weight	Peuravuori and Pihlaja (1997)
254	aromaticity	Abbt-Braun and Frimmel (1999), Croué et al. (2003), Hur and Schlautman (2003)
260	hydrophobic C content	Dilling and Kaiser (2002)
265	relative abundance of functional groups	Chen et al. (2002)
272	aromaticity	Traina et al. (1990)
280	hydrophobic C content, humification index, apparent molecular size	Chin et al. (1994), Korshin et al. (1999), Kalbitz et al. (2003)
285	humification index	Kalbitz et al. (2000)
300	characterization of humic substances	Artinger et al. (2000)
340	color	Scott et al. (2001)
350	apparent molecular size	Korshin et al. (1999)
365	aromaticity, apparent molecular weight	Peuravuori and Pihlaja (1997)
400	humic substances characterization	Artinger et al. (2000)
436	quality indicator	Abbt-Braun and Frimmel (1999)
465	relative abundance of functional groups	Chen et al. (2002)

matter than those in low-capillary soil solutions, which are closer to DOC transferred from the O horizon as litter leachates (Stevenson, 1994; Kaiser and Guggenberger, 2000).

We used the centrifuge drainage method to collect capillary solutions corresponding to a high matric potential (Giesler and Lundström, 1993; Ranger et al., 1993; Giesler et al., 1996; Gérard et al., 2003). A JOUAN KR4 22 centrifuge (Saint-Herblain, France) was used for this purpose. This apparatus enables the centrifugation of six soil samples of approximately 1600 cm^3 at a fixed temperature (20°C). The samples are placed in a double-bottomed polycarbonate tube consisting of an upper, soil-holding cylindrical part with a perforated base, and a lower solution-collecting cup. A stepwise procedure was adopted to extract that portion of the capillary solutions corresponding to the highest matric potential. A first extraction was performed at 1000 rpm for 20 min, yielding capillary solutions corresponding to a matric potential of <180 kPa. These solutions were discarded. The second step consisted in centrifuging the same samples for a further 20-min period at 3000 rpm. Capillary solutions corresponding to a matric potential within the range of 180 to 1600 kPa were thereby obtained.

Two replicates of the litter leachates were available for each forest stand. Suction cup lysimeters were located at depths of 15 and 30 cm (five replicates). These two types of soil solution were routinely collected during monthly sampling campaigns. For the present investigation, we took samples collected during five sampling campaigns unevenly distributed between June 2003 and late January 2004. More precisely, our database of litter leachates and low-capillary solutions corresponded to two set of samples collected in the autumn, two in the winter, and only one in the spring (calendar basis). We thus obtained a total of 30 samples of litter leachates and 98 samples of low-capillary soil solutions. Fresh soil samples used in the centrifugation method were collected at two soil depth intervals, 0 to 15 and 15 to 30 cm, which broadly corresponded to the A and B soil horizons, respectively. A total of 155 high-capillary solution samples were collected during six field campaigns, unevenly distributed during the winter, spring, and autumn of 2003. During the summer, drought conditions did not supply sufficient solution to perform chemical characterizations.

The samples were filtered at 0.45 µm (Pall Corp., East Hills, NY, Metricel membrane filter) in the laboratory and stored at 4°C in the dark before analysis, which was usually performed within 2 d. The Fe content was determined by inductively coupled plasma–optical emission spectroscopy (Jobin-Yvon Instruments, Longjumeau, France, Model JY180). Nitrate and DOC concentrations were measured by ionic chromatography (Dionex Corp., Sunnyvale, CA, Model X320) and using a C analyzer (Shimadzu Biotech, Manchester, UK, TOC 5050), respectively. A rod electrode was used to measure the pH (Sentron Europe BV, Roden, the Netherlands). Ultraviolet absorption spectra were measured at a constant temperature (25°C) with either a Cary 50 or Cary 500 UV-visible spectrophotometer (Varian Scientific Instruments, Palo Alto, CA), both instruments producing identical results. As suggested in the literature (Nowicka-Jankowska, 1986), we complied with the warm-up procedure recommended by the manufacturer. Spectra were acquired between 200 and 500 nm at a scan rate of 150 nm min^{-1} and with a uniform data point interval of 0.5 nm. Samples were placed in a quartz cell (Suprasil 300, Hellma, Mullheim, Germany) with a 1-cm optical path length. The cell holder was connected to a RE106 (Lauda, Lauda-Königshofen, Germany) water circulator (25°C), while each sample was equilibrated in a water bath for at least 15 min before measurement. Double-deionized high-purity water (18.2 MΩ cm), obtained using a Maxima (USF Elga, High Wycombe, UK) cartridge system designed for trace analysis, was used to collect baseline data and as a reference. Some measurements were duplicated randomly to ensure the validity and repeatability of the scans thus performed. The pH of the samples was neither adjusted nor buffered.

Statistical analysis of the results was performed using the commercial Unistat (Unistat Ltd., London) and Sigmastat (Systat Software, San Jose, CA) packages. Analyses of variance were run under the General Linear Model (Lane, 2002). Full interactions between factors were considered. We tested the effects of tree substitution and season in litter leachates using a two-way ANOVA, whereas in capillary solutions, the influence of plantations, soil depth, and time was tested by means of a three-way ANOVA. The normality and homoscedasticity postulates had been checked before variance analysis. Multiple comparisons were performed with the Holm Sidack test ($\alpha = 0.05$), as suggested by Glantz (2002).

RESULTS

Inorganic Absorbing Solutes

A commonly acknowledged problem using UV spectroscopy to evaluate DOC is that dissolved Fe and NO_3 also absorb light in the selected UV wavelength range (e.g., Simonsson et al., 2005). With respect to NO_3, this artifact can be corrected using the specific absorbance, or absorptivity, of the individual species and the additivity property of the Beer–Lambert law. It should be noted that NO_3 concentrations exhibited variations that depended on both the nature of the planted tree species and soil depth (Tables 2, 3, and 4). First of all, we corrected the absorbance measurements for the influence of NO_3 by making use of the additivity properties of the Beer–Lambert law (Wieteska, 1986; Wang and Hsieh, 2001). The extinction coefficients for NO_3 as a function of temperature were calculated from the work of Simeon et al. (2003). For all samples, we found that the maximum contribution of NO_3 absorption reached 5% of the total absorbance at 300 nm and was negligible at around 260 nm. Measured absorbance can also be corrected for the absorbance of dissolved Fe, based on the work of Weishaar et al. (2003) concerning the absorbance of Fe^{3+} in the presence of aromatic DOC. Knowledge of the absorptivity of Fe^{3+} is limited to the wavelength of 254 nm, however, which is commonly used in studies addressing the quality of natural organic matter (e.g., Korshin et al., 1996). Using the concentrations of dissolved Fe (see Tables 2, 3, and 4), we calculated that Fe^{3+} absorbance was slight, as it ranged

Table 2. Mean values for pH, specific absorbance at 254 nm ($SUVA_{254nm}$), and concentrations of dissolved organic carbon (DOC), NO_3, and Fe in litter leachates.

Forest type	pH		Fe		NO_3		DOC		$SUVA_{254nm}$	
	Mean	SE	Mean	SE	Mean	SE	Mean	SE	Mean	SE
			mg L^{-1}						L mg^{-1} cm^{-1}	
Beech	4.65 a†	0.1	0.28 a	0.05	2.91 a	0.57	25.89 a	2.95	0.0339 a	0.0008
Douglas-fir	4.55 a	0.15	0.3 a	0.05	5.26 a	1.77	33.32 a	3.93	0.0303 b	0.001
Native forest	4.17 b	0.07	0.35 a	0.06	0.56 b	0.21	41.6 a	5.9	0.036 a	0.0006

† Different letters denote mean values exhibiting significant differences ($P < 0.05$) with respect to tree species.

Table 3. Mean values for pH, specific absorbance at 254 nm ($SUVA_{254nm}$), and concentrations of dissolved organic carbon (DOC), NO_3, and Fe in low-capillary soil solutions (collected by means of tension lysimeters).

Depth	Forest type	pH		Fe		NO_3		DOC		$SUVA_{254nm}$	
		Mean	SE	Mean	SE	Mean	SE	Mean	SE	Mean	SE
cm				mg L^{-1}						– L mg^{-1} cm^{-1} –	
15	beech	5.2 a†	0.06	0.01 a	0.002	1.75 a	0.66	5.36 a	0.8	0.0116 a	0.0011
	Douglas-fir	4.68 b	0.04	0.05 b	0.007	18.27 b	3.07	19.02 b	2.93	0.0172 b	0.0016
	native forest	5.14 a	0.1	0.02 c	0.006	0.05 a	0.02	10.95 c	1.54	0.0186 b	0.0012
30	beech	5 a	0.12	0.006 a	0.001	0.9 a	0.33	4.05 a	0.5	0.0097 a	0.0010
	Douglas-fir	4.68 b	0.03	0.02 d	0.004	26.79 c	4.09	12.36 d	2.94	0.0105 a	0.0014
	native forest	5.32 a	0.06	0.006 a	0.002	0.03 a	0.01	4.65 a	0.34	0.0089 a	0.0011

† Different letters denote mean values exhibiting significant differences ($P < 0.05$) with respect to tree species and soil depth.

from 2% of the measured absorbance in litter leachates to 4% in high-capillary solutions. Such a small contribution of Fe^{3+} to the measured absorbance was expected, given the relatively low Fe concentrations encountered in this soil, which are typical of well-aerated soils (Weishaar et al., 2003).

Variations in the pH can also act on the absorption properties of aromatic C (e.g., Lawrence, 1980; De Haan et al., 1982; Baes and Bloom, 1990). Buffering the solution to a specific pH has even been recommended to enable an unbiased comparison between studies (e.g., Chen et al., 1977). Piccolo et al. (1999) suggested that this pH dependency of the UV absorption properties of DOC might be caused by the disruption of weak hydrophobic forces and subsequent conformational changes. During the present study, however, we decided to ignore the potential influence of pH on absorptivity. We believe that a clearer and more broad-based understanding is required before accounting for or correcting such pH effects, since several researchers found no influence across broad wavelength and pH ranges, such as Dilling and Kaiser (2002) and Wang and Hsieh (2001) in solutions containing humic substances only (from 200–600 nm and pH 2–9.5). More recently, Weishaar et al. (2003) investigated natural water samples and also observed a lack of pH effect across similar pH ranges. In our case, the mean pH of different types of soil solutions ranged from pH 4 to 5.3 (see Tables 2, 3, and 4). This narrow range reinforced the assumption that the influence of pH on the specific absorbance of DOC could be neglected in our case.

Quality of Dissolved Organic Matter

Based on the aforementioned theoretical relationship between UV absorbance properties and the aromatic content of DOC, the terms *specific absorbance* and *aromaticity* have been used to denote the quality of the DOC.

In all samples, we measured a relatively constant reduction in the specific absorbance of DOC as the wavelength increased. This trend was accompanied by a less marked influence of tree substitution. The greatest influence of tree substitution was observed in litter leachates at low wavelengths (around 254 nm). Variance analysis further revealed that the influence of tree substitution varied according to the type of soil solution and soil depth. Furthermore, in each solution type and at each soil depth, the effects of tree substitution on the quality (as well as on the quantity) of DOC were found to be unaffected by the sampling period.

In litter leachates, we detected a lack of significant influence of tree substitution on DOC concentrations, while we found that this factor significantly influenced specific absorbance, and thus the aromatic content, of the DOC released from the O horizon (Table 2). The lowest values were obtained in solutions collected beneath the O horizon in the Douglas-fir plantation (Table 2). The influence of this coniferous plantation on DOC quality in litter leachates was marked, as significant differences were observed throughout the wavelength range (see Fig. 1). Higher specific absorbance values were exhibited by litter leachates from the natural forest. Intermediate values were found in the beech plantation, between 272 and 400 nm.

In low-capillary solutions collected at a depth of 15 cm beneath the O horizon, we found that DOC concentrations varied significantly, as follows: Douglas-fir > native forest > beech (Table 3). The difference between the beech plantation and the native forest plot disappeared at a depth of 30 cm. Using UV spectrophotometry, it was possible to see that the effect of soil depth was more pronounced than that of tree species (Fig. 2), the influence of which was only noticeable from 250 to 350 nm and in samples collected at the surface (i.e., a depth of 15 cm). The aromatic content and related DOC properties were found to be significantly lower in low-capillary solutions collected in the beech planta-

Table 4. Mean values for pH, specific absorbance at 254 nm ($SUVA_{254nm}$), and concentrations of dissolved organic carbon (DOC), NO_3, and Fe in high-capillary soil solutions (collected by centrifugation).

Depth	Species	pH		Fe		NO_3		DOC		$SUVA_{254nm}$	
		Mean	SE	Mean	SE	Mean	SE	Mean	SE	Mean	SE
cm				mg L^{-1}						– L mg^{-1} cm^{-1} –	
0–15	beech	3.97 a†	0.05	0.37 a	0.03	34.23 a	5.21	39.84 a	2.28	0.0162 a	0.0005
	Douglas-fir	4.11 a,b	0.06	0.26 b	0.03	26.55 a	5.52	37.23 a	2.3	0.0119 b	0. 0005
	native forest	4.31 b	0.05	0.44 c	0.05	1.69 b	0.05	40.57 a	2.73	0.0145 c	0. 0006
15–30	beech	4.53 c	0.06	0.04 d	0.004	19.24 a,c	2.89	18.18 b	1.33	0.0089 d	0. 0005
	Douglas-fir	4.64 c	0.07	0.03 d	0.003	19.16 a	4.33	16.5 b	1.13	0.0062 e	0. 0006
	native forest	5.07 d	0.04	0.03 d	0.005	1.59 b	0.24	23 b	3.5	0.0065 e	0. 0005

† Different letters denote mean values exhibiting significant differences ($P < 0.05$) with respect to tree species and soil depth.

tion. By contrast, we found no significant difference between the Douglas-fir plantation and the native forest.

In high-capillary solutions (as in litter leachates), DOC concentrations were not significantly influenced by plantations of either Douglas-fir or beech planted 30 yr previously (Table 4). But soil depth had a significant influence, indicating that DOC was more concentrated in solutions from the topsoil layer (0–15 cm). Ultraviolet absorption spectrophotometry, however, showed that the aromatic content of DOC was significantly affected by the plantations, although this effect disappeared above 436 nm (Fig. 3). In solutions collected from topsoil (0–15 cm), DOC exhibited a lower aromatic content in the Douglas-fir plantation, as already observed in litter leachates. No difference was found between the two deciduous stands, except at 254 nm, after correction for the extra absorption induced by dissolved Fe. As for samples extracted from the deep soil layer (15–30 cm), no significant difference was found in those collected from the Douglas-fir stand. A pronounced effect of the beech plantation appeared, however, indicating higher DOC aromaticity.

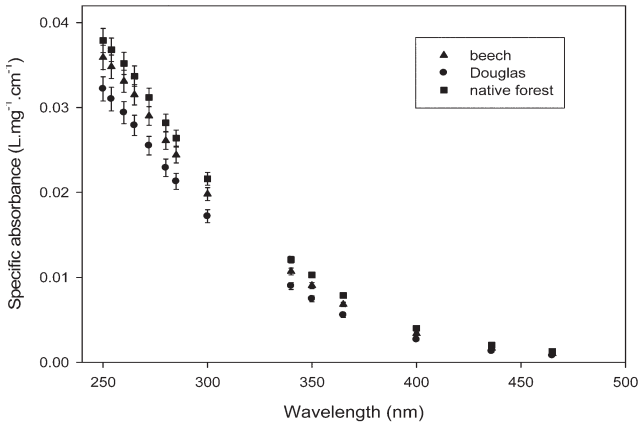

Fig. 1. Mean specific absorbance values for dissolved organic C in solutions collected beneath the O horizon in beech, Douglas-fir, and native forest stands. Error bars correspond to the standard error.

DISCUSSION

In our study, the time of sampling did not influence the effect of tree substitution, although the other factors tested (i.e., type of soil solution and soil depth) were found to interact strongly with the tree species. The effect of tree substitution on the quality and quantity of DOC thus appeared to persist over the seasons at the time span covered by our sampling campaigns.

In what follows, we focus on the effect of tree substitution and soil depth in the different types of soil solutions by considering the specific absorbance at 254 nm (hereafter referred to as $SUVA_{254nm}$). As noted above, the most marked effects were observed at this key wavelength, and $SUVA_{254nm}$ has been used widely in the literature for a variety of purposes relative to DOC quality. Moreover, the correction of measured absorbance due to the bias arising from the occurrence of dissolved Fe was limited to this wavelength, as explained above.

Overall, the significant variations observed in $SUVA_{254nm}$ values indicated that the substitution of natural forest by Douglas-fir or beech had an effect on organic C dynamics 30 yr after planting. In addition, the extent to which the aromaticity and related properties of DOC had been modified (e.g., hydrophobic C content, apparent molecular weight and size) depended on the nature of the planted tree species, soil depth, and type of soil solution.

More specifically, our results showed that, 30 yr after substitution, the O horizon of the beech stand released DOC that exhibited the same aromaticity and related properties as the DOC released by the native forest stand (see Table 2, Fig. 1). This showed that short-term DOC dynamics were unaffected by the planting of beech. This result tended to be in line with the composition of the native forest, which was mostly composed of beech. Interestingly, we also observed an influence of the beech plantation on C dynamics, from examination of the results concerning low-capillary solutions (see Table 3, Fig. 2). A significant difference was found in the topsoil (15-cm depth) of the beech plot, showing a lower $SUVA_{254nm}$ (i.e., less aromatic DOC). This difference in DOC quality disappeared when the solutions came from a depth of 30 cm. Even though no difference in terms of DOC aromaticity was observed in litter leachates, a significant effect "suddenly" appeared in this type of capillary solution collected from topsoil. As observed in high-capillary solutions, increasing the residence time not only reinforced the effect of the beech plantation on aromatic content but also altered it, as the DOC collected from the two soil depth layers became more aromatic (see Table 4, Fig. 3). These findings revealed the complex and considerable influence of soil processes on control of the aromatic content of DOC. Soil processes also reflected the long-term disturbance engendered by clear-cutting the natural beech-dominated forest and planting the same species. Such a change in the quality of DOC as a function of the residence time of solutions in soil suggested that the nature of these soil processes was controlled by the pore size network (Kaiser and Guggenberger, 2007).

The O horizon of the Douglas-fir stand released much less aromatic DOC than either planted or native deciduous stands, suggesting that its biodegradability might also be higher. This was consistent with the thinness of the O horizon in this plantation (about 1 cm as opposed to 6–8 cm under broadleaved species). Higher decomposition rates in the O horizon have been observed elsewhere under Douglas-fir when compared with beech (Hobbie et al., 2006; Moukoumi, 2006) Therefore, our results showed that short-term DOC dynamics were still modified by the Douglas-fir plantation 30 yr after substitution, as could be expected given the change from

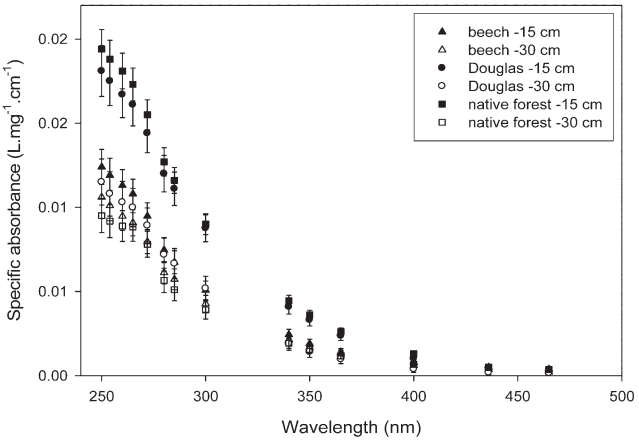

Fig. 2. Mean specific absorbance values for dissolved organic C in solutions collected by means of tension lysimeters (i.e., low-capillary solutions) in beech, Douglas-fir, and native forest stands at two depths. Error bars represent the standard error.

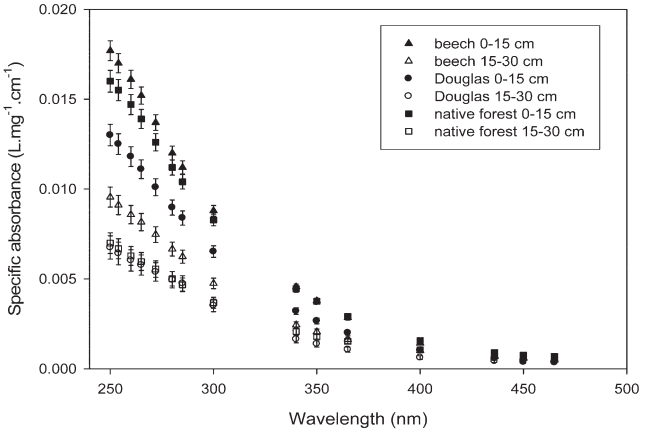

Fig. 3. Mean specific absorbance values for dissolved organic C in solutions collected by centrifugation (i.e., high-capillary solutions) in beech, Douglas-fir, and native forest stands at two depths. Error bars correspond to the standard error.

the broad-leaved litter of the native forest to a coniferous litter. The influence of soil processes was also marked in the Douglas-fir plantation, as no effect of substitution on $SUVA_{254nm}$ was observed in low-capillary solutions at depths of either 15 or 30 cm. Any difference in the DOC quality observed with respect to Douglas-fir litter leachates thus rapidly disappeared before the solutions passed through the first 15 cm of mineral soil. Nevertheless, a less aromatic DOC was found in high-capillary solutions collected from the topsoil, and this effect disappeared as soil depth increased.

Results in capillary solutions suggested that soil processes acted differently on DOC quality in the Douglas-fir and beech plantations. This suggests that the intensity or nature of the controlling soil processes responsible for drastic changes in DOC quality from litter leachates to soil solutions were notably affected by the nature of the planted species. Based on the close relationship between DOC in micropore solutions and soil organic matter (Stevenson, 1994; Kaiser and Guggenberger, 2000), it is very likely that the aforementioned differences concerning high-capillary waters better reflected the effects of substitution on the quality of soil organic matter (SOM). Thus SOM quality would also be changed by the type of tree species planted, and such changes varied with soil depth (0–15 and 15–30 cm).

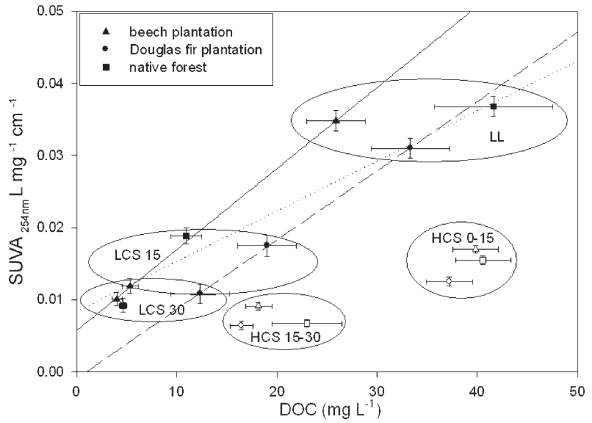

Fig. 4. Mean dissolved organic carbon (DOC) and specific ultraviolet absorbance at 254 nm ($SUVA_{254nm}$) values in the different types of solutions and as a function of forest type and soil depth. Errors bars correspond to the standard error. The lines represent the trends (linear regressions) obtained for the forest types (solid line, beech plantation; dashed line, Douglas-fir plantation; dotted line, native forest) in the light of measurements performed in litter leachates (LL), low-capillary solutions at 15- (LCS 15) and 30-cm (LCS 30) depths, and high-capillary solutions at 0- to 15- (HCS 0–15) and 15- to 30-cm (HCS 15–30) depths.

Overall, capillary solutions exhibited more marked disturbances resulting from the beech plantation in terms of the aromatic content of DOC. This could suggest that the planting of beech 30 yr previously more markedly modified present-day, and thus long-term, C dynamics. It is difficult to say, however, whether the planting of Douglas-fir has actually accelerated soil recovery, or whether there will be further changes to attain a completely new equilibrium. This contrasted markedly with the DOC in litter leachates, indicative of present-day and shorter term C dynamics, where $SUVA_{254nm}$ values did not differ significantly between the beech plantation and the native beech forest. This contrast may have stemmed from the source of aromatic DOC, which should differ as a function of solution type, that is, decomposition of fresh organic residues in litter leachates and close control by reactions with SOM in high-capillary solutions. Figure 4 illustrates the relationships between $SUVA_{254nm}$ and DOC for the different types of soil solutions, and highlights the plausible relationship between DOC in litter leachates and in low-capillary solutions (litter influenced), and the particular quality of DOC contained in high-capillary solutions (SOM influenced).

Irrespective of the nature of the planted tree species, the high $SUVA_{254nm}$ values found in litter leachates and the decrease with soil depth in capillary waters were also of interest in terms of attempting to clarify the nature of the soil process influencing DOC quality. The higher degree of aromaticity in DOC collected beneath an O horizon was in line with its unfractionated status (Ströbel et al., 2001). The $SUVA_{254nm}$ values in capillary solutions, which declined in line with soil depth (see Fig. 2 and 3, Tables 3 and 4), indicating that DOC became less aromatic and thus more biodegradable as soil depth increased, may have been caused by a cumulative effect of biodegradation and adsorption processes. The aromatic portion of DOC is less bioavailable to microorganisms (Qualls, 2005) and is preferentially adsorbed by soil solids, particularly Fe oxyhydroxides (e.g., Jardine et al., 1989; Kaiser et al., 2002). It is therefore very likely that adsorption was the major process involved in the decrease in aromatic C with soil depth. It should be noted that the noticeable rise in pH with soil depth (see Tables 3 and 4) may have increased the number of intermolecular bonds and the apparent molecular weight of DOC, as well as its hydrophobicity (Piccolo et al., 1999), thereby promoting the adsorption process. In addition, the pH-driven deprotonation of binding sites can also alter the affinity of hydrophobic C for sorption onto oxyhydroxides (Gu et al., 1995, 1996; Kaiser et al., 1996; Guo and Chorover, 2003). No clear correlation was observed, however, between pH and $SUVA_{254nm}$ values (see Tables 2, 3, and 4). These observations thus provide further evidence of an effect of planted species on the quantity, quality, and accessibility of the surfaces adsorbing the aromatic portion of DOC.

CONCLUSIONS

Use of the UV absorption spectrophotometry method made it possible to monitor, 30 yr after planting, the influence of two tree species (Douglas-fir and beech) on the aromatic C content and

related properties of DOC, and by extension, on several aspects of C dynamics in these ecosystems by comparison with a reference native forest plot. Our major findings can be summed up as follows:

1. During this 1-yr study, we found no time dependence for the effect of tree substitution. This result may reveal the predominance over time of the same effect of tree species on the quality (and quantity) of DOC.
2. At present, short-term C dynamics are only influenced by the planting of coniferous species. The same aromatic-C content in DOC ($SUVA_{254nm}$) was observed in litter leachates from the two deciduous stands, the beech plantation and the natural forest, which is dominated by this tree species.
3. Long-term C dynamics were more clearly disturbed by the planting of beech, as revealed by more marked differences in the aromatic-C content of DOC in the various types of capillary soil solutions collected from this stand. The effect was more pronounced in the DOC of solutions filling soil micropores. This result could be extended to soil organic matter. It was not clear, however, whether the planting of Douglas-fir had actually accelerated soil recovery after clear-cutting, or whether there would be future changes to attain a completely new equilibrium.
4. Soil processes, including adsorption, probably played a central role in controlling the aromatic C content of DOC vs. soil depth.
5. The degree of adsorption processes could depend on the nature of the planted tree species and could also be ascribed to variations in solid phases (quantity, nature, and accessibility of adsorbing surfaces, including soil organic matter).

ACKNOWLEDGMENTS

We gratefully acknowledge the financial support received from the GIP-Ecofor, which enabled maintenance of the field site within the French Ministry of Research's Observatoire de Recherche pour l'Environnement network (ORE). We are also grateful to the Ministry of Research's Ecologie Quantitative program for funding this work.

REFERENCES

Abbt-Braun, G., and F.H. Frimmel. 1999. Basic characterization of Norwegian NOM samples: Similarities and differences. Environ. Int. 25:161–180.

AFES. 1992. Principaux sols d'Europe. Référentiel pédologique. INRA Editions, Paris.

Artinger, R., G. Buckau, S. Geyer, P. Fritz, M. Wolf, and J.I. Kim. 2000. Characterization of groundwater humic substances: Influence of sedimentary organic carbon. Appl. Geochem. 15:97–116.

Baes, A.U., and P.R. Bloom. 1990. Fulvic acid ultraviolet–visible spectra: Influence of solvent and pH. Soil Sci. Soc. Am. J. 54:1248–1254.

Binkley, D. 1995. The influence of tree species on forest soils: Processes and patterns. *In* D.J. Mead and I.S. Cornforth (ed.) Proc. Trees and Soil Worksh., Canterbury, UK. 28 Feb.–2 Mar. 1994. Vol. 10. Lincoln Univ. Press, Canterbury, UK.

Chen, J., B. Gu, E.J. LeBoeuf, H. Pan, and S. Dai. 2002. Spectroscopic characterization of the structural and functional properties of natural organic matter fractions. Chemosphere 48:59–68.

Chen, Y., N. Senesi, and M. Schnitzer. 1977. Information provided on humic substances by E4/E6 ratios. Soil Sci. Soc. Am. J. 41:352–358.

Chin, Y.-P., G.R. Aiken, and E. O'Loughlin. 1994. Molecular weight, polydispersity, and spectroscopic properties of aquatic humic substances. Environ. Sci. Technol. 28:1853–1858.

Croué, J.-P., M.F. Benedetti, D. Violleau, and J.A. Leenheer. 2003. Characterization and copper binding of humic and nonhumic organic matter isolated from the South Platte River: Evidence for the presence of nitrogenous binding site. Environ. Sci. Technol. 37:328–336.

De Haan, H., T. De Boer, H.A. Kramer, and J. Voerman. 1982. Applicability of light absorbance as a measure of organic carbon in humic lake water. Water Res. 16:1047–1050.

Dilling, J., and K. Kaiser. 2002. Estimation of the hydrophobic fraction of dissolved organic matter in water samples using UV photometry. Water Res. 36:5037–5044.

Gérard, F., J. Ranger, C. Ménétrier, and P. Bonnaud. 2003. Silicate weathering mechanisms determined using soil solutions held at high matric potential. Chem. Geol. 202:443–460.

Giesler, R., and U.S. Lundström. 1993. Soil solution chemistry: Effects of bulking soil samples. Soil Sci. Soc. Am. J. 57:1283–1288.

Giesler, R., U.S. Lundström, and H. Grip. 1996. Comparison of soil solution chemistry assessment using zero-tension lysimeters or centrifugation. Eur. J. Soil Sci. 47:395–405.

Glantz, S.A. 2002. Primer of biostatistics. 5th ed. McGraw-Hill, New York.

Gu, B., T.L. Mehlhorn, L. Liang, and J.F. McCarthy. 1996. Competitive adsorption, displacement, and transport of organic matter on iron oxide: I. Competitive adsorption. Geochim. Cosmochim. Acta 60:1943–1950.

Gu, B., J. Schmitt, Z. Chen, L. Liang, and J.F. McCarthy. 1995. Adsorption and desorption of different organic matter fractions on iron oxide. Geochim. Cosmochim. Acta 59:219–229.

Guo, M., and J. Chorover. 2003. Transport and fractionation of dissolved organic matter in soil columns. Soil Sci. 168:108–118.

Hautala, K., J. Peuravuori, and K. Pihlaja. 2000. Measurement of aquatic humus content by spectroscopic analyses. Water Res. 34:246–258.

Hobbie, S.E., P.B. Reich, J. Oleksyn, M. Ogdahl, R. Zytkowiak, C. Hale, and P. Karolewski. 2006. Tree species effects on decomposition and forest floor dynamics in a common garden. Ecology 87:2288–2297.

Hur, J., and M.A. Schlautman. 2003. Using selected operational descriptors to examine the heterogeneity within a bulk humic substance. Environ. Sci. Technol. 37:880–887.

Jardine, P.M., N.L. Weber, and J.F. McCarthy. 1989. Mechanisms of dissolved organic carbon adsorption on soil. Soil Sci. Soc. Am. J. 53:1378–1385.

Kaiser, K., and G. Guggenberger. 2000. The role of DOM sorption to mineral surfaces in the preservation of organic matter in soils. Org. Geochem. 31:711–725.

Kaiser, K., and G. Guggenberger. 2007. Sorptive stabilization of organic matter by microporous goethite: Sorption into small pores vs. surface complexation. Eur. J. Soil Sci. 58:45–59.

Kaiser, K., G. Guggenberger, L. Haumaier, and W. Zech. 2002. The composition of dissolved organic matter in forest soil solutions: Changes induced by seasons and passage through the mineral soil. Org. Geochem. 33:307–318.

Kaiser, K., G. Guggenberger, and W. Zech. 1996. Sorption of DOM and DOM fractions to forest soils. Geoderma 74:281–303.

Kalbitz, K. 2001. Properties of organic matter in soil solution in a German fen area as dependent on land use and depth. Geoderma 104:203–214.

Kalbitz, K., S. Geyer, and W. Geyer. 2000. A comparative characterization of dissolved organic matter by means of aqueous samples and isolated humic substances. Chemosphere 40:1305–1312.

Kalbitz, K., J. Schmerwitz, D. Schwesig, and E. Matzner. 2003. Biodegradation of soil-derived dissolved organic matter as related to its properties. Geoderma 113:273–291.

Korshin, G.V., J.P. Croué, C.W. Li, and M.M. Benjamin. 1999. Comprehensive study of UV absorption and fluorescence spectra of Suwannee River NOM fractions. p. 147–156. *In* J. Davies and E. Ghabbour (ed.) Understanding humic substances. Advanced methods, properties and applications. Spec. Publ. 247. R. Soc. Chem., Cambridge, UK.

Korshin, G.V., C.W. Li, and M.M. Benjamin. 1996. Use of UV spectroscopy to study chlorination of natural organic matter. p. 182–195. *In* R.A. Minear and G. Amy (ed.) Water disinfection and natural organic matter. Am. Chem. Soc., Chicago.

Lane, P.W. 2002. Generalized linear models in soil science. Eur. J. Soil Sci. 53:241–251.

Lawrence, J. 1980. Semi-quantitative determination of fulvic acid, tannin and lignin in natural waters. Water Res. 14:373–377.

Leenheer, J.A., and J.-P. Croué. 2003. Characterizing dissolved aquatic organic matter. Environ. Sci. Technol. 37:18A–26A.

Levrel, G., and J. Ranger. 2006. Effet des substitutions d essences forestières et des

amendements sur les propriétés physiques d un Alocrisol: Site expérimental de la forêt de Breuil-Chenue, Morvan, France. Etude Gest. Sols 13:71–88.
Marschner, B., and K. Kalbitz. 2003. Controls of bioavailability and biodegradability of dissolved organic matter in soils. Geoderma 113:211–235.
Martin-Mousset, B., J.P. Croué, E. Lefebvre, and B. Legube. 1997. Distribution and characterization of dissolved organic matter of surface waters. Water Res. 31:541–553.
Maurice, P.A., S.E. Cabaniss, J. Drummond, and E. Ito. 2002. Hydrogeochemical controls on the variations in chemical characteristics of natural organic matter at a small freshwater wetland. Chem. Geol. 187:59–77.
McKnight, D.M., R. Harnish, R.L. Wershaw, J.S. Baron, and S. Schiff. 1997. Chemical characteristics of particulate, colloidal, and dissolved organic material in Loch Vale watershed, Rocky Mountain National Park. Biogeochemistry 36:99–124.
Moukoumi, J. 2006. Effet des essences forestières sur la biodégradation des matières organiques: Impact sur la dynamique et le cycle du carbone, de l'azote et des éléments minéraux. Univ. Henri Poincaré, Nancy, France.
Nowicka-Jankowska, T. 1986. Experimental techniques. p. 229–265. *In* T. Nowicka-Jankowska et al. (ed.) Analytical visible and ultraviolet spectroscopy. Vol. 19. Elsevier Science Publ., Amsterdam.
O'Loughlin, E., and Y.-P. Chin. 2004. Quantification and characterization of dissolved organic carbon and iron in sedimantary porewater from Green Bay, WI, USA. Biogeochemistry 71:371–386.
Peuravuori, J., and K. Pihlaja. 1997. Molecular size distribution and spectroscopic properties of aquatic humic substances. Anal. Chim. Acta 337:133–149.
Piccolo, A., P. Conte, and A. Cozzolino. 1999. Effects of mineral and monocarboxylic acids in the molecular association of dissolved humic substances. Eur. J. Soil Sci. 50:687–694.
Qualls, R.G. 2005. Biodegradability of fractions of dissolved organic carbon leached from decomposing leaf litter. Environ. Sci. Technol. 39:1616–1622.
Ranger, J., D. Discours, D. Mohamed Ahamed, C. Moares, E. Dambrine, D. Merlet, and J. Rouiller. 1993. Comparaison des eaux liées et des eaux libres des sols de trois peuplements d'épicéa (Picea abies Karst) des Vosges. Application à l'étude du fonctionnement actuel des sols et conséquences pour l'état sanitaire des peuplements. Ann. Sci. For. 50:425–444.
Ranger, J., R. Marques, and J.-H. Jussy. 2001. Forest soil dynamics during stand development assessed by lysimeter and centrifuge solutions. For. Ecol. Manage. 144:129–145.
Scott, M.J., M.N. Jones, C. Woof, B.M. Simon, and E. Tipping. 2001. The molecular properties of humic substances isolated from a UK upland peat system. A temporal investigation. Environ. Int. 27:449–462.
Simeon, V., V. Butorac, V. Tomisic, and N. Kallay. 2003. Existence of two forms of nitrate ion in dilute aqueous solutions: Thermodynamic parameters of interconversion. Phys. Chem. Chem. Phys. 5:2015–2019.
Simonsson, M., K. Kaiser, F. Andreux, and J. Ranger. 2005. Estimating nitrate, dissolved organic carbon and DOC fractions in forest floor leachates using ultraviolet absorbance spectra and multivariate analysis. Geoderma 124:157–168.
Smethurst, P.J. 2000. Soil solution and other soil analyses as indicators of nutrient supply: A review. For. Ecol. Manage. 138:397–411.
Soil Survey Staff. 1994. Keys to Soil Taxonomy. 6th ed. U.S. Gov. Print. Office, Washington, DC.
Stevenson, F.J. 1994. Humus chemistry: Genesis, composition, reactions. John Wiley & Sons, New York.
Ströbel, B.W., H.C.B. Hansen, O.K. Borggaard, M.K. Andersen, and K. Raulund-Rasmussen. 2001. Composition and reactivity of DOC in forest floor soil solutions in relation to tree species and soil type. Biogeochemistry 56:1–26.
Traina, S.J., J. Novak, and N.E. Smeck. 1990. An ultraviolet absorbance method for estimating the percent aromatic carbon content of humic acids. J. Environ. Monit. 19:151–153.
Uyguner, C.S., C. Hellriegel, W. Otto, and C. Larive. 2004. Characterization of humic substances: Implications for trihalomethane formation. Anal. Bioanal. Chem. 378:1579–1586.
Wang, G.-S., and S.-T. Hsieh. 2001. Monitoring natural organic matter in water with scanning spectrophotometer. Environ. Int. 26:205–212.
Weishaar, J.L., G.R. Aiken, B.A. Bergamaschi, M.S. Fram, R. Fuji, and K. Mopper. 2003. Evaluation of specific ultraviolet absorbance as an indicator of the chemical composition and reactivity of dissolved organic carbon. Environ. Sci. Technol. 37:4702–4708.
Wieteska, E. 1986. Fundamentals of ultraviolet and visible spectroscopy. p. 19–97. *In* T. Nowicka-Jankowska et al. (ed.) Analytical visible and ultraviolet spectroscopy. Vol. 19. Elsevier Science Publ., Amsterdam.
Zabowski, D., and F.C. Ugolini. 1990. Lysimeter and centrifuge soil solutions: Seasonal differences between methods. Soil Sci. Soc. Am. J. 54:1130–1135.

Modélisation du cycle biogéochimique du silicium

Gérard F., Mayer K. U., Hodson M. J., et Ranger J. (2008) Modelling the biogeochemical cycle of silicon in soils: application to a temperate forest ecosystem. *Geochimica Cosmochimica Acta* **72**, 741-758.

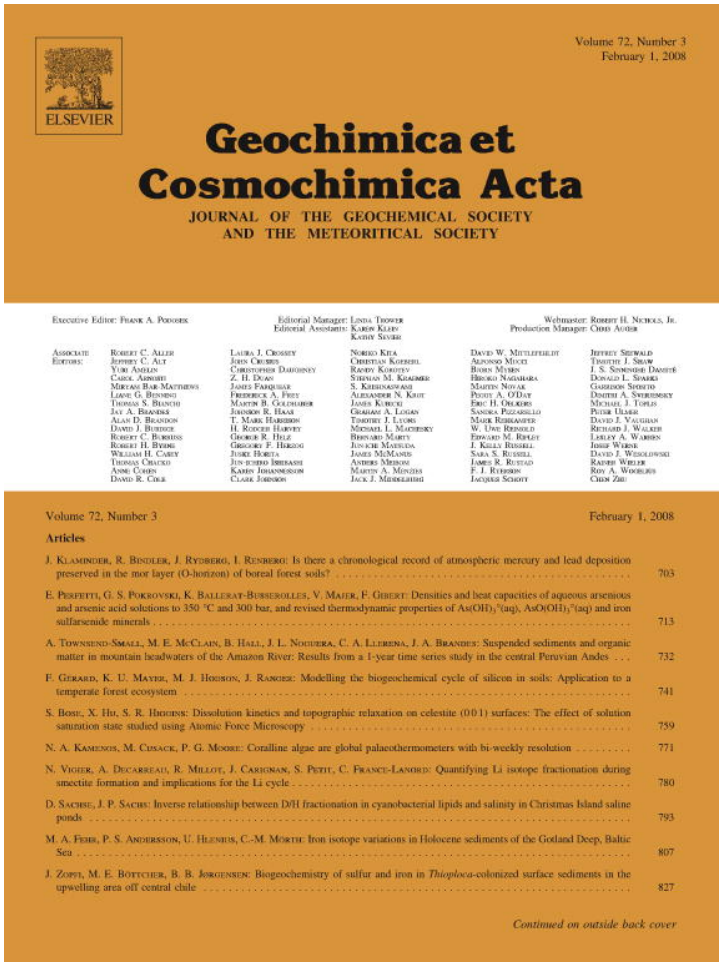

Volume 72, Number 3
February 1, 2008

ELSEVIER

Geochimica et Cosmochimica Acta

JOURNAL OF THE GEOCHEMICAL SOCIETY
AND THE METEORITICAL SOCIETY

Continued on outside back cover

Available online at www.sciencedirect.com
ScienceDirect
Geochimica et Cosmochimica Acta 72 (2008) 741–758
Geochimica et Cosmochimica Acta
www.elsevier.com/locate/gca

Modelling the biogeochemical cycle of silicon in soils: Application to a temperate forest ecosystem

F. Gérard [a,*,1], K.U. Mayer [b], M.J. Hodson [c], J. Ranger [a]

[a] *Biogéochimie des Ecosystèmes Forestiers, UPR1138, INRA, F-54280 Champenoux, France*
[b] *Department of Earth and Ocean Sciences, University of British Colombia, Vancouver, Canada V6T 1Z4*
[c] *School of Life Sciences, Oxford Brookes University, Oxford OX3 0BP, UK*

Received 26 June 2006; accepted in revised form 13 November 2007; available online 22 November 2007

Abstract

We investigated the biogeochemical cycling of silicon (Si) in an acidic brown soil covered by a coniferous forest (Douglas fir). Based on published and original data, we constructed a conceptual model and used a modified version of the reactive transport code MIN3P for model testing and quantification purposes. The model was first calibrated and further validated with respect to biomass data and Si-concentrations in capillary solutions, which were collected monthly over several years by means of suction-cup lysimeters placed at different soil depths.

Following sensitivity tests, the model was calibrated quite accurately (limited to a 10% concentration error) by the adjustment of kinetic constants, longitudinal dispersion, and apparent activation energy for K-feldspar dissolution. Calibrated parameter values were constrained by ranges reported in the literature, when available. Mass balance calculations indicate that an average of 60% of the biogeochemical cycle of Si was controlled by biological processes (i.e. Si-uptake and dissolution of phytoliths). Sensitivity analyses suggest that no more than 55% of the Si-cycle is controlled by weathering of primary silicates. Such a large contribution of biological turnover to Si-cycling may be explained by the combined effects of a relatively large Si-content in the litter fall (i.e. specifically in the needles) and high biomass productivity of the coniferous species considered. In addition to potential implications for the global Si cycle, this investigation raises several fundamental questions concerning the nature of Si-uptake mechanisms and physiological use of Si by trees in natural systems.

1. INTRODUCTION

Silicon (Si) is crucial in numerous biochemical and geochemical subsurface processes, ranging from chemical weathering to soil development, plant growth, and toxicity of metals to living organisms (e.g. Epstein, 1999; Pregitzer, 2003). Despite the importance of Si, several recent review articles have drawn attention to the lack of knowledge regarding the role of plants in the terrestrial Si cycle (Conley, 2002; Meunier, 2003; Sommer et al., 2006). This shortcoming generates uncertainties for the global Si cycle, because Si-discharge to oceans is closely related to events occurring on land. Another aspect of geochemical interest is related to the effects of plants on the weathering rate of silicates. Plants can influence chemical weathering rates by producing various organic ligands and acidity, by affecting the soil water budget through transpiration, and by root uptake of Si (Drever and Zobrist, 1992; Kelly et al., 1998; Hinsinger et al., 2001; Lucas, 2001). A general conceptual model of the biogeochemical cycle of Si in the soil-plant-atmosphere system is depicted in Fig. 1. Biological uptake of Si (flux F_4) can enhance silicate weathering by decreasing aqueous silica concentrations. Conversely, the release of Si from dead plant biomass and its decomposition in the organic soil layer (O-horizon) (F_3) leads to increased silica concentrations in the soil and may therefore inhibit the rate

* Corresponding author. Fax: +33 4 99 613088.
E-mail address: gerard@supagro.inra.fr (F. Gérard).
[1] Present address: Biogéochimie du Sol et de la Rhizosphère, UMR1222, INRA, SupAgro, F-34060 Montpellier, France.

0016-7037/$ - see front matter © 2007 Elsevier Ltd. All rights reserved.
doi:10.1016/j.gca.2007.11.010

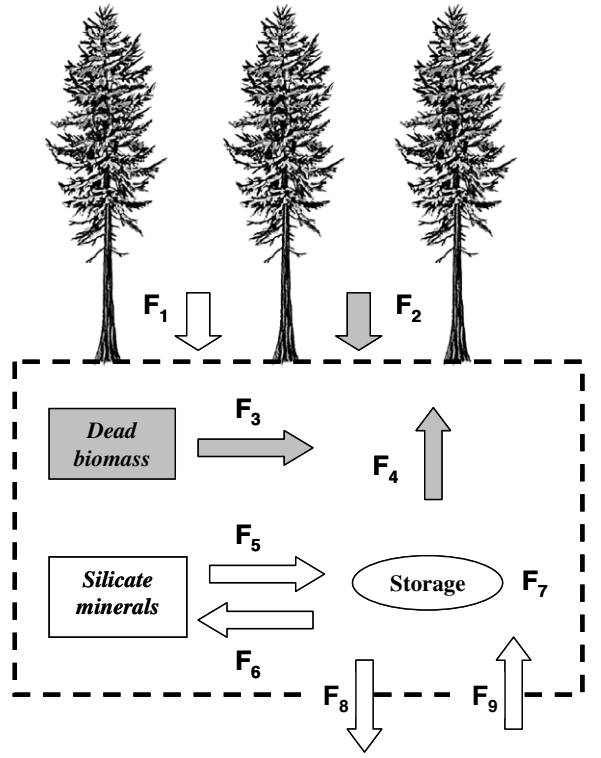

Fig. 1. General conceptual model of the biogeochemical cycle of silicon (Si) in terrestrial ecosystems. Shaded arrows include the biological cycle of Si, and open arrows the geochemical cycle. The flux F_1 is the Si influx from atmospheric precipitation, F_2 is the flux associated with litter fall, F_3 represents the flux released by the dissolution of biogenic Si (phytoliths), F_4 is the vegetation uptake flux, F_5 stands for the flux of Si released by the dissolution of silicate minerals, and F_6 is the flux of Si precipitated with secondary silicates. The storage of Si corresponds to the mass of this element contained in soil solutions, and given by the product of the concentration and the volume of water filling the soil pores. Correspondingly, the flux F_7 is the change in storage with time caused by a variation in the other fluxes. F_8 is the flux draining out of the system, and F_9 is the flux entering the system by capillary upward flows.

of chemical weathering. The biological cycle of Si has also been reported to promote and sustain the neoformation of Si-containing minerals such as kaolinite in the top horizon of tropical soils (Lucas, 1993, 2001), (F_6).

In most of the higher-order plants, including trees, Si accumulates in the shoots; i.e. in leaves and non-woody tissues (Hodson and Evans, 1995; Hodson and Sangster, 1999; Carnelli et al., 2001; Hodson et al., 2005). This makes Si widely recyclable through falling plant litter. In plant tissues, Si precipitates in the form of microporous and hydrated silica particles (i.e. biogenic opal or phytoliths). Reported dissolution rates for phytoliths fall within the range of those determined for quartz (Bartoli and Wilding, 1980; Drees et al., 1989; Fraysse et al., 2006). However, there are also reports that phytoliths exhibit an extremely high specific surface area and are significantly more soluble than quartz (Bartoli and Wilding, 1980; Bartoli, 1985; Fraysse et al., 2006). These properties may be the reason for the rapid dissolution of fresh phytoliths reported for tropical climates (Alexandre et al., 1997). The influence of the dissolution of the biogenic pool on dissolved Si is commonly believed less significant in temperate climate regimes, because soils are often rich in silicates that are prone to weathering (Bartoli and Wilding, 1980; Bartoli, 1981, 1983). However, it is conceivable that the contribution towards Si-release from the biogenic pool stored in the silicate-mineral poor O-horizon is still considerable. The annual flux of biogenic Si returned by litter fall is also influenced by the climate. Generally, more Si is recycled by forest trees growing in the tropics (Lucas, 2001; Conley, 2002).

Accordingly, there exists ample evidence for strong interactions between biological and geochemical processes in tropical soils (e.g. Alexandre et al., 1997; Meunier et al., 1999; Derry et al., 2005; Ziegler et al., 2005). In contrast, much less attention has been given to the biogeochemical cycle of Si under temperate climates, since the work by Bartoli and co-workers on acid forest ecosystems in the 1970s and 1980s (Bartoli and Souchier, 1978; Bartoli, 1981, 1983). Alexandre et al. (1997) found in a rain forest ecosystem that the flux of Si released by the dissolution of fresh phytoliths stored in the topsoil was about three times larger than the flux from mineral weathering. More recently, Meunier et al. (1999) obtained similar results for the soil-plant system at Reunion Island (Indian Ocean). Control of Si concentration by the dissolution of phytoliths has been found in some Hawaiian streams and soil waters by Derry et al. (2005) and Ziegler et al. (2005), using germanium concentrations and Si isotopes as tracers, respectively. Bartoli and Souchier (1978) determined that the type of tree species also had an effect on biological turnover in temperate ecosystems. They calculated an Si-uptake by pure deciduous (beech) forests ranging from 36 to 46 $kg\,ha^{-1}\,yr^{-1}$, which falls within the range of the minimum uptake flux determined for forest ecosystems in the tropics (Lucas, 2001). In contrast, the uptake flux by a pine forest ecosystem was much lower, on the order of 7 $kg\,ha^{-1}\,yr^{-1}$, whereas mixed beech-fir and fir forests exhibited intermediate values. Consequently, Bartoli (1983) calculated that the flux of Si as a result of weathering was about three times that of the biological flux (i.e. uptake and phytolith dissolution) in the pine forest soil, and that the biogeochemical cycle of Si in a beech forest was dominated by biological processes.

Since Bartoli's early work, increasing interest in Si dynamics in acid forest soils has provided the motivation for recent studies under temperate to Mediterranean climatic regimes (e.g. Berner et al., 1998; Markewitz and Richter, 1998; Giesler et al., 2000; Gérard et al., 2002; Gérard et al., 2003; Johnson-Maynard et al., 2005; Goddéris et al., 2006). However, an assessment of the biogeochemical Si-cycle has not been made in these studies, with the exception of work by Markewitz and Richter (1998), who estimated that the biological Si-uptake from a pine forest at an experimental site in South Carolina (USA) was approximately equivalent to Si-release by chemical weathering. This is in contrast to the common belief that chemical weathering dominates Si-dynamics in temperate regimes and at the catchment scale (e.g. White and Blum, 1995;

White et al., 1999; Goddéris et al., 2006). However, exceptions exist, as described in Fulweiler and Nixon (2005), who explained the seasonality of dissolved Si in New England Rivers by biological pumping in the watershed forests.

Previous studies targeting the dynamics of Si in soils also point to the need for development of numerical models that allow the integrated investigation of plant-related processes, chemical weathering, and solute transport. The current understanding of Si-cycling may be affected by the fact that most previous studies assumed that ecosystems are at a quasi steady-state (i.e. all fluxes seen in Fig. 1 are assumed constant in time), although marked seasonal variations in Si concentration and water fluxes are typically observed in natural systems (e.g. Kelly et al., 1998). A steady state assumption is also not applicable to managed forest systems, which tend to take up nutrients including Si during their growth cycle.

Our objectives include: (a) the derivation of a site-specific conceptual model for the biogeochemical cycling of Si in a forest ecosystem situated on an acidic soil and under a temperate climatic regime; and (b) the development and use of a numerical model to investigate the relevant geochemical, biological, and mass transfer processes in an unsaturated soil profile under transient field conditions. Furthermore, we attempt to demonstrate how integrative modelling of biogeochemical cycling of Si can be used to assess the extent of the control of chemical weathering on dissolved Si, and to provide a preliminary estimate of the relative importance of different plant uptake mechanisms under field conditions.

2. MATERIALS AND METHODS

2.1. Field site and mineralogy

The field site is an acidic brown soil classified as a 'Typic Dystrochrept' (USDA, 1994) or an Alocrisol (AFES, 1992) covered by a 40-year-old plantation of Douglas fir (*Pseudotsuga menziesii* (Mirb.) Franco). Its area covers approximately 2500 m^2. Tree density is 490 trees ha^{-1} with no significant vegetation on the forest floor. Average stand height reached 28 m after 40 years (Ranger et al., 2003). The site is located in the 'Montagne des Aiguilettes' in the Beaujolais region (Rhône, France), at an altitude of about 750 m a.s.l. The mean annual temperature is 7 °C and the mean annual precipitation and potential evapotranspiration during the period 1995–1999 were about 1000 mm and 800 mm, respectively. A winter storm on December 27th 1999 destroyed the plantation. Representative site monitoring was no longer possible after this natural disaster.

Soil mineralogy has been studied extensively at the site (Ezzaïm et al., 1999). The bedrock is an Upper Visean volcanic tuff that has undergone hydrothermal alteration. It is composed of approximately even proportions of phenocrysts and devitrified groundmass both composed of quartz, K-feldspar, albite, andesine, a white mica, biotite and minor apatite. Extensive Ca and Na depletion can be observed in the soil material, corresponding to the almost complete dissolution of andesine and an 80% removal of albite. Biotite is almost absent in the soil material and has been intensely transformed into clays. Al-hydroxides (amorphous to poorly-crystallized forms), hydroxy-Al interlayered vermiculites and interstratified vermiculite-biotite have been identified as the main weathering products. Only trace quantities of kaolinite have been observed in this temperate soil. Imogolite-type-materials (ITM) and allophanes are most likely to be formed in a temperate environment, but these secondary Si-containing minerals have not been detected either directly by SEM and XRD or indirectly using chemical extractions (Ezzaïm et al., 1999).

2.2. Controlling geochemical processes

Statistical analyses and speciation modelling of capillary solutions from the site suggest that the dissolution kinetics of primary silicates (i.e. chemical weathering) provide the main control on Si (Gérard et al., 2002, 2003). Capillary solutions were collected at different soil depths by means of suction-cup lysimeters. Samples were collected monthly over 52 successive months, and at a number of different locations, to capture effects of both temporal and spatial variability (Gérard et al., 2002). A control of chemical weathering of primary silicates on Si was supported by the positive correlation of Si-concentrations with soil temperature. The solubility of kaolinite, ITM and other allophanic compounds typically exhibit an inverse variation with temperature (Gérard et al., 2002), suggesting that these secondary phases do not exhibit a strong control on Si. This observation can also be applied to 2:1 clay minerals. Although the thermodynamic properties of clay minerals are poorly known, the temperature-dependence of their thermodynamic equilibrium constants, and thus to a great extent their solubility, can be appreciated from existing thermodynamic databases. Furthermore, vermiculites observed in this soil were not the products of a precipitation reaction but were formed from the transformation of biotite (Ezzaïm et al., 1999). In addition, the concentration of Si was not affected by this process, as vermiculization reactions are widely recognized as not altering the Si-content of minerals (e.g. Jeong and Kim, 2003).

A more recent complementary study at the same site, but with capillary solutions extracted by centrifugation (Gérard et al., 2003), suggests that the dissolution of alkali feldspars may control Si-concentrations. The contribution of Si release from albite can be neglected because only trace amounts of this phase remain in the soil material. This implied that the reactive surface area of albite was much less than that of K-feldspar, thus suggesting that the dissolution kinetics of K-feldspars provide the main control for Si-release. No significant relationships were found between K (or Na) and Si-concentrations, indicating that different processes are controlling the dynamics of these alkali ions.

In the study conducted by Gérard et al. (2002), it was further shown that the average rate of primary silicate dissolution yields far-from-equilibrium conditions for chemical weathering (i.e. the influence of the chemical affinity term on the rates is small). It was also found that the influence of solution pH on the kinetics was insignificant because of the dominant influence of temperature together

with the relatively narrow pH range. Thermodynamic equilibrium constants (K) used in the speciation model in order to evaluate the presence of far-from-equilibrium conditions are given by Gérard et al. (2001), except for K-feldspar for which log K (25 °C) = −0.96 was used. This value was calculated with the SUPCRT92 program (Johnson et al., 1992) and using the revised Helgeson–Kirkham–Flowers parameters proposed by Shock et al. (1997). Kinetic calculations are based on the linear Transition State Theory (TST) formalism for the dissolution kinetics of primary silicates (e.g. Lasaga et al., 1994; Maher et al., 2006). The corresponding rate expression is given by:

$$r_d = k_{eff}\{H^+\}^n\left(1 - \exp\left(-\frac{A_r}{RT}\right)\right)\exp^{(E_a/RT)} \quad (1)$$

where r_d is the dissolution rate of the mineral (mol L^{-1} s^{-1}), k_{eff} stands for an effective dissolution rate constant given by the product of the mineral reactive surface with a surface-area normalized specific rate constant, the following term corresponds to the aqueous activity of the H^+ ion, n is an experimental exponent that represents the order of the reaction with respect to H^+, A_r is the chemical affinity (J mol^{-1}), R is the gas constant (8.32 J mol^{-1} K^{-1}), T is the temperature in Kelvin (K), and E_a is the apparent activation energy (J mol^{-1}).

These findings on controlling geochemical processes have important implications for the modelling analysis to follow. The fact that K-feldspar likely dominates present-day mineral weathering at this site allows considerable simplification of the geochemical system. In addition, the flux F6 (precipitation of secondary silicate minerals, Fig. 1) is unlikely to be a significant component in this soil. The presence of only trace quantities of kaolinite and the absence of ITM and other allophanes from the soil profile allows us to neglect the formation of secondary silicate minerals from the simulations as a first approximation. In this context, it is acknowledged that marked supersaturations were obtained with respect to poorly-crystallized kaolinite for select solution samples; however, calculating saturation indices based on the mean of the Si-concentrations of all replicates (Gérard et al., 2002) suggests that supersaturated conditions are not common and do not persist.

2.3. Hydrological modelling

Previously, soil water transfer has been simulated at this site (Gérard et al., 2004) by coupling the evapotranspiration processes to hydrological processes in the vadose zone. Simulations were conducted using the modified flow module of the reactive transport code MIN3P (Mayer et al., 2002; Gérard et al., 2004). This numerical model allows for simulating daily variations in soil moisture at different soil depths based on the daily values of throughfall, intercepted water by the tree canopy, potential soil evaporation, and potential plant transpiration. The model was calibrated and validated by comparison with on-site soil moisture measurements. Modelling of the soil water budget was performed for the same time period as the investigation of Si-controlling processes in Gérard et al. (2002); i.e. from mid 1995 to late 1999.

Daily water drainage and transpiration rates for the Douglas fir forest, i.e. the root water uptake, are some of the model outputs. Both fluxes may be important for the modelling of biogeochemical cycling of Si. Vadose zone flow has been simulated by solving Richard's equation using the van Genuchten–Mualem formalism to describe the relationships between pressure head and soil water content, and between unsaturated hydraulic conductivity and soil water content (van Genuchten, 1980). An additional term was used to account for the occurrence of preferential flow (Gérard et al., 2004). The daily transpiration flux (i.e. root water uptake) was based on the water budget at the soil surface:

$$PET = T + E_u + f_i I \quad (2)$$

where PET, T and E_u are the rates of potential evapotranspiration, tree transpiration, and soil evaporation, respectively (m s^{-1}). I stands for the water interception rate by the tree canopy (m s^{-1}) and f_i is a dimensionless factor, which accounts for the reduction of tree transpiration by the evaporative demand of a wet canopy on days with precipitation. The potential tree transpiration rate was distributed over the discretized domain based on the root length density in the corresponding soil layer, the local soil moisture, and a reduction factor that accounts for the transpiration decrease in case of water stress.

An important outcome of this modelling for the present investigation is that capillary upward flows within the soil profile and across its bottom boundary were insignificant because of the well-drained conditions prevailing in the soil and the presence of a very deep water table. Therefore, the flux F9 (Fig. 1) is unlikely to be a significant component in this soil.

2.4. Assessment of the uptake flux

Si-uptake by the Douglas fir forest was estimated by the sum of the mean annual flux of Si returned by litter fall and that accumulated by tree growth (e.g. Bartoli, 1983; Markewitz and Richter, 1998). Fifteen litter-traps (30 × 45 cm from 1995 to 1996 and 71 cm × 71 cm since 1997) were systematically distributed and installed in the stand for tree litter fall collection. After drying at 65 °C, samples were manually sorted into nine components (brown needles, dead wood, green needles, green wood, bark, cones, flowers and buds, and various plant debris), and their dry mass was recorded. The main steps for stand biomass quantification were: (a) provision of a full inventory of the stand; (b) cutting 12 trees that were well distributed throughout the girth classes defined from the inventory, and isolation of the two tree components (branches and trunk); (c) calculation of biomass tables in order to predict the compartmental biomass for each tree of the stand from their circumference. The tree dimensions and fresh mass were recorded in the field. Sub-samples were collected for quantifying branches, and bark and wood from stems separately. Material was dried until there was no mass variation at 65 °C.

The Si content in Douglas fir biomass samples was analyzed gravimetrically (e.g. Eliott et al., 1988; Carnelli et al., 2001). This method has recently been compared with diges-

tion in hydrofluoric acid (Saito et al., 2005), and there was excellent agreement between the two methods ($R^2 = 0.98$). Samples were dried in an oven at 80 °C, weighed, and ashed in a muffle furnace at 450 °C overnight. After cooling, 10 ml 1 M HCl was added to each sample, the sample was agitated, and the residue was allowed to settle. The supernatant solution was pipetted off into a volumetric flask. The ash was then rinsed twice with a small amount of HCl and the rinse solution was added to the volumetric flask, which was made up to volume with deionised water. The residue was dried in an oven at 80 °C overnight, allowed to cool to room temperature and weighed. These solids were assumed to consist of SiO_2, an assumption that was supported by x-ray microanalysis of phytoliths from Douglas fir needles (Sangster et al., 2007). Combined supernatants were analyzed by inductively coupled plasma spectrophotometer (Jobin Youn 70C ICP AES) for soluble Si. Total Si was calculated as the sum of insoluble and soluble Si fractions.

To calculate the mean annual uptake of Si for our Douglas fir forest, we have considered the different compartments of litter fall as defined by Ranger et al. (2003) and their flux measured over the period 1995-1999 (Table 1). Concentrations measured in the major compartments of the living biomass were used in combination with the annual growth of these compartments as derived from Ranger and Gelhaye (2001), in order to calculate the mass of Si stored in biomass from tree growth. Reports on the Si-content of tree roots are rarely found in the literature, mainly because of the difficulty in cleaning roots from all sources of mineral contamination (Fu et al., 2002). As such the values of Gordon and Jackson (2000) for spruce, a mean concentration of 4 mmol of Si per kg of dry matter, and the primary production (~2500 kg ha^{-1} yr^{-1}) for Douglas fir roots reported by Gill and Jackson (2000) were utilized.

2.5. Assessing the uptake mechanisms

Si concentrations in capillary solutions sharply increase below the O-horizon to a depth of 15 cm (Gérard et al., 2002). A marked decrease of concentrations was also observed between capillary solutions sampled at 15 cm and 60 cm depth (Fig. 2). The concentration increase is likely dominated by K-feldspar dissolution that enriches capillary waters with Si as they progressively move downward. In the absence of a significant Si sink caused by secondary mineral precipitation, the observed decrease of Si-concentrations with soil depth can only be explained through an active uptake mechanism by the plants (e.g. Marschner, 1995; Tamai and Ma, 2003). Active uptake is characterized by a rate of solute uptake faster than transpiration, which results in decreased dissolved Si with soil depth as the pore water progressively moves throughout the soil profile. This is in contrast to passive solute uptake where solute is removed together with the pore water and concentrations remain unchanged. In our conceptual and numerical models, we consider a preferential uptake of Si by the Douglas fir forest.

2.6. Modelling approach

To allow for a quantitative analysis and to test the conceptual model, we modified the reactive transport code MIN3P (Mayer et al., 2002) to simulate the biogeochemical cycle of Si (and other plant nutrients) in terrestrial ecosystems. The MIN3P code was designed to simulate one- to three-dimensional flow and multicomponent reactive transport in variably saturated media involving a set of homogeneous and heterogeneous reactions. The model is also capable of simulating networks of equilibrium and kinetic reactions. A number of geochemical processes can be considered with MIN3P, including aqueous speciation, mineral dissolution-precipitation, intra-aqueous kinetic reactions, gas exchange, ion exchange, surface complexation, and linear sorption. Thermodynamic and kinetic constants are determined using the van't Hoff and Arrhenius equations, respectively, based on an externally defined temperature field that can vary in space and time.

For the objectives of the present work, we have added the process of passive solute uptake as an additional sink

Table 1
Concentration of silicon and flux of the different litter fall and living biomass compartments used to estimate the mean annual uptake of the Douglas fir forest

Type	Compartment	Si concentration (mmol $kg^{-1}_{drymatter}$)	Biomass flux[a] ($kg_{dry\,matter}$ ha^{-1} yr^{-1})
Litter fall	Brown needles	403(123)	2345(545)
	Brown wood	105(24)	475(156)
	Green needles	446(121)	390(268)
	Green wood	143(55)	332(505)
	Cones	57	124(45)
	Branches	268	8(11)
	Flowers[b] and buds	194	83(23)
	Various vegetal debris	638	78(43)
Living biomass	Stem wood	15(11)	8000
	Stem bark	74(46)	1200
	Branches	55(23)	1000

Values in parenthesis denote the standard deviation.
[a] Calculated over the period 1995–1999. Standard deviation corresponding to inter-annual variations.
[b] In *forestry*, the terminology of *flowering plants* has commonly though inaccurately been applied to cone-bearing trees as well. The male cone and unfertilized female cone are called "male flower" and "female flower", respectively.

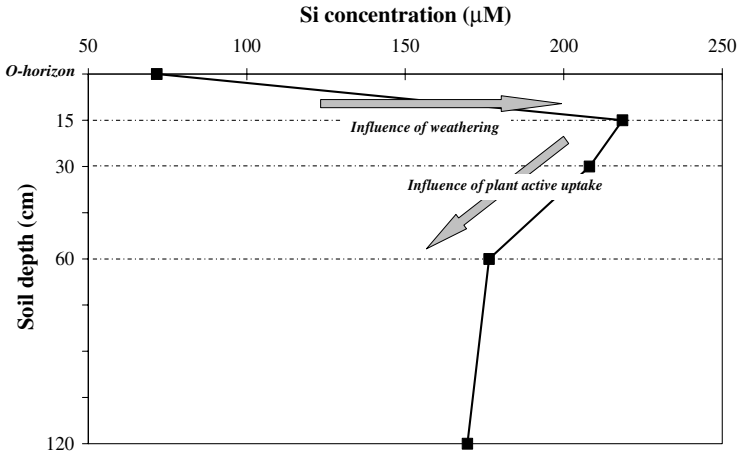

Fig. 2. Mean concentration of dissolved silica expressed as a function of soil depth. Shaded arrows outline variations that are indicative of the significant influence of weathering and plant active uptake.

term in the mass balance equation for the reactive transport of solute species:

$$\frac{\partial}{\partial t}\left(S_a \phi T_j^a\right) = \nabla.\left(S_a \phi D_a \nabla T_j^a\right) - \nabla.\left(v T_j^a\right) - R_j - q T_j^a \quad (3)$$

where S_a stands for water saturation, ϕ is the total porosity, T_j^a is the total aqueous concentration of component j (mol L^{-1}), v is the Darcy velocity (m s^{-1}), D_a is the hydrodynamic dispersion coefficient (m^2 s^{-1}), for a 1D system defined as $D_a = \alpha_L v + D_{eff}$, where α_L is the longitudinal dispersivity (m) and D_{eff} is the effective diffusion coefficient (m^2 s^{-1}). R_j is the sink/source term for kinetically-controlled reactions (mol L^{-1} s^{-1}), and q is the water uptake flux (s^{-1}).

The dissolution rate of K-feldspar (Eq. (1)) is included using the generalized kinetic expressions available in MIN3P (Mayer et al., 2002). The Michaelis-Menten (Monod) rate expression that is commonly used to simulate microbially-mediated reactions (e.g. Salvage and Yeh, 1998; Watson et al., 2003) and nutrient uptake by plants (e.g. Nowack et al., 2006) was used to describe the active uptake of Si:

$$r_a = k_M \left(\frac{[Si]}{K_M + [Si]}\right) \quad (4)$$

where r_a is the active uptake rate (mol L^{-1} s^{-1}), k_M is the kinetic constant (mol L^{-1} s^{-1}), and K_M is the half saturation constant (mol L^{-1}). The brackets in the equation denote the total concentration of dissolved Si.

We adopted the same system geometry and simulation parameters for water transfer as Gérard et al. (2004). The geometry consists of a 1.20 m depth soil profile discretized into 120 grid blocks (of 1 cm each) and comprised of 6 soil horizons with different hydrodynamic properties.

We have not measured the longitudinal dispersivity (α_L) in this soil (Eq. (3)), but have estimated this parameter based on correlating the observation scale to the value of the longitudinal dispersivity (e.g. Gelhar et al., 1992). For the present model application, i.e. a 1.2 m thick soil profile, a maximum of the order of a tenth of a metre is expected for α_L. We neglected the influence of molecular diffusion on Si transfers, as we calculated that $\alpha_L v \gg D_{eff}$. Calculations were made by considering a diffusion coefficient in free water of 1×10^{-10} m^2 s^{-1} and the Millington correction for the influence of tortuosity and soil moisture on D_{eff}.

Model calibration is required because of the empirical nature of the kinetic parameters, E_a and k_{eff} involved in Eq. (1), particularly at the field scale. This is a well-known issue when studying and modelling heterogeneous reactions, and is the focus of intensive research efforts (e.g. Hodson, 1999; Oelkers, 2001; Jové Colon et al., 2004; Dove et al., 2005). The kinetic constant k_M to describe active uptake (Eq. (4)) was also calibrated, but not the half saturation constant, K_M, which was set to a large value in order to minimize the number of parameters to calibrate. Such a simplification implies that Eq. (4) was approximated by the following first order rate equation (Bekins et al., 1998):

$$r_a = k_M^* [Si] \quad (5)$$

where k_M^* is the first order rate constant, with $k_M^* = k_M / K_M$. The root-soil interface (i.e. the rhizosphere) is affected by processes that differ to various extents from those occurring in the bulk soil. These processes are taken into account implicitly in this study, which has been conducted at the soil profile scale. This provides another reason for the apparent nature of the kinetic parameters used to calibrate the model.

Model calibration was performed over the first half of the period covered by the measurements of Si-concentrations in capillary solutions. We evaluated the validity of the model over the second half of the period using identical model parameters. Two statistical criteria were used for evaluating model accuracy. The first criterion is the normalized mean residual error (NMRE, in percent), which evaluates the mean direction of the error and the deviation regarding the mean observed concentration:

$$\mathrm{NMRE} = \left[\frac{\sum_{i=1}^{N}(P_i - O_i)}{N}\right]\frac{100}{\overline{O}} \quad (6)$$

where P_i is the model prediction, O_i the observed value, $\overline{O}$ is the observed mean, and N is the number of observations. A value of the NMRE close to zero indicates that measured and simulated concentrations do not differ systematically

from each other. For practical reasons, we accepted a certain tolerance for the NMRE (±2.5%) while adjusting the relevant controlling parameters in order to obtain the best concentration fit.

The second criterion is the normalized root mean square error (NRMSE), also expressed in percent. This NRMSE is a measure for the scatter between observed and simulated values:

$$\mathrm{NRMSE} = \left[\frac{\sum_{i=1}^{n}(P_i - O_i)^2}{N}\right]^{\frac{1}{2}} \frac{100}{\overline{O}} \quad (7)$$

For calibration purposes we defined different reactive zones or layers in the soil profile wherein the kinetic parameters can be calibrated independently. We considered three reactive layers: a top layer between the inlet boundary to 20 cm depth, where the kinetic parameters directly control the concentrations simulated at 15 cm depth; for the concentrations at 30 cm depth, we set a second reactive layer ranging from 20 to 35 cm depth; for concentrations at 60 cm depth, the deeper reactive layer reaches to the bottom of the soil profile (120 cm depth).

Initial and boundary conditions are identical to values used in a previous study carried out at the site (Gérard et al., 2004) to ensure an accurate and consistent calculation of water drainage and Douglas fir transpiration in the coupled modelling. Transport boundary conditions are represented by measured concentrations in the litter leachates for the inlet, and a free exit condition is set at the outlet boundary. Solutions leached from the O-horizon were collected daily and analyzed in the laboratory (Ranger et al., 2001). The initial temperature profile is set according to on-site measurements performed at the initial simulation time and at five soil depths (0, 15, 30, 60 and 120 cm). Daily temperature values measured over the simulated period (Gérard et al., 2002) are defined in an external file read by the model. At each simulation day, the temperature field is updated automatically and nodal values are obtained by spatial interpolation between the monitoring points.

3. RESULTS

3.1. Si-uptake flux and recycling

Si concentrations measured in the major compartments of the dead and living biomass are given in Table 1. Based on these data, we calculated that 157 mmol m^{-2} yr^{-1} (~44 kg ha^{-1} yr^{-1}) of Si was taken up by the Douglas fir forest of the Vauxrenard field site. Up to 129 mmol m^{-2} (36.2 kg ha^{-1}) of Si were annually recycled to the ground by litter fall. The calculated Si-mass contained in roots represents less than 1% of the total uptake.

3.2. Testing the conceptual model

The concentration of Si at 15, 30 and 60 cm depth (Fig. 3) was initially simulated assuming passive uptake, and by progressively increasing the dissolution rate of K-feldspar (i.e. by increasing k_{eff}) in the top reactive zone (0–20 cm depth) until a reasonable fit of the concentrations measured at 15 cm depth was obtained. We neglected dispersion (i.e. $\alpha_L = 0$) for these initial simulations, and E_a equals the apparent activation energy for K-feldspar dissolution in acid and abiotic conditions; i.e. 51.7 kJ mol^{-1} (Blum and Stillings, 1995). Simulated Si-concentrations at 15 cm depth increased with increasing dissolution rates, and progressively exhibited temporal variations consistent with the measurements (see Fig. 3A). These results reveal the effect of both advective transport and K-feldspar dissolution on dissolved Si-concentrations. At 30 and 60 cm depth, the concentration of Si increased as well but had inconsistent temporal variations, because the concentration fronts were delayed compared to measurements (Fig. 3B and C). In addition, the concentration of Si peaked at higher values compared to the measurements. The delay of the concentration fronts reflects the travel time of soil solutions from 15 to 60 cm depth, as advection is the dominant Si-controlling process in the absence of significant K-feldspar dissolution beneath the top reactive zone. Such a transport-control on Si-concentrations is not reflected in the actual data, which suggests that variations in the rates of reaction processes also occur at depth and overwhelm variations induced by transport.

In an attempt to correct the results for the excessive concentration peaks we first incorporated active uptake, but this process was unsuccessful in remediating temporal discrepancies. Although active uptake improves the fit during periods of elevated Si concentrations, larger discrepancies are obtained during periods of low Si-concentrations (Fig. 4). As expected, the addition of K-feldspar dissolution in the deeper reactive zones improves the fit throughout the soil profile. Si release by K-feldspar dissolution compensates for the concentration decrease by active uptake provided the feldspar dissolution rate is set large enough to ensure consistent seasonal variations (Fig. 5).

Based on this finding, a further increase in the active uptake flux should lead to the same concentration variations if compensated by the equivalent increase in the dissolution rate. In addition, a larger total uptake flux of Si should be obtained as well, since passive uptake would be basically unaltered whereas the active uptake flux increases. This is a crucial factor for the remaining modelling, as it implies that we can first calibrate the model regarding the concentrations irrespective of the uptake flux of Si by the Douglas fir forest, which thus may be calibrated in a second step by re-adjusting k_M and k_{eff}.

3.3. Model calibration

By considering passive uptake, K-feldspar dissolution with E_a based on the literature, and active Si uptake, the above modelling provides Si-concentrations as a function of time and soil depth that are consistent with field data. Unfortunately, despite meeting the NMRE criterion (±2.5%), the NRMSE is appreciably larger, especially at 15 cm depth (Table 2). As expected, gradually increasing the longitudinal dispersivity induced a significant moderation of the seasonal variations at 15 cm and thus improved the goodness-of-fit at this depth (Fig. 6). However, the NRMSE remained high (20%) at this soil depth

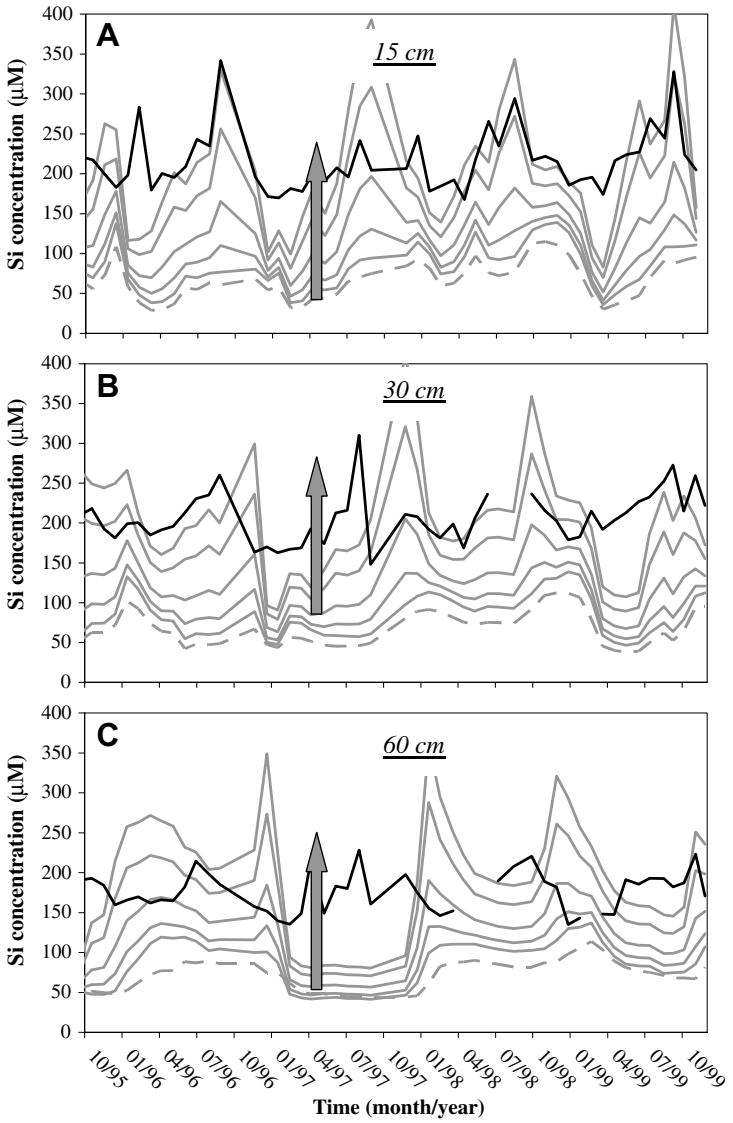

Fig. 3. Concentrations of Si at 15, 30 and 60 cm as a function of time calculated with the model MIN3P by setting different K-feldspar dissolution rates in the top reactive zone (0–20 cm) and passive solute uptake through the soil profile. The shaded arrows outline the overall change in the concentrations obtained by increasing the dissolution rate of K-feldspar. Only advection is considered in these simulations. Black line: measured concentrations. Dashed grey line: concentrations simulated with no K-feldspar dissolution.

(see Table 2). Moreover, it can be seen that the influence of dispersion on NRMSE decreased with soil depth, and the concentrations calculated at 60 cm depth were relatively insensitive to this transport process (not shown). This can be attributed to limited concentration gradients in the deep soil, along with a strong control of the concentrations by K-feldspar dissolution and active uptake as opposed to a control by solute transport processes.

The apparent activation energy for K-feldspar dissolution, E_a, controls the influence of soil temperature on the reaction rate and therefore the amplitude of the concentration variations *vs.* time calculated by the model at the different soil depths. We show in Fig. 7 Si-concentrations obtained for different values of E_a and $\alpha_L = 0.10$ m. Decreasing E_a and re-adjusting k_{eff} accordingly to ensure the goodness-of-fit in terms of the NMRE (±2.5%) decreased the scatter (NRMSE) substantially. However, decreasing E_a further again led to an increase in the scatter (Table 3). We obtained the best fit of the concentrations by setting E_a to half the value reported under acidic and abiotic conditions, which yields a value of approximately 25 kJ mol^{-1}. By doing so, the capacity of the model to simulate the Si concentration in capillary waters was quite good as concentration scatters of about 10% were obtained at 30 and 60 cm depth against ~18% for the topsoil.

3.4. Model validation

Before examining the capability of the model to predict Si-concentrations during the validation period, we used mass balance calculations to derive the mean annual uptake flux corresponding to the previous best concentration fit.

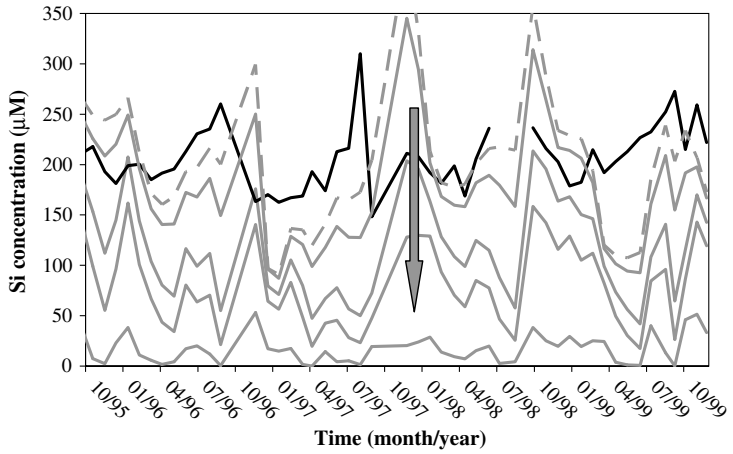

Fig. 4. Influence of active uptake on the concentrations of Si as a function of time calculated with the model MIN3P by assuming K-feldspar dissolution in the top reactive zone (0–20 cm), passive uptake through the soil profile, and active uptake in the two deeper reactive zones. Example given at 30 cm depth. The shaded arrow outlines the overall change in the concentrations obtained by increasing the active uptake flux. Solute transport proceeds by advection only. Black line: measured concentrations. Dashed grey line: concentrations simulated without active uptake (initial case).

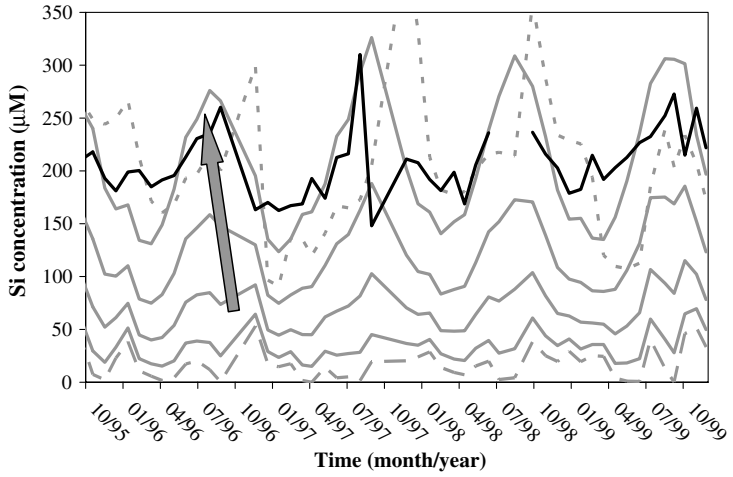

Fig. 5. Influence of increasing the dissolution rate of K-feldspar on the concentrations of Si calculated at 30 cm depth as a function of time with the model MIN3P. These simulations follow those depicted by Fig. 4, where excess Si (dotted line) has been drastically diminished by adding the relevant active uptake flux (dashed line). Setting K-feldspar dissolution in the intermediate reactive zone (20–35 cm depth) leads to consistent seasonal variations and to consistent concentration levels at the 30 cm depth. The shaded arrow outlines the overall change in the concentrations obtained by increasing K-feldspar dissolution rate. Pure advective solute transport is considered. Black line: measured concentrations.

Table 2
Normalized root mean square error (NRMSE, in percent) calculated for the best concentration fit ($-2.5\% <$ normalized mean residual error (NMRE) $< 2.5\%$) assuming different longitudinal dispersion coefficients, ranging from pure advection ($\alpha_L = 0$) to highly dispersed Si transport ($\alpha_L = 0.25$ m)

Soil depth (cm)	Longitudinal dispersion coefficient, α_L (m)				
	0	0.01	0.05	0.1	0.25
15	29.4	26.8	22.8	21.7	21.0
30	17.1	16.8	16.2	15.9	15.7
60	20.7	20.7	20.7	20.7	20.6

Simulations are performed with fixed passive uptake. Results obtained after calibration of the dissolution rate of K-feldspar (using $E_a = 51.7$ kJ mol^{-1}) and active uptake flux.

This test must be performed because a passive uptake flux that exceeds the uptake flux determined from the biomass would invalidate the present simulation results, and the calculation of the transpiration flux and water transfers performed in Gérard et al., 2004).

The flux of passive Si-uptake is defined by the product between the concentration and the transpiration flux. Since the transpiration flux was obtained from previous unsaturated flow modelling, the passive uptake flux is thus imposed by the best fit of the concentrations as obtained from the calibration. Consistent results were obtained in the previous best-fit simulation as a passive Si-flux equal to 97.9 mmol m^{-2} yr^{-1} ($\sim$27.5 kg ha^{-1} yr^{-1}) was calculated, which is much less than required by the biomass

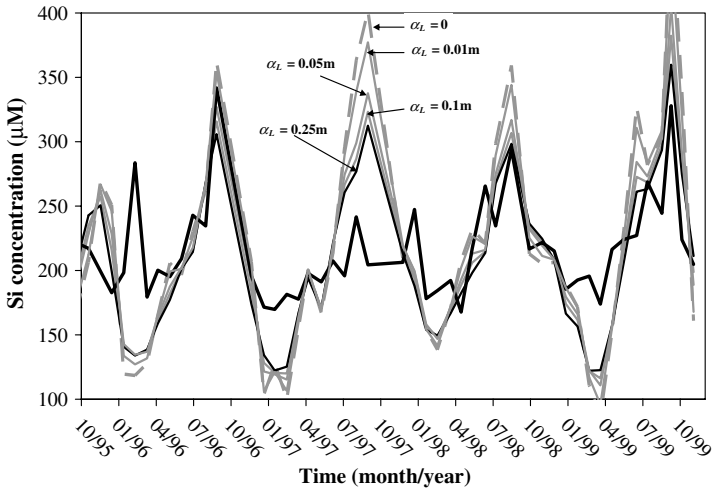

Fig. 6. Concentrations of Si as a function of time calculated with the model MIN3P for different values of the longitudinal dispersion coefficient, ranging from $\alpha_L = 0$ (i.e. pure advection; dashed grey line) to $\alpha_L = 0.25$ m (thin black line). Example given at 15 cm depth. Thick black line: measured concentrations.

(44 kg ha^{-1} yr^{-1}). The mean annual flux actively taken up by the vegetation was estimated to be 23.7 mmol m^{-2} yr^{-1} (~6.7 kg ha^{-1} yr^{-1}). Therefore, the total simulated uptake flux amounted to 121.6 mmol m^{-2} yr^{-1} (~34.2 kg ha^{-1} yr^{-1}), which is about 22% less than assessed from the biomass analysis.

To compensate, we performed a last simulation wherein both the active uptake flux and the dissolution rate of K-feldspar were readjusted. This readjustment induces no significant changes in the simulated concentrations and thus in the passive uptake flux (Fig. 8). Corresponding Si-uptake flux by the Douglas fir forest was 157.8 mmol m^{-2} yr^{-1} (~44.3 kg ha^{-1} yr^{-1}). The ability of the model to predict Si concentrations measured in capillary solutions is quite good (Table 4). The NMRE ranged from −2% to about 4% at 15 and 60 cm depth, respectively. The scatter criterion, NRMSE, ranged around 12% depending on the soil depth. The maximum scatter (13.7%) was obtained at 30 cm.

3.5. Biogeochemical Si cycle

As it can be seen in Fig. 9, the mean flux of Si from K-feldspar dissolution was estimated at 132 mmol m^{-2} yr^{-1} (~37.2 kg ha^{-1} yr^{-1}). In the calibrated model, 53 mmol m^{-2} yr^{-1}(~14.9 kg ha^{-1} yr^{-1}) of Si was released from the O-horizon. As discussed above, about 158 mmol m^{-2} yr^{-1} (~44.4 kg ha^{-1} yr^{-1}) of Si was taken up by the Douglas fir forest. The modelling suggests that this flux was distributed between a passive component of 100 mmol m^{-2} yr^{-1} (~28.1 kg ha^{-1} yr^{-1}) and a more moderate active uptake flux of 58 mmol m^{-2} yr^{-1} (~16.3 kg ha^{-1} yr^{-1}). The sum of all biological flux components including active and passive uptake by the Douglas fir forest and the flux of Si from litter leachates is 211 mmol m^{-2} yr^{-1} (~59.3 kg ha^{-1} yr^{-1}). By assuming that all the Si in litter leachates was released from dissolving biogenic Si, the present modelling suggests the predominance of the biological cycle for the control of Si-concentrations in capillary solutions (biologically-controlled at 62%, i.e. 211/343 × 100), leaving only 38% for geochemical contributions from K-feldspar dissolution. The mean flux of Si draining out of the soil profile was estimated at 18 mmol m^{-2} yr^{-1} (~5.1 kg ha^{-1} yr^{-1}), small in comparison to the uptake by the forest stand.

4. DISCUSSION

4.1. Sources for Si in litter leachate

Previously, the predominance of biological turnover *vs.* geochemistry has only been found in tropical forest ecosystems (e.g. Alexandre et al., 1997; Meunier et al., 1999; Derry et al., 2005; Ziegler et al., 2005), and in two forests exposed to temperate and Mediterranean conditions and covered by deciduous species (Bartoli, 1983; Markewitz and Richter, 1998). Even if it is assumed that Si in litter leachates originates from the dissolution of silicate minerals admixed into the O-horizon, the geochemical and biological cycles would be equal to 185 and 158 mmol ha^{-1} yr^{-1}, respectively (Fig. 9), and thus would be similar. Therefore, regardless of the origin of Si leached from the O-horizon, this modelling exercise points to a very substantial contribution of biological processes for controlling the Si cycle at this site.

We did not attempt to quantify the amount of primary silicates stored in the forest floor, and quantitative data are absent from the literature. However, the study of Rustad and Cronan (1995) on Al-cycling in the forest floor of a similar ecosystem may be used to assess the potential for mineral Si sources in the O-horizon. These authors found that the solution Al-flux (2.1 kg ha^{-1} yr^{-1}) from the O-horizon was much larger than the aboveground inputs (0.9 kg ha^{-1} yr^{-1}) and thus hypothesized a contribution of Al from the mineral horizon underneath. At the present site, utilizing existing data (Ranger et al., 2003), a litter leachate Al flux of roughly 5 kg ha^{-1} yr^{-1} (18 mmol m^{-2} yr^{-1}) was estimated while aboveground

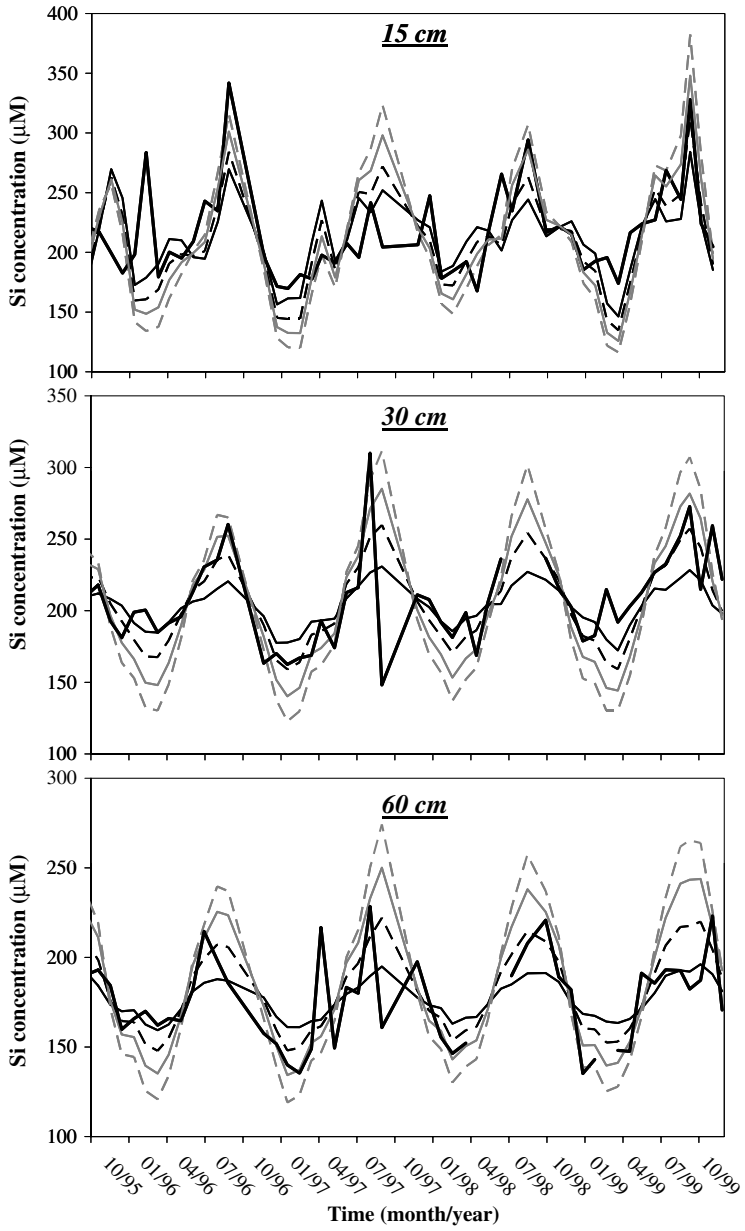

Fig. 7. Concentrations of Si as a function of time calculated with the model MIN3P by setting different values of the apparent activation energy (E_a) of K-feldspar dissolution. Dashed grey line: $E_a = 51.7$ kJ mol^{-1} (Blum and Stillings, 1995), continuous grey line: E_a 25% decrease, thin dashed black line: E_a 50% decrease, thin continuous black line: E_a 75% decrease. Thick continuous black line: measured concentrations.

input of Al returned by falling plant litter was estimated to be only 0.4 kg ha^{-1} yr^{-1} (1.5 mmol ha^{-1} yr^{-1}). Considering the relative contribution of the litter fall to the above-ground Al inputs calculated by Rustad and Cronan (1995), i.e. 69%, we found that at least 15 mmol m^{-2} yr^{-1} of Al was brought to the O-horizon from the mineral soil at the Vauxrenard field site by bioturbation. Assuming that K-feldspar was the sole admixed mineral form responsible for this accumulation, the flux of mineral Si in litter leachates is estimated as 45 mmol m^{-2} yr^{-1}. This mineral flux could account for virtually all the measured Si flux in litter leachate (Fig. 9), and the contribution of chemical weathering to the biogeochemical cycle of Si would approach 52% (i.e. $(132 + 45)/343)) \times 100$.

Table 3
Normalized root mean square errors (NRMSE, in percent) obtained for the best concentration fit ($-2.5\% <$ normalized mean residual error (NMRE) $< 2.5\%$) assuming a dispersivity (α_L) of 0.1 m and progressively decreasing the activation energy of K-feldspar dissolution

Soil depth (cm)	E_a [a]	$0.75E_a$	$0.5E_a$	$0.25E_a$
15	21.7	19.2	18.5	19.2
30	15.9	11.3	9.3	12.0
60	20.7	15.4	11.0	11.1

[a] $E_a = 51.7$ kJ mol^{-1} (Blum and Stillings, 1995).

However, several observations contradict such an important contribution of primary mineral dissolution to

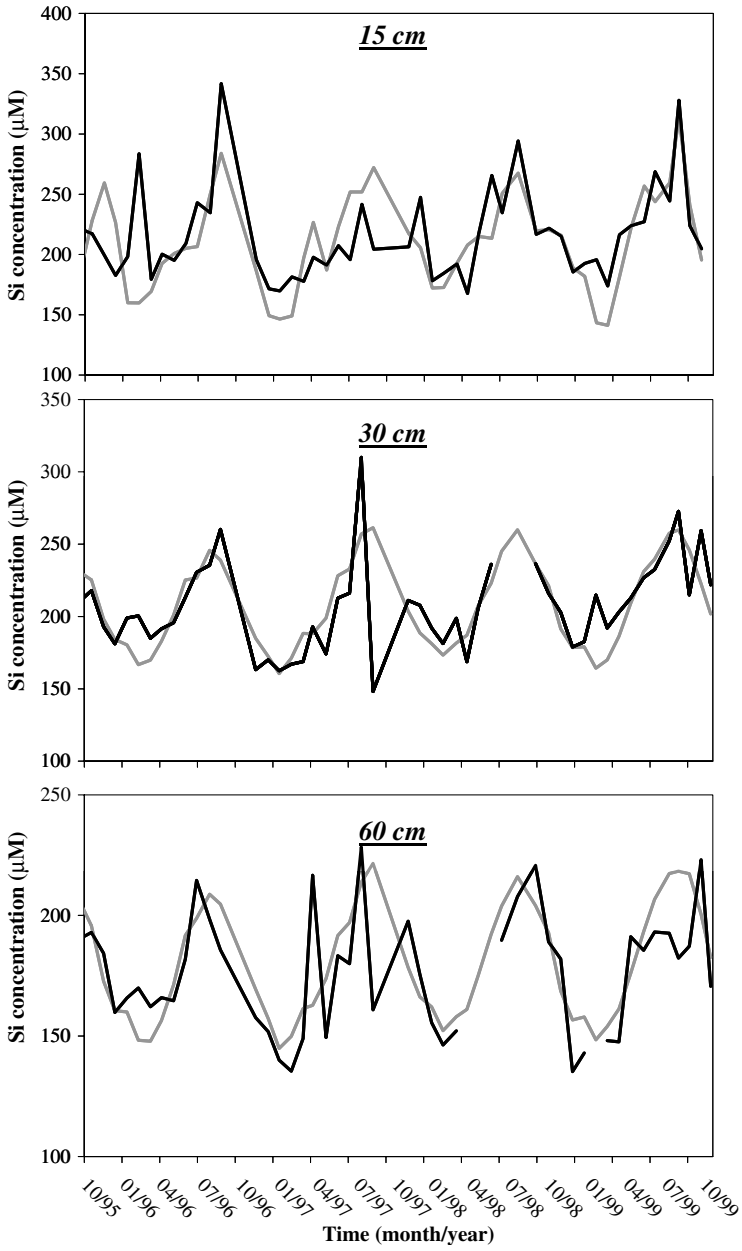

Fig. 8. Concentrations of Si as a function of time calculated with the model MIN3P after adjusting active uptake and dissolution rates to get the best concentration fit together with a consistent value of the mean annual uptake flux. Thick continuous black line: measured concentrations.

Table 4
Normalized mean residual error (NMRE, in percent) and normalized root mean square errors (NRMSE, in percent) calculated for the reference simulation over the validation period (Fig. 10)

Soil depth (cm)	NMRE	NRMSE
15	−2.0	12.4
30	−1.3	13.7
60	3.9	10.8

Si in litter leachates. First, we neglected the contribution of admixed Al-hydroxides although these phases are quite abundant (Ezzaïm et al., 1999). Second, most likely the storage of Al in the O-horizon was caused by its adsorption onto carboxylic groups of the organic material (e.g. Rustad and Cronan, 1995). Third, Si-concentrations in waters leached from the O-horizon exhibited a very large silica enrichment compared with the concentration in throughfall and the maximum Si-concentration measured in litter leachates was reached in autumn, when the amount of falling litter is largest (Ranger et al., 2003). Si-concentrations in litter leachates were not related to the amount of throughfall occurring in winter (Fig. 10). In addition, we estimated residual biogenic Si from the difference between the flux

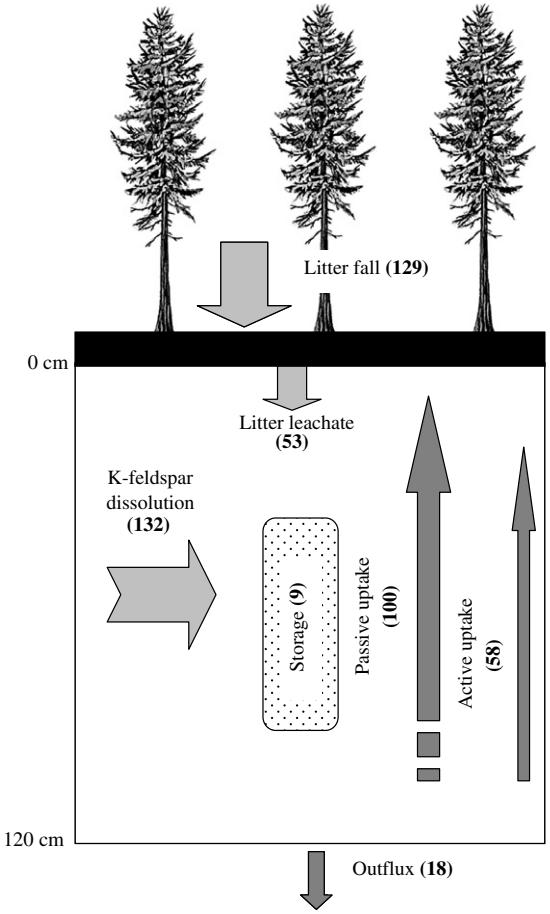

Fig. 9. Illustration of the simulated biogeochemical cycle of Si calculated by MIN3P. The numbers given in parenthesis correspond to the mean annual values (given in mmol m^{-2} yr^{-1}) of the different Si flows involved in the biogeochemical Si-cycle.

of Si released from litter fall (129 mmol m^{-2} yr^{-1}) and Si contained in litter leachates (53 mmol m^{-2} yr^{-1}) to 76 mmol m^{-2} yr^{-1} (~21.3 kg ha^{-1} yr^{-1}). This fraction amounts to 59% of the influx of Si released from litterfall. Residual biogenic Si remains in the O-horizon and may be subjected to translocation by bioturbation and stored in the mineral soil (e.g. Colin et al., 1992; Meunier et al., 1999). Assuming all the residual biogenic Si underwent translocation, was preserved in the mineral soil, and that a steady-state has been established since the planting of the Douglas fir forest (over 40 years), a maximum value for the accumulation of soil phytoliths in the soil column can be calculated. The resulting value is 852 kg ha^{-1}, which is much less than 26,600 kg ha^{-1} determined by Alexandre et al. (1997) for a tropical forest. Considering the accumulation period in the tropical forest was estimated at 458 yrs (see Alexandre et al., 1997), we calculated a flux equal to 58.1 kg ha^{-1} yr^{-1}, which is more than twice as large than in the present temperate ecosystem. The difference would increase if only a portion of Si in litter leachates is released by dissolution of phytoliths. These observations provide further support for a significant biogenic contribution to Si present in litter leachate.

4.2. Uptake flux and mechanisms

The value for the uptake of Si estimated from biomass analysis is large compared with the limited data for coniferous species reported in the literature. This uptake rate falls within the range of values reported for deciduous forests (e.g. Conley, 2002) in a similar pedo-climatic context (moderate elevation, temperate climate, acidic brown soil). Generally conifers are low silicon accumulators when compared with other groups of plants (Hodson et al., 2005). However, high biomass productivity of the Douglas fir investigated here is accompanied by comparatively large quantities of falling litter and annual growth (Ranger and Gelhaye, 2001; Ranger et al., 2003). In addition, the mean Si content measured in the major compartments of the litter fall; i.e. the needles (Table 1), ranged from 1.13% to 1.25% Si in green and brown needles, respectively. Therefore, it is likely that the large uptake flux calculated in this work reflects both the high productivity of the Douglas fir forest and

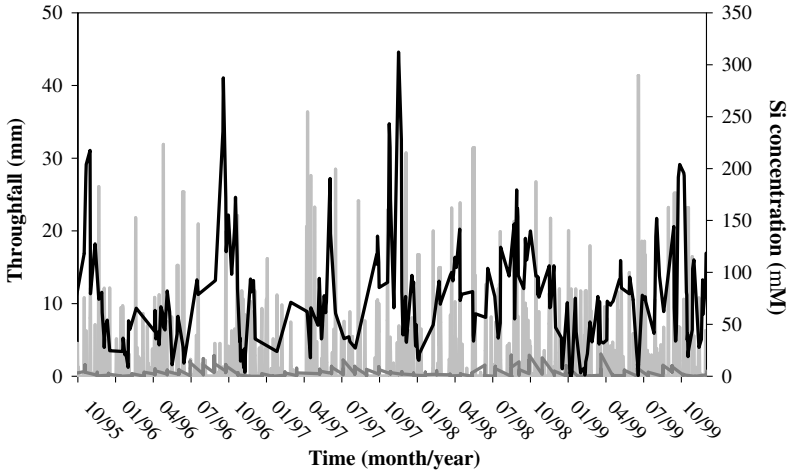

Fig. 10. Daily amount of throughfall (light grey line), mean dissolved silica concentration measured in throughfall (dark grey line) and in litter leachates (black line) of the Vauxrenard field site.

the quite large Si concentration in the needles. Previous work has shown that Si concentrations in the needles of Douglas fir vary quite considerably depending on the location sampled (Beaton et al., 1965; Klein and Geis, 1978; Hodson et al., 1997; Hodson and Sangster, 1999), and the present analyses fall in the upper part of this range.

These high Si contents suggest an active uptake of Si by Douglas fir in this forest. This mechanism was also required by our model to explain the decrease of Si-concentrations with soil depth and to fit the uptake flux calculated from biomass analysis. Furthermore, it was calculated that ~63% of Si uptake occurred passively (Fig. 9) and as much as ~37% of Si would be actively taken up by the trees, which therefore appeared to spend significant metabolic energy for Si uptake. The predominance of passive uptake appears quite consistent with the preferential accumulation of Si in the plant transpiration termini, the needles, with greater amounts in the tip and middle (Sangster et al., 2007). To our knowledge, Si-uptake mechanisms have never been studied in woody species, and certainly not in trees growing in the field.

Direct proof (i.e. by identifying the gene) of the presence of an Si transporter in higher plants has been provided by Ma et al. (2006). Their work concerned rice, a non-woody species, and a heavy Si accumulator, confirming the study of Tamai and Ma (2003), which was based on indirect evidence (i.e. on the observation of the Si concentration decrease in hydroponic solutions). This method was also used by Rains et al. (2006) to show active uptake by wheat, another heavy Si-accumulator species. Such a relationship between the occurrence of active uptake and the Si content of plants follows earlier investigations that attributed the difference in Si accumulation to the ability of the root to take up Si (e.g. Takahashi et al., 1990). This idea was reiterated by Ma and Takahashi (2002) who proposed criteria for the presence of active uptake, based on Si concentrations and Si/Ca molar ratios in plant shoots. They defined a Si accumulator as a species with above 1% Si and a Si/Ca molar ratio above unity. We used the data of Ranger et al. (2003) for the mean Ca concentration in needles and our analysis for Si and found that Douglas fir at the Vauxrenard site met these criteria (Si/Ca = 3.51 and 2.18 in green and brown needles, respectively).

Note that Ranger et al. (2003) also reported 1.4% and 1.18% nitrogen in green and brown needles, respectively, implying that N was more than two times more concentrated (on a molar basis) than Si in Douglas fir needles, which is in line with the well-known macronutrient status of nitrogen. However, the occurrence of larger N-concentrations has not always been found. Epstein and Bloom (2005) reported Si-concentrations for various species ranging between 0.1% and 10% and N-concentrations ranging from 0.5% to 6%, thus suggesting that Si is higher than N in some plants. In rice, N concentrations between 0.8% and 3.34% were measured by Sahrawat (1983), depending on soil nitrogen availability, while Si concentrations in this heavy Si accumulator species are above 1% (e.g. Ma and Takahashi, 2002) as in the present case for the Douglas-fir of the Vauxrenard field site.

Hodson et al. (2005) have carried out a meta-analysis of published data summarizing relative Si-concentrations in leaves and non-woody tissues of 735 plant species. This work demonstrated that both dicotyledons and monocotyledons contained Si accumulator species. Moreover, woody species can also accumulate much Si, since common beech (*Fagus sylvatica*) exhibited a relative abundance indicator as high as 6.1, while rice (*Oryza sativa*) exhibited a value of only 4.2. Thus it is likely that active uptake of Si is not restricted to a few grass and cereal species and such a mechanism in Douglas fir would seem tenable.

The present modelling investigation was based on the observation of Si-concentration data in capillary waters—a nutritive solution—and can be seen as equivalent to the indirect method commonly used in the literature to demonstrate the occurrence of active uptake for non woody plants (Tamai and Ma, 2003; Rains et al., 2006). In other words, biogeochemical modelling together with soil solution data has enabled us to present indirect evidence for this process in a woody species, and more specifically for mature trees in the field. This result supports the study of Markewitz and Richter (1998) carried out in a coniferous ecosystem under a Mediterranean-type climate, where the need for the active uptake of Si was also proposed to meet mass balance calculations.

4.3. Chemical weathering

The flux of Si released by weathering reactions occurring in the soil material (37.2 kg ha^{-1} yr^{-1}) is similar to an estimate for K-feldspar weathering made for the same field site (Ranger et al., 2002) with no provision for the biological Si-cycle. They used the Profile model (Sverdrup and Warfvinge, 1995) and determined the Si-weathering rate at 30 kg ha^{-1} yr^{-1} based on K-release (assuming that the flux of K originates from K-feldspar). This is 24% smaller than calculated here, where we accounted for the influence of the biological Si-cycle. Given the uncertainties prevailing in these calculations, the difference cannot be ascribed to the effect of biology on the weathering flux. However, the comparison showed that modelling with the MIN3P-code has provided a value for chemical weathering flux consistent with a well-established model.

We also calculated estimates of the reactive surface area for K-feldspar based on the flux of Si released by chemical weathering. By using the calibrated effective rate constants together with the specific dissolution rate constant in abiotic and acidic media (Blum and Stillings, 1995) we calculated a reactive surface area of 0.15 m^2 g^{-1} and roughly 3 m^2 g^{-1} in the top and in the underlying reactive layers, respectively. A sound comparison between these estimates and field-scale values of the literature is difficult, as these values are model-dependent. In the present modelling we assumed that active uptake was absent from the top reactive layer since we did not observe a concentration decrease between 0 and 15 cm depth. Therefore, we have not been led to increase the K-feldspar dissolution rate in the top reactive layer in order to preserve the goodness-of-fit of the concentrations after adjusting the active uptake flux, hence the much lower value taken by the reactive surface area of K-feldspar in this layer. Nevertheless, this result is consistent with more advanced weathering in shallow soil layers.

We have shown that the model-calculated concentrations fit reasonably well with measured concentrations, provided that we decreased E_a by about 50% of the value taken by default and derived from experimental studies in similar pH conditions. This is consistent with laboratory studies showing that E_a can significantly decrease for moderately acidic pH conditions (e.g. Blum and Stillings, 1995) and/or when organic ligands promote dissolution (Brady et al., 1999; Welch and Ullman, 1999, 2000). A dissolution rate enhancement driven by organic ligands is a likely process in surface environments (e.g. Drever and Stillings, 1997). The pH of capillary soil solutions exhibited a mean value consistent with acid conditions at the different soil depths (i.e. pH ~4.3, see Gérard et al., 2002), but it varied and locally reached a value close to pH 5. This pH range overlaps with the boundary of the neutral domain commonly defined for the dissolution kinetic of feldspars (e.g. Drever and Stillings, 1997).

The important influence of biological turnover observed here, although likely to be applicable to many acid soils, does not preclude control of Si in surface waters by chemical weathering (e.g. White and Blum, 1995; White et al., 1999; Goddéris et al., 2006). The influence of biological processes is normally attenuated as soil waters leach through the subsoil before reaching rivers. Accordingly, Si in infiltrating water progressively turns from a control by biological processes to a control by weathering reactions occurring in the regolith. This was observed by Ziegler et al. (2005) in Hawaiian soil and stream waters through Si isotopic composition measurements. However, Nédeltcheva et al. (2006) showed for the much cooler climate of the Vosges Mountains that soil solutions contribute significantly to concentrations in streams; for Si, it appears that almost 70% of the Si-concentrations measured in streams was acquired from the root zone.

4.4. Spatial variability and uncertainties

An indication of the spatial variability at the forest stand scale can be seen in Table 1 for Si in the major litter fall compartments, in Gérard et al. (2002) for the concentrations in capillary solutions, and in Gérard et al. (2004) for the soil water content. Indeed, spatial variation was important for all these master variables, and this is presumably the same for the processes under investigation. Although a detailed account of spatial variability was beyond the scope of the present work, the consideration of spatial-average master variables may question the effects of simplification on the modelling outcomes, and particularly the relative importance of biology *vs.* geochemistry and the need of an active mechanism for uptake of Si by Douglas fir in order to close the mass balance.

For evaluation purposes, a simple sensitivity analysis is conducted to assess the relative variability of the fluxes shown in Fig. 9 in response to the combined effect of a 15% variation in the uptake by the vegetation and of a variation in the transpiration rate. For example, if one assumes 15% less Si-uptake as calculated from biomass analysis (i.e. $\sim$134 mmol m^{-2} yr^{-1}) and 15% more transpiration, which results in a 15% increase of the passive uptake flux, the flux of Si that is actively taken up by the Douglas fir forest must be decreased by a factor three (i.e. $\sim$19 mmol m^{-2} yr^{-1}) to compensate for the decrease in the total uptake flux. The recalculated active uptake flux amounts to only 14% of the diminished total uptake, highlighting the uncertainty associated with the active uptake mechanism. Simultaneously, the weathering flux must be decreased to compensate for the decrease of active uptake. We have shown that the same quality of fit can be obtained for Si-concentrations by calibrating the active uptake flux and the weathering flux, through the adjustment of the kinetic constants. Mass balance calculations showed that a weathering flux of 93 mmol m^{-2} yr^{-1} (i.e. 132–39 mmol m^{-2} yr^{-1}) should be sufficient, which indicates that only 33% of the biogeochemical Si cycle is controlled by chemical weathering of K-feldspars, in comparison to the initial estimate of 38% (Fig. 9). In relative terms this would point towards an even greater importance of biological processes in contribution to Si-cycling in comparison to our calibrated model. The opposite scenario, (i.e. 15% additional total Si-uptake and 15% less transpiration) promotes the contribution of geochemistry *vs.* biology. For this case, we calculated that 42% of the biogeochemical Si cycle was controlled by chemical weathering, against 38% initially (Fig. 9), still leaving a substantial contribution for the biological fluxes. In addition, this scenario would point to an even larger contribution of active uptake, than suggested by our simulations. We also tested different combinations of such variations in Si-uptake and transpiration fluxes. The calculations suggested that for variations not exceeding 15%, the weathering flux cannot exceed 42% of the biogeochemical cycle, but can be much less (decrease to 27%).

The question of the effect of the formation of trace quantities of kaolinite on the modelling of the biogeochemical Si cycle can also be posed. To maintain the uptake flux at the calibrated level, the occurrence of kaolinite formation must be compensated by an equivalent increase of K-feldspar weathering. This would lead to a relative decrease in the importance of the biological contribution towards Si-cycling. However, even if uncertainties associated with the uptake flux are combined with the formation of kaolinite and enhanced feldspar dissolution, measured Si accumulation in live and dead biomass indicate that biogenic fluxes remain significant and in magnitude remain at least comparable to geochemical fluxes.

4.5. On the influence of soil phytoliths

Based on our calibrated model (Fig. 9), 41% (53 mmol m^{-2} yr^{-1}) of the biogenic Si introduced by plant litter (129 mmol m^{-2} yr^{-1}) dissolves in the O-horizon and is released by litter leachates into the underlying mineral soil, while the remainder accumulates in the O-horizon (76 mmol m^{-2} yr^{-1}). However, it is also conceivable that phytoliths are transported to deeper regions of the soil profile by biologic activity. Subsequent to translocation and depending on the geochemical conditions, phytoliths may undergo either dissolution or provide a substrate for formation of secondary silicates (Farmer et al., 2005).

Assuming that complete dissolution of the phytoliths occurs, the rate of feldspar dissolution must be reduced by 76 mmol m^{-2} yr^{-1} to maintain a closed mass balance (Fig. 9). This scenario would result in complete recycling of Si from litter fall and would imply that biological processes contribute even more significantly to Si-cycling than in our calibrated model (84% *vs.* 62%). However, such a weak influence of geochemical weathering appears unrealistic. Even in a tropical climate, phytoliths in the litter fall were not completely dissolved in the soil column with 8% remaining in the soil profile (Alexandre et al., 1997).

On the other hand, Farmer et al. (2005) argued that soil phytoliths introduced by translocation may provide a suitable substrate for the formation of secondary amorphous silica and may therefore be responsible for the sink of Si in Bs horizons of podzols. Geochemical modelling performed for the current site produced data that were rather well aligned with the stability line of an hypothetical Si-rich phase (Gérard et al., 2002), providing support for a control by secondary silica-like compounds. However, these secondary products have never been identified - neither in the soil studied in the present investigation, nor in the Bs horizons studied by Farmer et al. (2005). The effect of this process on Si-cycling would be similar to that of kaolinite formation, i.e. resulting in an increase of the importance of chemical contributions to the overall Si mass balance.

5. CONCLUSIONS

In the present study we developed a numerical model to investigate the biogeochemical Si-cycle in a temperate soil covered by a mature (40 year-old) Douglas fir forest. We attempted to simulate the concentrations of Si measured in capillary solutions over several years and at different soil depths. The ability of the model to reproduce concentrations was satisfactory (about 10% of scatter error) and the simulations were particularly useful to estimate fluxes that are not directly attainable by measurements.

Results showed that the presence of this coniferous forest, which exhibited a high productivity and contained significant Si in needles, can significantly contribute to the biogeochemical cycling of Si. On average, we estimated that only 38% of the Si cycle is attributed to chemical weathering, while the remainder is comprised of plant uptake (47%) and, to a lesser extent (15%), the ingress of biogenic Si dissolving from phytoliths present in the O-horizon. The large contribution of biological processes appears consistent with studies performed in temperate and Mediterranean forest ecosystems. Uncertainties remain with respect to the role of phytoliths, the formation of secondary minerals, and Si-uptake by plants, which warrant further investigation in future studies. However, despite these uncertainties, the present results indicate that the influence of plants on the biogeochemical Si cycle, and thus on the global cycle of Si, can be important, even in a temperate climate.

ACKNOWLEDGMENTS

The authors are indebted with the technical assistance in the field and the laboratory provided by D. Gelhaye, B. Pollier, S. Prabagar. Model developments and the present application were partially funded by the contribution of the 'Agence Nationale pour la Recherche' (ANR), program 'Ecosphère continentale: processus et modélisation', and the 'GIP-Ecofor' for help in the maintenance of the field site within the French Ministry of Research's Observatoire de Recherche pour l'Environnement network (ORE). We also acknowledge financial support for this cooperative research from the French Embassy in Ottawa ('Fonds France-Canada pour la Recherche', FFCR) and NSERC (Natural Sciences and Engineering Research Council of Canada). Finally, we believe that the manuscript has been greatly improved by the recommendations made by C. Steefel and two anonymous reviewers.

REFERENCES

AFES (1992) *Principaux sols d'Europe. Référentiel pédologique*. Association Française pour l'Etude des Sols. Institut National de Recherches Agronomique.

Alexandre A., Meunier J.-D., Colin F. and Koud J.-M. (1997) Plant impact on the biogeochemical cycle of silicon and related weathering processes. *Geochim. Cosmochim. Acta* **61**, 677–682.

Bartoli F. (1981) Le cycle biogeochimique du silicium sur roche acide: application à deux écosystèmes forestiers tempérés (Vosges). Thesis, Univ. Henri Poincaré, Nancy, France, p. 188.

Bartoli F. (1983) The biogeochemical cycle of silicon in two temperate forest ecosystems. *Environ. Biogeochem. Ecol. Bull.* **35**, 469–476.

Bartoli F. (1985) Crystallochemistry and surface properties of biogenic opal. *J. Soil Sci.* **36**, 335–350.

Bartoli F. and Souchier B. (1978) Cycle et rôle du silicium d'origine végétale dans les écosystèmes tempérés. *Ann. Sci. Forest.* **35**, 187–202.

Bartoli F. and Wilding L. P. (1980) Dissolution of biogenic opal as a function of its physical and chemical properties. *Soil Sci. Soc. Am. J.* **44**, 873–878.

Beaton J. D., Brown G., Speer R. C., Masrae I., McGhee W. P. T., Moss A. and Kosick R. (1965) Concentration of micronutrients in foliage of three coniferous tree species in British Columbia. *Soil Sci. Soc. Am. Proc.* **29**, 299–302.

Bekins B. A., Warren E. and Godsy E. M. (1998) A comparison of zero-order; first-order, and monod biotransformation models. *Groundwater* **36**, 261–268.

Berner R. A., Rao J.-L., Chang S., O'Brien R. and Keller C. K. (1998) Seasonal variability of adsorption and exchange equilibria in soil waters. *Aqu. Geochem.* **4**, 279–290.

Blum A. E. and Stillings L. L. (1995) Feldspar dissolution kinetics. In *Chemical Weathering Rates of Silicate Minerals*, vol. 31 (eds. A . F. White and S. L. Brantley). Mineral. Soc. Am., pp. 291–351.

Brady P. V., Dorn R. I., Brazel A. J., Clark J., Moore R. B. and Glidewell T. (1999) Direct measurement of the combined effects of lichen, rainfall, and temperature on silicate weathering. *Geochim. Cosmochim. Acta* **63**, 3293–3300.

Carnelli A. L., Madella M. and Theurillat J.-P. (2001) Biogenic silica production in selected alpine plant species and plant communities. *Ann. Bot.* **87**, 425–434.

Colin F., Brimhall G. H., Nahon D., Lewis C. J., Baronnet A. and Danty K. (1992) Equatorial rainforest lateritic mantles: a geomembrane filter. *Geology* **20**, 523–526.

Conley D. J. (2002) Terrestrial ecosystems and the global biogeochemical silica cycle. *Global Biogeochem. Cycles* **16**, 1121–1128.

Derry L. A., Kurtz A. C., Ziegler K. and Chadwick O. A. (2005) Biological control of terrestrial silica cycling and export fluxes to watersheds. *Nature* **433**, 728–731.

Dove P. M., Han N. and De Yoreo J. J. (2005) Mechanisms of classical crystal growth theory explain quartz and silicate dissolution behavior. *PNAS* **102**, 15357–15362.

Drees L. R., Wilding L. P., Smeck N. E. and Senkayi A. L. (1989) Silica in soils: quartz and disordered silica polymorphs. In *Mineral in Soil Environments* (eds. J. B. Dixon and S. B. Weed). Soil Sci. Soc. Am., pp. 913–974.

Drever J. I. and Stillings L. L. (1997) The role of organic acids in mineral weathering. *Colloids Surf. A: Physicochem. Eng. Aspects* **120**, 167–181.

Drever J. I. and Zobrist J. (1992) Chemical weathering of silicate rocks as a function of elevation in the southern Swiss Alps. *Geochim. Cosmochim. Acta* **56**, 3209–3216.

Eliott C. L., Snyder G. H. and Jones D. B. (1988) Rapid gravimetric determination of silicon in rice straw. *Commun. Soil Sci. Plant Anal.* **19**, 1543–1550.

Epstein E. (1999) Silicon. *Annu. Rev. Plant Physiol. Plant. Mol. Biol.* **50**, 641–644.

Epstein E. and Bloom A. J. (2005) *Mineral Nutrition of Plants: Principles and Perspectives*, second ed. Sinauer, Sunderland, USA.

Ezzaïm A., Turpault M.-P. and Ranger J. (1999) Quantification of weathering processes in an acid brown soil developed from tuff (Beaujolais, France). Part II. Soil formation. *Geoderma* **87**, 155–177.

Farmer V. C., Delbos E. and Miller J. D. (2005) The role of phytolith formation and dissolution in controlling concentrations of silica in soil solutions and streams. *Geoderma* **127**, 71–79.

Fraysse F., Pokrovsky O. S., Schott J. and Meunier J.-D. (2006) Surface properties, solubility and dissolution kinetics of bamboos phytoliths. *Geochim. Cosmochim. Acta* **70**, 1939–1951.

Fu F., Akagi T. and Yabuki S. (2002) Origin of silica particles found in the cortex of Matteuccia roots. *Soil Sci. Soc. Am. J.* **66**, 1265–1271.

Fulweiler R. W. and Nixon S. W. (2005) Terrestrial vegetation and the seasonal cycle of dissolved silica in a southern New England coastal river. *Biogeochemistry* **74**, 115–130.

Gelhar L. W., Welty C. and Rehfeldt K. R. (1992) A critical review of data on field-scale dispersion in aquifers. *Water Resour. Res.* **28**, 2017–2032.

Gérard F., Boudot J.-P. and Ranger J. (2001) Consideration on the occurence of the Al_{13} polycation in natural soil solutions and surface waters. *Appl. Geochem.* **16**, 513–529.

Gérard F., François M. and Ranger J. (2002) Processes controlling silica concentration in leaching and capillary soil solutions of an acidic brown forest soil (Rhône, France). *Geoderma* **107**, 197–226.

Gérard F., Ranger J., Ménétrier C. and Bonnaud P. (2003) Silicate weathering mechanisms determined using soil solutions held at high matric potential. *Chem. Geol.* **202**, 443–460.

Gérard F., Tinsley M. and Mayer K. U. (2004) Preferential flow revealed by hydrologic modeling based on predicted hydraulic properties. *Soil Sci. Soc. Am. J.* **68**, 1526–1538.

Giesler R., Ilvesniemi H., Nyberg L., van Hees P., Starr M., Bishop K., Kareinen T. and Lundström U. S. (2000) Distribution and mobilization of Al, Fe and Si in three podzolic soil profiles in relation to the humus layer. *Geoderma* **94**, 249–263.

Gill R. and Jackson R. B. (2000) Global patterns of root turnover for terrestrial ecosystems. *New Phytol.* **81**, 275–280.

Goddéris Y., François L. M., Probst A., Schott J., Moncoulon D., Labat D. and Viville D. (2006) Modelling weathering processes at the catchment scale: the WITCH numerical model. *Geochim. Cosmochim. Acta* **70**, 1128–1147.

Gordon W. S. and Jackson R. B. (2000) Nutrient concentrations in fine roots. *Ecology* **81**, 275–280.

Hinsinger P., Fernandes Barros O. N., Benedetti M. F., Noack Y. and Callot G. (2001) Plant-induced weathering of a basaltic rock: experimental evidence. *Geochim. Cosmochim. Acta* **25**, 137–152.

Hodson M. E. (1999) Micropore surface area variation with grain size in unweathered alkali feldspars: implications for surface roughness and dissolution studies. *Geochim. Cosmochim. Acta* **62**, 3429–3435.

Hodson M. J. and Evans D. E. (1995) Aluminium/silicon interactions in higher plants. *J. Exp. Bot.* **46**, 161–171.

Hodson M. J. and Sangster A. G. (1999) Aluminium/silicon interactions in conifers. *J. Inorg. Biochem.* **76**, 89–98.

Hodson M. J., White P. J., Mead A. and Broadley M. R. (2005) Phylogenetic variation in the silicon composition of plants. *Ann. Bot.* **96**, 1027–1046.

Hodson M. J., Williams S. E. and Sangster A. G. (1997) Silica deposition in the needles of the gymnosperms. I. Chemical analysis and light microscopy. In *The State-of-the-Art of Phytoliths in Soils and Plants*, vol. Monograph, 4 (eds. A. Pinilla, J. Juan-Tresserras and M. Machado). Centro de Ciencias Medioambientales, pp. 123–133.

Jeong G. Y. and Kim H. B. (2003) Mineralogy, chemistry, and formation of oxidized biotite in the weathering profile of granitic rocks. *Am. Mineral.* **88**, 352–364.

Johnson J. W., Oelkers E. H. and Helgeson H. C. (1992) SUPCRT92: a software package for calculating the standard molal thermodynamic of minerals, gases, aqueous species, and reactions from 1 to 5000 bars and 0° to 1000 °C. *Comput. Geosci.* **18**, 899–947.

Johnson-Maynard J. L., Graham R. C., Shouse P. J. and Quideau S. A. (2005) Base cation and silicon biogeochemistry under pine and scrub oak monocultures: implications for weathering rates. *Geoderma* **126**, 353–365.

Jové Colon C. F., Oelkers E. H. and Schott J. (2004) Experimental investigation of the effect of dissolution on sandstone permeability, porosity, and reactive surface area. *Geochim. Cosmochim. Acta* **68**, 805–817.

Kelly E. F., Chadwick O. A. and Hilinski T. E. (1998) The effects of plants on mineral weathering. *Biogeochemistry* **42**, 21–53.

Klein R. L. and Geis J. W. (1978) Biogenic silica in the Pinaceae. *Soil Sci.* **126**, 145–156.

Lasaga A. C., Soler J. M., Ganor J., Burch T. E. and Nagy K. L. (1994) Chemical weathering rate laws and global geochemical cycles. *Geochim. Cosmochim. Acta* **58**, 2361–2386.

Lucas Y. (1993) The relation between biological activity of the rain forest and mineral composition of soils. *Science* **260**, 521–523.

Lucas Y. (2001) The role of plants in controlling rates and products of weathering: importance of biological pumping. *Annu. Rev. Earth Planet. Sci.* **29**, 135–163.

Ma J. F. and Takahashi E. (2002) *Soil, Fertilizer, and Plant Silicon Research in Japan*. Elsevier Science.

Ma J. F., Tamai K., Yamaji N., Mitani N., Konishi S., Katsuhara M., Ishiguro M., Murata Y. and Masahiro Y. (2006) A silicon transporter in rice. *Nature* **440**, 688–691.

Maher K., Steefel C. I., DePaolo D. J. and Viani B. E. (2006) The mineral dissolution rate conundrum: insights from reactive transport modelling of U isotopes and pore fluid chemistry in marine sediments. *Geochim. Cosmochim. Acta* **70**, 337–363.

Markewitz D. and Richter D. D. (1998) The bio in aluminum and silicon geochemistry. *Biogeochemistry* **42**, 235–252.

Marschner H. (1995) *Mineral Nutrition in Higher Plants*. Academic Press Limited.

Mayer K. U., Frind E. O. and Blowes D. W. (2002) Multicomponent reactive transport modeling in variably saturated porous media using a generalized formulation for kinetically controlled reactions. *Water Resour. Res.* **38**, 1174–1195.

Meunier J.-D. (2003) Le rôle des plantes dans le transfert du silicium à la surface des continents. *C.R. Geosci.* **335**, 1199–1206.

Meunier J.-D., Colin F. and Alarcon C. (1999) Biogenic silica storage in soils. *Geology* **27**, 835–838.

Nédeltcheva T., Piedallu C., Gégout J.-C., Stussi J.-M., Boudot J.-P., Angéli N. and Dambrine E. (2006) Influence of granite mineralogy, rainfall, vegetation and relief on stream water chemistry (Vosges Mountains, north-eastern France). *Chem. Geol.* **231**, 1–15.

Nowack B., Mayer K. U., Oswald S. E., Van-Beinum W., Appelo C. A. J., Jacques D., Seuntjens P., Gérard F., Jaillard B., Schnepf A. and Roose T. (2006) Verification and intercomparison of reactive transport codes to describe root-uptake. *Plant Soil* **285**, 305–321.

Oelkers E. H. (2001) General kinetic description of multioxide silicate mineral and glass dissolution. *Geochim. Cosmochim. Acta* **65**, 3703–3719.

Pregitzer K. S. (2003) Cycling silicon—the role of accumulation in plants. *New Phytol.* **158**, 419–430.

Rains D., Epstein E., Zasoski R. and Aslam M. (2006) Active silicon uptake by wheat. *Plant Soil* **280**, 223–228.

Ranger J., Allie S., Gelhaye D., Pollier B., Turpault M.-P. and Granier A. (2002) Nutrient budgets for a rotation of a Douglas-fir plantation in the Beaujolais (France) based on a chronosequence study. *For. Ecol. Manage.* **171**, 3–16.

Ranger J. and Gelhaye D. (2001) Belowground biomass and nutrient content in a 47-year-old Douglas-fir plantation. *Ann. For. Sci.* **58**, 423–430.

Ranger J., Gérard F., Lindemann M., Gelhaye D. and Gelhaye L. (2003) Dynamics of litterfall in a chronosequence of Douglas-fir (*Pseudotsuga menziesii* Franco) stands in the Beaujolais mounts (France). *Ann. For. Sci.* **60**, 475–488.

Ranger J., Marques R. and Jussy J.-H. (2001) Forest soil dynamics during stand development assessed by lysimeter and centrifuge solutions. *For. Ecol. Manage.* **144**, 129–145.

Rustad L. E. and Cronan C. S. (1995) Biogeochemical controls of aluminium chemistry in the O horizon of a red spruce (*Picea rubens* Sarg.) stand in central Maine, USA. *Biogeochemistry* **29**, 107–129.

Sahrawat K. L. (1983) Correlations between indexes of soil nitrogen availability and nitrogen percent in plant, nitrogen uptake, and dry-matter yield of rice grown in the greenhouse. *Plant Soil* **74**, 223–228.

Saito K., Yamamoto A., Sa T. and Saigusa M. (2005) Rapid, micro-methods to estimate plant silicon content by dilute hydrofluoric acid extraction and spectrometric molybdenum method. I. Silicon in rice plants and molybdenum yellow method. *Soil Sci. Plant Nutr.* **51**, 29–36.

Salvage K. M. and Yeh G. T. (1998) Development and application of a numerical model of kinetic and equilibrium microbiological and geochemical reactions (BIOKEMOD). *J. Hydrol.* **209**, 27–52.

Sangster A. G., Ling L., Gérard F. and Hodson M. J. (2007) X-ray microanalysis of needles from Douglas fir growing in environments of contrasting acidity. *Water, Air Soil Pollut.: Focus* **7**, 143–149.

Shock E. L., Sassani D. C., Willis M. and Sverjensky D. A. (1997) Inorganic species in geologic fluids: correlations among standard molal thermodynamic properties of aqueous ions and hydroxide complexes. *Geochim. Cosmochim. Acta* **61**, 907–950.

Sommer M., Kaczorek D., Kuzyakov Y. and Breuer J. (2006) Silicon pools and fluxes in soils and landscapes – a review. *J. Plant Nutr. Soil Sci.* **169**, 310–329.

Sverdrup H. and Warfvinge P. (1995) Estimating weathering rates using laboratory kinetics. In *Chemical Weathering Rates of Silicate Minerals*, vol. 31 (eds. A. F. White and S. L. Brantley). Mineral. Soc. Am., pp. 485–539.

Takahashi E., Ma J. F. and Miyake Y. (1990) The possibility of silicon as an essential element for higher plants. *Comments Agric. Food Chem.* **2**, 99–122.

Tamai K. and Ma J. F. (2003) Characterization of silicon uptake by rice roots. *New Phytol.* **158**, 431–436.

USDA (1994) *Keys for soil taxonomy*. Soil Conservation Service.

van Genuchten M. T. (1980) A closed-form equation for predicting the hydraulic conductivity of unsaturated soils. *Soil Sci. Soc. Am. J.* **44**, 892–898.

Watson I. A., Oswald S. E., Mayer K. U., Wu Y. X. and Banwart S. A. (2003) Modeling kinetic processes controlling hydrogen and acetate concentrations in an aquifer-derived microcosm. *Environ. Sci. Technol.* **37**, 3910–3919.

Welch S. A. and Ullman W. J. (1999) The effect of microbial glucose metabolism on bytownite feldspar dissolution rates between 5° and 35 °C. *Geochim. Cosmochim. Acta* **63**, 3247–3259.

Welch S. A. and Ullman W. J. (2000) The temperature dependence of bytownite feldspar dissolution in neutral aqueous solutions of inorganic and organic ligands at low temperature 5–35 °C. *Chem. Geol.* **167**, 337–354.

White A. F. and Blum A. E. (1995) Effects of climate on chemical weathering in watersheds. *Geochim. Cosmochim. Acta* **59**, 1729–1747.

White A. F., Blum A. E., Bullen T. D., Vivit D. V., Schulz M. and Fitzpatrick J. (1999) The effect of temperature on experimental and natural chemical weathering rates of granitoid rocks. *Geochim. Cosmochim. Acta* **63**, 3277–3291.

Ziegler K., Chadwick O. A., Brzezinski M. A. and Kelly E. F. (2005) Natural variations of δ^{30}Si ratios during progressive basalt weathering Hawaian islands. *Geochim. Cosmochim. Acta* **69**, 4597–4610.

Associate editor: Donald L. Sparks